BOUNDARY LAYER TRANSITION IN SIMULATED TURBINE BLADE FLOW

by

Derek Graham BSc

Department of Mechanical and Industrial Engineering, Dundee Institute of Technology

Thesis submitted to the C.N.A.A. in partial fulfilment of the requirements of the degree of Doctor of Philosophy

August 1990

DECLARATION

I hereby declare that the following work has been composed by myself and that this thesis has not been presented for any previous award of the C.N.A.A. or any other university

Derek Graham

CONTENTS

Boundary Layer Transition in Simulated Turbine Blade Flow

by

Derek Graham

Abstract

An experimental investigation of the development of the boundary layer in a simulated turbine blade flow is described.

A velocity distribution typical of a "squared-off" turbine blade was reproduced in an open return wind tunnel. Measurements were made in the boundary layer formed on a flat, polished aluminium plate using standard hot wire instrumentation. An automatic data acquisition and control system was based around an Amstrad PC1640 16-bit microcomputer. By using assembly language subroutines, very fast sampling rates could be achieved which allowed a detailed digital representation of the raw signal to be captured. The relatively large RAM capacity of the Amstrad PC1640 allowed samples of sufficient duration to be stored. The mean flow variables, such as the mean velocity and RMS, were calculated by software thus reducing the requirement for external instrumentation. Assembly language subroutines were again necessary to process the large quantities of data involved within acceptable timescales.

An algorithm was developed to discriminate between laminar and turbulent flow. This was used to conditionally sample the signal in the transition region and hence provide mean laminar and turbulent velocity profiles in the transition region. It also provided a measurement of the intermittency. Boundary layer profiles were measured under the imposed velocity distribution at various levels of freestream turbulence giving a range of normal and separation bubble type transitions. The concept of statistical similarity of transition regions was observed to remain intact for severe adverse pressure gradients, including cases where separation bubbles were present during the early stages of transition.

An original correlation for the spot formation rate parameter, N, was developed using the adverse pressure gradient data of Gostelow (1989b). This correlation accounted for the combined effects of freestream turbulence and adverse pressure gradient. The correlation was found to give better prediction of the transition length in turbine blade flows than currently used methods.

The conditionally sampled velocity profiles indicate that intermittent laminar separation can occur in the early part of the transition region.

PUBLICATIONS

Fraser C J, Milne J S & Graham D - "Fast Data Acquisition and Digital Signal Processing in Studies of Turbulent Flow" 4th Joint International Conference on Mechanical Engineering and Technology, Zagazig Univ. Cairo, 1989
Paper presented by Dr C J Fraser

Graham D, Fraser C J & Milne J S - "Digital Measurement in Intermittently Turbulent Flows" AMSE conference on Signals and Systems, Brighton, 1989
Paper presented by D Graham

Fraser C J, Graham D & Milne J S - "Digital Processing of Hot Wire Anemometer Signals in Intermittently Turbulent Flows" Flow Measurement and Instrumentation, Vol. 1, 1990

ACKNOWLEDGEMENTS

I would like to sincerely thank the following people;

My supervisors, Dr C J Fraser and Mr J S Milne, who at all times have shown a keen interest in the development of the project.

Dr P Stow and Mr N T Birch of Rolls-Royce PLC who provided much information and valuable comment during the course of the project.

The technical staff, in particular Mr W Keating for assistance in the laboratory and Mr I McNab and Mr R Greig. Also Noreen and Liz of the secretarial staff.

Finally a special thanks to my collegues Sumant Mathure and George Kotsikos.

The financial support of Rolls Royce PLC and the SERC is gratefully acknowledged.

NOTATION

A		dependence area
a		velocity ratio of upstream edge of a turbulent spot
b		velocity ratio of downstream edge of a turbulent spot
C		constant in the law of the wall
C_f		skin friction coefficient
c		wave propagation speed
f		dimensionless stream function
G		spot formation rate parameter
g		spot production rate (from Emmons (1951))
H_{12} or H	δ^*/θ	shape factor
i		$\sqrt{-1}$
L		mixing length
m	$\frac{\theta^2}{\nu}\frac{dU}{dx}$	pressure gradient parameter
m	$\frac{x}{U}\frac{dU}{dx}$	pressure gradient parameter (chapter 6)
n		spot formation rate (no./s m)
n		number of points (section 4.1.3)
N		non-dimensional spot formation rate
R		influence volume
R_x	$\frac{xU}{\nu}$	length Reynolds number
R_θ	$\frac{\theta U}{\nu}$	momentum thickness Reynolds number
R_λ	$\frac{\lambda U}{\nu}$	transition length Reynolds number
r		body radius
s		streamwise surface distance

Tu%		freestream turbulence level
t		time
Δt		small, finite time interval
u, v, w		instantaneous velocity components (m/s)
u',v', w'		fluctuating velocity components (m/s)
$\bar{u}$, $\bar{v}$, $\bar{w}$		mean velocity components (m/s)
u_τ	$\sqrt{\tau_w/\rho}$	friction velocity (m/s)
u^+	U/u_τ	dimensionless velocity
U		freestream velocity (m/s)
V		volume in xyt space
x, y, z		cartesian coordinates (mm)
$\bar{x}$		location of 50% intermittency point (mm)
Δx		transition length as defined by Chen and Thyson (1971)
y^+	yu_τ/ν	dimensionless y coordinate
α		angle
α		wave number
β		non dimensional coordinate (equation 4.19)
ψ		stream function
ϵ		eddy viscosity
λ		distance between 25% and 75% intermittency points (mm)
η	$\frac{x - \bar{x}}{\sigma}$	transition normalising coordinate (Schubauer and Klebanoff (1955))
κ		constant in the law of the wall
ω		vorticity
μ		fluid dynamic viscosity (kg/ms)
ν		fluid kinematic viscosity (m^2/s)
ρ		fluid density (kg/m^3)
Π		Coles' wake parameter

γ		near wall intermittency
θ		momentum thickness (mm)
σ		dependence area factor
σ		standard deviation of mean intermittency distribution (mm)
τ		shear stress
ξ	$\frac{x - x_t}{\lambda}$	transition normalising coordinate (Dhawan and Narasimha (1958))
δ		boundary layer thickness (mm)
δ^*		displacement thickness (mm)

subscripts

L	laminar flow
d	downstream edge of turbulent spot
i	inner region (chapter 6)
o	outer region (chapter 6)
o	zero pressure gradient flows
s	start of transition (1% intermittency point)
t	start of transition (Narasimha's criterion)
tr	related to the transition region
T	turbulent flow
u	upstream edge of turbulent spot
w	conditions at the wall

CHAPTER 1

INTRODUCTION

The first gas turbine design was patented in 1791 by John Barber but it was not until the early years of the twentieth century that the first successful turbines were built. In Britain nearly 200 patents for gas and steam turbines were registered between 1784 and 1884, the year in which Parsons successfully constructed a steam turbine. The implications of Parsons invention became clear in 1897 when his turbine propelled boat, the Turbinia proved to be faster than the Royal Navy's fastest destroyers of the time. The 1930s proved to be a productive period in the development of the gas turbine. In 1939 the first jet powered flight was made in Germany and the Brown Boveri company demonstrated the first gas turbine power plant at the Swiss National Exhibition in Zurich. Gas and steam turbines are now used in many applications and have become increasingly more efficient as improvements in materials, cooling techniques and subsequent operating temperatures have been achieved. However, in recent years factors such as increased competition, government regulations on noise and emissions and dramatic changes in prices and availability of fuel have ensured continuing efforts to further improve the performance and efficiency of gas and steam turbine engines. Although the present work is specific to gas turbines it does have some relevance to non condensing steam turbines.

In the past intuitive design played a considerable role with the design and construction of working engines often preceding a theoretical understanding of all the processes involved. Even now the ideal of purely theoretical prediction of the performance of an arbitrary blade cascade is far in the future. The flow fields associated with turbomachinery are extremely complex. They are

three dimensional, unsteady, highly turbulent and subject to strong rotational effects. Theoretical analysis can be further complicated by other factors such as supersonic effects and the need to apply external and internal cooling to turbine blading. These effects are illustrated in figures 1.1a and 1.1b

According to Dzung and Seippel (1970) one of the first attempts to calculate the flow field around a blade was made in 1906 by Lorentz, who made the unjustified assumption that all streamlines were congruent to the blade shape. The 1920s saw the advent of the aircraft industry and the accumulation of aerofoil data which prompted the application of aerofoil theory to the prediction of turbine blade performance. The theory of two dimensional, inviscid flow was already well developed and methods of solving the Laplace equation, for example conformal mapping, were well known and could be applied to simple blade shapes. Arbitrary blade shapes, however, only became more readily analysed after the introduction of digital computers. Schlichting and Scholz were the first to account for the effect of viscosity by utilising Prandtl's boundary layer concept in 1951, almost fifty years after it was introduced.

Accurate flow prediction methods can play an important part in the design of turbine blading. In particular, prediction of the development of the boundary layer over blade profiles is important since it directly represents the aerodynamic losses and heat transfer associated with the blade. Current boundary layer prediction methods, however, are unreliable in important areas such as laminar to turbulent transition. Faster, more reliable, prediction methods, which can be used to analyse on-design and

off-design conditions, will allow more detailed optimisation without increasing development costs and should lead to better final designs.

1.1 BLADE DESIGN

Computer aided blade design systems typically consist of two parts, a through-flow analysis and a blade to blade analysis. The through-flow analysis gives information about the inlet and outlet flow conditions which are necessary to determine parameters such as stage pressure ratio or work output and the blade to blade analysis is used to determine the flow behaviour between individual blades.

The through-flow calculation considers the flow through a number of stages. Small scale unsteadiness in the flow, such as blade wakes, are ignored and the three dimensional equations of motion are usually reduced to a two dimensional form. The equations of motion are further modified to allow the effects of the blades on the through-flow to be modelled. For example, a dissipative force is included to account for the viscous losses through a blade row. Other effects which are modelled include; end wall boundary layers, secondary flows, various leakage flows etc. A more detailed description of through-flow modelling is given by Stow (1989).

The detailed flow over individual blades is normally calculated by coupling inviscid and boundary layer calculations, however methods which solve the Navier-Stokes equations have emerged in recent years. Solution of the complete Navier-Stokes equations requires considerable computing time with the fastest computers and is impractical for most cases. For turbulent flows

the time averaged, or Reynolds averaged, form of the Navier-Stokes equations are often used in conjunction with a model for the turbulence. Two approaches to inviscid analysis are possible; the design approach where the desired velocity over the blade is prescribed and the analysis gives the necessary blade geometry, and the analysis approach where the blade geometry is prescribed and the external velocity is calculated. Both approaches are useful and methods have been developed which combine both, for example the method of Cedar and Stow (1985) which is based on the finite element technique.

The boundary layer equations are a simplification of the Navier-Stokes equations and are valid in the region close to the surface of a body when the Reynolds number, based on the length of the body, is greater than about 1000. However the boundary layer equations are still complex, non-linear partial differential equations which are not readily solved for general boundary conditions. Various analytic approaches have been developed for laminar boundary layers. For example similarity solutions which reduce the number of variables, by one or more, by means of a coordinate transform. More general boundary layer calculation methods are based on either the von Karman integral momentum equation or direct numerical solution of the boundary layer equations using the finite difference technique. Integral methods are fast and acceptably accurate in many cases. Finite difference techniques require longer solution times and also rely on experimental data at some stage in the development of accurate turbulence models. For transitional flows integral methods and most finite difference methods require correlations to determine

the start and end of transition.

Inviscid - boundary layer coupling involves using the solution from a boundary layer calculation to modify the inviscid mainstream calculation. This is done by thickening the blade by the boundary layer displacement thickness before recalculating the inviscid flow over the modified blade shape. The boundary layer calculation is then repeated to give a new modified blade shape and this procedure is repeated until subsequent boundary layer calculations converge within specified limits.

At off design conditions laminar separation bubbles, where the flow reattaches as a turbulent boundary layer, can occur near the leading edge, Also, in some cases, complete turbulent separation can occur towards the trailing edge. Under these conditions the coupled inviscid - boundary layer approach can become very unreliable as the boundary layer approximations become invalid. Because of the importance of being able to predict off design losses, methods of solving the Reynolds averaged Navier-Stokes equations in two dimensions are currently being developed and used. These methods still rely on relatively simple turbulence models and the start and end of transition is specified or determined by correlation. Birch however (1987a) uses a one equation kinetic energy model for turbulence and transition. Although these methods have proved better able to predict off design flow conditions they will not replace the inviscid - boundary layer methods as every day design tools unless they become faster and cheaper to run. Three dimensional Navier-Stokes methods have also been developed and are used to some extent in design applications at present.

1.2 THE BOUNDARY LAYER

The introduction of the boundary layer concept by Prandtl in 1904 has proved to be one of the most significant achievements in the development of viscous flow theory and its importance in turbomachinery design has already been stated. The boundary layer concept allowed the theory of ideal fluid flow, which had been developed in the eighteenth century by such as Bernoulli, Euler, Lagrange and Laplace, to be reconciled with observations of the real world and the viscous-inviscid matching procedure permitted meaningful analysis of viscous flows.

The behaviour of the boundary layer is rather complex. Near the leading edge, in two dimensional flow, the flow is always laminar but at some point downstream it becomes unstable. Stability theory for viscous flow originated with the work of Orr (1907) and Sommerfeld (1908) who independently derived what is now known as the Orr-Sommerfeld equation ie.

$$(\bar{u} - c)(\hat{v}'' - \alpha^2\hat{v}) - \bar{u}''\hat{v} + \frac{i\nu}{\alpha}(\hat{v}'''' - 2\alpha^2\hat{v}'' + \alpha^4\hat{v}) = 0 \qquad (1.1)$$

where α = disturbance wave number, c = wave propagation speed, $i = \sqrt{-1}$, $\hat{v}$ = the disturbance variable and the prime, ', denotes differentiation w.r.t. y.

Solution of this equation can reveal whether infinitesimal disturbances are damped (stable flow) or amplified. The Reynolds number at which laminar flow becomes unstable to a travelling wave disturbance was calculated by Tollmein (1929) and extended to amplified two dimensional disturbances by Schlichting in the 1930s. These disturbances, which are now called Tollmein-Schlichting waves, were not observed experimentally until 1940-1941 by

Schubauer and Skramstad (1948). Previous to this the existence of Tollmein-Schlichting waves had not been accepted outwith Germany partly because of the political situation prior to the second world war and partly because of the lack of experimental evidence. As the flow develops, the Tollmein-Schlichting waves are amplified and soon become three dimensional. Ultimately, isolated spots of turbulence emerge which grow as they travel downstream and merge to form a fully turbulent boundary layer. The transition region consists of spots of turbulence surrounded by essentially laminar flow and is quantified by the intermittency function, γ, which defines the probability of encountering turbulence at any point and varies from 0 in laminar flow to 1 in the fully turbulent boundary layer.

Schubauer and Klebanoff (1955) provided the first quantitative data on the shape, growth and propagation of turbulent spots. Various workers including Chen and Thyson (1971), McCormick (1968) and more recently Walker (1987) have subsequently approximated the turbulent spot as a two dimensional triangle with the vertex downstream. Since then various workers have made more detailed studies of the structure and behaviour of turbulent spots. Wygnanski et al (1976) have measured the three dimensional mean flow field within a spot using ensemble averaging techniques. Cantwell et al (1978) studied the structure and growth in the plane of symmetry of a spot and Gad-el-Hak et al (1981) further investigated the growth of spots both normal to the plate and in the spanwise direction. All the above work was carried out in zero pressure gradient flows.

The first integral method, which was appropriate only for

laminar boundary layers, was devised by Pohlhausen (1921) and was based on the integral momentum equation of von Karman. Pohlhausen's method was widely used for about twenty years before better methods were developed. Twenty integral methods for turbulent boundary layers are described in the proceedings of the Stanford conference, see Kline et al (1968), and four of those were graded good when tested against a variety of data. Dhawan and Narasimha (1958) showed that the transitional boundary layer could be adequately described by performing laminar and turbulent calculations and weighting the solutions using the intermittency. This represented a considerable improvement over the assumption of point transition, particularly when the transition region occupied a considerable proportion of the flow. The finite difference technique is an old one but has only been a practical tool for solving the boundary layer equations since the introduction of the digital computer. The laminar boundary layer equations can be solved with arbitrary accuracy but turbulent boundary layer calculations depend on the accuracy of the turbulence model used. The most popular approach is to use an eddy-viscosity model as used by two of the three methods which were graded "good" at the Stanford conference. Various methods have been used to predict transition, for example McDonald and Fish (1973) use the turbulent kinetic energy transport equation, but it is still common to find empirical and semi empirical correlations for the start and length of transition, eg. Cebeci and Smith (1974).

The assumptions which allow the Navier-Stokes equations to be reduced to the boundary layer equations do not apply close to the point of separation, in particular velocities in the y direction

become significant. As a result both integral and differential methods have difficulty in predicting flows with severe adverse pressure gradients where separation is present. Integral methods resort to empirical correlations, such as Horton (1967), for laminar separation and reattachment. The so called FLARE approximation used by Cebeci, Keller and Williams (1979) allows the method of Cebeci and Smith (1974) to continue through small regions of separated flow but requires that the displacement thickness be specified.

1.3 TRANSITION PREDICTION

Integral and differential methods can give good predictions of the behaviour of the important parameters through transition but only if the start and end of transition are known. However, the inability to predict the start and length of the transition region is perhaps the most severe limitation to accurate prediction of typical blade boundary layers, Birch (1987b). The theory of linear stability can predict the point where laminar flow becomes unstable but it becomes increasingly more difficult to continue when three dimensionality becomes important. The boundary layer remains essentially laminar until the first turbulent spots form in the flow marking the start of transition. Various semi-empirical approaches to the prediction of transition onset, such as the so called e^n methods which relate the location of the start of transition to the amplification of Tollmein-Schlichting waves, have been proposed. However in some applications, such as turbine blade flows, it is still more common to find empirical correlations being used. A very commonly applied correlation is that of Abu-Ghannam

and Shaw (1980) which is the most recent and is based on the most data.

Dhawan and Narasimha (1958) proposed a correlation for transition length which related the transition length Reynolds number to the Reynolds number based on the location of the start of transition. Good correlation has been observed for zero pressure gradient flows with much of the scatter attributable to the differing techniques used to detect the start and end of transition. However, direct application of the Dhawan and Narasimha correlation to flows with pressure gradients can give poor accuracy. The transition length prediction method of Chen and Thyson (1971) is based on a similar correlation but also allows local conditions to affect the growth of turbulent spots and thus affect the calculated length of transition. A correlation for transition length which takes into account the effects of freestream turbulence and pressure gradient was proposed by Fraser et al (1988), for adverse pressure gradients only.

Emmons (1951) made the first attempt to quantify the transition process by means of a probability analysis. He assumed the existence of a function, $g(x,y,t)$, of position on the surface and time which specified the rate of spot production per unit area and followed the subsequent development of each spot produced. The fraction of time, $\gamma(x,y)$, (Emmons used the notation $f(x,y)$) that a point $P(x,y)$ is turbulent is obtained by summing the times that it is covered by a spot, taking care not to count overlapping spots twice. A spot generated at P_o (x_o, y_o, t_o) sweeps out a volume in xyt space which Emmons called the "propagation cone". He also noted that the cone need not have straight generators, allowing for

non linear growth of the spot as in axi-symmetric flows, for example. Emmons also defined the "dependence cone" which, for $P(x,y,t)$, is the locus in xyt space of all points $P_o(x_o,y_o,t_o)$ such that spots generated at these points will cover P. To eliminate errors due to overlaps Emmons assumed that the spot formed closest to the leading edge would be taken as causing the turbulence. Thus he developed an expression for the fraction of time, $\gamma(P)$, during which the flow at P is turbulent ie.

$$\gamma(P) = 1 - \exp(-\int_R g(P_o)dV_o) \qquad (1.2)$$

which can be calculated numerically if $g(P_o)$ is known and the influence volume R is defined. Emmons considered flat plate flow and assumed that g was constant. He also assumed that both the propagation and dependence cones had straight generators and thus the volume, V, of the dependence cone was given by $V = A_1x^3/3$ where A_1 is the cone cross section at unit distance from the apex. Thus Emmons derived the intermittency distribution

$$\gamma(x) = 1 - \exp(-\sigma g x^3/3U) \qquad (1.3)$$

where σ is a dimensionless propagation parameter of the spot related to the base area of the cone at unit distance from the apex.

The spot concept of transition was investigated by the experiments of Schubauer and Klebanoff (1955), however their intermittency measurements did not agree with Emmons' theory. Instead they fitted their data to a cumulative normal distribution and showed that, when scaled by the standard deviation, all the data collapsed onto a single curve. Dhawan and Narasimha (1958) managed to reconcile Emmons' theory with experimental data by introducing the concept of concentrated breakdown. This stated

that turbulent spots were most likely to appear at a fixed point in the flow and this point was observed experimentally to be the start of transition. They assumed g to be a Gaussian error curve with its maximum at x_t and found the best agreement with experimental data when the Gaussian curve had a standard deviation approaching zero. Thus they assumed g to be best approximated by a Dirac delta function. Using Emmons' theory this gave the intermittency distribution

$$\gamma = 1 - \exp[-(x - x_t)^2 n\sigma/U] \qquad (1.4)$$

where n is the number of spots occurring per unit of time and spanwise distance at x_t. This can be modified to give the "universal" distribution

$$\gamma = 1 - \exp(-0.412\xi^2) \qquad (1.5)$$

where $\xi = (x - x_t)/\lambda$ with λ being the distance between the points where the intermittency is 0.25 and 0.75. Dhawan and Narasimha showed that intermittency data for a flat plate collapsed onto this single curve, when normalised by λ, whether transition was natural or provoked by a trip wire. The concept of statistical similarity of transition regions has been extended to moderate adverse pressure gradients by Fraser et al (1988), Gostelow and Blunden (1988) and Gostelow (1989) and was shown to remain intact, in fact the present work has indicated that it holds true in severe adverse pressure gradients.

From the above two equations it can be shown that

$$n = 0.412U/\sigma\lambda^2 \qquad (1.6)$$

ie. that the transition length varies as the inverse square root of the spot formation rate, if σ is constant. Emmons estimated the value of σ as about 0.1 and Narasimha (1985) found that σ varies

from about 0.25 to 0.29. Knowledge of the behaviour of σ is limited since detailed measurements of spot shapes only exist for zero pressure gradient flows. Narasimha (1985) defined the non dimensional parameter

$$N = n\sigma\theta_t^3/\nu \tag{1.7}$$

and suggested that it has a constant value of 0.7×10^{-3} in zero pressure gradient flows. Data indicates that this value increases at low freestream turbulence levels. The work of Gostelow and Blunden (1988), Gostelow (1989a), Walker and Gostelow (1989) and the present work have shown that N rises rapidly in adverse pressure gradients and also varies greatly with freestream turbulence. In the course of the present work the data set of Gostelow (1989b) has been used to correlate N with the pressure gradient and freestream turbulence level.

Chen and Thyson (1971) extended Emmons theory to include blunt, axisymmetric bodies with pressure gradients. They accepted the hypothesis of concentrated breakdown and assumed that a) spot propagation velocities were proportional to the local external velocity and b) the spot grows at a constant angle, α, relative to the local external streamline. Thus they developed the following expression for intermittency

$$\gamma = 1 - \exp[\ -Gr(s_t)(\int_{s_t}^{s} r^{-1}ds)(\int_{s_t}^{s} Ue^{-1}ds)\ ] \tag{1.8}$$

where G is a new spot formation rate parameter

$$G = n\tan\alpha(a^{-1} - b^{-1}), \quad \text{with } a = Uu/Ue \text{ and } b = Ud/Ue$$

G was then correlated with the start of transition Reynolds number, Re , and Mach number for a flat plate. The method is still widely used but has been found to predict transition lengths which are far too long in adverse pressure gradients. The fact that the method

is not solely dependent on the conditions at the start of transition has lead to suggestions that it may be better able to predict transitions which occur in flows with rapidly varying pressure gradients, for example a flow where transition starts in a favourable pressure gradient and continues into a region of adverse pressure gradient, although this has been disputed by Narasimha (1985).

The fact that the intermittency distribution remains statistically similar in favourable and adverse pressure gradients might be taken to indicate that effects on the spot growth and propagation characteristics may have a secondary influence on the transition length. In fact Narasimha (1985) quotes one case where a pressure gradient occuring in the downstream half of the transition region has no effect on the intermittency distribution. This suggests that the most important factor influencing the extent of the transition region is the rate at which spots are produced at the start of transition, which can be quantified by the parameter N. This also gives some physical justification to the correlations which relate the length of transition to conditions at the start of transition although more sophisticated correlations may be necessary to account for pressure gradient and other effects. It is this physical justification which makes the spot formation rate approach to transition length prediction more attractive than purely empirical correlation.

1.4 EXPERIMENTAL MEASUREMENT OF INTERMITTENT FLOWS

Schubauer and Klebanoff (1955) obtained measurements of intermittency in the transition region directly from photographic

records of an oscilloscope trace. At around the same time Corrsin and Kistler (1955) were using conditional sampling to investigate the intermittent turbulence which occurs in the outer region of the turbulent boundary layer. This area was further studied by Kovasznay et al (1970) who developed new techniques of conditional sampling and conditional averaging using analogue equipment, and also by Kaplan and Laufer (1962) and, more recently, by Murlis et al (1982) using large digital computers. Arnal et al (1977) applied conditional sampling to the transition region on a flat plate and showed that the behaviour of turbulent spots was very similar to that of a fully developed turbulent boundary layer from an early stage, giving credence to the assumption adopted by Dhawan and Narasimha (1958). The signal from a hot wire anemometer was first recorded in analogue form and then digitised at an effective sampling rate of 10kHz before processing in a digital computer.

During the course of the present work a data acquisition and control system, based on the IBM compatible AMSTRAD PC1640, was developed. A real time sampling rate of 10kHz was employed and sufficient memory space was available to allow long sample times to be obtained. The use of the 16-bit microcomputer has allowed the development of a powerful digital system which would previously have required access to an expensive mainframe or mini computer.

Using a conditional sampling technique the system was used to investigate the transitional boundary layer on a simulation of the suction surface of a turbine blade. One feature of particular interest was the possibility of intermittent separation occurring in a transitional boundary layer where the turbulent component of the flow remains attached as suggested by Gardiner (1987). The

development of the data acquisition system has resulted in the presentation of two conference papers; Fraser et al (1989) and Graham et al (1989), and one journal publication; Fraser et al (1990) (see appendix 4).

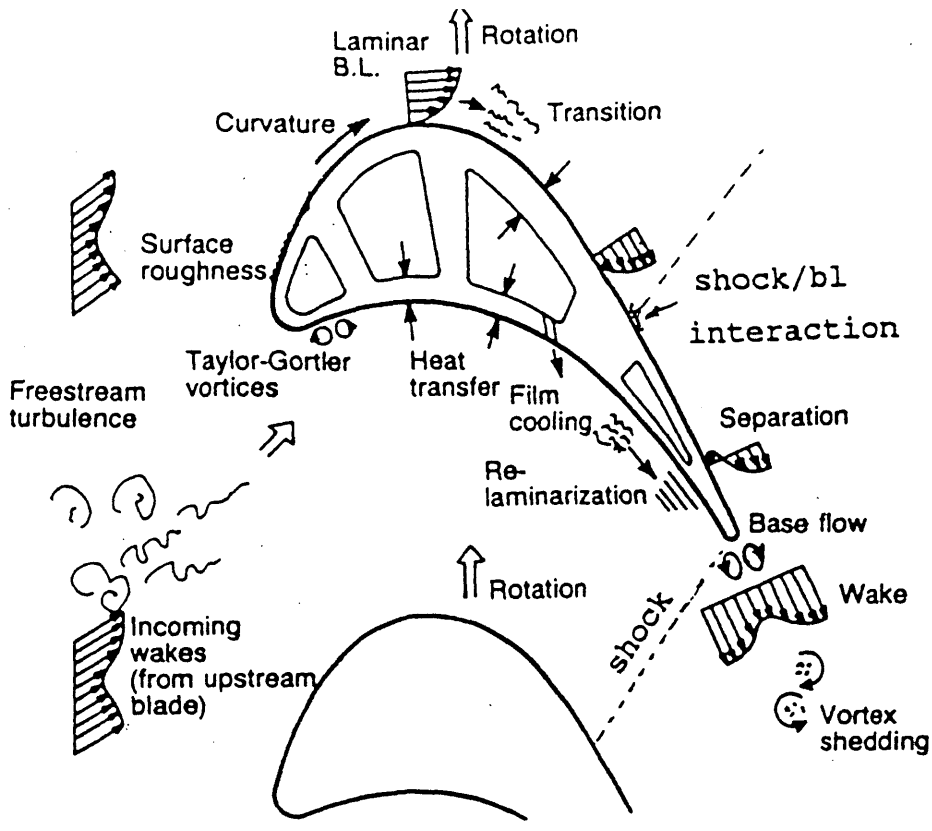

Figure 1.1a: 2D Turbine Blade Flow

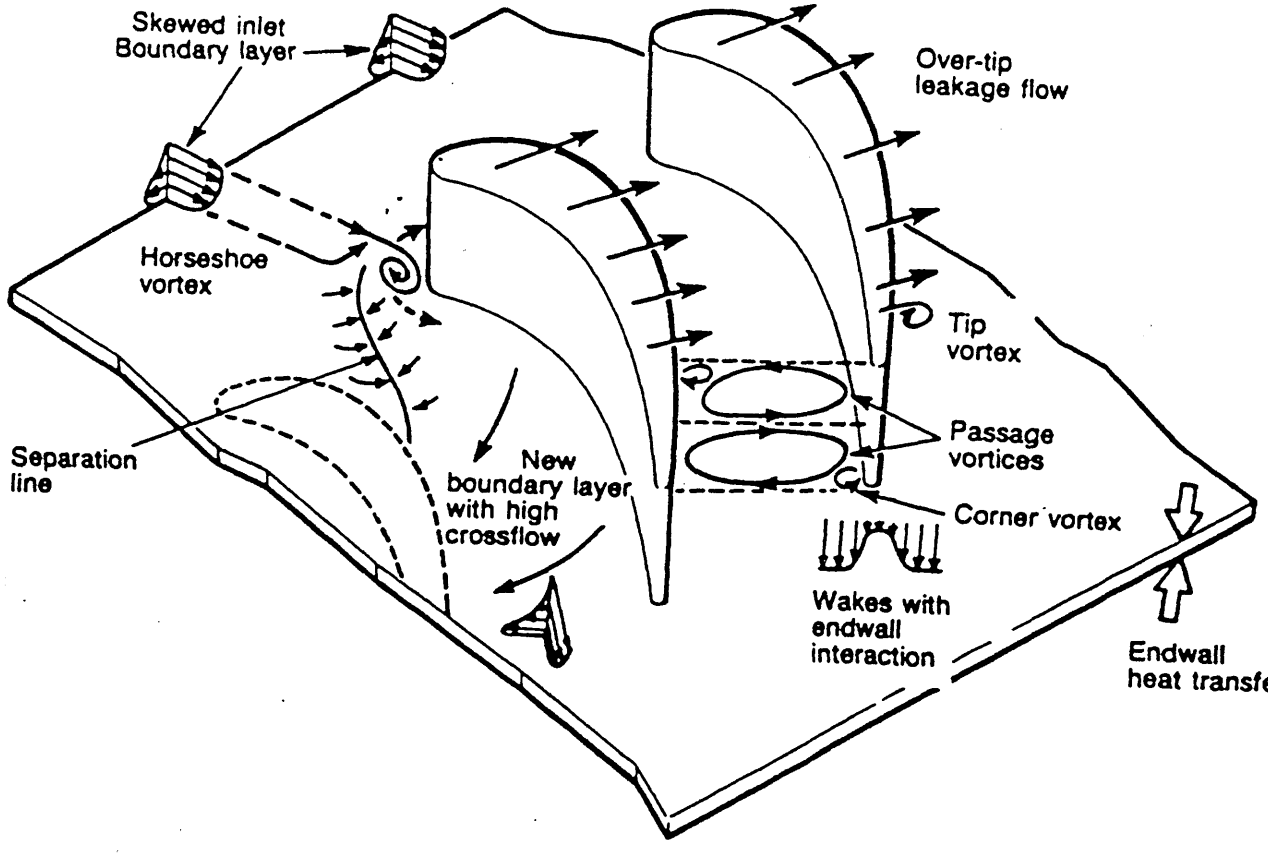

Figure 1.1b: 3D Turbine Blade Flow

CHAPTER 2

EXPERIMENTAL FACILITIES

2.1 WIND TUNNEL FACILITY

The wind tunnel used throughout the present investigation was that designed and built by Fraser (1979) and subsequently modified by Gardiner (1987). It was purpose built for the study of two dimensional, incompressible flat plate boundary layer flow and has an adjustable roof to allow the external pressure distribution to be varied. Various freestream turbulence levels can be generated by means of grids which are located in the inlet contraction prior to the working section. Fig 2.1 shows a schematic diagram of the wind tunnel.

The inlet contraction is preceded by a series of turbulence damping screens which are designed to reduce spanwise nonuniformity in the flow and also reduce the freestream turbulence. The inlet contraction itself is of rectangular section with an aspect ratio of 2:1 and has an area reduction ratio of 9:1 over a length of 1.5m. The working section is 2.5m long and 450mm wide and the height at the inlet is 227mm. The existing flexible roof had to be modified to enable a pressure distribution typical of turbine blade flow to be reproduced. A fixed insert was introduced over the first 260mm of the working section to reproduce the rapid acceleration encountered near the leading edge of a blade. Further downstream the flexible roof could be used normally to adjust the flow field. The insert was designed using a simple one dimensional analysis however a two dimensional inviscid analysis and subsequent measurements showed that any two dimensional effects were small.

Simulation of the rapid acceleration near the leading edge resulted in considerable reduction of the height of the working section. This meant that the existing instrument carriage, which

ran inside the working section on two horizontal rails fixed to the side walls, would produce an unacceptably large blockage to the flow. The solution adopted was to move the carriage outside the working section and provide access for the hot wire probe by means of a slot in the roof. The slot was then sealed using an adhesive tape. This arrangement, however, limited all measurements to the centre line of the working section. Streamwise positioning of the probe was carried out manually and vertical traversing was driven remotely by means of a DISA sweep drive unit (type 52B01) in conjunction with a stepper motor (type 52C01). A pitot static tube coupled to an inclined manometer, which was used to calibrate the probe and monitor the reference velocity had to be moved from the leading edge to a point 780mm downstream.

A flexible coupling connects the exit of the working section to the diffuser. This prevents vibrations being transmitted from the fan and the motor to the working section and also provides a pliable seal between the variable height roof and the diffuser. The diffuser merges from a 450mm by 450mm square section at the upstream end to an 800mm diameter round section over its 1.5m length. The six blade fan is driven by a 2hp variable speed motor which has a maximum speed of 1440rpm and is housed in a 700mm long cylindrical casing.

The wind tunnel is equipped with an aluminium boundary layer plate which is 6mm thick, 2.4m long and spans the full width of the working section. The plate was originally positioned 50mm above the floor of the working section at zero incidence to oncoming flow. The symmetrically sharpened leading edge was bent downwards to ensure that the stagnation point would occur on the upper

surface of the leading edge. Gardiner (1987) modified the leading edge design, returning it to a symmetrical shape and ensured that the stagnation point would occur on the top surface by inclining the plate at -0.5 degrees to the oncoming flow.

2.2 TURBULENCE GENERATING GRIDS

Various levels of freestream turbulence were generated in the working section by inserting grids close to the contraction entrance, about 400mm downstream of the front edge. This arrangement was suggested by Blair et al (1981) and differs from the arrangement employed by most other wind tunnels in which the grids are located at the start of the working section itself, eg. Roach (1988). The advantage of this arrangement is that the turbulence generated will be more homogeneous and have a lower decay rate along the test section although a coarser grid will be required for a given turbulence intensity. Four existing grids were used to produce turbulence levels at the leading edge of between 1% and 1.5%. A further grid was designed to give a leading edge turbulence level of about 2%.

2.3 FREESTREAM PRESSURE DISTRIBUTION

The wind tunnel was arranged to reproduce the velocity distribution found on the suction surface of a forward loaded aerofoil ("squared-off" design). The velocity distribution was based on that used by Sharma et al (1982) which is described in detail by Gardner (1981) and is shown in fig 2.2. The rapid acceleration which occurs over the first 10-15% of the blade could not be achieved simply by means of the existing flexible roof so a

section was designed which would be fixed in place over the leading edge region. The shape of the insert was calculated using the one dimensional continuity equation. A two dimensional, inviscid calculation was carried out using a finite element package, the results of which indicated that variation of the velocity in the y direction would be small and would thus not affect the development of the boundary layer. This was confirmed experimentally after the roof insert was installed. Measurements also showed that the roof boundary layer was turbulent from the earliest measuring station and there appeared to be no separation from the roof which could have caused problems in setting up the required velocity distribution.

Figure 2.3 shows the variation of the freestream turbulence intensity and the RMS of u' along the test section, with the highest turbulence generating grid present. The turbulence intensity appears to vary in inverse proportion to the freestream velocity. The RMS of the fluctuations in u do not appear to be strongly influenced by the rapid acceleration and deceleration of the flow, varying by less than 10% over the first 700mm of the test section.

2.4 HOT WIRE INSTRUMENTATION

All velocity measurements were made using standard DISA, series 55M hot wire instrumentation. Boundary layer probes were connected via a probe support and a 5m length of coaxial cable to a 55M10 constant temperature anemometer. The voltage output from the anemometer is related to the velocity over the probe but the relationship is non-linear. The signal is passed through a 55M25

lineariser which can be calibrated to give an output which is linearly proportional to the flow velocity. The output from the lineariser is passed through a 55D25 auxiliary unit to filter out frequencies above 2kHz since most of the turbulent energy is contained well below this frequency.

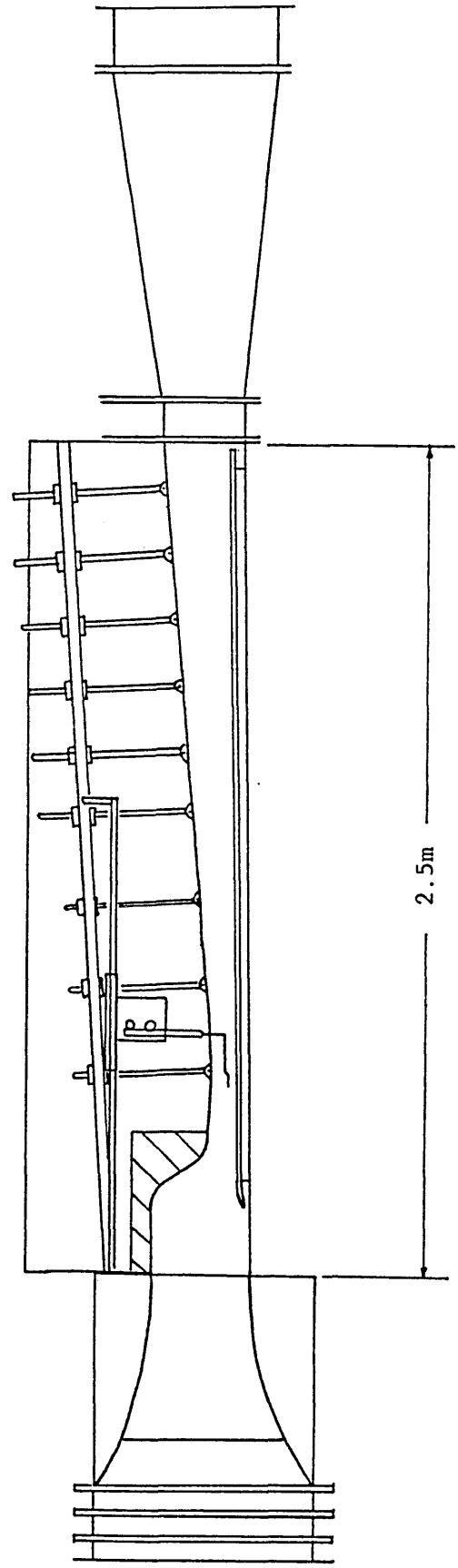

figure 2.1 Cross section of the wind tunnel

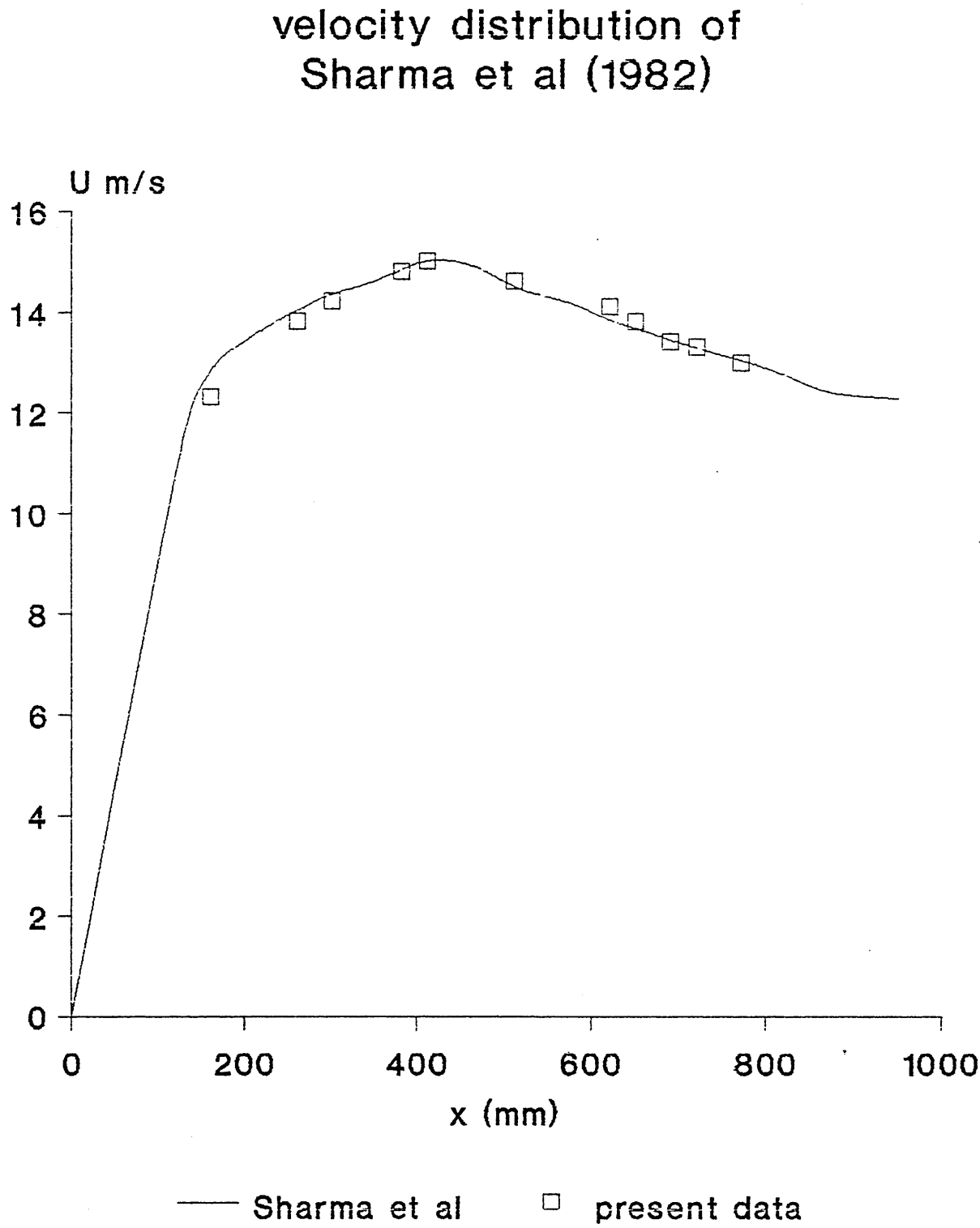
velocity distribution of
Sharma et al (1982)
U m/s
16
14
12
10
8
6
4
2
0
0
200
400
600
800
1000
x (mm)
Sharma et al
present data

figure 2.2

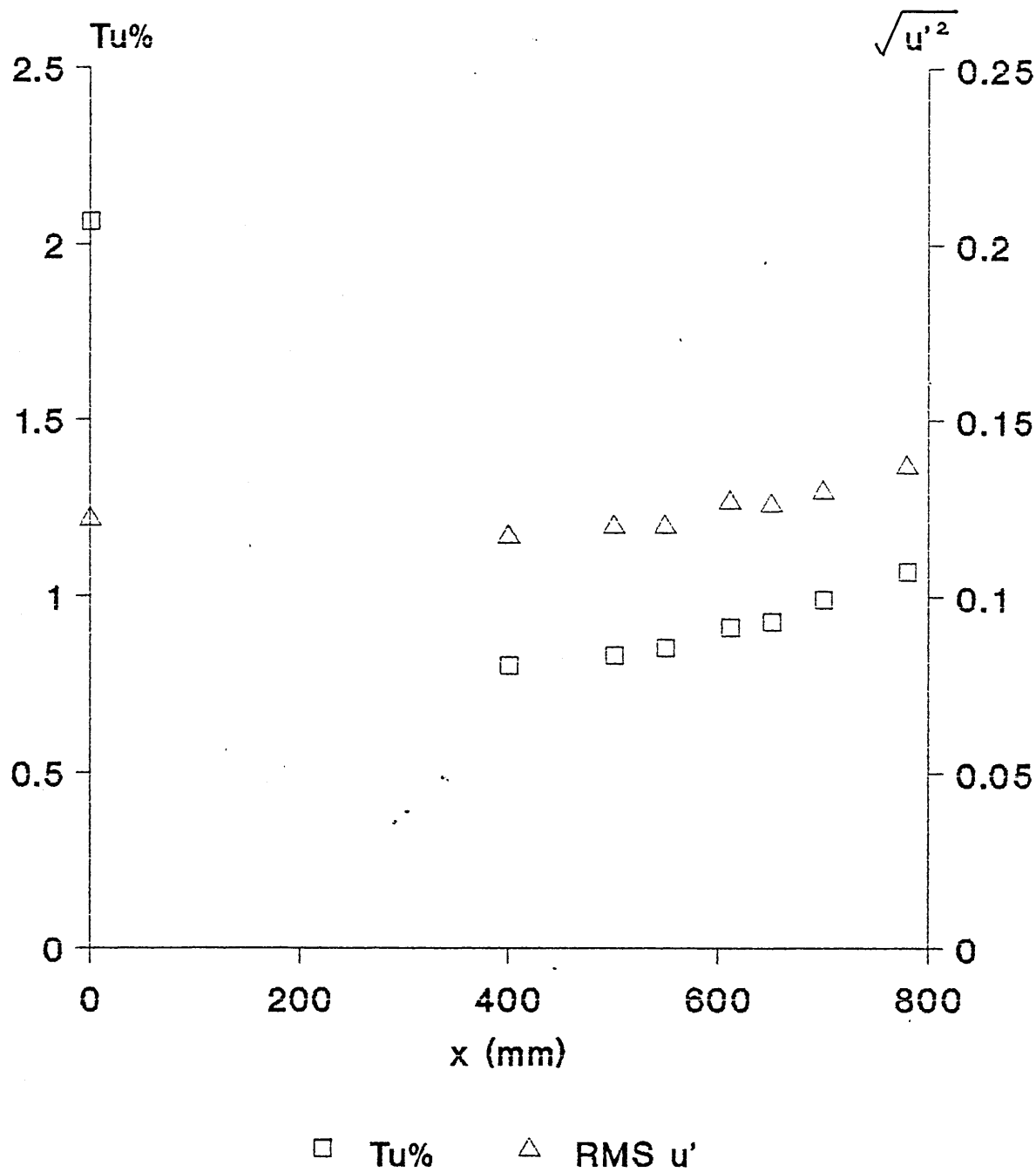

figure 2.3 distribution of freestream turbulence and RMS of u'

CHAPTER 3

DATA ACQUISITION

Since the introduction of the first commercial microprocessor chip by Intel, the 4-bit Intel 4004 in 1971, the microcomputer has found increasing application to engineering problems. 8-bit machines, such as the BBC microcomputer, have proved very successful in measurement and control systems but it is only with the advent of 16-bit machines, such as the IBM and compatible machines, that the microcomputer has begun to pose a threat to mainframe computers in some applications.

Traditionally the measurement of turbulent flows has involved the use of expensive analogue instrumentation but a digital computer based approach can be much more flexible. Previously this required access to a mainframe or mini computer but the increased memory capacity of the 16-bit computers allows these machines to be used in data acquisition applications although there may be a time penalty when analysing large quantities of numerical data. This chapter describes the development of a data acquisition and control system, based on an IBM compatible 16-bit machine, which allows detailed digital measurements to be made in transitional boundary layers. The sophistication of the system is comparable to that achieved in the past by workers using mainframe computers but at a fraction of the cost.

3.1 DATA TRANSFER

An important consideration in the development of a computer based data acquisition system is the process by which data is to be transferred between the external instrumentation and the computer itself. One approach is to use a standard digital transmission bus such as the IEEE-488 parallel bus or the RS232 serial bus. Many

microcomputers have serial and parallel input/output ports and can communicate data directly in digital format with a wide range of compatible laboratory instruments. However, many instruments produce analogue signals, normally in the form of a voltage, to represent the physical quantity being measured or require an analogue input to control their operation. Under these conditions an interface is required which can convert analogue voltages into digital form and vice versa. An IEEE interface is available on the DISA 5600 series of hot wire equipment but not on the 55M series used in the present system. For this reason an interface approach was adopted. Some microcomputers, such as the BBC microcomputer, have an on board analogue to digital converter (ADC) and most machines have facilities to allow the addition of peripheral devices such as ADCs.

The AMSTRAD PC1640, a typical IBM compatible, is equipped with a parallel port and a serial port and also has three expansion slots which will accept any IBM compatible expansion cards. A great variety of expansion cards are available and a good general purpose interface card will normally provide multi channel analogue input to an ADC, multi channel analogue output from a DAC, multi channel digital input/output and possibly other features. The input/output space is "port addressed" and is accessed using the BASIC commands INP and OUT or IN and OUT in assembly language. Most interface cards can be hardware set to appear at a specified address in the port map. Available locations are shown in Fig 3.1 with location &h300 being recommended by some card manufacturers. The address which is chosen is effectively the base address of the card from which the various ports are offset. Fig 3.2 shows an

example port map for the BLUECHIP TECHNOLOGY ACM-44 card, reference BLUECHIP TECHNOLOGY (1988).

3.2 DATA ACQUISITION HARDWARE

To obtain a true digital representation of an analogue signal, suitable sampling rates and sample lengths must be employed. These will depend very much on the nature of the signal itself and the information required from the signal. To avoid aliasing errors the sampling theorem states that the sampling rate should be at least twice the highest frequency occurring in the signal. It is commonly accepted that a sampling rate of at least five times the highest frequency should be used for most engineering applications. Very fast analogue to digital conversion is required when digitising turbulence signals, for example the boundary layer produced in the present wind tunnel contains velocity fluctuations at frequencies of up to about 2kHz requiring a sampling rate of 10kHz.

The high sampling rates required to give an accurate representation of a turbulence signal lead to the generation of large quantities of numerical data very quickly. This can cause problems when using microcomputers with low RAM capabilities. For example, Shaw et al (1983) used the 48k Apple II microcomputer to record and analyse signals from turbulent and transitional boundary layers but could only record samples of less than one second while sampling at 20kHz. This may have been sufficient to obtain accurate values of the mean flow parameters in a fully developed turbulent boundary layer but is almost certainly too short to obtain a representative sample of an intermittently turbulent

signal, particularly at low or high intermittencies. Gardiner (1987) overcame the limited memory capacity of the BBC microcomputer by taking a large number of samples from appropriate analogue instrumentation and storing only the mean value in the computer memory. This also allowed lower sampling rates to be used which simplified the acquisition software. However there are advantages in recording a complete digital signal in that the processing can be carried out digitally at a later time, thus reducing the quantity of analogue instrumentation required.

The newer 16-bit machines are more suited to this type of data acquisition application since they have up to twenty times as much RAM as many 8-bit machines. They also have faster processors, eg. the 8MHz Intel 8086 which is used in the AMSTRAD PC against the 1MHz 6502 used in the BBC microcomputer. It was decided at an early stage to use a 16-bit machine as the basis of the data acquisition system because of the increased RAM and processor speed. Because of the availability of a wide range of accessories, such as expansion boards, it was decided to use an IBM or compatible machine and the AMSTRAD PC1640, which is fully compatible, was chosen. This machine has 640k of RAM, a 20 megabyte hard disc and a 5.25" floppy disc drive but costs about the same as a BBC microcomputer with a double disc drive and a colour monitor. All programs and data could be stored on the hard disc which proved to be more convenient and quicker to access than floppy discs.

The main factors which influence the choice of ADC are the conversion time and the resolution. The conversion time must obviously be short enough to allow the appropriate sampling rates

to be achieved, while bearing in mind that cost will increase with decreasing conversion time. A "safety factor" should be allowed for however, as experience has shown that the theoretical maximum sampling rate, based on the manufacturers quoted conversion time, cannot always be achieved. The most common ADC resolutions available are 8-bit or 12-bit. 12-bit conversion would require two bytes ie. 16-bits, to store each piece of data and would therefore consume twice as much memory as 8-bit resolution. The I8086 processor is equally capable of handling 8-bit or 16-bit inputs but it was decided that the increased accuracy of 12-bit conversion would not give any significant advantage therefore 8-bit resolution was selected.

The current data acquisition and control software was developed using the BLUECHIP TECHNOLOGY ACM-44 Multi Channel Analogue/Digital Combination Card which offered sixteen single ended analogue inputs with 8-bit resolution and a conversion time of two microseconds, four analogue outputs and twenty four digital input/output channels. However the ADC developed a non linearity which ultimately led to the device being withdrawn from the market, and had to be replaced before the experimental work commenced. The replacement card was the ML-16 Multi-Lab Board from Industrial Computer Source which had very similar features and a specified conversion time of ten microseconds. The main difference as far as the software was concerned was a slight rearrangement of the input/output address map, shown in fig 3.3.

3.3 DATA ACQUISITION SOFTWARE

The AMSTRAD PC1640 uses the MS-DOS version 3.2 operating

system and as a result has a wide range of software available to it, including a variety of programming languages. BASIC has been popular with engineers for many years because it is easy to use and was the standard language on many microcomputers. It has retained its popularity as newer, more powerful, versions of the language have been developed. The most recent development is the introduction of BASIC compilers which allow programs written in BASIC to be compiled to machine code. These programs can run significantly faster than those executed by the more common BASIC interpreters. Despite this increase in speed programs written in compiled BASIC can still only achieve data sampling rates which are a fraction of that required in the present application.

Programs written in assembly language can execute many times faster than corresponding programs written in a high level language, however it is extremely impractical to write lengthy programs entirely in assembly language. Fortunately it is possible to incorporate assembly language subroutines in a program written in a high level language. Thus assembly language can be used only when speed of execution is critical and a more convenient high level language used elsewhere. A typical assembler can produce ".COM" files which can be run immediately as stand alone programs, or ".OBJ" files (object modules) which can be joined to other object modules by the MS-DOS linker. High level language compilers also produce object modules and the MS-DOS linker can be used to join a number of object modules, whether produced by an assembler or a compiler, to produce a single executable program. Recently Borland have introduced Turbo Basic which is a combined editor, compiler and linker. It is entirely menu driven and to include

assembly routines it requires only ".COM" files from an assembler. In practice an assembly language routine is given a label and the high level command "CALL label" is used when the subroutine is required. For the present application a subroutine was written in assembly language to sample the signal at about 10kHz and to store the numerical data at an appropriate location in the computer memory. Control of the hot wire probe position and transfer of the data from memory to the hard disc was programmed in BASIC.

3.3.1 Programming the I8086

The 8086 Central Processing Unit logic is divided into two separate units, the execution unit (EU) and the bus interface unit (BIU), which operate asynchronously. A significant speed improvement is achieved in the 8086 as a result of the overlapping functions of the EU and the BIU. While the EU is executing instructions the BIU looks ahead to fetch successive instructions from memory. These instructions are stored in the instruction queue, a 6-byte FIFO, for use by the EU. While the program calls for sequential execution of instructions the EU has almost immediate access to the next instruction to be executed. When a branch to a non-sequential instruction is encountered the instructions in the queue become invalid and are overwritten.

The 8086 has fourteen 16-bit registers which are grouped as shown in fig 3.4. There are four 16-bit general purpose registers AX, BX, CX and DX, each of which can be referenced as two 8-bit registers AL, AH, BL, BH etc. This is an advantage in that 16-bit operations need not necessarily be performed on 8-bit quantities.

The AX register serves as the primary accumulator. All

Input/Output operations are performed through this register and operations utilising immediate data typically require less memory space when performed on this register. Also some string operations and arithmetic instructions require the use of this register. The BX register is referred to as the base register. This is the only general purpose register which is used in the calculation of 8086 memory addresses. All memory references which use this register in the calculation of memory addresses use the DS register as the default segment register (see next paragraph). The CX register is referred to as the count register. This register is decremented by string and loop operations. CX is typically used to control the number of iterations a loop will perform. The DX register is referred to as the data register, mainly for mnemonic reasons. This register provides the I/O address for some I/O instructions.

There are four 16-bit segment registers CS, DS, SS and ES. The segment registers are used in the calculation of all memory addresses. Each segment register defines a 64k block of memory in the 8086 memory addressing space, which is referred to as the segment registers current segment eg. the DS register defines a 64k segment referred to as the current data segment. CS is the code segment register and the memory address of each instruction to be fetched is calculated by adding the contents of the program counter to the CS register contents. DS is known as the data segment register and most data memory references are taken relative to the DS register. SS is the stack segment register and all stack oriented instructions (eg. PUSH, POP etc.) use the SS register. The ES register is referred to as the extra segment register which is normally used for certain string operations. The use of segment

registers is usually implied by the instruction however it is possible to override the implied register in most circumstances.

The 8086 is a 16-bit device, however the address bus consists of twenty lines allowing direct access to one megabyte of external memory. Each 20-bit memory address is formed by combining the contents of a segment register with an effective memory address or offset as shown in fig 3.5. The contents of the selected, or implied, segment register are shifted four bits to the left and then the effective address is added to generate the actual address. Thus each segment register identifies the beginning of a 64k memory segment which must lie at an address which is an even multiple of 16. At any instant there will be four selected 64k segments which may or may not overlap each other.

The instruction set of the 8086 is fairly complex, consisting of approximately 70 basic instruction with up to 30 addressing modes available for memory reference instructions. The 8086 instructions can be grouped according to function, the groups being

1. Data movement instructions
2. Arithmetic instructions
3. Logical instructions
4. String primitive instructions
5. Program counter control instructions
6. Input/Output instructions
7. Interupt instructions
8. Rotate and shift instructions

The MOV instruction is used to transfer data from a source to a destination. Data transfers possible are register to register, memory to register, register to memory and immediate data to

register or memory. Note, it is not possible to load the segment registers directly with immediate data. PUSH and POP instructions allow registers or memory to exchange data with the stack. There are five types of 8086 arithmetic instructions; addition, subtraction, multiplication, division and compare instructions. Both 8-bit and 16-bit arithmetic can be performed. The program counter and control instructions include CALL, LOOP and a number of conditional jump instructions. The LOOP instruction has the same effect as the combination

```
DEC CX
JNZ          ; Jump if Not Zero
```

Some of the conditional jumps available are JA (Jump if Above), JB (Jump if Below), JCXZ (Jump if CX is Zero) etc. The instructions IN and OUT are used to access input/output space eg.

```
IN  AL,DX    ; Inputs an 8-bit number into the AL register
               from the I/O port specified by the DX
               register
OUT DX,AX    ; Outputs the 16-bit contents of AX to the I/O
               port specified by the DX register
```

Reference has been made to the texts by Rector and Alexy (1980) and Liu and Gibson (1984) for the above information.

3.3.2 Data Acquisition Subroutine

The extra segment register was used to address the data read from the ADC, thus allowing it to be stored separately from other program data and at a location determined by the user. Sampling at approximately 10kHz meant that a 64k segment was filled in about 6.5 seconds. This was observed to be close to the absolute minimum

sample time which could be relied on to give reasonable repeatability of intermittency measurements in a typical transitional flow. It was therefore decided to use two memory segments giving a sample time of about 13 seconds.

The operation of the BLUE CHIP TECHNOLOGY ACM-44 interface card is straightforward and a simple BASIC program to read n consecutive values might be

```
10 PORT = &H300            base address = 300 (hex)
20 OUT PORT,0              selects channel 0
30 FOR i=1 TO n
40  OUT PORT+2,0           outputing a zero starts conversion
50  A = INP(PORT+2)        reads value into A
60 NEXT i
```

The assembly language subroutine ACQ.DG reads 128k of data as 8-bit numbers at about 10kHz to provide a sample of about 13 seconds duration. This data is stored in two memory segments at physical addresses &30000 to &4FFFF and is addressed using the ES register which is set to &3000 and &4000 respectively and the offset (0 - &FFFF) is provided by the BX register. The subroutine ACQ.DG is now described in detail. Note, the channel number is selected previously by the main program.

```
ACQ:
 MOV CX,02H
 MOV DX,302H
 MOV AX,3000H
START:
```

ACQ: is the label for the subroutine. CX is loaded with the number 2 since the main loop must be executed twice to read 128k of

data into two 64k memory segments. The value &302 stored in DX is simply the value PORT+2 used to start the conversion and to read the input value. &3000 is the value to be loaded into ES to provide the starting address for data storage and is loaded via AX since ES cannot be loaded directly with immediate data. START: is the label marking the start of the outer loop which is repeated twice.

```
PUSH CX
MOV ES,AX
MOV BX,00H
MOV CX,0FFFFH
CONV_1:
```

The current value of CX is stored on the stack and the value &3000 is stored in ES. The BX register is set to zero and CX is loaded with &FFFF to control the loop which reads in and stores one complete segment of data. CONV_1: is the label marking the start of this loop.

```
MOV AL,00H
OUT DX,AL
```

AL is loaded with zero and the zero is output to the address specified by DX (ie. &302) to start the analogue to digital conversion.

```
PUSH CX
MOV CX,24H
DELAY:
NOP
LOOP DELAY
POP CX
```

The current value of CX is stored on the stack and a new value of &24 is loaded to control a delay loop. This loop is necessary to ensure conversion is complete before the value is read in and also to control the sampling frequency. Finally, the previous value of CX is restored from the stack.

```
IN AL,DX
MOV ES:[BX],AL
INC BX
LOOP CONV_1
```

The 8-bit digital value is read from the I/O address specified in DX (again &302) and stored in the 8-bit AL register. This value is then stored in the "extra segment" which starts at &30000, offset by the number contained in BX. A segment override is used since data is normally stored relative to DS. The contents of BX are incremented by one to allow the next datum to be stored at the next consecutive address.

```
POP CX
MOV AX,04000H
LOOP START
RETF
```

The original value of CX is restored from the stack and AX is loaded with &4000. Looping back to START: allows the second 64k segment of memory, starting at &40000, to be filled with data. The RETF instruction returns control to the main program.

The full listing of ACQ.DG in appendix 1 shows the clock cycles required for each instruction. The data acquisition loop is contained between the CONV_1: label and the LOOP CONV_1 instruction and contains a delay loop. The LOOP instruction requires 17 clock

cycles when the loop is repeated and only 5 when it is exited, thus the total number of clock cycles taken by the delay loop is

&23*(3 + 17) + 3 + 5 = 708

The number of clock cycles taken by the remaining instructions in the data acquisition loop is

4 + 8 + 10 + 4 + 8 + 8 + 16 + 2 + 17 = 77

Thus the total number of clock cycles for one execution of the data acquisition loop is 785. The clock frequency is 8 MHz, ie. the time for one cycle is 0.125μs. Thus the time per loop is 98.125μs giving a sampling rate of 10.19kHz.

3.3.3 Main Data Acquisition Program

The assembly language routine described in the previous section is responsible for reading a succession of data from an ADC, at high speed, and storing the data in the computers RAM. To obtain a boundary layer profile, measurements must be made from as close to the plate as possible out to the freestream. The probe datum was set manually using a scaled block placed behind the probe and viewed through a cathetometer and was normally set at 0.5mm above the plate. The main program, which is written in BASIC, controls the movement of the probe, from the datum to the freestream, and records its position at each step. It also calls the data acquisition subroutine, transfers the data from RAM to the hard disc and stops the traverse after the probe is outside the boundary layer.

The signal from the hot wire anemometer was connected to channel zero on the card and the signal from the sweep drive unit was input to channel two. The digital output channel zero is

connected to the switch which controls the sweep drive unit. Outputing a "1" closes the switch and stops the SDU while outputing a "0" opens the switch causing the stepper motor to move the probe. The stepper motor on/off interface is shown in fig 3.6.

The data acquisition program DGDATA5.BAS is listed in appendix 1 and the main features are described here.

```
PORT = &H300
OUT PORT+2,&H12
OUT PORT+3,1
```

The base address is set to &h300 and the "command byte" is set at &h12. The command byte controls the various A/D functions and in the case of the ML-16 card also selects the channel number for analogue input. Fig 3.7 shows the functions of the command byte. Setting it to &H12 selects channel 2, analogue input is unipolar in the range 0-10v and conversion is started by writing to PORT+0. The third command outputs a digital "1" to ensure that the probe does not move before the first reading is taken.

After inputing initial data such as atmospheric temperature and pressure and the initial location of the probe the data acquisition loop is entered (at line 5). A loop reads 500 values from channel two and takes the average to obtain the probe position.

```
OUT PORT+2,&H10
CALL ACQ
SUB ACQ INLINE
 $INLINE
END SUB
```

The first two commands select channel two and transfer

control to the assembly language routine. The $INLINE is a so called metastatement which controls the compiler during compilation of the program.

```
CALL TOTAL
C1 = PEEK(&HA000)
C2 = PEEK(&HA001)
C3 = PEEK(&HA002)
C4 = PEEK(&HA003)
TOTAL = C4*(2^24) + C3*(2^16) + C3*256 + C1
MEAN = TOTAL/(65535*?)
```

Another assembly language subroutine called TOTAL, which is described in the next section, is called. This subroutine sums all the values which have been read in and stores the result as a 32-bit number in locations &HA000 - &HA003 in the current data segment. This total is retrieved using PEEK commands, converted to a decimal number and divided by the number of points to obtain the mean value.

```
DEF SEG=&H3000
BSAVE FILE$+STR$(2*N-1),0,&HFFFF
DEF SEG=&H4000
BSAVE FILE$+STR$(2*N),0,&HFFFF
DEF SEG
```

The DEF SEG command defines the data segment to be used by various commands such as BLOAD and BSAVE. The BSAVE command saves a memory range of up to 64k to disc. For example if N=1 the data contained in memory locations &H30000 to &H3FFFF would be saved in the file FILE$ 1 and the data contained in locations &H40000 to &H4FFFF would be saved in the file FILE$ 2. Thus each 128k sample

is stored in two disc files. The BSAVE command is very quick, transferring 128k of data from memory to disc in about 2 seconds.

The section of code headed "test for profile complete" causes the loop to be exited if three consecutive values of mean velocity are within ±0.5% of each other. If the loop is not exited the probe is raised in the boundary layer and the loop repeated. The probe is moved by outputing a digital "0" and pausing using the DELAY command, before sending out a digital "1" to stop the probe. Since the velocity varies most rapidly close to the plate smaller steps were taken for the first six points. To avoid excessive numbers of points in a traverse the step length was increased after six points and again after twelve points. Finally initial data and the probe position data are written to a separate file.

3.4 SIGNAL CONDITIONING

Two signals are required to be recorded by the computer ie. the linearised hot wire signal and the output voltage from the sweep drive unit. To ensure that the ADC is used to its full capability the maximum reading expected from each instrument must be conditioned to approximately 10v. Both signals were passed through a FYLDE modular instrumentation rack which contained ×0.1 and ×1 switched gains with a ×10 variable control and a digital display.

The hot wire signal was linearised such that the voltage output was equivalent to 1/10th of the fluid velocity eg. 2v = 20m/s. The maximum velocity expected in the planned experiments was about 15m/s. It was decided to allow a maximum of 20m/s to be equivalent to 250 bits giving a calibration constant of 0.08. This

was particularly convenient when using the ACM-44 card where 250 bits corresponded to exactly 10v requiring an amplification of exactly 5. The amplification was adjusted when the ACM-44 card was replaced to retain the calibration constant.

The position of the probe above the plate is determined from the output voltage of the DISA 55D35 sweep drive unit. The output is made proportional to the linear displacement of the hot wire probe via a stepper motor and a traverse mechanism. Calibration of the sweep drive unit, fig 3.8, gives a linear relationship between the voltage and the displacement. The calibration constant was found to be 0.2022 mm/bit.

PC/XT/AT Port Map
I/O Address Map

Address	
000-01F	DMA Controller 1, 8237A-5
020-03F	Interrupt Controller 1, 8259A
040-05F	Timer, 8254
060-06F	Keyboard Controller, 8742; Control Port B
070-07F	RTC and CMOS RAM, NMI Mask (Write)
080-09F	DMA Page Register (Memory Mapper)
0A0-0BF	Interrupt Controller, 8259
0F0	Clear NPX (80287) Busy
0F1	Reset NPX, 80287
0F8-0FF	Numeric Processor Extension, 80287
1F0-1F8	Hard Disk Drive Controller
200-207	Reserved
278-27F	Reserved for Parallel Printer Port 2
2F8-2FF	Reserved for Serial Port 2
300-31F	Reserved
360-36F	Reserved
378-37F	Parallel printer Port 1
380-38F	Reserved for SDLC Communucations, Bisynchronous 2
3A0-3AF	Reserved for Bisynchronous 1
3B0-3BF	Reserved
3C0-3CF	Reserved
3D0-3DF	Display Controller
3F0-3F7	Diskette Drive Controller
3F8-3FF	Serial Port 1

figure 3.1

Port Map (Bluechip Technology ACM-44 card)

```
BASE     = Analogue Input Channel Select
BASE+2   = Analogue Input Value (READ)
         = Start Conversion (WRITE)
BASE+3   = Timer control
BASE+4   = Analogue Output Channel 0
BASE+5   = Analogue Output Channel 1
BASE+6   = Analogue Output Channel 2
BASE+7   = Analogue Output Channel 3
BASE+8   = Digital I/O Port A
BASE+9   = Digital I/O Port B
BASE+10  = Digital I/O Port C
BASE+11  = Digital Port control
```

figure 3.2

I/O Address Map (ML-16 card)

BASE+0	Start A/D Conversion (write)
	A/D Data (read)
BASE+1	Reset Interrupt
BASE+2	Command Byte
BASE+3	Digital Output (write)
	Digital Output (read)
BASE+4	D/A 1
BASE+5	D/A 0
BASE+6	D/A 1
BASE+7	D/A 0
BASE+8	CTR0 Load (write)
	CTR0 Data (read)
BASE+9	CTR1 Load (write)
	CTR1 Data (read)
BASE+A	CTR2 Load (write)
	CTR2 Data (read)
BASE+B	Counter/Timer Mode Byte

figure 3.3

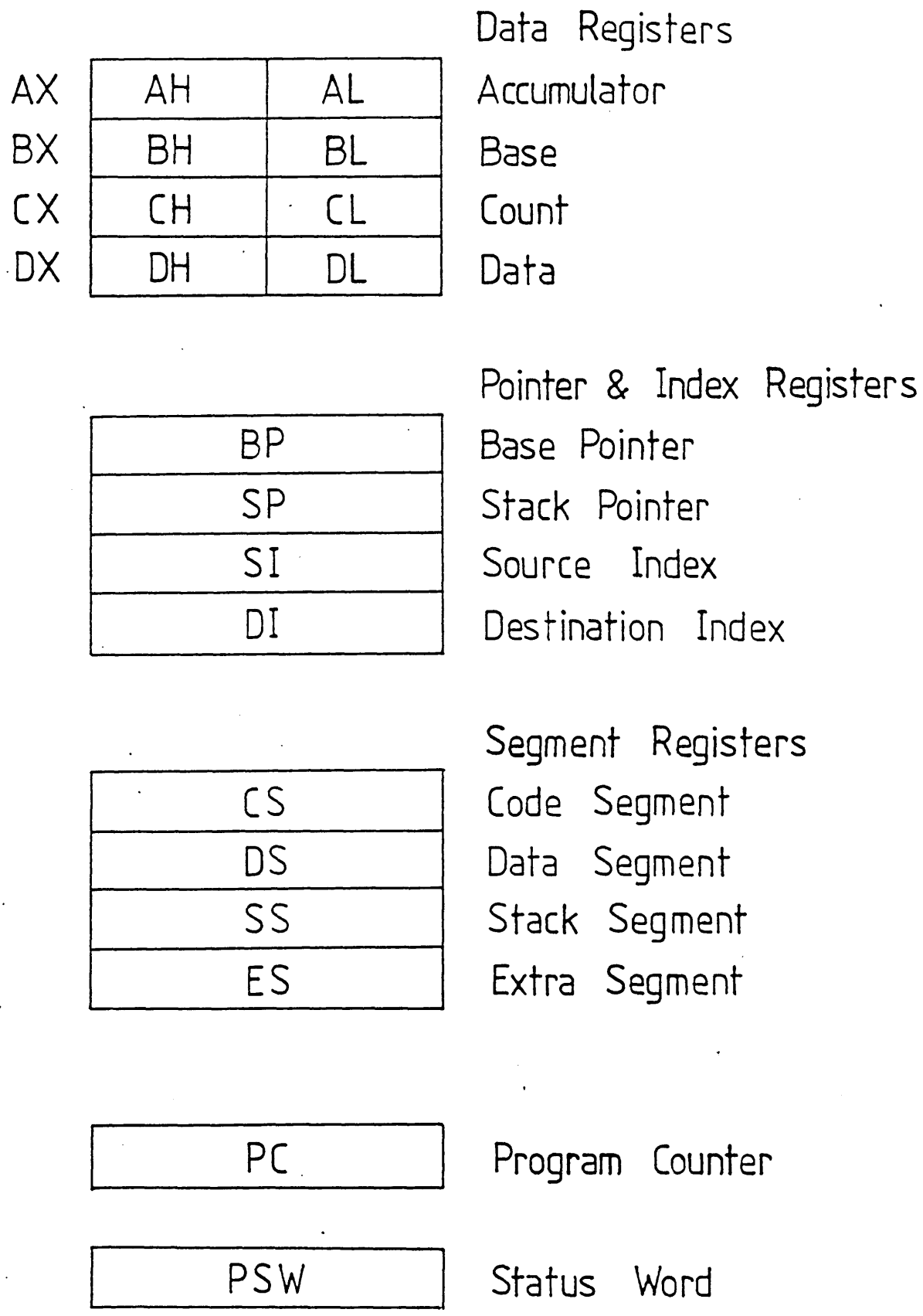

figure 3.4 8086 registers

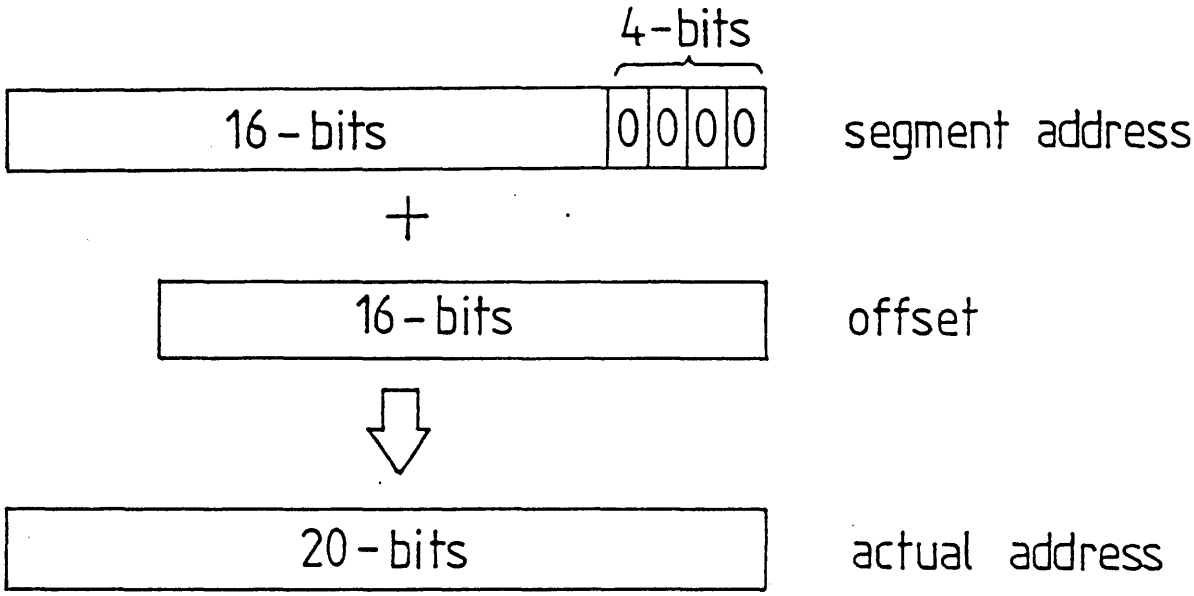

figure 3.5 memory addressing

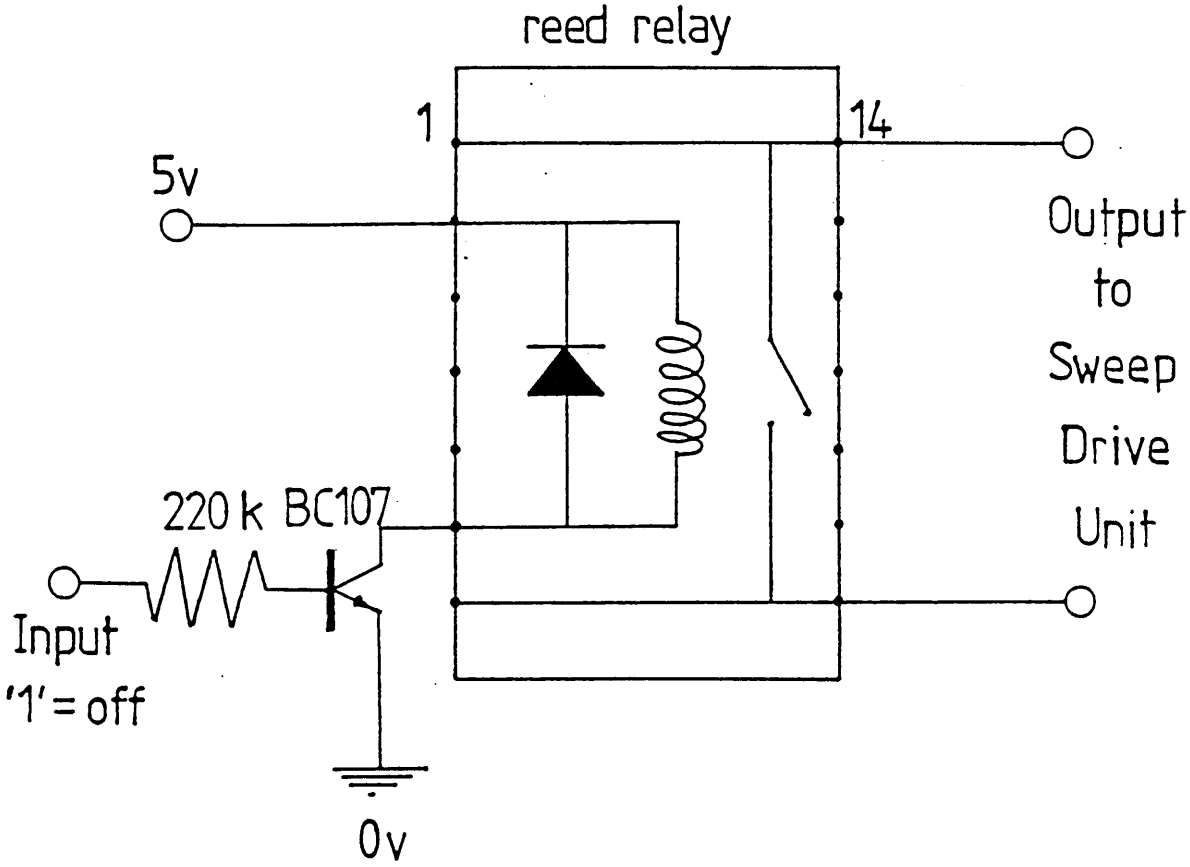

figure 3.6 stepper motor on/off interface

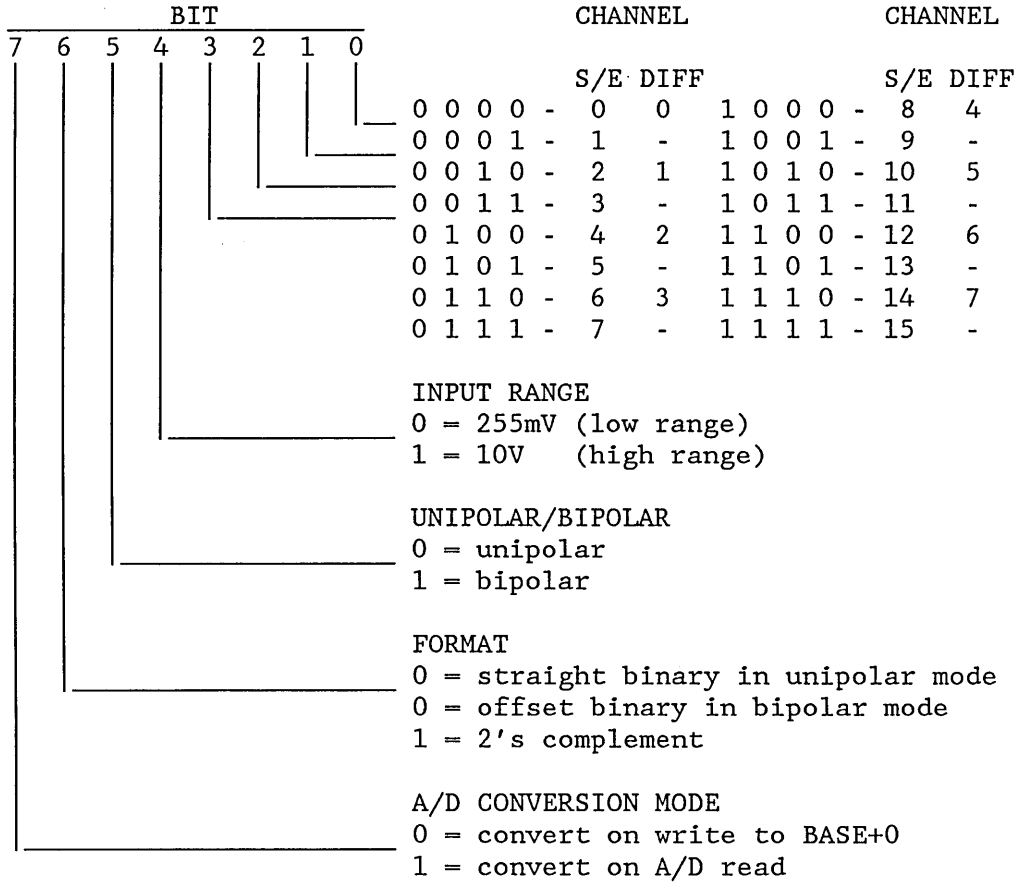

figure 3.7 command register bit assignments for the ML-16 multi-lab board

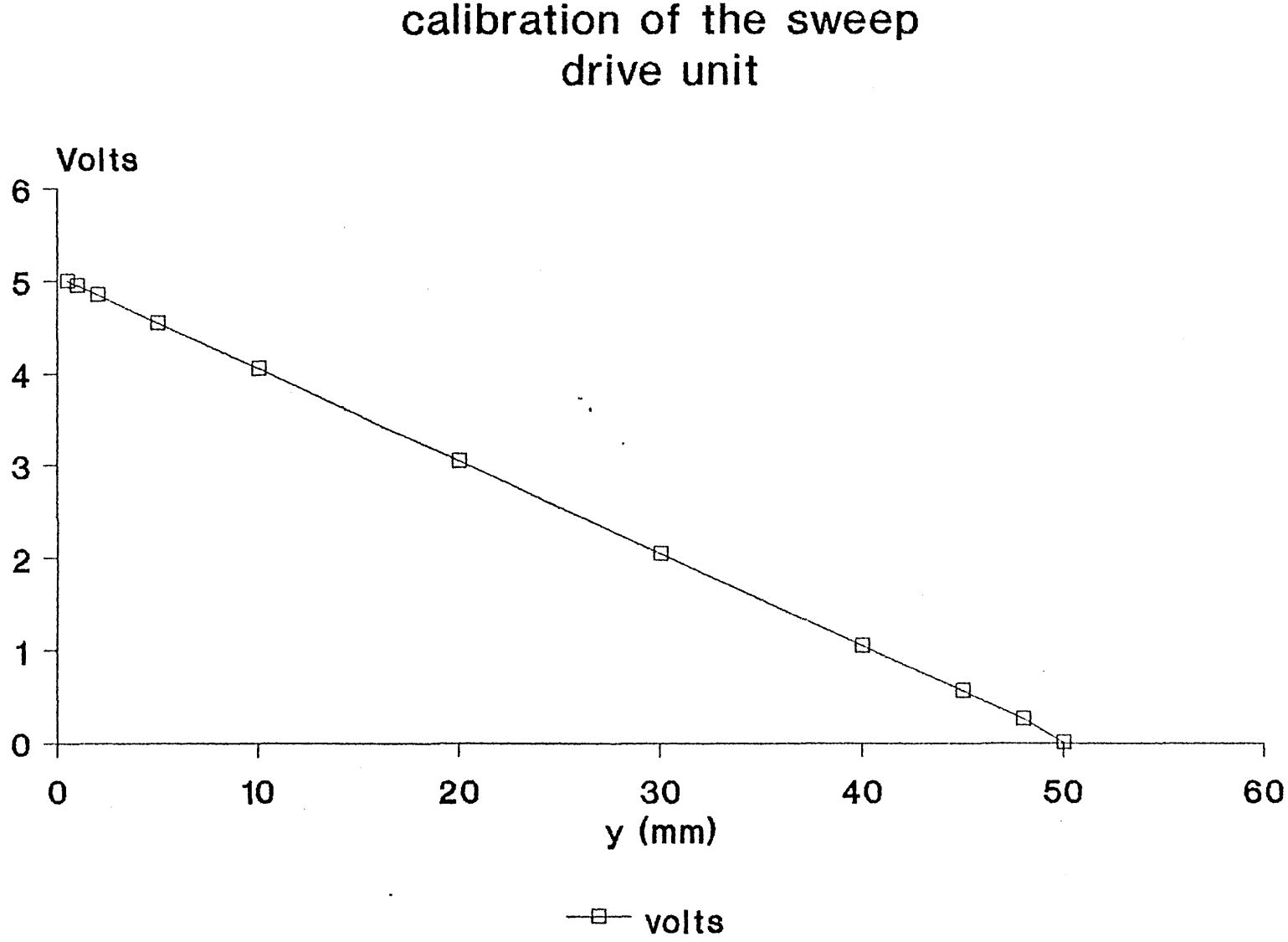
calibration of the sweep drive unit
Volts
6
5
4
3
2
1
0
0
10
20
30
40
50
60
y (mm)
volts

figure 3.8

CHAPTER 4

DATA REDUCTION

It has already been noted that high frequency digital sampling of an analogue signal can quickly generate large quantities of numerical data. In the present case a 13 second sample of the velocity signal requires 128k of memory and a profile consisting of up to about 28 such samples can require as much as 3.5 Megabytes of space on the hard disc. Depending on the number of points per profile there is enough room to store only five or six complete profiles on the computers hard disc at any one time. To keep a complete digital record of all the flows measured would require a vast amount of storage so it was necessary to process the raw signal to reduce the data to a more manageable format. As well as the mean velocity and RMS of each sample the intermittency was calculated and, in transitional flows, the mean laminar and turbulent velocities were also determined. All processing was to be carried out digitally, however it soon became apparent that processing time could become a significant issue. For example, summing the 131,072 individual values, which make up a sample, took over two minutes using compiled BASIC ie. it could take almost an hour just to determine the mean velocity profile of one traverse. However, judicious use of an assembly language subroutine to execute the summation reduced the time from two minutes to less than two seconds thus giving more acceptable processing times. All summation procedures were programmed in assembly language with final divisions, square root operations etc, which need to be performed only once for each sample, being programmed in BASIC for simplicity.

4.1 REDUCTION OF THE RAW DATA

The data reduction program DGDATA6.BAS reloads the raw data into the computers memory and calculates the mean velocity, RMS, intermittency and the mean laminar and turbulent components of velocity. Finally, the mean data for a complete profile is saved in a new file. This data can be further processed to provide the usual integral parameters, both for the mean velocity profile and for the laminar and turbulent component profiles.

4.1.1 Mean Velocity

The first value required from the data reduction is the mean velocity which is given by

$$\bar{u} = \frac{\Sigma u}{n}$$

The calculation of the mean velocity is greatly accelerated by the use of an assembly language routine to calculate Σu. The division occurs only once and can be easily performed in BASIC with no loss of speed. The data is accessed in much the same way as it was stored by ACQ.DG in that the main loop must be executed twice to access the two segments of data. A complete listing of TOTAL.DG is contained in appendix 1 and the main aspects of the routine are detailed below.

```
MOV AX,00H
MOV [0A000H],AX
MOV [0A002H],AX
```

The total, Σu, is to be stored as a 32-bit number at memory locations &A000, &A001, &A002 and &A003, relative to DS. MOV [ ],AX moves the low byte of AX to the address in the square

brackets and the high byte to address+1. These memory addresses are cleared to zero initially.

```
MOV DL,ES:[BX]
MOV DH,00H
MOV AX,[0A000H]
```

The 8-bit value held in ES:[BX] is stored in the DX register. The quantity currently held in addresses &A000 and &A001 is moved to AX.

```
ADD AX,DX
MOV [0A000H],AX
MOV AX,[0A002H]
ADC AX,00H
MOV [0A002H],AX
```

Standard 32-bit addition is used to add the value in DX to the running total held at addresses &A000 to &A003 and the new total is returned to the same addresses.

The main program obtains the value Σu by peeking the memory locations thus

```
U1 = PEEK(&HA000)
U2 = PEEK(&HA001)
U3 = PEEK(&HA002)
U4 = PEEK(&HA003)
```

and

$$\Sigma u = U4*2^{24} + U3*2^{16} + U2*2^{8} + U1$$

4.1.2 RMS Subroutine

The RMS of the velocity fluctuations is given by

$$RMS = \sqrt{\frac{\Sigma\ (u - \bar{u})^2}{n}}$$

The mean velocity, $\bar{u}$, will involve decimal fractions thus the evaluation of the above expression will involve floating point arithmetic. This can be handled by the I8087 numeric coprocessor but the need for this was eliminated by rewriting the expression for RMS.

$$RMS = \frac{1}{n} \sqrt{\Sigma\ \frac{(un - \bar{un})^2}{n}}$$

Note that the value $\bar{un}$ is the same as Σu calculated by the previous routine. A relatively straight forward assembly language routine can now be used to evaluate $\Sigma\ (un - \bar{un})^2$.

The division and square root operations need only be performed once and can again be implemented in BASIC.

The construction of this loop is again similar to the data acquisition loop since the same data is being accessed in the same manner. The main features of the loop are now described.

RMS: Start of subroutine

Various data locations are cleared initially to zero and the numbers 2 and &FFFF are stored at locations &A01C and &A01E for future use.

RMS1: Start of calculation loop

The instruction MUL W[n] causes the contents of AX to be multiplied by the WORD contained in n and n+1. The result is stored in AX (low order 16-bits) and DX (high order 16-bits).

```
MUL W[0A01CH]
MUL W[0A01EH]
MOV [0A004H],AX
MOV [0A006H],DX
```

The first instruction gives u*2, which has a maximum value of 2*255 = 510, which is stored in AX. The second MUL instruction gives u*2*&FFFF ie. the quantity un which is stored as a 32-bit number.

Before calculating $(un - \overline{un})^2$ the two quantities, un and $\overline{un}$, are compared, high bytes first, to determine which is the larger. To avoid confusion with two's complement negative numbers, the smaller of the two values is subtracted from the larger to give the absolute value of $(un - \overline{un})$. This has no effect on the final result since squaring results in a positive number anyway. 32-bit subtraction is employed and the result is stored in locations &A008 - &A00B.

The squaring routine is modified from a 32-bit multiplication routine given by Rector and Alexy (1980) which gives a 64-bit answer. The quantity $\Sigma (un - \overline{un})^2$ is obtained by 64-bit addition which is a simple extension to the procedure used in TOTAL.

The LOOP command failed in this program because the jump was greater than 128 hence CX was decremented explicitly and an unconditional jump was used when CX > 0.

Mean velocity and RMS values obtained digitally were compared with measurements made by analogue instrumentation over a range of flow conditions. Errors were within about one percent and were probably due to the fact that the analogue instrumentation was read manually.

4.1.3 Intermittency Measurement

To discriminate between laminar and turbulent flow some characteristic of the flow must be found which is significantly different in each type of flow. In the literature various criteria have been used as "detector functions". Corrsin and Kistler (1955) used the streamwise component of vorticity, ω_x, to identify turbulent and non-turbulent regions in the intermittent interface of the turbulent boundary layer. This technique however, required the use of an array of four hot wire anemometers. Kovasznay et al (1970) used $\partial u/\partial y$, which is effectively a measure of the spanwise vorticity, ω_z, as the basis of detection. The flow was considered to be turbulent if either $\partial^2 u/\partial y \partial t$ or $\partial^3 u/\partial y \partial t^2$ exceeded set threshold values. These quantities are not necessarily zero in non-turbulent flow and can cross zero in turbulent flow therefore some smoothing was applied to average out these errors. Here two hot wires, separated by 5mm in the y direction, were required to measure $\partial u/\partial y$. Kaplan and Laufer (1969) used a digital computer to process their data and based their detector function on the short time variance of $\partial u/\partial t$. Murlis et al (1982) used the product uv as the detector function. In a similar procedure to Kovasznay et al (1970) turbulence was registered if either the first or second time derivatives of uv exceeded separate thresholds. Measurement of uv however, necessitates the use of a cross wire probe which is impractical in thin boundary layers.

Using a single wire probe, it is only possible to consider the level of the signal or its variation with respect to time as a potential detector function. A turbulent signal consists of higher frequency, higher amplitude fluctuations than a laminar signal and

it would be expected therefore that the rate of change of the signal, with respect to time ($\partial u/\partial t$), would be greater, on average, in a turbulent region. It was decided to investigate both $\partial u/\partial t$ and $\partial^2 u/\partial t^2$ as possible means of discriminating between laminar and turbulent flow. As with other criteria however, both $\partial u/\partial t$ and $\partial^2 u/\partial t^2$ can be non zero in non-turbulent flow while momentary zero values can occur in turbulent flow. To reduce these discrepancies the signal was digitally rectified and smoothed.

The rate of change of u with respect to time at a point i, can be represented by the forward difference approximation

$$\frac{\partial u}{\partial t} = \frac{u_{i+1} - u_i}{\Delta t} \tag{4.1}$$

where u_i and u_{i+1} are two consecutive data points and Δt is the sampling period. The signal is rectified by taking the absolute value of expression (4.1) and smoothing is achieved by summing over a number of points, n. The smoothing period, $n\Delta t$, should remain small relative to the average time duration of a turbulent spot or laminar region. Thus

$$F(t) = \frac{1}{n\Delta t} \sum_{i=1}^{n} |u_{i+1} - u_i| \tag{4.2}$$

Since Δt is constant a function S1(t), which is proportional to a smoothed and rectified $\partial u/\partial t$ signal can be given as

$$S1(t) = \sum_{i=1}^{n} |u_{i+1} - u_i| \tag{4.3}$$

Similarly a function S2(t), which is proportional to a

smoothed and rectified $\partial^2 u/\partial t^2$ signal is given by

$$S2(t) = \sum_{i=2}^{n} |u_{i+1} - 2u_i + u_{i-1}| \qquad (4.4)$$

Sufficient smoothing must be applied to the detector functions to allow a threshold to be fixed which will allow an intermittency of 1 to be recorded in a fully turbulent boundary layer and zero to be recorded in laminar flow or the freestream. Figure 4.1 shows intermittencies obtained using S1(t) in a fully turbulent boundary layer and the freestream. Smoothing over 10 points and 20 points has been used and the graph has been normalised by plotting on a base of threshold value divided by the number of smoothing points. Increased smoothing appears to have little effect on intermittency measurement in the freastream with both 10 and 20 point smoothing behaving almost identically as the threshold value is decreased. In the fully turbulent boundary layer, increasing the smoothing period slightly reduces the effects of momentary zero values of S1(t). Smoothing of 15 points, ie. n = 14, was found to be about the minimum reliable value for both S1(t) and S2(t) and increasing this had little effect on the results other than to increase computing time. It is clear from figure 4.1 that there is a range of possible threshold values which will satisfy the above criterion. The optimum threshold was found to be about S1(t) = S2(t) = 26.

The most accurate identification of the interface between a turbulent spot and the surrounding laminar flow was obtained if the smoothing was centered about the point under consideration eg. if the function S1(t), defined in equation 4.2, exceeded the threshold

value then the point at at the centre of the smoothing sample, ie. at i+7, was considered to be turbulent. Figures 4.2, 4.3 and 4.4 show sections ,of about 0.06 second duration, from three velocity traces obtained at different points in a transitional boundary layer. Also shown are the behaviours of S1(t) and S2(t), the shaded regions below each trace indicating the flow identified as turbulent by each function.

The trace in fig 4.2 was obtained fairly close to the plate and shows a fairly definite turbulent burst, on the left hand side of the trace, followed by a region of fairly disturbed laminar flow and a sharp spike close to the right hand end which may well be considered to be a short region of turbulent flow. It can be seen from fig 4.2(a) that S1(t) frequently registers turbulence in the disturbed laminar flow because of the rapid accelerations which are present. S2(t), fig 4.2(b), is slightly less clear at the trailing edge of the spot, but performs better overall. In practice S1(t) predicts a considerably higher intermittency factor than S2(t) for this region of the flow field, $\gamma = 0.55$ against $\gamma = 0.38$ over the full 13 second sample. The trace shown in fig 4.3 was obtained towards the outer edge of the boundary layer. Both S1(t) and S2(t) appear to cope well but S2(t) registers a brief burst of turbulence in a region which is clearly non-turbulent. This is not an isolated occurrence and leads to S2(t) predicting a higher intermittency factor than S1(t), $\gamma = 0.08$ from S2(t) and $\gamma = 0.06$ from S1(t). Fig 4.4 illustrates the complex nature of the flow involved. Here again S1(t) appears to overestimate γ by including regions of flow which, although highly disturbed, are not strictly turbulent. The overall values of γ obtained in this case from

S1(t) and S2(t) were 0.46 and 0.36 respectively.

Figures 4.2 to 4.4 show only a small sample of the variety of flow conditions which occur in the present set up but the features observed appear to apply generally in that neither S1(t) nor S2(t) is entirely satisfactory as a turbulence detector function throughout the complete transition region. Both S1(t) and S2(t) rise rapidly immediately turbulence is encountered but, because of the smoothing, the functions have a finite slope. This means that the intermittency recorded will depend, to some extent, on the level of the threshold. It is desirable to set the threshold as low as possible to register turbulence as soon as it occurs but lowering the threshold leads to an increase of false readings in the non turbulent flow, as previously described. This was overcome by registering turbulence only when S1(t) and S2(t) exceeded their threshold values. This ensures that turbulence is registered as soon as both S1 and S2 begin to rise rapidly but eliminates errors due to minor excursions, above the threshold, of S1(t) or S2(t) individually. Figures 4.5 to 4.7 repeat the previously described signals and show the turbulence registered using an S1(t) AND S2(t) criterion.

The use of an arbitrary fixed threshold is satisfactory in the present application where the transition region is fairly short and external conditions do not vary excessively over the transition region. It is clear however, that the optimum threshold may vary from flow to flow and possibly from location to location in a particular flow. Boundary layer transition under an imposed adverse pressure gradient is particularly complex and the measurement of intermittency in such a flow is subjective. While

turbulent regions and obviously non-turbulent regions can be defined there is a proportion of the flow which cannot be unambiguously assigned to either category. The non-turbulent flow is in a disturbed state and exhibits high amplitude, low frequency fluctuations and occasional bursts of relatively high frequency sinusoid like fluctuations. Using a single wire signal, ie. direct measurement of u, and its time derivatives is the simplest approach to conditional sampling. The evidence presented in figures 4.5 to 4.7 suggests that the technique developed is no less reliable than any of the more complex methods which have been used.

The program DATA9.BAS, see appendix 1, allows a 13 second sample to be taken and examined visually, on the computer screen, in sections of 640 points, ie. about 64mseconds, at a time. Since only 640 points are considered at any one time all calculations are executed in BASIC. The variables VLAM and VTURB, which will hold the sum of the laminar and turbulent velocities respectively, and CLAM and CTURB, which will hold the number of laminar and turbulent points, are initially set to zero. Fifteen consecutive points are loaded into the array VEL( ) using the PEEK command and the variables SUM1 and SUM2, ie. S1(t) and S2(t), are set to zero. The values of SUM1 and SUM2 are calculated and if both exceed 26 the appropriate point is added to VTURB and CTURB is incremented by one. Otherwise the point is added to VLAM and CLAM is incremented by one. Finally the mean laminar and turbulent velocities are calculated and the intermittency is given by the number of turbulent points divided by the total number of points.

Again it is necessary to use an assembly language routine in the calculation of the intermittency and mean laminar and turbulent

components of velocity for a complete sample. This assembly language subroutine determines the intermittency and the values equivalent to VLAM, VTURB, CLAM and CTURB. The divisions required to obtain the mean laminar and turbulent velocities are again performed once each in BASIC. The subroutine follows exactly the same logic as the previously described BASIC program.

4.2 REDUCTION OF MEAN VELOCITY PROFILES

The program ANLYS4.BAS reduces the mean velocity data from laminar, turbulent and transitional boundary layers to give the usual integral parameters. In the case of transitional boundary layers the mean laminar and turbulent component profiles are also reduced separately. The boundary layer thickness, δ, is estimated from the mean profile by linear interpolation and is taken to be the point where $\overline{u} = 0.995U$. The program also calculates the "near wall" intermittency which is the most commonly used factor in describing transitional boundary layers. The intermittency remains more or less constant up to about $y/\delta = 0.4$ and the near wall intermittency was taken to be the average for all points below this value. Following the approach of Gardiner (1987) the laminar analysis, described in section 4.2.1, was used to reduce mean transitional profiles when $\gamma < 0.5$ and the turbulent analysis, described in section 4.2.2, when $\gamma > 0.5$. A typical printout from the analysis program is shown in fig 4.8.

4.2.1 Reduction of Laminar Mean Velocity Profiles

Both Gardiner (1987) and Fraser (1979) obtained the integral parameters for laminar velocity profiles by direct integration of a

polynomial which was fitted through data points of u/U against y/δ using a least squares technique. Fraser (1979) used a fourth order polynomial while Gardiner (1987) found that a third order polynomial was sufficient. The present work involved the measurement of inflectional and separating laminar velocity profiles and it was found that fitting a polynomial to the data was unreliable in these cases. To obtain more reliable integration of the laminar profiles a technique described by Coles and Hirst (1968) and used by Fraser (1979) and Gardiner (1987) for turbulent boundary layers was adapted.

The procedure was to fit a parabola through three consecutive points and compute the integrals from the first to the second and from the second to the third using Simpson's Rule. The central point is then moved out one and the process repeated. The two values which are obtained for each interval, other than the first and last, are then averaged to provide an element of smoothing. The integrals of

$$\left(\frac{\bar{u}}{U}\right), \left(1 - \frac{\bar{u}}{U}\right), \left(\frac{\bar{u}}{U}\right)^2 \text{ and } \left(\frac{\bar{u}}{U}\right)^3$$

which are obtained are appropriately combined to give the required integral parameters.

In a laminar layer the shear stress is directly proportional to the rate of strain ie.

$$\tau = \mu\left(\frac{\partial \bar{u}}{\partial y}\right) \tag{4.5}$$

By assuming a linear profile between the wall and the first data point an estimate of the wall shear stress could be made. Since the first data point is always 0.5mm above the surface this

estimate will be unreliable in thin boundary layers and also as separation is approached.

4.2.2 Reduction of Turbulent Mean Velocity Profiles

Turbulent boundary layer velocity profiles were reduced using the analysis of Coles (1968), as applied by Coles and Hirst (1968) to the data presented at the Stanford conference. Fig 4.9 shows the structure of a typical turbulent boundary layer which consists of a thin viscous sublayer, "so-called" inner and outer layers and an irregular but sharp interface with the freestream. In the viscous sublayer, viscous forces dominate and the mean velocity profile can be approximated by

$$\frac{\bar{u}}{u_\tau} = \frac{y u_\tau}{\nu} \tag{4.6}$$

where $u_\tau = \sqrt{\frac{\tau_w}{\rho}}$

This equation is often written as $u^+ = y^+$

Coles (1956) used two similarity laws, the law of the wall and the law of the wake, to develop an empirical equation for the mean velocity profile ie.

$$u^+ = f(y^+) + \frac{\Pi}{\kappa} W\left(\frac{y}{\delta}\right) \tag{4.7}$$

The law of the wall (the function $f(y^+)$) has the form

$$f(y^+) = \frac{1}{\kappa} \ln y^+ + C \tag{4.8}$$

where κ and C are empirical constants. Equation 4.8 applies outside the viscous sublayer and the buffer layer, ie. for $y^+ > 50$ The values of κ and C are slightly controversial because of scatter in the data. Coles (1968) used the values κ=0.41 and C=5.0 but

since the present investigation was concerned with low Reynolds number turbulent boundary layers the value of C = 5.2, as suggested by Murlis (1975) and used by Fraser (1979) and Gardiner (1987) among others, was adopted.

The law of the wake describes the deviation of the velocity, above the law of the wall, in the outer layer. Coles (1968) noted that the velocity deviations were a single wakelike function when normalised by the maximum deviation at $y = \delta$. The wake function, W, is approximately antisymmetric about $y = \delta/2$, $W = 1$ therefore Coles proposed the following curve fit.

$$W\left(\frac{y}{\delta}\right) = 2\sin^2\left(\frac{\pi y}{2\delta}\right) \tag{4.9}$$

Equation 4.7 written in full is therefore

$$\frac{\bar{u}}{u_\tau} = \frac{1}{\kappa}\ln\left[\frac{yu_\tau}{\nu}\right] + C + \frac{2\Pi}{\kappa}\sin^2\left(\frac{\pi y}{2\delta}\right) \tag{4.10}$$

where Π is called the wake parameter. At the edge of the boundary layer equation 4.10 becomes

$$\frac{\bar{U}}{u_\tau} = \frac{1}{\kappa}\ln\left[\frac{\delta u_\tau}{\nu}\right] + C + \frac{2\Pi}{\kappa} \tag{4.11}$$

This equation relates the three parameters u_τ , δ and Π and can be used to determine any one if the other two are known.

The law of the wall, eqn 4.8, is assumed to be valid in the region $y^+ > 50$ and $y/\delta < 0.2$ following the suggestion of Murlis et al (1982) to allow for the low Reynolds number flows in the present work. For each point within the specified region equation 4.8 is solved iteratively for u_τ. The averaged value of u_τ from all such points is then taken to be the representative value for the velocity profile under consideration. With δ and u_τ now known the

value of Π can be obtained from equation 4.11.

For the calculation of the integral parameters Coles used the following standard integrals for the viscous sublayer.

$$\int_0^{50} \left[\frac{\bar{u}}{u}\right] d\left[\frac{yu_\tau}{\nu}\right] = 540.6$$

$$\int_0^{50} \left[\frac{\bar{u}}{u}\right]^2 d\left[\frac{yu_\tau}{\nu}\right] = 6546$$

$$\int_0^{50} \left[\frac{\bar{u}}{u}\right]^3 d\left[\frac{yu_\tau}{\nu}\right] = 82770$$

Equation 4.8 is then used to continue the integration from $y^+ = 50$ to some point in the log law region. Following Gardiner (1987) this point was taken to be the third data point in the traverse. In some cases the value of y^+ of the third point was less than 50 and in such cases the first point is automatically deleted and the data renumbered. The integration from the third data point to the freestream is carried out by the parabolic fitting method used for the laminar profiles, see section 4.2.1

When applying this analysis to the turbulent component profile and, in some cases, the mean profile in the transition region it was found that some traverses had no points in the region where the law of the wall was valid. In these cases no value of u_τ could be obtained and the parabolic fitting method was used from the wall to obtain the integral parameters.

An alternative method was used to obtain values of the skin friction coefficient, c_f. The correlation of Ludwieg and Tillman (1950) is one of a number of correlations which relate c_f to the

shape factor, H_{12}, and the momentum thickness, θ, ie.

$$c_f = 0.246R_\theta^{-0.268} \exp(-1.561H_{12}) \quad (4.12)$$

The wall shear stress, τ_w, can also be calculated from the value of u_τ obtained from the law of the wall analysis ie.

$$\tau_w = \rho u_\tau^2 \quad (4.13)$$

and the skin friction coefficient follows from

$$c_f = \frac{2\tau_w}{\rho U^2} = 2\left(\frac{u_\tau}{U}\right)^2 \quad (4.14)$$

4.2.3 Transitional Mean Velocity Profiles

Dhawan and Narasimha (1958) represented the mean velocity in a transitional boundary layer by the intermittency weighted average of the mean laminar and turbulent component velocities, ie.

$$\bar{u}_{tr} = (1-\gamma)\bar{u}_L + \gamma\bar{u}_T \quad (4.15)$$

They also stated that although γ varied across the boundary layer, the value measured close to the wall gives sufficiently accurate results for the whole profile. The effect of γ variation with y was briefly investigated during the present work. Klebanoff (1955) measured the intermittency in a boundary layer in a zero pressure gradient flow and White (1974) proposed the following curve fit.

$$\gamma = [1 + 5(y/\delta)^6]^{-1} \quad (4.16)$$

Equation 4.16 was compared with some of the data of Gardiner (1987). Fig 4.10 shows a set of intermittency profiles from a transitional boundary layer in a zero pressure gradient flow. The similarity of the curves is apparent. Each set of data was normalised by the "near wall" intermittency and replotted. The data was found to collapse on to the curve as shown in fig 4.11. This suggested that equation 4.16 could be used, along with the near wall intermittency, to describe the intermittency variation

with y in transitional boundary layers. All intermittency profiles measured during the present work were normalised and plotted against White's curve fit and good agreement was found in most cases. Two typical examples are shown in figures 4.12 and 4.13. This, along with some of the results of Gardiner (1987), indicate that equation 4.16 can also be applied, at least as a first approximation, to turbulent flows in adverse pressure gradients.

Using equation 4.15 Dhawan and Narasimha (1958) showed that the displacement thickness in the transition region was given by

$$\delta^*_{tr} = (1-\gamma)\delta^*_{L} + \gamma\delta^*_{T} \qquad (4.17)$$

They also calculated the corresponding expressions for θ and H although these turn out to be more complex. Taking intermittency to be a function of x and y, ie.

$$\gamma' = \gamma\,\gamma_y \qquad (4.18)$$

where $\gamma_y = [1 + 5(y/\delta)^6]^{-1}$

it can be shown that

$$\delta^*_{tr} = \delta^*_{L} - \gamma\,\delta\int_0^1 \frac{1 - u_L/U}{[1 + 5\beta^6]}\,d\beta + \gamma\,\delta\int_0^1 \frac{1 - u_T/U}{[1 + 5\beta^6]}\,d\beta \qquad (4.19)$$

where $\beta = y/\delta$

In the transition region equations 4.17 and 4.19 were both used to obtain a value for the transitional displacement thickness from the laminar and turbulent values. When these were compared with the value obtained by reducing the mean velocity profile equation 4.19 was found to be much more accurate. This improvement might have been expected since the measured turbulent displacement thickness is based on measurements which isolate the completely turbulent flow. However methods which use equation 4.17 and the

corresponding expressions for momentum thickness and shape factor, see for example Fraser and Milne (1986) or Fraser et al (1987), are not incorrect for the following reason. These methods use standard integral techniques to provide laminar and turbulent values in the transition region. Most integral techniques for turbulent boundary layers take the intermittent outer region into account, eg. through the law of the wake (eqn. 4.10). Thus the near wall intermittency is appropriate when combining the laminar and turbulent values.

The previously described methods for obtaining the skin friction were used separately for the laminar and turbulent profiles and could be combined to give a transitional value using a near wall intermittency weighting, ie.

$$(\tau_w)_{tr} = (1 - \gamma)(\tau_w)_{\llcorner} + \gamma(\tau_w)_{\urcorner} \qquad (4.20)$$

as suggested by Dhawan and Narasimha (1958). Again this is physically more realistic than simply using a laminar analysis in a predominantly laminar boundary layer and a turbulent analysis in a predominantly turbulent boundary layer.

4.2.4 Start and End of Transition

Various techniques have been used in the past to determine the locations of the start and end of transition. This has undoubtedly contributed to the considerable scatter in transition data. During the present work the start and end of transition were determined from intermittency measurements with two techniques being considered. One method was to define the start of transition as the point where the near wall intermittency was 0.01 and the end of transition as the point where it was 0.99, the two points being estimated from a plot of the complete intermittency distribution.

Although this method has been popular it is still very difficult to locate these points accurately. An alternative approach was that used by Narasimha (1985) and also by Dey (1988). The function $F(\gamma)$, given by

$$F(\gamma) = [-\ln(1 - \gamma)]^{0.5} \qquad (4.20)$$

varies linearly with x and the start of transition is obtained by linear interpolation to $F(\gamma) = 0$. This method leads to different measured values of γ at the start of transition however. Because of the variety of techniques available to locate the start and end of transition a useful measure of the transition length is the distance between the points of 0.25 and 0.75 intermittency which can be more readily located. This value is given the symbol λ and has been described in section 1.3.

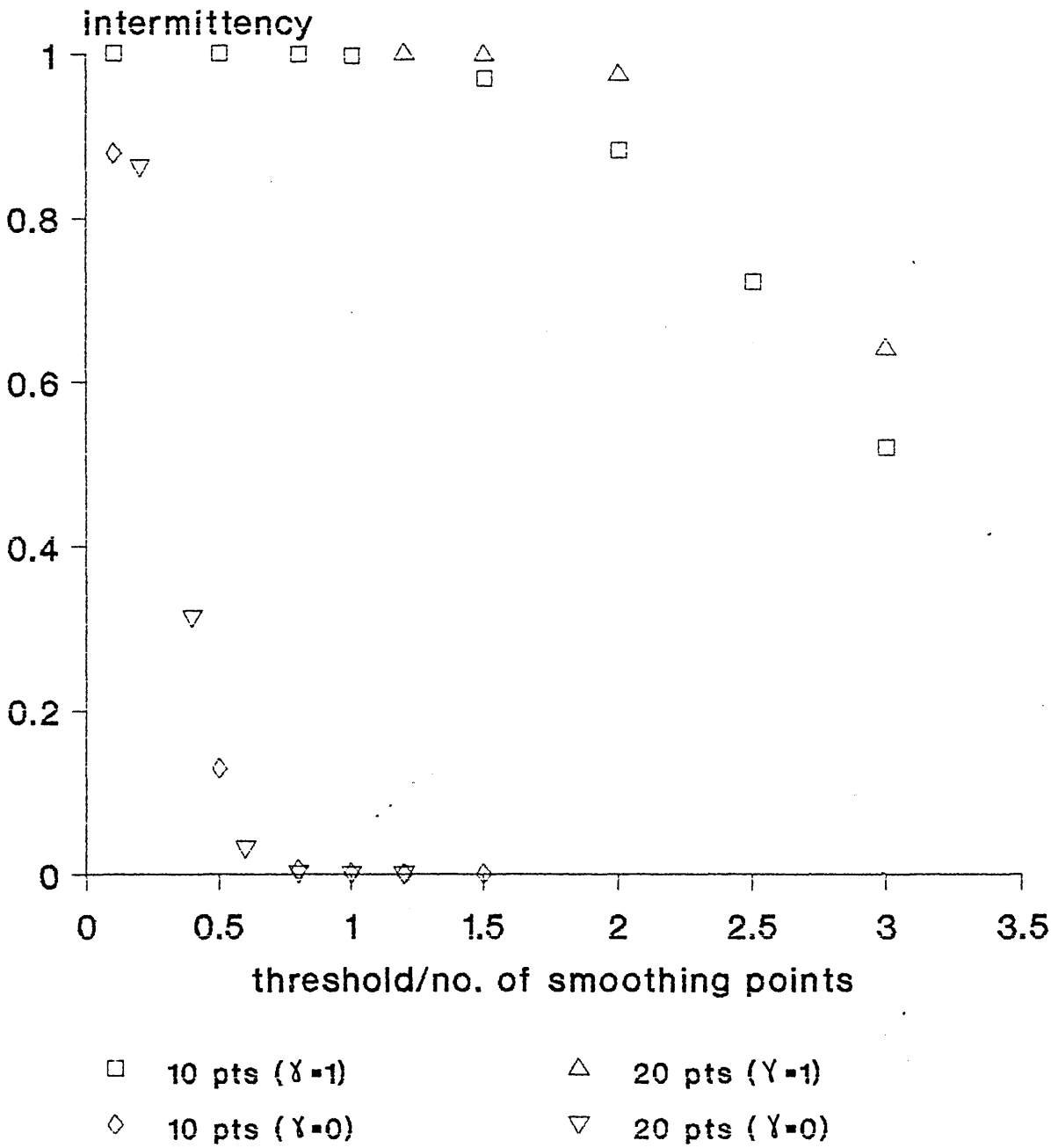

figure 4.1 measurements in a fully turbulent b.l. and the freestream

figure 4.2a velocity trace close to wall and S1

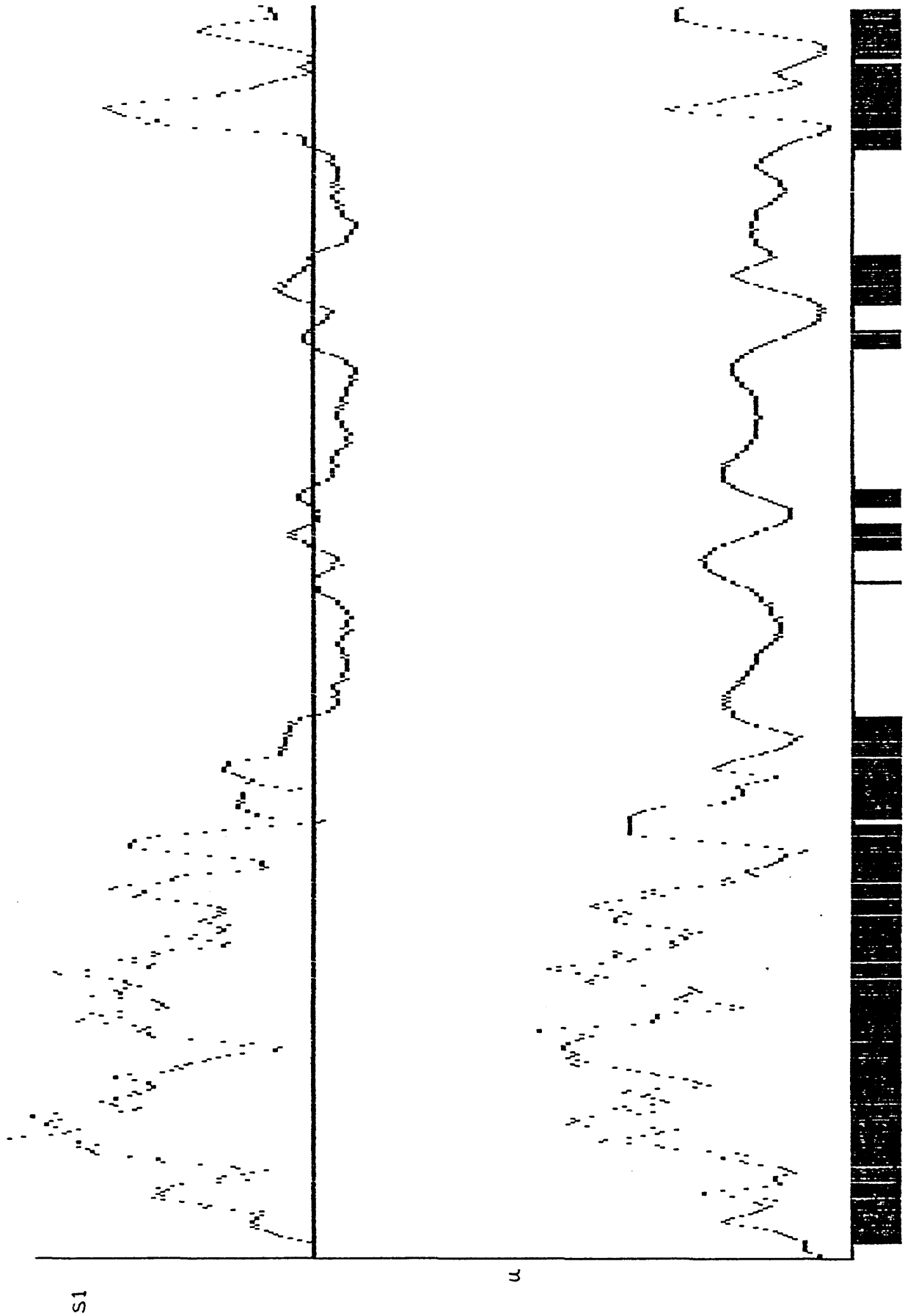

figure 4.2b velocity trace close to wall and S2

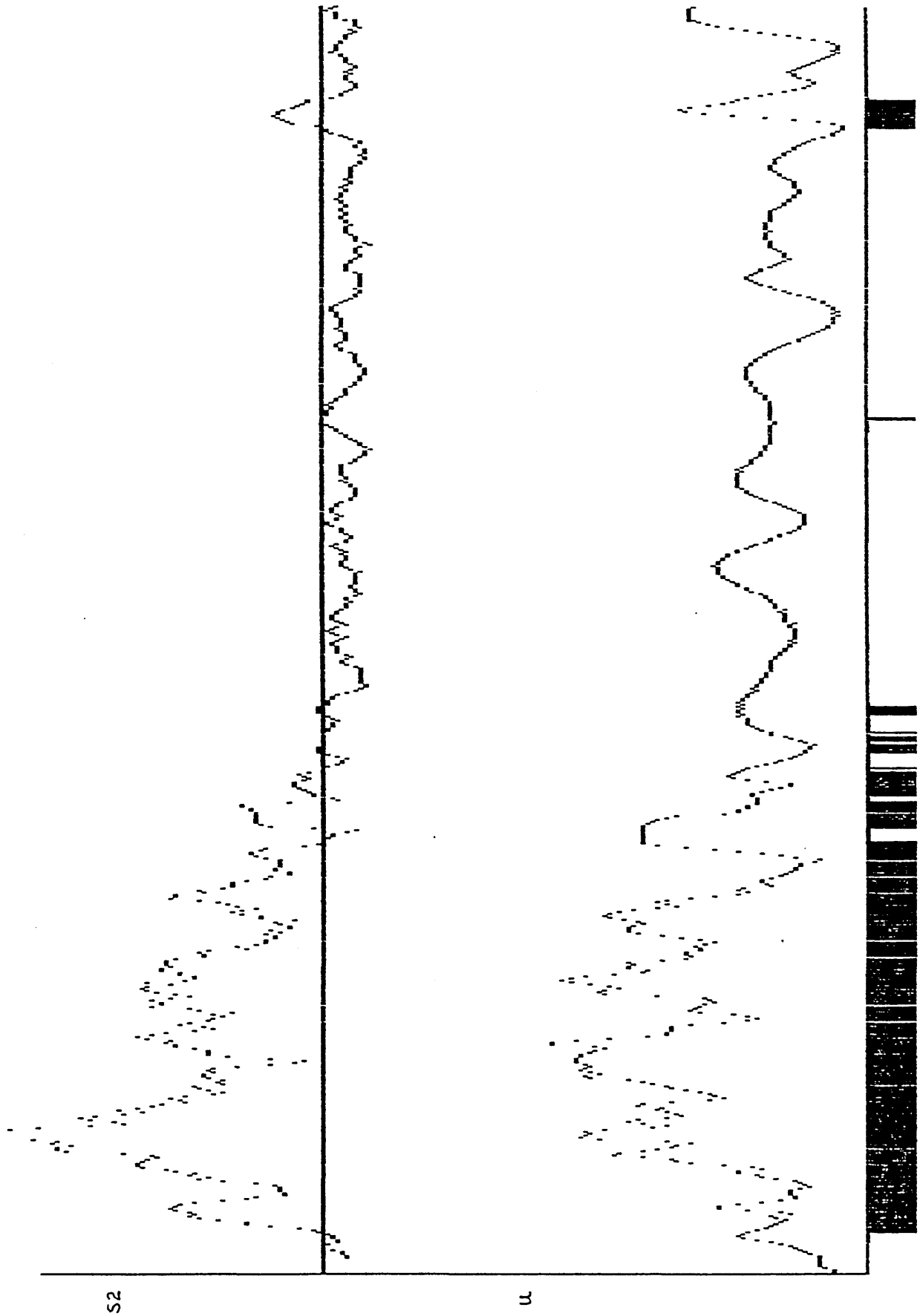

figure 4.3a velocity trace near b.l. edge and S1

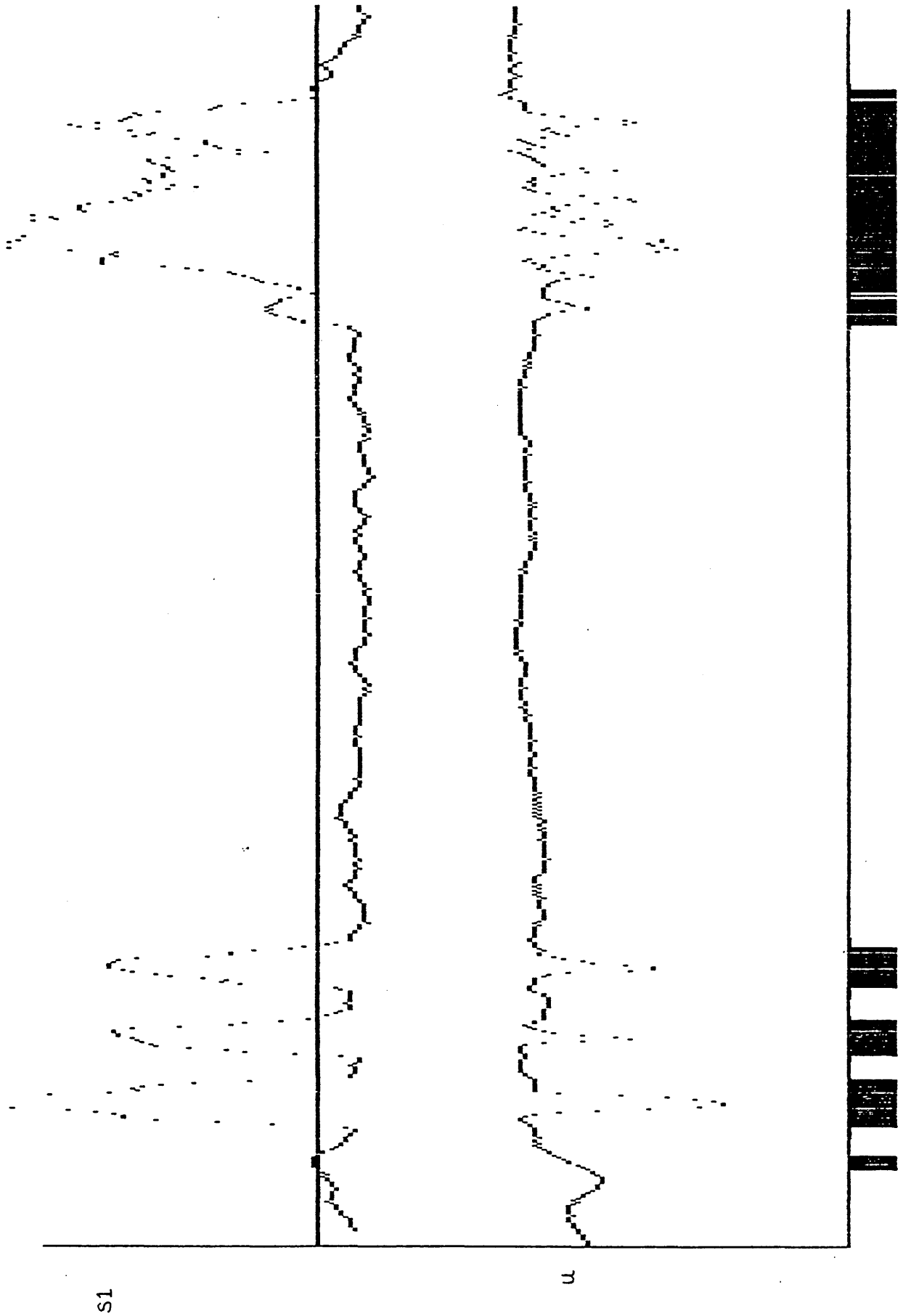

figure 4.3b velocity trace near b.l. edge and S2

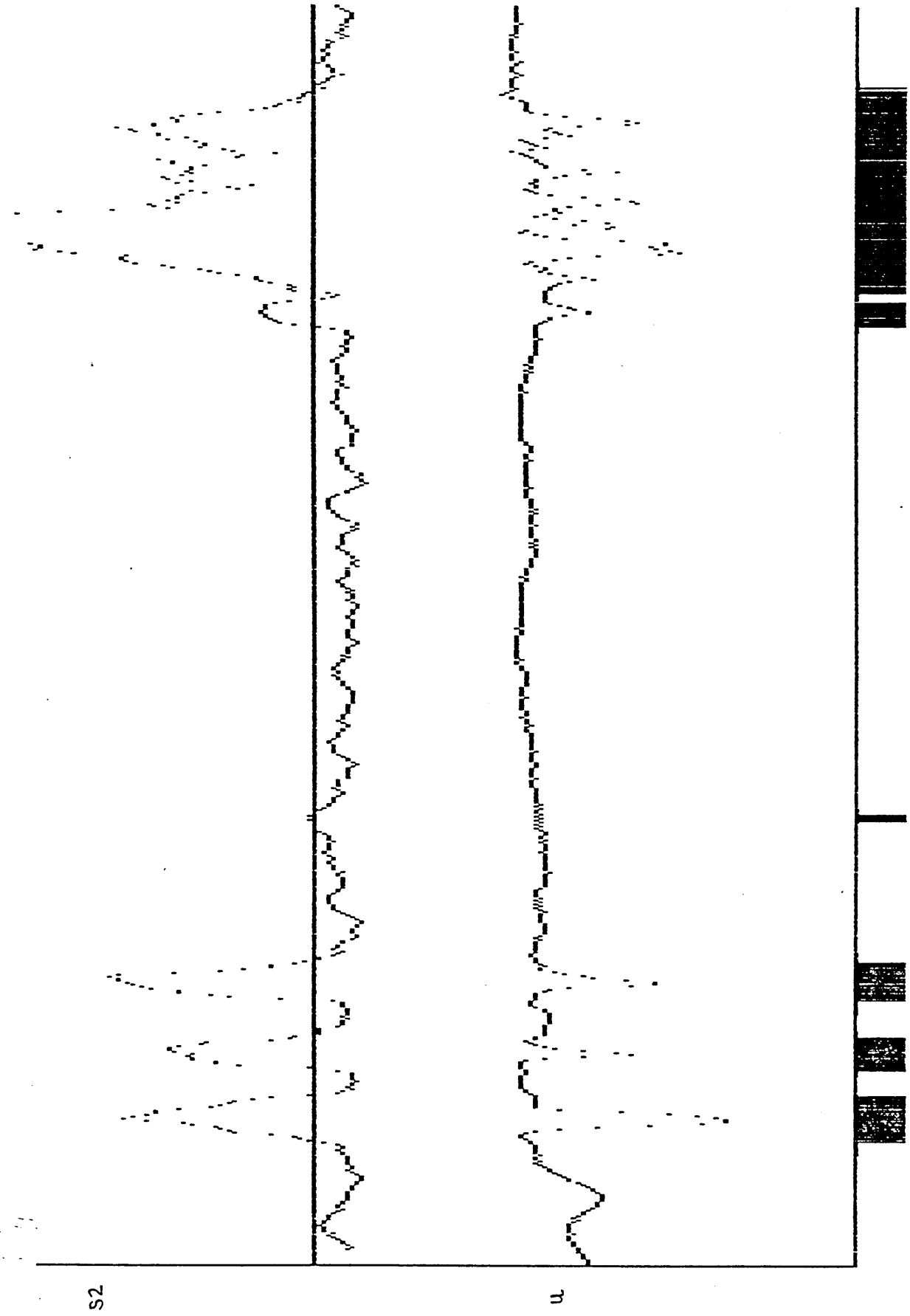

figure 4.4a intermediate velocity trace and S1

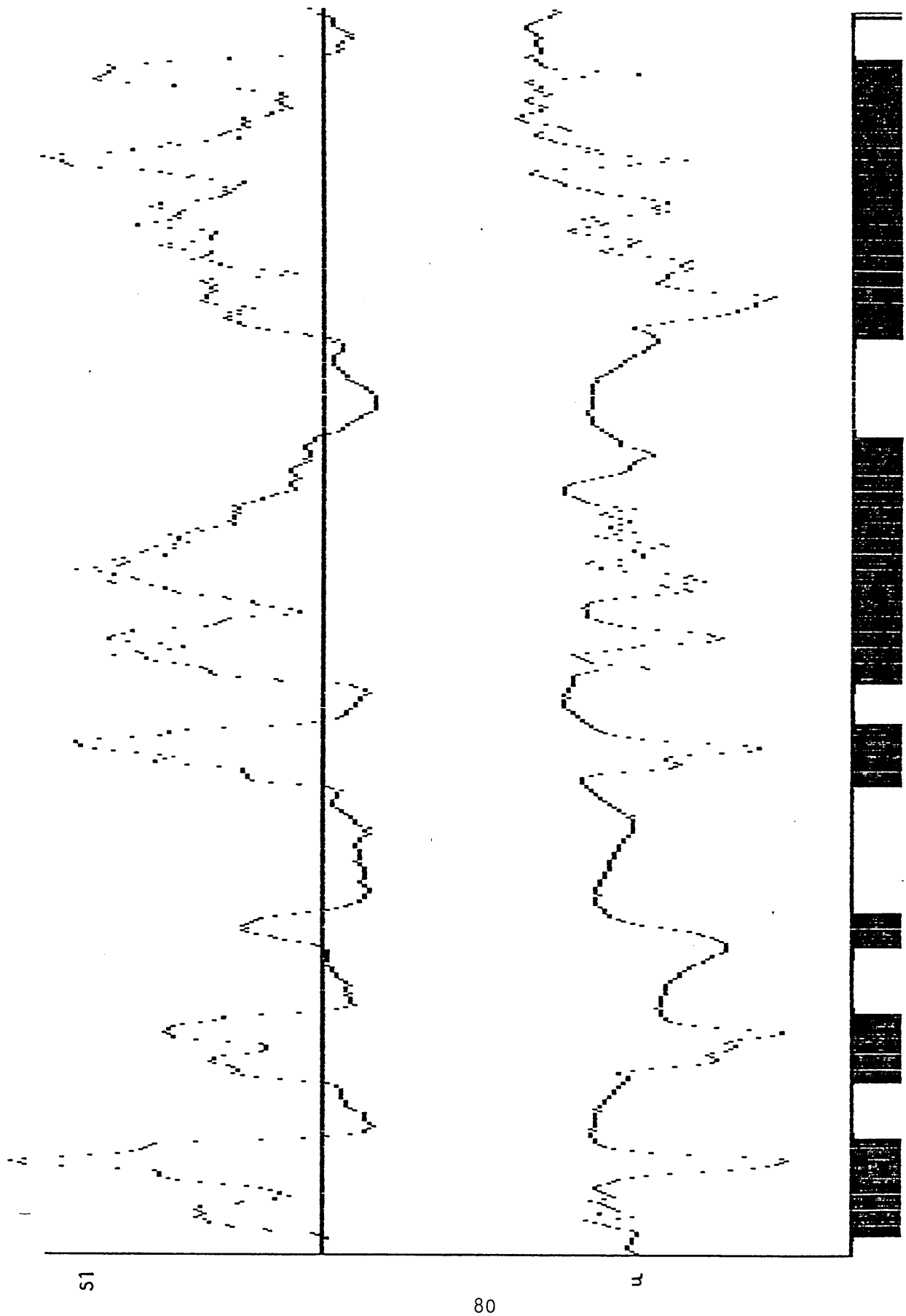

figure 4.4b intermediate velocity trace and S2

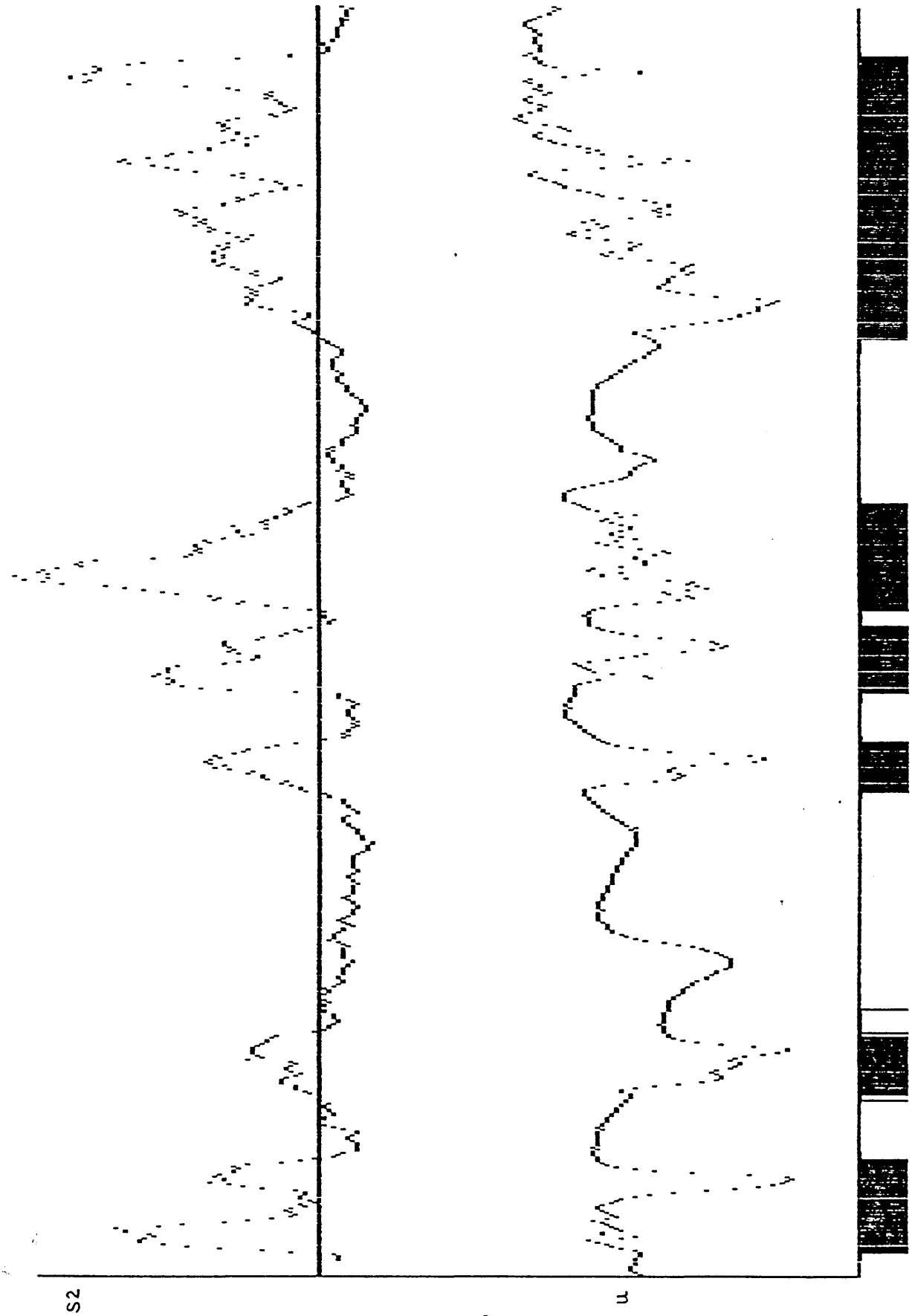

figure 4.5 velocity trace close to wall with S1 AND S2

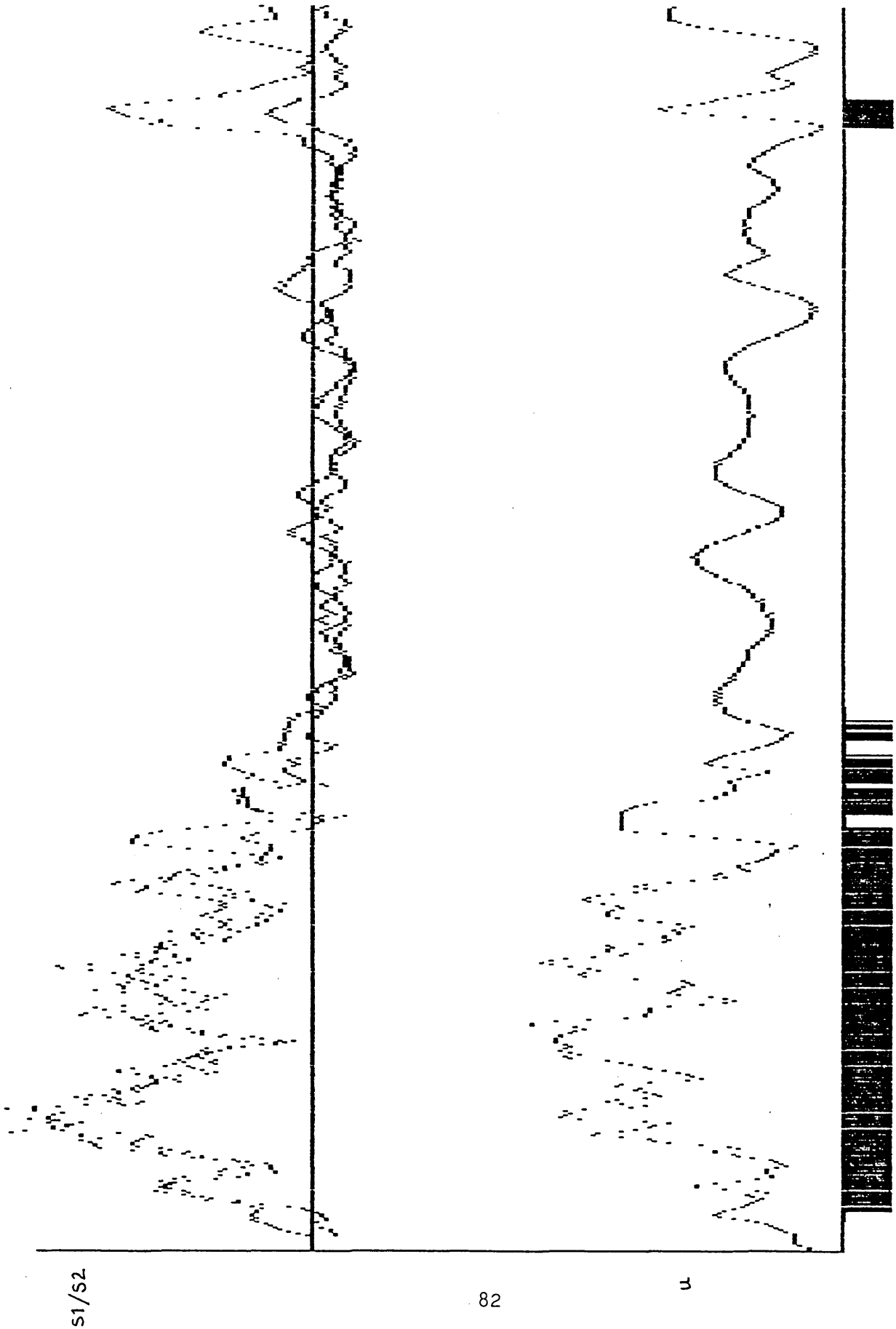

figure 4.6 velocity trace near b.l. edge with S1 AND S2

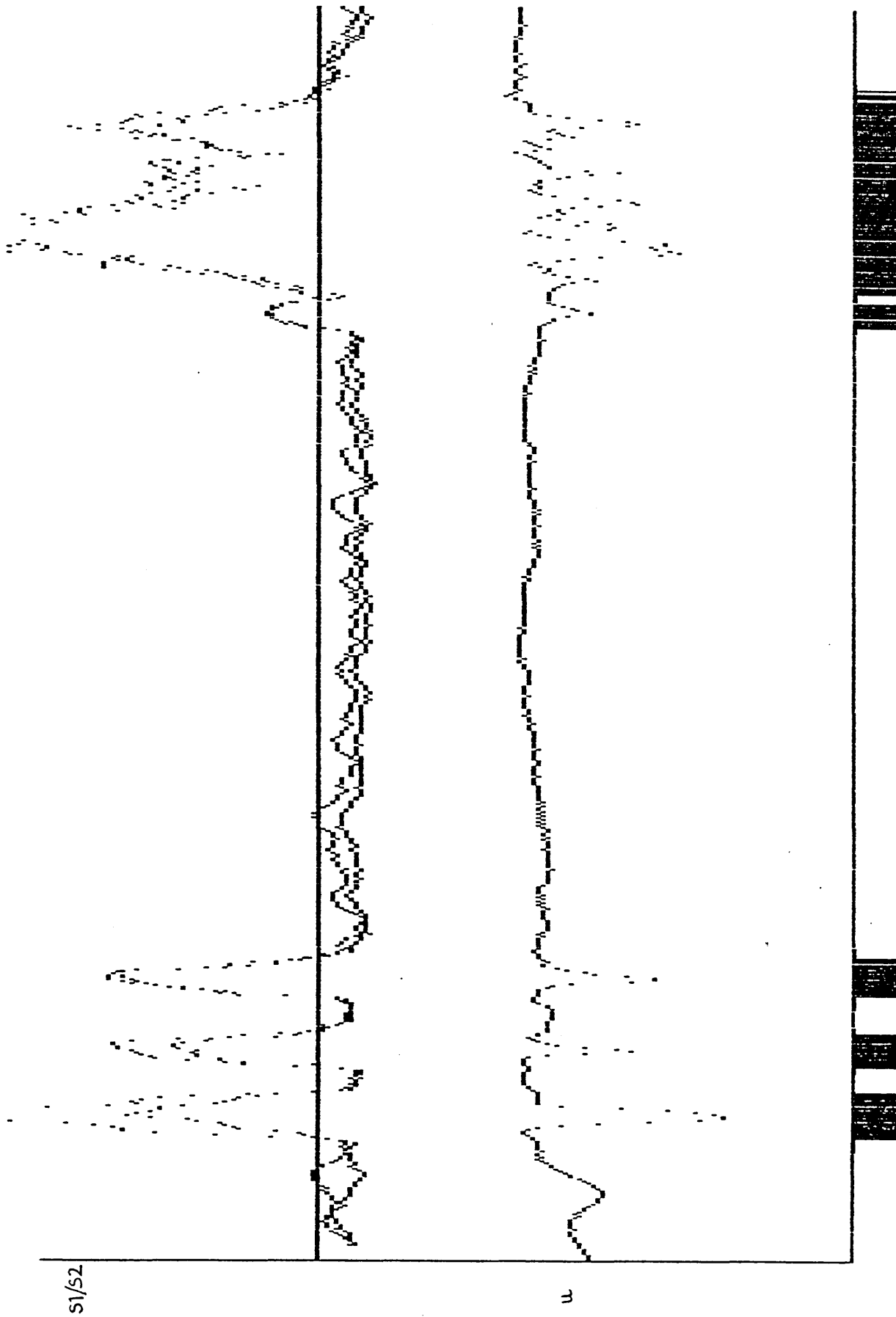

figure 4.7 intermediate velocity trace with S1 AND S2

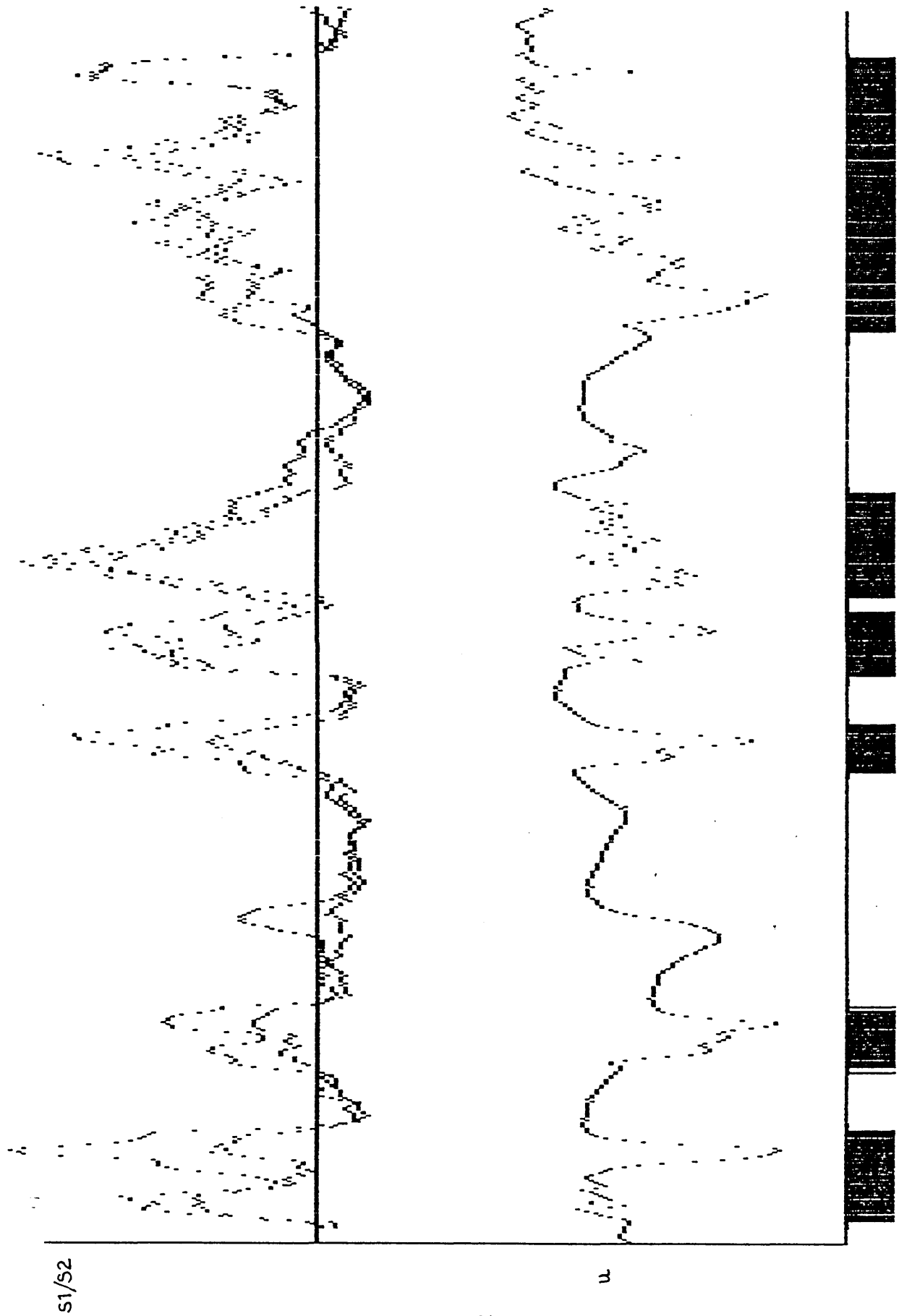

FILE NAME test1\t1668

b.l. thickness	5.01 mm
Intermittency	.411
freestream velocity	14.06 m/s
Reynolds number (x)	611355.38

Simpsons rule is used from the wall

TRANSITIONAL B.L. PARAMETERS

PARAMETER	LAMINAR	TURBULENT
disp thk (mm)	1.876	1.821
mom thk (mm)	.591	.899
energy thk (mm)	.911	1.445
H12	3.176	2.025
H32	1.543	1.607
Rdisp	1717	1667
Rmom	541	823
Cf	4.03E-004	--
Cf Lud/till	--	1.724E-003
Cf Log-plot	--	0
TO (N/m^2)	4.7E-002	.102
Wake par.	--	0

COMBINED PARAMETERS

a) Dhawan and Narasimha dislacement thickness	1.853 mm
b) Modified intermittency displacement thickness	1.805 mm

TRANSITIONAL MEAN PROFILE

LAMINAR BOUNDARY LAYER PARAMETERS

displacement thickness	1.811 mm
momentum thickness	.685 mm
energy thickness	1.061 mm
shape factor 12	2.646
shape factor 32	1.55
displacement thickness Reynolds no	1657
momentum thickness Reynolds no	626
tO	9E-002 N/m^2
cf	7.65E-004

figure 4.8 sample output from analysis program

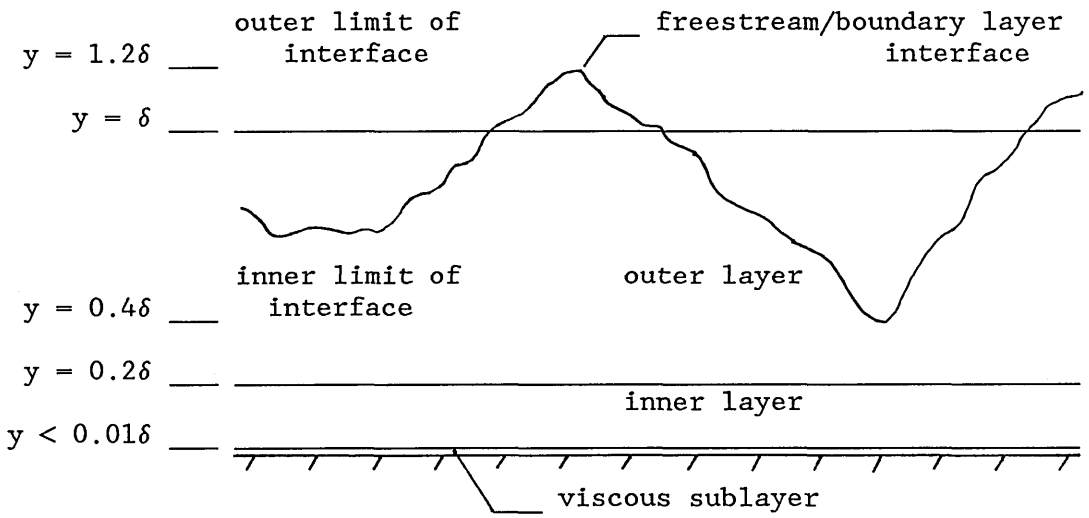

figure 4.9 schematic representation of a turbulent boundary layer

figure 4.10 transitional intermittency data from Gardiner (1987)

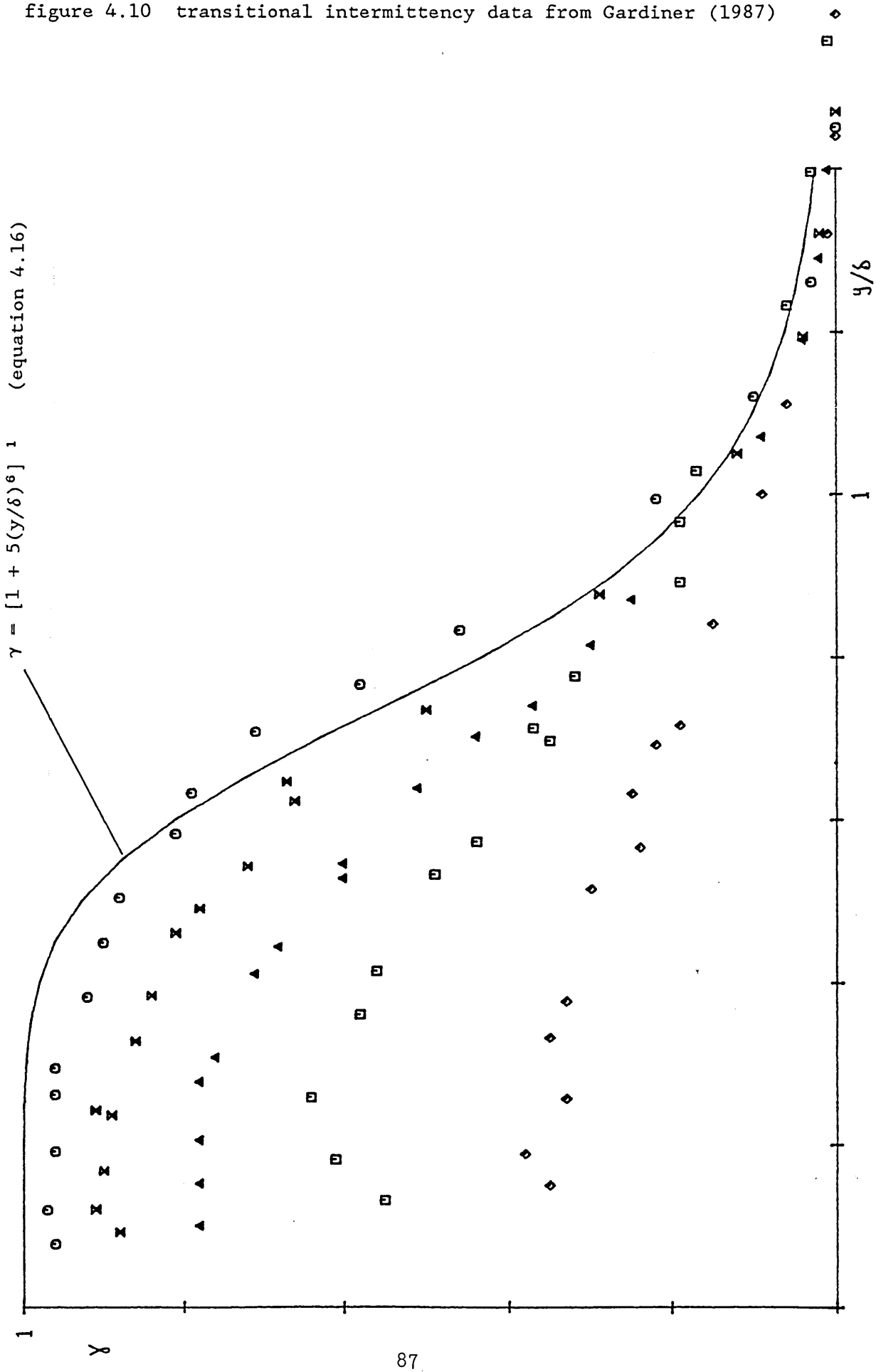

figure 4.11 previous data normalised by near wall intermittency

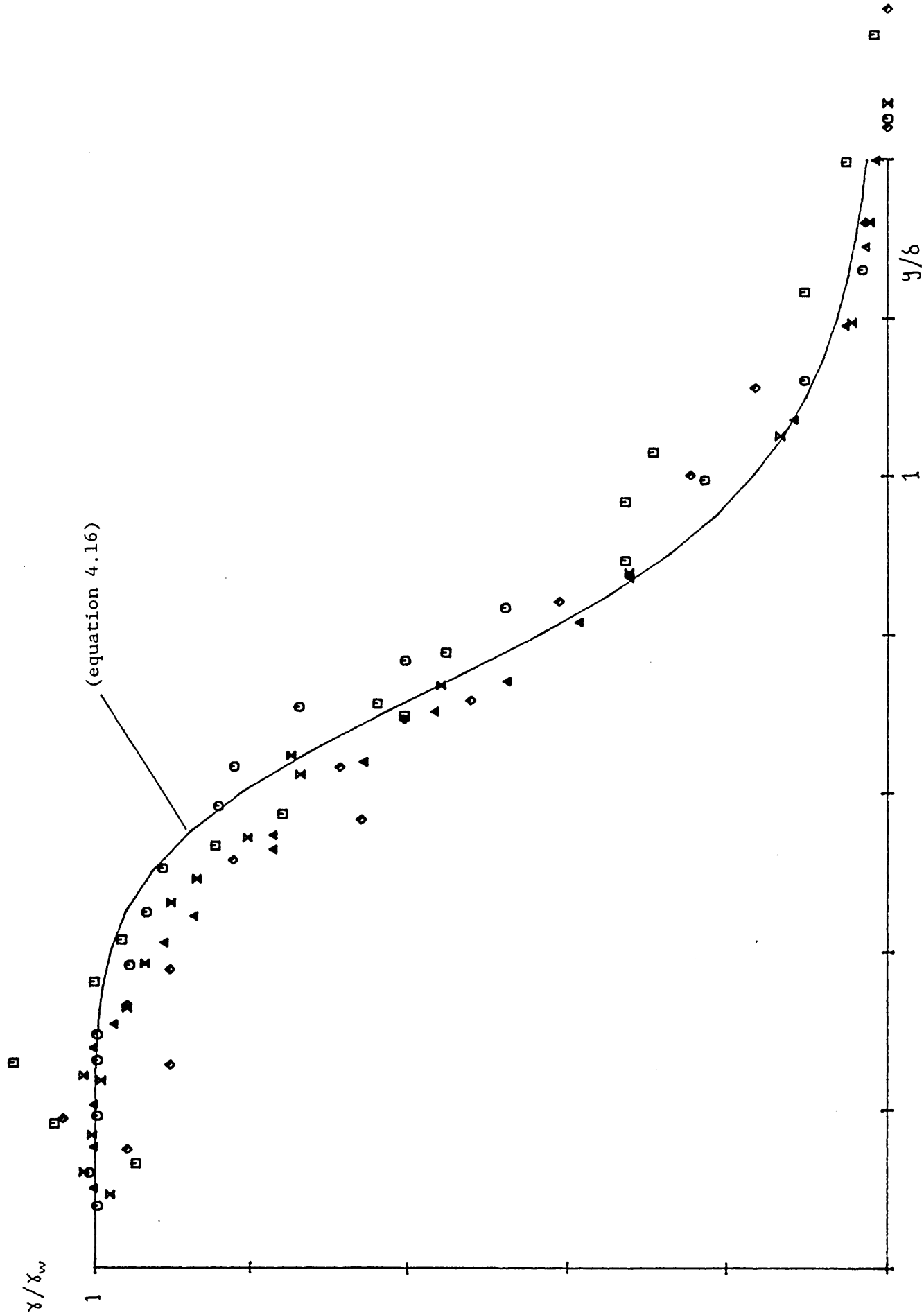

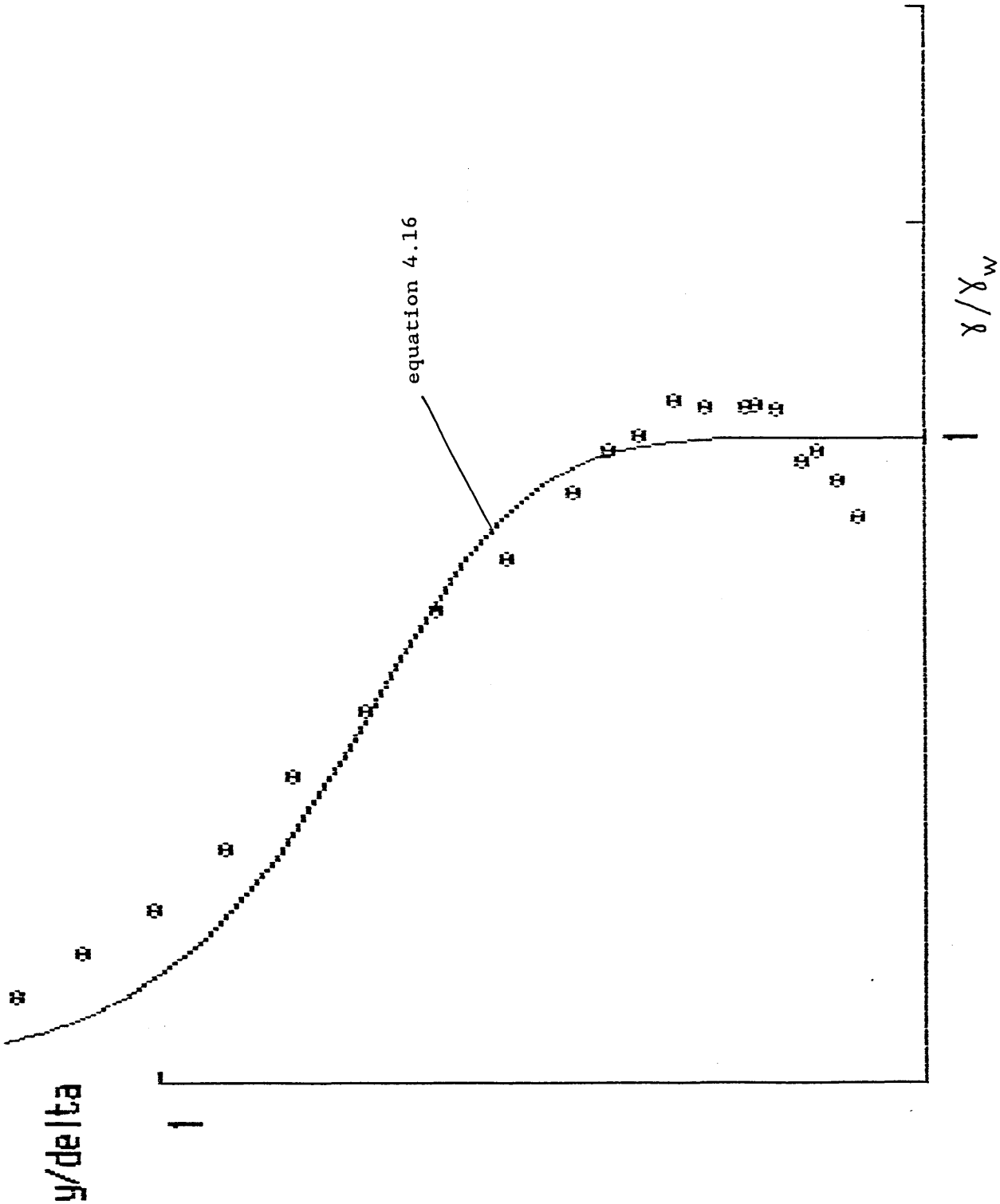

figure 4.12 example of present data plotted against equation 4.16

(near wall intermittency = 0.65)

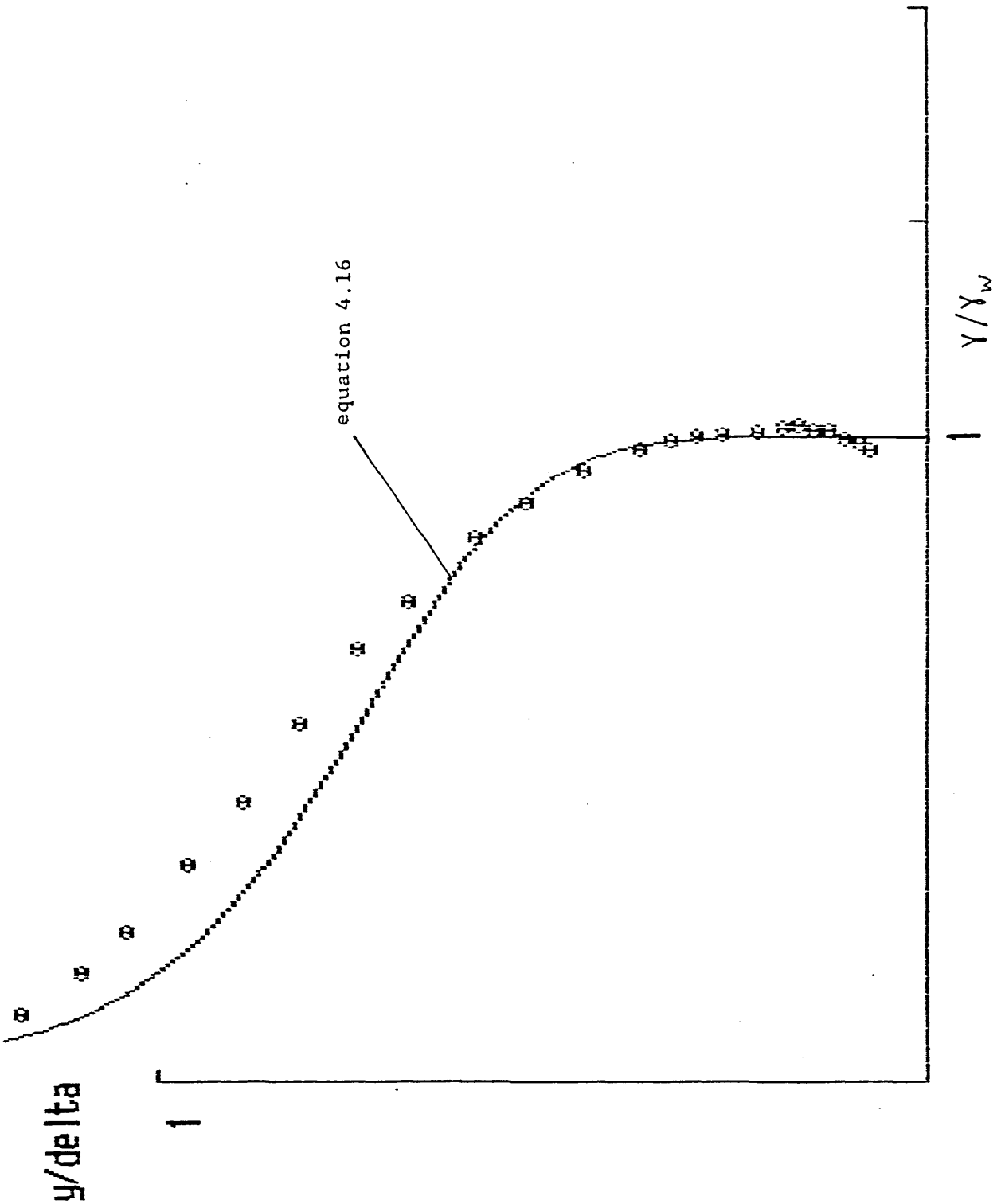

figure 4.13 example of present data plotted against equation 4.16

(near wall intermittency = 0.96)

CHAPTER 5

DISCUSSION OF EXPERIMENTAL RESULTS

Detailed measurements were made of the boundary layer which developed in a simulated turbine blade flow. A velocity distribution typical of the suction surface of a forward loaded, or "squared-off" design, aerofoil was reproduced in a low speed wind tunnel. Particular attention was paid to the transition region. Conditional sampling techniques were used to investigate the behaviour of the laminar and turbulent components of the flow. One feature of interest was the possibility of intermittent separation, as described in chapter one, which was first raised by Gardiner (1987). The effect of varying freestream turbulence on the location and extent of transition was also investigated. Intermittency data collected showed that the concept of statistical similarity of transition regions was also applicable to the present case which involved fairly severe adverse pressure gradients.

The boundary layer was allowed to develop naturally from the leading edge of the smooth aluminium plate and transition was considered to be influenced mainly by the freestream turbulence level and the streamwise pressure distribution. It was found that three of the existing turbulence generating grids all produced a turbulence level at the inlet of about 1%. Only the coarsest grid produced a higher turbulence level of about 1.5%. A further grid, of similar design, which gave an inlet turbulence level of about 2% was constructed.

In common with Gardiner (1987) and other workers it was assumed that the turbulence was isotropic ie.

$$Tu = \frac{\sqrt{u'^2 + v'^2 + w'^2}}{3\,U} = \frac{\sqrt{u'^2}}{U} \qquad (5.1)$$

No measurements of v' and w' were made to justify this but Blair

and Werle (1980) showed that the fluctuating velocity components were approximately equal by the time grid generated turbulence had decayed to a constant value. It might be expected that the rapid accelerations and decelerations experienced by the flow would affect the components u', v' and w' differently. However, it was noted in chapter two that the RMS of the fluctuations in u vary by less than 10% over most of the test flow. Since it might be expected that u' would be most affected by rapid variation of u it would therefore seem reasonable to assume that the flow remains approximately isotropic. This is supported by measurements of u', v' and w' by Sharma et al (1982) in a very similar flow.

In all, six different values of inlet turbulence were used. In the case of flow 1, which gave the lowest level of 1%, no turbulence grid was used. Results from this flow may have been affected by the different length scale of this turbulence compared with the grid generated turbulence. For each of the flows a series of boundary layer traverses were made measuring the mean velocity, the rms velocity and, in the transition region, the intermittency distribution and the laminar and turbulent components of velocity. From the intermittency measurements the most usefull average value, the near wall intermittency was calculated. All experimental data is summarised graphically in appendix 2. A further flow, flow 7, was also investigated in an attempt to observe the effect of rapidly changing pressure gradient on transition. By altering the roof slightly and running the wind tunnel at a higher speed transition was brought just forward of the point of maximum velocity ie. transition was initiated in a favourable pressure gradient region but most of the transitional boundary layer

developed in a region of adverse pressure gradient. This did not constitute a complete study but the results are considered in this chapter.

5.1 START OF TRANSITION

The linearised stability theory has proved successful in predicting the point of instability ie. the location at which a laminar boundary layer first becomes unstable. Following the initial amplification of two dimensional Tollmein-Schlichting waves the flow becomes increasingly complex, as outlined in chapter one, before the appearance of turbulent spots which effectively mark the start of transition to a fully turbulent boundary layer. Theoretical analysis is not readily extended to predict the onset of turbulence. Also, the linear stability theory is not strictly applicable to flows with high freestream turbulence hence the multitude of correlations and semi-theoretical prediction methods which exist. Transition data exhibits considerable scatter which, as was noted in the previous chapter, can be partly attributed to the variety of techniques used to detect the onset of transition. For example Hall and Gibbings (1972) and others have used the surface pitot method. Here, the start and end of transition are located by maximum and minimum readings from a surface pitot. Abu-Ghannam and Shaw (1980) used hot wire instrumentation and used the variation of the ratio of surface velocity to reference velocity to determine the start and end of transition Reynolds numbers. For the present work the more direct approach of using intermittency measurements to locate the transition region was adopted.

Two techniques for determining the location of the start of transition have been considered. The first was the method used by Fraser et al (1988) whereby the start of transition is defined as the point where the flow becomes 1% turbulent, ie. the intermittency reaches 0.01, and the end of transition is the point where the flow becomes 99% turbulent. These points can be reasonably well estimated from a plot of intermittency against streamwise location. Fraser et al (1988) noted that this technique could be expected to give the start of transition earlier than that of Abu-Ghannam and Shaw (1980) under the same experimental conditions.

Alternatively a technique first introduced by Narasimha (1957) was used to locate the start of transition. The function $F(\gamma)$,

$$F(\gamma) = [-\ln(1 - \gamma)]^{0.5} \qquad (4.20)$$

has been shown to vary linearly with x in zero pressure gradient flows. The start of transition location, x_t, is obtained by extrapolating to F = 0 from the best fit straight line through the data. This method can give various values of intermittency at the start of transition but Narasimha (1985) suggests that the x_t given by this method is the most appropriate since it is the effective origin of the turbulent boundary layer which follows the transition region. Narasimha (1985) has observed that pressure gradients can affect the linearity of F with x, particularly if they are applied close to x_t.

Table 5.1, on page 112, gives details of the experimental

flows and summarises the transition data. Figures 5.1 to 5.6 show the present intermittency data plotted in the form suggested by Narasimha and described above. It can be seen that the lower turbulence flows, ie. flows 1 to 4, give good straight lines and x can be readily obtained. Flow 5 shows a kink and can be best fit by two straight line segments while flow 6 appears to be best fit by three straight line segments. These kinks were described as "subtransitions" by Narasimha (1985). Thus there is some ambiguity about the values of x_t for flows 5 and 6. In all cases x_t is larger than x_s.

The velocity gradient is fairly constant over the range of locations of the start of transition at about -6.15 ms^{-1}/m (see figure 2.2). This value was used to obtain values for the pressure gradient parameter, m, at the start of transition. As can be seen from table 5.1 the values of m at the start of transition are very low indicating that laminar separation may be imminent or indeed have already occurred. In fact shape factor data and velocity profiles, as described in section 5.4, indicate that laminar separation occurs in flows 1 - 4 and probably flow 5 with only flow 6 remaining attached.

Table 5.2 shows a comparison of the measured momentum thickness Reynolds number at the start of transition with that predicted by the correlation of Abu-Ghannam and Shaw (1980) for the same pressure gradient and turbulence conditions. It can be seen that better agreement is achieved when the local turbulence level is used as opposed to the leading edge value. Abu-Ghannam and Shaw (1980) suggested using an average value for the turbulence level, obtained midway between the leading edge and the point under

consideration. This is unlikely to be strictly applicable in the present case since the freestream turbulence varies greatly between the leading edge and the transition point. The turbulence level varies essentially in inverse proportion to freestream velocity. This is due to the fact that the rms of the fluctuations remains more or less constant in spite of the flow being accelerated then decelerated.

The errors in the predicted values of R_{θ_t} are possibly due, in part, to the fact that transition is not dependent entirely on local conditions. All measured values of R_{θ_t} are higher than the predicted values, ie. transition appears to be delayed. It is possible therefore, that the boundary layer is better able to resist the adverse pressure gradient region as a consequence of the stabilising effect of the rapid acceleration in the initially favourable pressure gradient region.

Table 5.3 summarises the details of flow 7 and figure 5.7 shows that the intermittency data is also well represented by Narasimha's distribution. The correlation of Abu-Ghannam and Shaw (1980) gives $R_{\theta_t} = 550$ when the turbulence level at the start of transition, of about 1%, is used. This is in excellent agreement with the measured value of 540.

5.2 STATISTICAL SIMILARITY OF TRANSITION REGIONS

When the intermittency data is plotted in the coordinates suggested by Schubauer and Klebanoff (1955) it is found to collapse on to a single curve, see figure 5.8. Schubauer and Klebanoff (1955) plotted the intermittency against the coordinate

$$\eta = \frac{x - \bar{x}}{\sigma}$$

where $\bar{x}$ is the x location of the point where the intermittency is 50% and σ is the standard deviation of the intermittency distribution. Fraser et al (1988) noted that σ was simply related to λ by

$$\lambda = 1.37\sigma \qquad (5.2)$$

Figure 5.8 gives further evidence that the concept of statistical similarity applies to transition regions in adverse pressure gradient flows. The intermittency distribution of Schubauer and Klebanoff (1955) is often found to give better agreement with data than other distributions such as Dhawan and Narasimha (1958) and Abu-Ghannam and Shaw (1980). This is simply because the normalising coordinate $\bar{x}$, can be more accurately obtained from experimental data than the start of transition. Narasimha (1985) attributes scatter from the distribution of Dhawan and Narasimha (1958) to "incorrect" choice of x_t. Fig 5.9 shows the intermittency data plotted against Dhawan and Narasimha's distribution and it can be seen that there is greater scatter than in fig 5.8 despite using x_t values obtained as described by Narasimha. Difficulty arises in cases such as flows 5 and 6 where there are two or more possible values of x_t. Flow 5 gives a better fit if the later value is used but flow 6 can be made to fit if the mean of the last two possible values of x_t is used (see fig 5.6).

Figures 5.1 to 5.6 show that there is always some deviation from the linear relationship at low intermittency values but this is normally neglected when determining x_t. Other workers who have

used Narasimha's method of describing intermittency have observed this deviation at low intermittencies, even in zero pressure gradient flows eg. Dey (1988) and Gostelow (1989a). Narasimha (1985) suggests that this is due to errors in measurements of low intermittencies and recommends that the straight line be fitted only to points in the range $0.25 < \gamma < 0.75$. However, as has been noted above, flows 5 and 6 of the present work and those reported by Narasimha (1985) show significant deviation and, even ignoring the low intermittency points, the data is still best fit by two straight line segments giving rise to two possible values of x_t . Fig 5.10 shows flow 6 replotted using three possible values of x_t obtained from figure 5.6. The third value is simply the mean of the first two and gives the best fit. Thus in certain cases such as flow 6 it may be best to use a mean value for x_t but even in such cases the low intermittency data should be neglected.

Figure 5.11 shows the intermittency data of flow 7 plotted against Narasimha's distribution. There is some scatter but the graph does suggest that the distribution is still a fair representation of the growth of intermittency even under the present conditions where the pressure gradient changes from favourable to fairly severely adverse over the transition region.

5.3 TRANSITION LENGTH

The difficulty of predicting the onset of transition is well known and much effort has been devoted to this problem. The problem of predicting the end of transition has attracted less effort but can also be of crucial importance. Local maxima of skin friction and heat transfer rate occur at the end of the transition

region which can lead to hot spots on turbine blading for example. Dhawan and Narasimha (1958) offered, for zero pressure gradient flows, the rough correlation

$$R_\lambda = 5\, R_{x_t}^{0.8} \qquad (5.3)$$

which has found wide application despite considerable scatter in the available data. Abu-Ghannam and Shaw (1980) used equation 5.3 for both zero and non-zero pressure gradient flows. Figure 5.12 shows the present data and that of Sharma et al (1982) plotted against equation 5.3 and it can be seen that comparison is poor. Chen and Thyson (1971) have used a similar correlation which allows for Mach number ie.

$$R_{\Delta x} = A\, R_{x_t}^{0.67} \qquad (5.4)$$

where $A = 60 + 4.68M^{1.92}$

Gardiner (1987) has developed a correlation, for adverse pressure gradients, which relates the transition length directly to the pressure gradient parameter and the turbulence level at the start of transition ie.

$$R_\sigma = R_{\sigma_o}[1 + 1710m^{1.4}\ \exp\{-\sqrt{(1 + Tu^{3.5})}\}]^{-1} \qquad (5.5)$$

where

$$R_{\sigma_o} = (270 - (250Tu^{3.5})/(1 + Tu^{3.5})) \times 10^3 \qquad (5.6)$$

and $R_\sigma = U\sigma/\nu$

where σ is the standard deviation of the Schubauer and Klebanoff (1955) distribution and can be related to λ by

$$\lambda = 1.37\sigma \tag{5.2}$$

Equation 5.5 was developed only for constant, mild adverse or zero pressure gradients ie. $0 < m < -0.04$. Table 5.4 shows measured values of λ alongside those predicted by equation 5.5. Bearing in mind the limitation of equation 5.5 the results are probably as good as could be expected.

More recently Narasimha (1985) has suggested that the transition length can be predicted from knowledge of the rate of spot production at the start of transition (see section 1.3). He suggested that the most appropriate non dimensional parameter is

$$N = n\sigma\theta_t^3/\nu \tag{1.7}$$

Using equation 1.6 the above equation can be rewritten as

$$N = \frac{0.412\theta_t^3 U}{\lambda^2\nu} \tag{5.7}$$

or, alternatively

$$N = \frac{0.412R_{\theta_t}^3}{R_\lambda^2} \tag{5.8}$$

Narasimha then suggests that in zero pressure gradient flows N has a "universal" value of 0.7×10^{-3} for turbulence levels above about 1%. This value appears to rise for low values of freestream turbulence. Using this universal value of N, if the start of transition can be located and θ_t calculated, then λ follows from

equation 5.7 and the intermittency distribution and the extent of transition can be obtained from equation 1.5. However, as was mentioned in section 1.3, N has been shown to vary rapidly with the application of an adverse pressure gradient. Gostelow (1989b) has summarised a large amount of experimental data concerning boundary layer transition in adverse pressure gradients. This data was used to formulate a correlation for N based on pressure gradient parameter and freestream turbulence. The data was particularly suitable since it covered a wide range of freestream turbulence (0.3% - 5.3%) and the velocity gradients were all more or less linear. Firstly a range of zero pressure gradient data was considered.

5.3.1 N in Zero Pressure Gradient Flows

Figure 5.13 shows N values in zero pressure gradient flows from a variety of sources. The N values are not measured themselves but are determined via equation 5.7 or 5.8. Narasimha's assertion that the value of N tends towards 0.7×10^{-3} as the freestream turbulence increases seems to be reasonable although it is clear that this value rises below about Tu% = 1%. It was decided to use an expression of the form

$$N = A + \exp(B - kTu\%) \qquad (5.9)$$

to describe the behavour of N under zero pressure gradient conditions. This expression will have a value of A + exp(B) when Tu% = 0 and will asymptote to the value A, at a rate determined by the constant k, as Tu% increases. A then becomes 0.7 and, choosing

a value of 2.5 for $N\times10^3$ when Tu% = 0 leads equation 5.9 to become

$$N_o\times10^3 = 0.7 + \exp(0.588 - 3Tu) \qquad (5.10)$$

The zero turbulence value of 2.5 has little effect on the function and is perhaps irrelevant anyway as zero turbulence is an unobtainable ideal. Using a value of 3 for the constant k brings the function down to about 0.8 at Tu% = 1%. Equation 5.10 is shown along with the data of Gostelow (1989b) in figure 5.14 where the agreement is seen to be reasonable.

5.3.2 N in Adverse Pressure Gradient Flows

The data of Gostelow (1989b) is shown in figure 5.15. It can be seen that the non dimensional parameter N rises rapidly as the pressure gradient parameter becomes increasingly adverse but also that increased freestream turbulence has the effect of reducing N. This suggests that increasingly adverse pressure gradient dramatically increases the rate at which turbulent spots are produced, resulting in shorter transition lengths. It also suggests that increasing the freestream turbulence level reduces the rate of spot production leading to an increase in transition length which is in direct contrast with observations that increasing turbulence leads to a reduction in transition length eg. Hall and Gibbings (1972), Abu-Ghannam and Shaw (1980) and Fraser et al (1988).

The effect of adverse pressure gradient on the stability of laminar flow is well known. Stability theory has shown that, as the pressure gradient parameter becomes more negative, the critical

Reynolds number decreases and the maximum rate at which disturbances can be amplified increases. This has the effect of bringing the start of transition forward. It is possible that modification of the disturbance amplification rates is linked to the increase in spot production rate which leads to shorter transition lengths.

Increasing the freestream turbulence also has the effect of bringing the start of transition forward. In the flows of Gostelow (1989b), and in the present flows, dU/dx is reasonably constant, at least in the area of interest. Thus, bringing the start of transition forward, by increasing the freestream turbulence, will result in the pressure gradient parameter, at the start of transition, becoming smaller in magnitude. This will result in a reduced spot formation rate which will lead to an increase in the transition length. This would appear to outweigh any effective reduction of the transition length due to the freestream turbulence. It therefore appears that, at least for Gostelow's data, the net effect of increasing the freestream turbulence is to increase the transition length. The data of Gostelow (1989b), and the present data, covers a wide range of adverse pressure gradients and freestream turbulence levels which are found in typical turbine blade flows but obvious care should be taken to avoid using the following correlation outwith this range.

Figure 5.15 suggests an exponential type of relationship between N and the pressure gradient parameter at the start of transition, m , however log/linear plots failed to produce linear relationships. However, plotting ln(N) against freestream turbulence level for selected values of pressure gradient parameter

did reveal a near linear relationship as shown in figure 5.16. The mean slope of all the lines plotted in figure 5.16 was found to be about -0.45 thus

$$\ln(N\times10^3) = -0.45Tu + k \qquad (5.11)$$

where k is the value of $\ln(N\times10^3)$ at the intercept where Tu = 0 and is obviously a function of the pressure gradient parameter. Figure 5.17 shows the values of k, obtained from fig 5.16, plotted against ln(m) which also produces a straight line relationship. A straight line fit gave a slope of 1.96 and an intercept of k=0.90. Since this was a purely empirical fit the slope was adjusted to 2 which gave an intercept of k=0.82 without significantly altering the fit of the straight line. Thus

$$k = 2\ln(-m\times10^2) + 0.82 \qquad (5.12)$$

When substituted into equation 5.11 this gives

$$N = 22.7m^2\exp(-0.45Tu) \qquad (5.13)$$

which shows that the data of Gostelow (1989b) can be used to correlate N, fairly simply, to the freestream turbulence level at the leading edge and the pressure gradient parameter at the start of transition (x_t determined by Narasimha's procedure). Equation 5.13 has one flaw in that it becomes zero when m becomes zero. This was overcome by simply adding the zero pressure gradient value of N obtained from equation 5.10, ie.

$$N = N_o + 22.7m^2\exp(-0.45Tu) \qquad (5.14)$$

Both equations 5.13 and 5.14 are shown in figures 5.18a - d. It can be seen that the modified equation, 5.14, deviates from the original correlation, 5.13, as the turbulence level increases, particularly for low values of m. However this effect is exagerated by the logarithmic nature of the plot and it can be seen from figures 5.18a - d that equation 5.14 in fact gives a better correlation of the data. The data of Gostelow (1989b) is replotted, along with equation 5.14 for the appropriate turbulence levels, on a linear scale in figures 5.19 and 5.20.

Figure 5.21 shows the present data plotted against the correlation, equation 5.14. Good agreement is obtained with flows 2, 3 and 4. Flows 5 and 6 are less satisfactory but they do at least follow the trend of decreasing N with increasing turbulence. Figure 5.22 shows the data of Gardiner (1987). This shows a fair amount of scatter but again the general trends are evident. It should be noted that the start of transition for this data is the 1% intermittency point rather than that obtained by Narasimha's procedure.

5.4 DETAILS OF TRANSITION

5.4.1 Integral Parameters

The behaviour of the main integral parameters through transition are shown graphically in appendix 2. As well as the overall mean values, the values for the laminar and turbulent

components of the flow through the transition region are also shown. On the whole the mean parameters behave similarly to the results reported by Sharma et al (1982), particularly flow 6 which most closely resembled the flow studied by Sharma et al.

The behaviour of the momentum thickness Reynolds number, R_θ, is shown in figures A2.1 to A2.6. The behaviour of the mean value is typical of a transitional boundary layer in that the rate of growth increases fairly suddenly after the start of transition. This is a result of the increasing influence of the turbulent component of the flow which has a much higher value of R_θ from its inception. After the start of transition, R_θ for the laminar component of the flow continues to grow at the same rate. However, towards the end of the transition region R_θ for the laminar component shows a tendency to decrease.

Figures A2.7 to A2.12 show the behaviour of the shape factor H_{12}. In flow 6 the flow remains attached but the mean shape factor reaches a value of about 3 at the start of transition which is indicative of the adverse pressure gradient. The shape factor of the turbulent component has a much lower value, typical of a fully developed turbulent boundary layer, from the start of transition. This causes the mean value to drop as the proportion of turbulent flow increases. H_{12} of the laminar flow remains high before dropping off rapidly towards the end of transition. This may be due to the stabilising effect of the passage of turbulent spots first reported by Schubauer and Klebanoff (1955). It can be seen from the velocity profiles (see appendix 3) that towards the end of transition the laminar profiles become fuller indicating increased stability of the remaining laminar flow. Flows 1 to 5 follow a

similar pattern but separation prior to transition leads to higher values of the shape factor at the start of transition. In all cases the shape factor levels out at a value of about 1.5 after transition is complete.

5.4.2 Velocity Profiles

Appendix 3 shows all the velocity profiles measured in flows 1 to 6. Again both the mean velocity and the laminar and turbulent component profiles are shown for the transition region. The velocity profiles tend to confirm, by their inflectional nature, that separation occurs prior to, and in the early stages of, transition in flows 1 to 4. They show that flow 6 remains attached and that flow 5 possibly also remains attached in spite of the shape factor reaching a value of over 3.5 at the start of transition.

Consider, for example, flow 2 which was the flow with the lowest grid generated freestream turbulence. The profiles at x=301mm and x=401mm, figures A3.14 and A3.15, were difficult to measure since the boundary layer was only 1.9mm and 2.3mm thick respectively. Since the probe could only be brought to 0.5mm from the plate, to avoid errors due to heat loss to the plate, there is a relatively large step before the first measured point and the error in the initial value of y/δ will be greatest in these profiles. However the profiles exhibit the full, stable shape which is typical of favourable pressure gradient flows. At x=500mm, figure A3.16, the profile is less full and by x=549mm, figure A3.17 the first signs of a point of inflection in the profile are apparent. The profiles at x=650mm, 661mm and 668mm look highly

inflectional and, with shape factors of almost 4, indicate that the flow has separated.

At the next measurement station, x=680mm, figure A3.22, transition is underway and the near wall intermittency has a value of 0.12. The bulk of the flow, which is laminar, still appears to be separated with a shape factor of about 3.5 and a velocity profile which is highly inflectional. The turbulent component velocity profile is typical of a fully turbulent boundary layer in a severe adverse pressure gradient, however it appears to be attached. Thus it would seem that developing turbulent spots can remain attached in a separating laminar flow from an early stage in the transition process. This would lead to the observation of intermittent laminar separation in the transition region. A similar pattern is observed at the next point, x=691mm, figure A3.23, but because of the increased proportion of turbulent flow, the mean velocity profile is less severely inflectional than the laminar component. At x=695mm, figure A3.24, the laminar profile is still inflectional and has a shape factor of 3.2, indicating that it may still be separated, but because the intermittency is almost 0.5, the mean velocity profile no longer has a point of inflection. As the turbulence becomes the dominant flow regime the laminar component profiles become more stable as can be seen in figures A3.25 to A3.28. The turbulent boundary layer is much more resistant to adverse pressure gradients than the laminar boundary layer as is illustrated by the profiles in figures A3.29 to A3.32. These profiles show some effect of the adverse pressure gradient but are obviously in no imminent danger of separating.

As the turbulence level is increased the start of transition

is brought forward. This is shown in figure 5.23 which also includes data from Sharma et al (1982). Since the end of transition is not affected as much, the transition length increases as shown in figure 5.24. Bringing the start of transition forward ultimately means that the start of transition occurs before the point of laminar separation and the growth of the turbulent spots can prevent separation as in flow 6 and possibly flow 5. In both flows 5 and 6 the mean profiles show slight inflections prior to the start of transition. After the start of transition the inflection becomes more marked in the mean and laminar profiles, see figures A3.68, A3.69 and A3.86. Again, however, as the turbulence occupies increasingly more of the flow the laminar flow becomes stabilised while an attached turbulent boundary layer eventually emerges.

5.4.3 Flow 7

The velocity distribution of flow 7 is shown in figure A2.13 in appendix 2 and the integral parameters are shown in figures A2.14 and A2.15. The velocity profiles are shown in figures A3.103 to A3.113 in appendix 3. The momentum thickness Reynolds number exhibits similar behaviour through transition to flows 1 to 6. The shape factor also behaves similarly to flows 1 to 6 although the shape factor for the laminar component profile rises more sharply than the mean value after the pressure gradient changes from favourable to adverse. The shape factor for the turbulent component profile seems to be unaffected by the change in pressure gradient and the remaining laminar flow becomes stabilised by the increasing proportion of turbulent flow. The velocity profiles show

that the laminar component profile becomes slightly inflectional between x=750, figure A3.110, and x=780, figure A3.111, but this does not lead to laminar separation before the boundary layer becomes fully turbulent.

DATA SUMMARIES

FLOW	Tu	x_s (mm)	x_t (mm)	θ_t (mm)	$R\theta_t$	λ (mm)	$R\lambda$	-m
1	1.00	663	669	0.56	525	23	21563	0.129
2	1.06	670	673	0.60	560	17	15867	0.148
3	1.08	669	679	0.58	530	16	14621	0.138
4	1.12	658	663	0.56	510	17	15482	0.129
5	1.53	610	634	0.57	525	30	27632	0.133
6	2.06	564	592	0.53	500	51	48113	0.115

Table 5.1 Summary of transition data

	measured	Abu-Ghannam and Shaw	
FLOW	$R\theta_t$	Tu (L.E.)	$Tu(x_t)$
1	525	381	507
2	560	381	529
3	530	368	511
4	510	359	507
5	525	296	434
6	500	245	397

Table 5.2 Comparison of measured and predicted values of R_{θ_t}

x_t (mm)	625
θ_t (mm)	0.34
λ (mm)	68
m	0.027

Table 5.3 Data for flow 7

FLOW	λ (meas)	λ (eqn 5.5)
1	23	11
2	17	8
3	16	11
4	17	11
5	30	11
6	51	13

Table 5.4 Measured and calculated values of λ

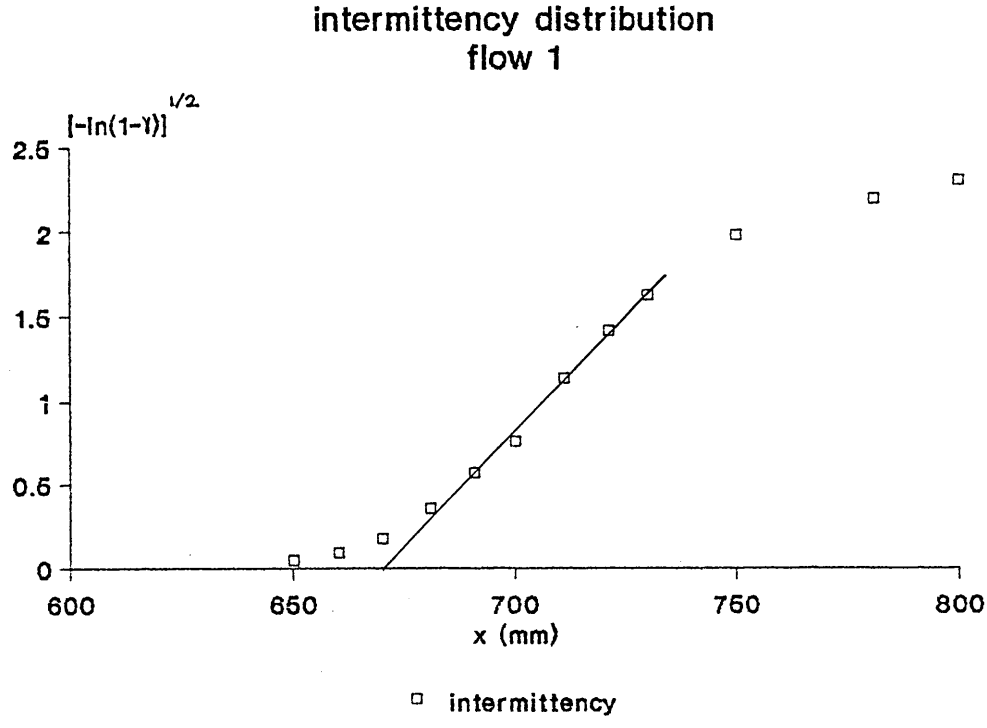

figure 5.1

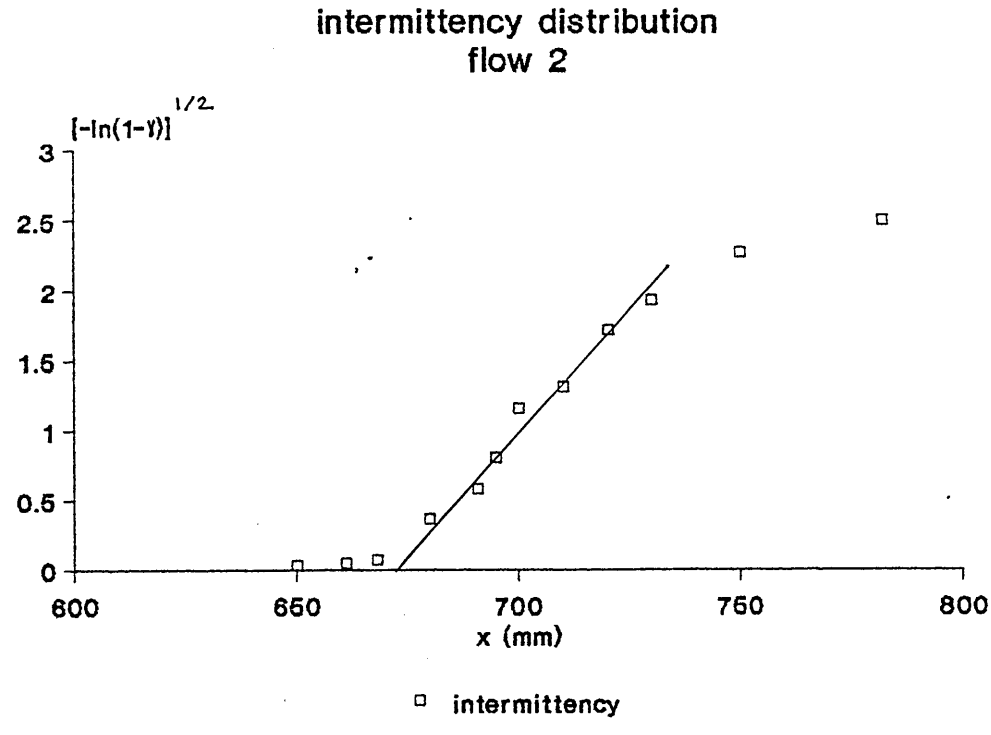

figure 5.2

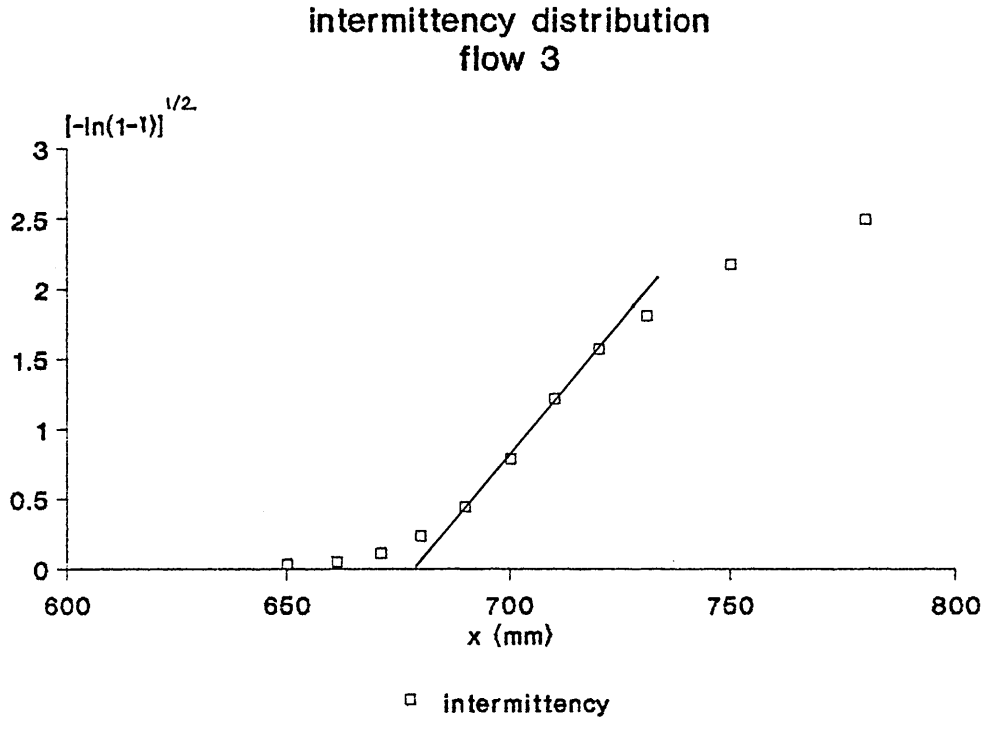

figure 5.3

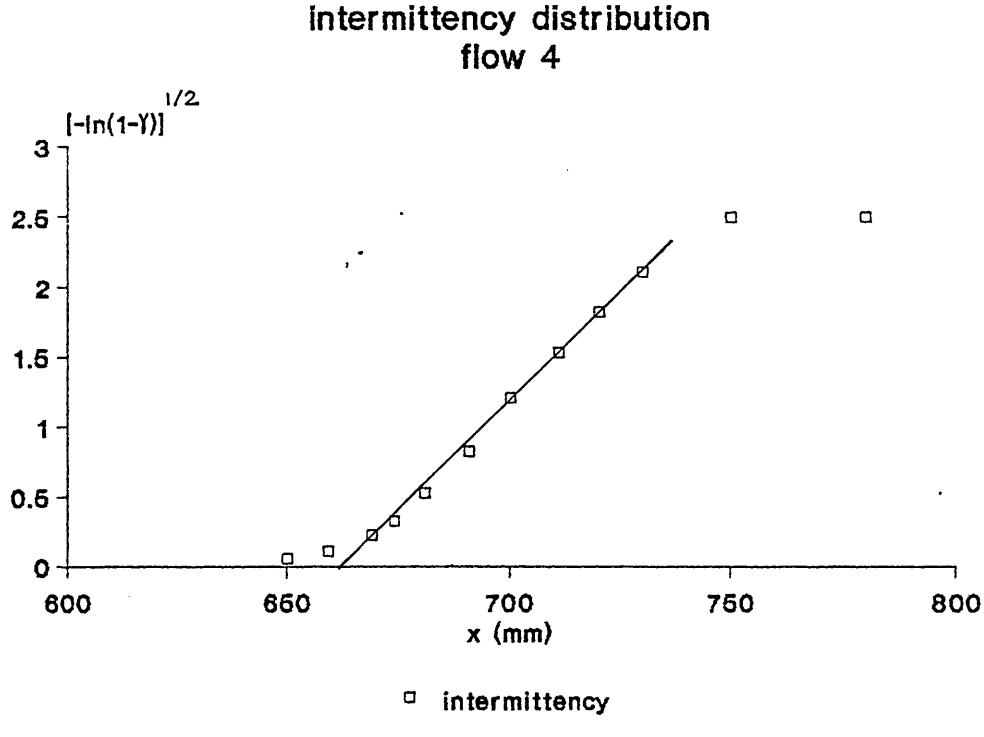

figure 5.4

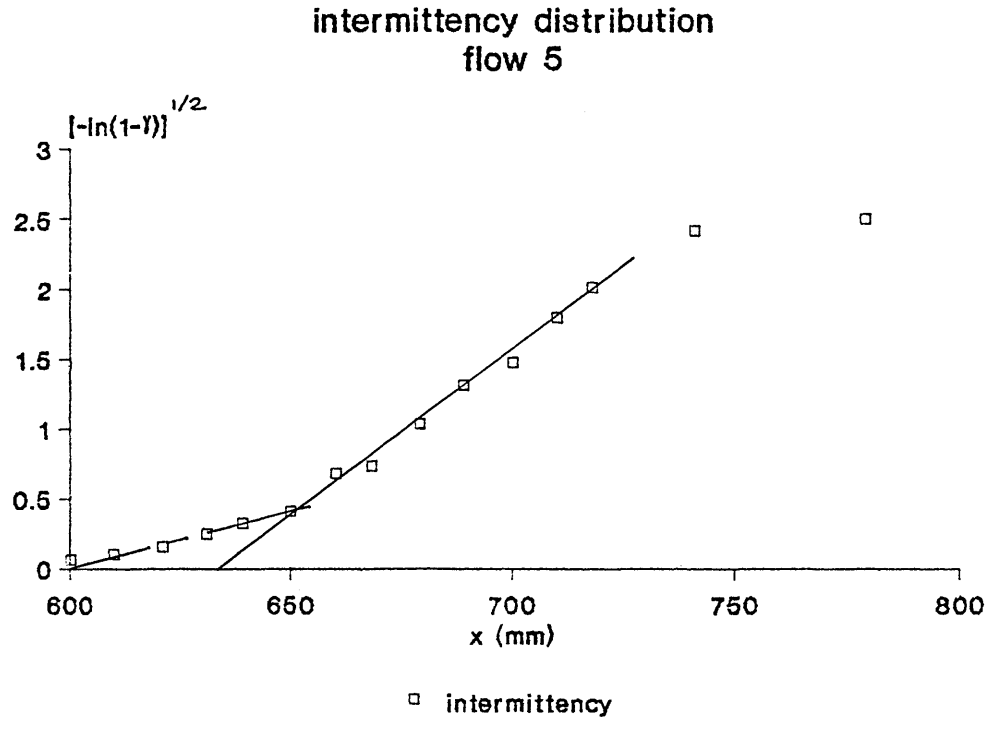

figure 5.5

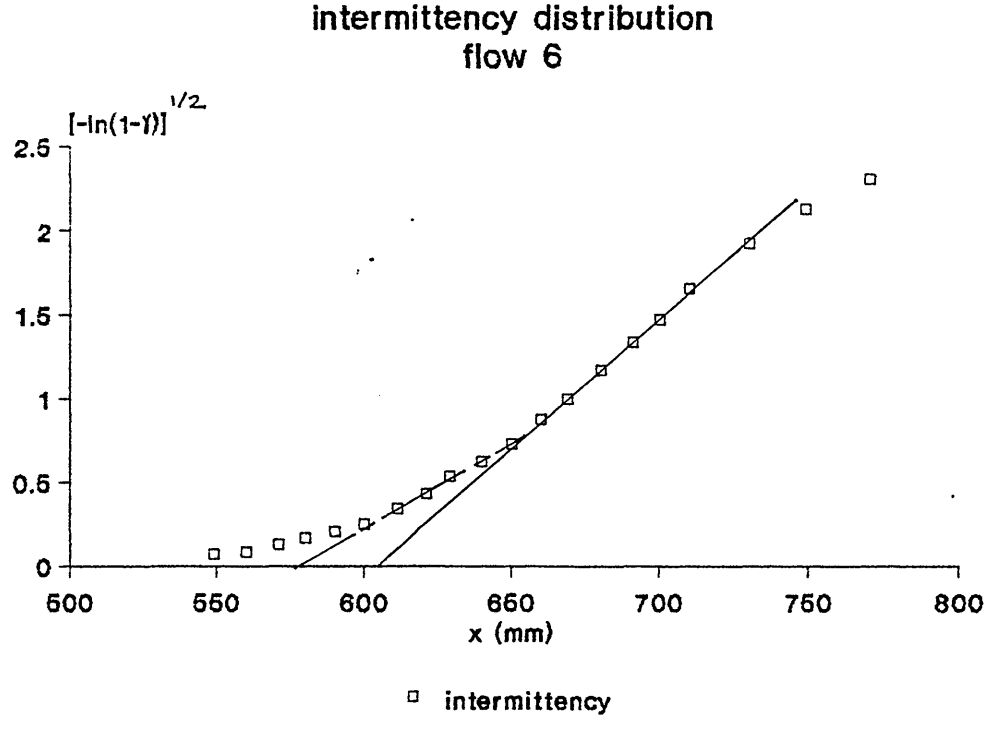

figure 5.6

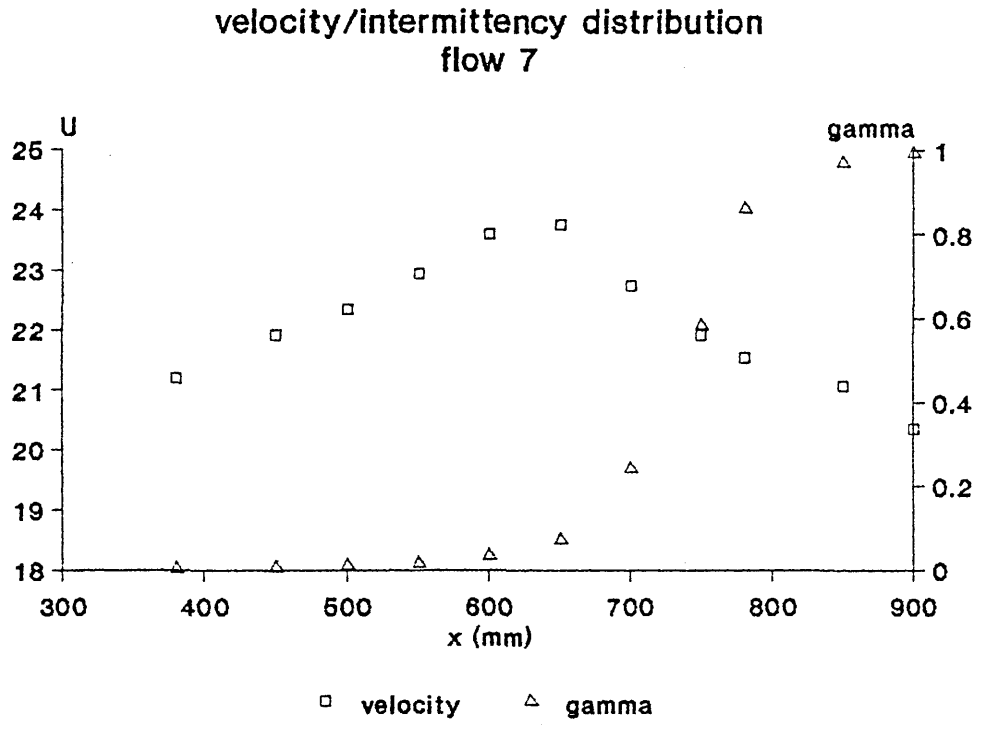

figure 5.7a

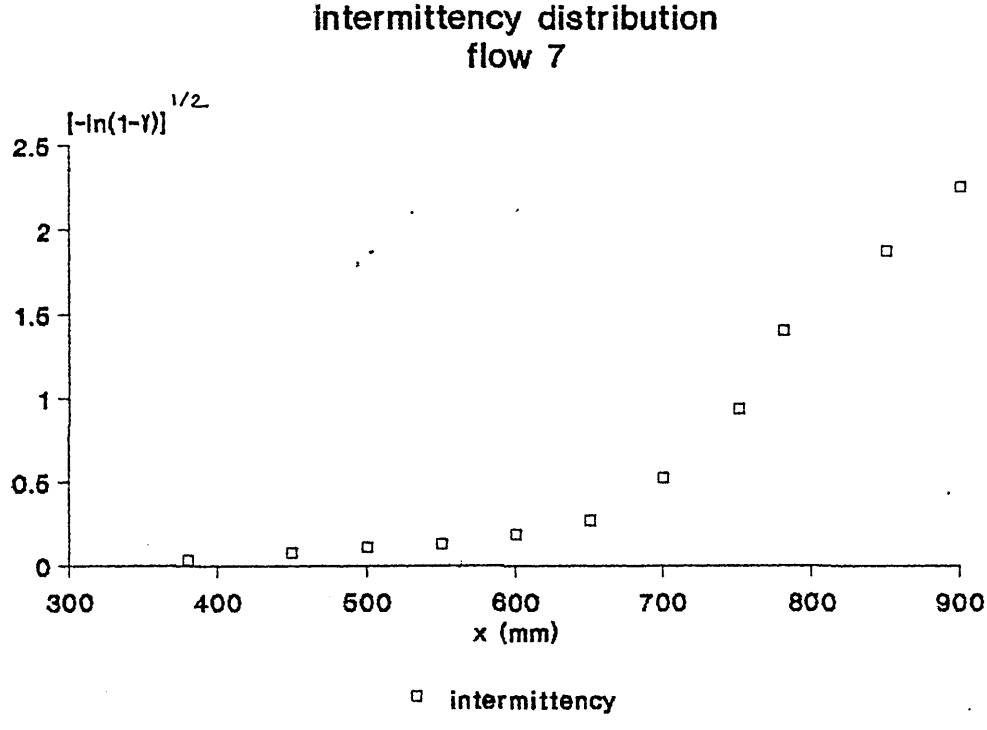

figure 5.7b

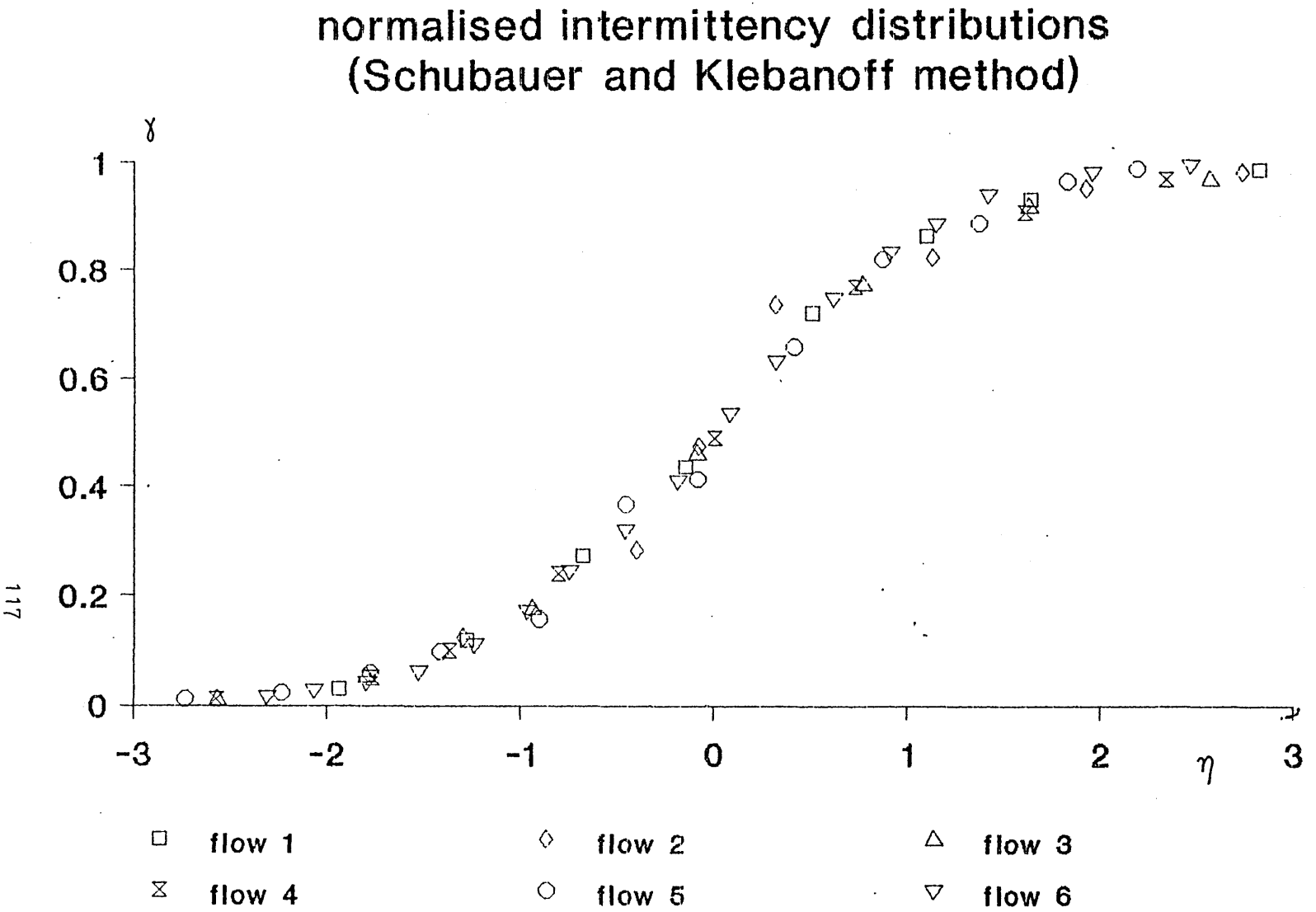
normalised intermittency distributions
(Schubauer and Klebanoff method)
γ
1
0.8
0.6
0.4
0.2
0
-3
-2
-1
0
1
2
3
η
flow 1
flow 2
flow 3
flow 4
flow 5
flow 6

figure 5.8

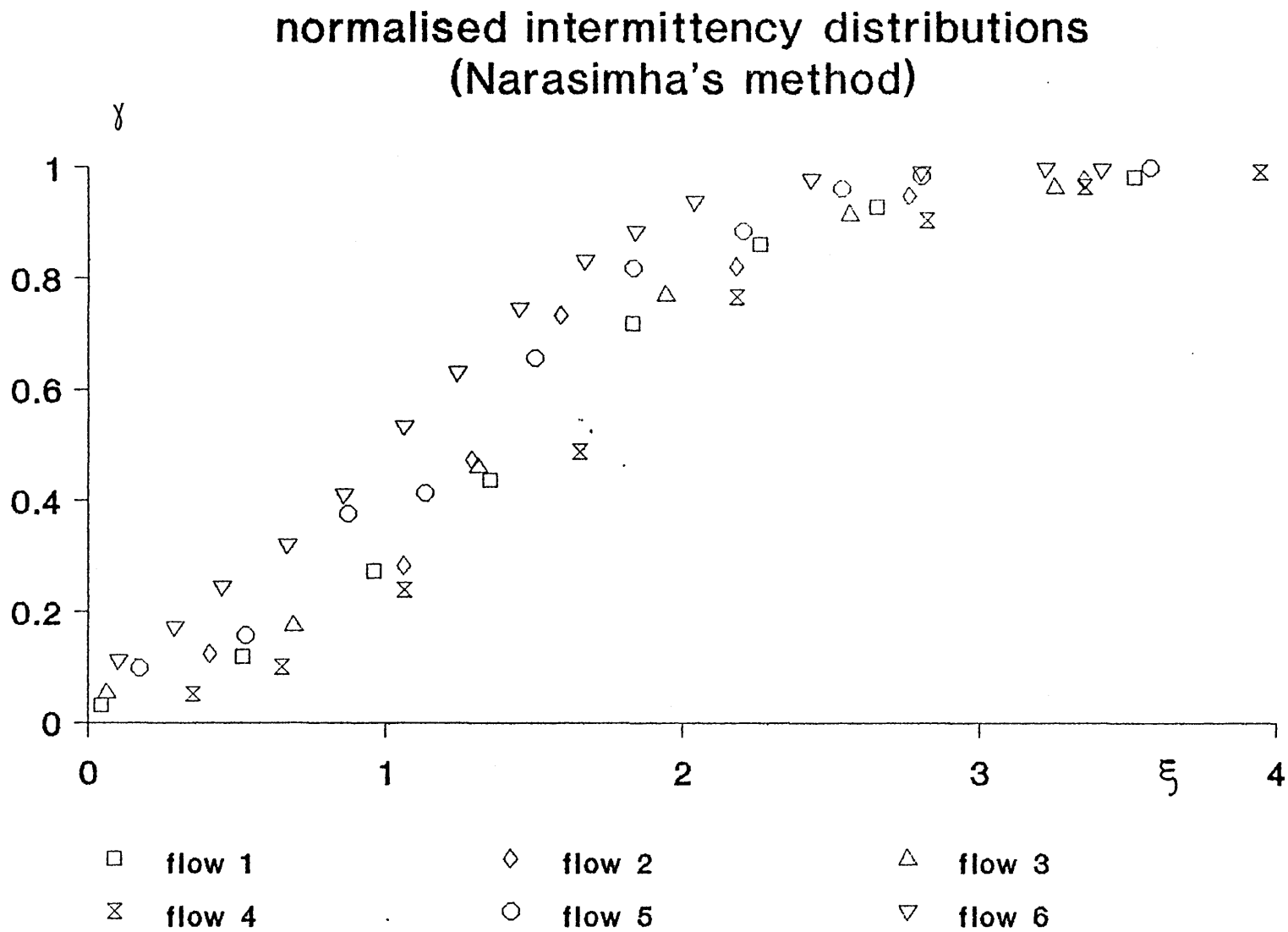
normalised intermittency distributions
(Narasimha's method)
γ
1
0.8
0.6
0.4
0.2
0
0
1
2
3
ξ
4
flow 1
flow 2
flow 3
flow 4
flow 5
flow 6

figure 5.9

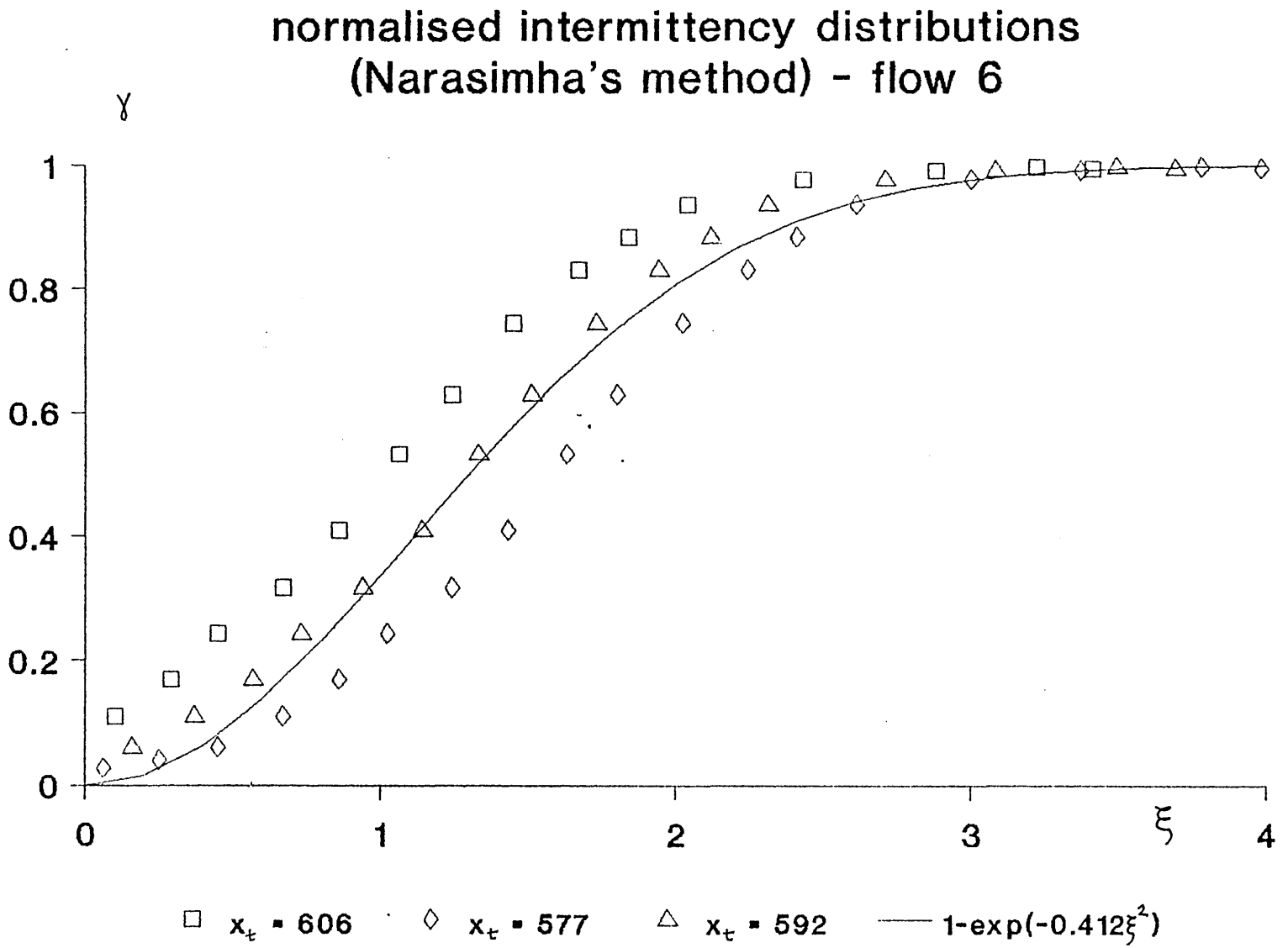
normalised intermittency distributions
(Narasimha's method) - flow 6
γ
1
0.8
0.6
0.4
0.2
0
0
1
2
3
ξ
4
□ x_t = 606
◇ x_t = 577
△ x_t = 592
1-exp(-0.412ξ^2)

figure 5.10

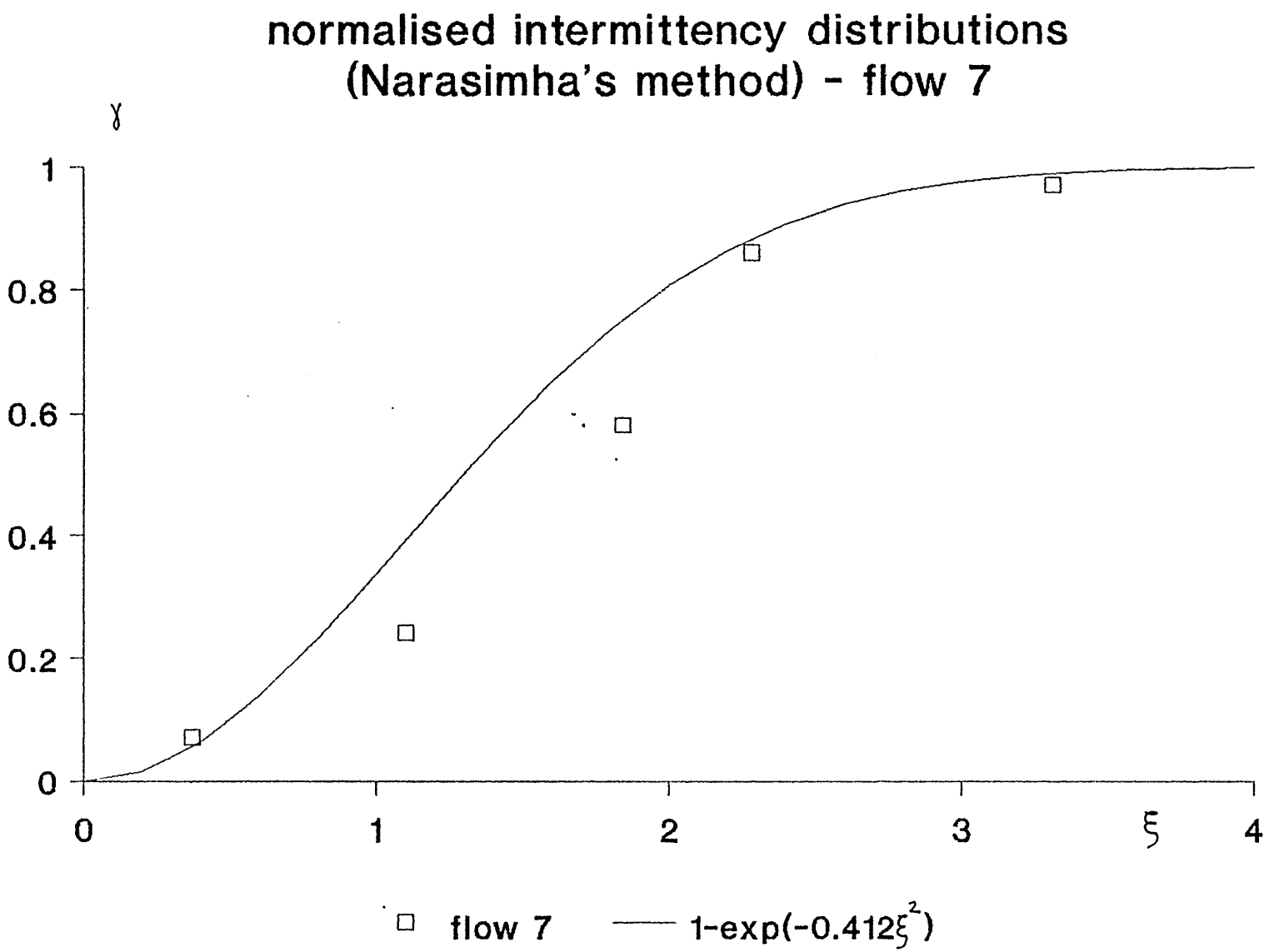
normalised intermittency distributions
(Narasimha's method) - flow 7
γ
1
0.8
0.6
0.4
0.2
0
0
1
2
3
ξ
4
flow 7
1-exp(-0.412ξ²)

figure 5.11

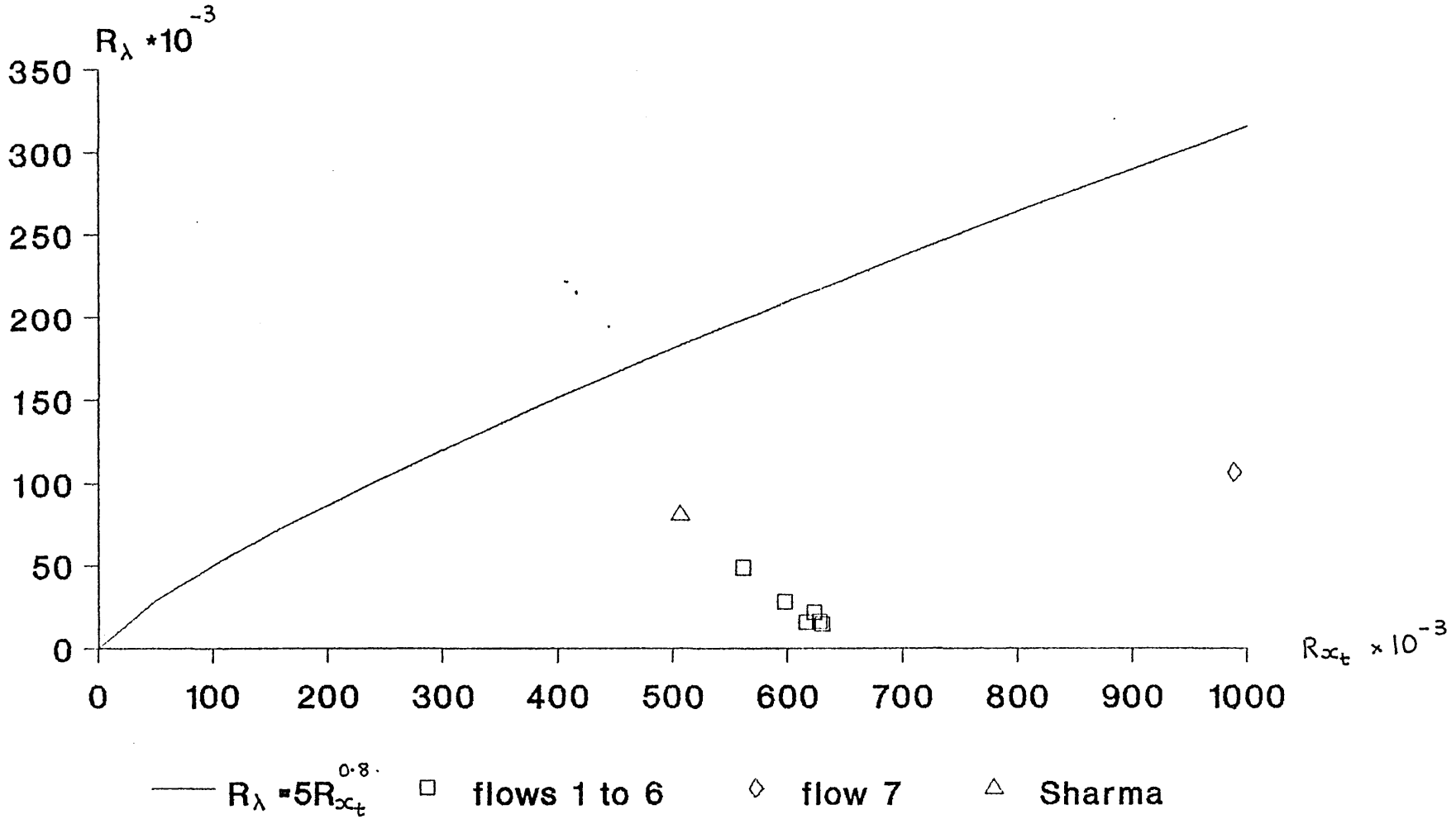
transition length correlation of
Dhawan and Narasimha
$R_\lambda * 10^{-3}$
350
300
250
200
150
100
50
0
0
100
200
300
400
500
600
700
800
900
1000
$R_{\alpha_t} \times 10^{-3}$
$R_\lambda = 5R_{\alpha_t}^{0.8}$
flows 1 to 6
flow 7
Sharma

figure 5.12

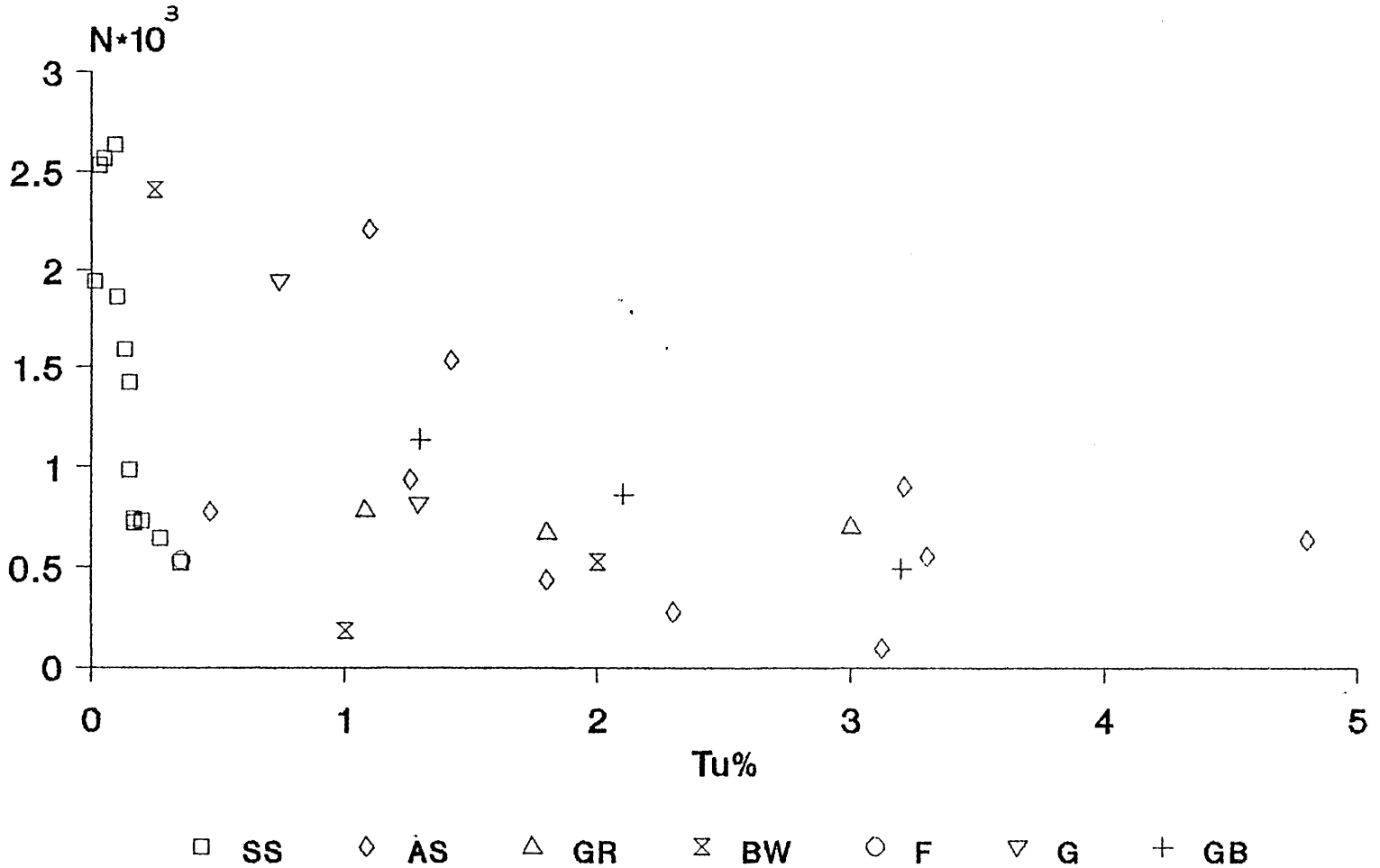
spot formation rate in
zero pressure gradient
N*10^3
3
2.5
2
1.5
1
0.5
0
0
1
2
3
4
5
Tu%
SS
AS
GR
BW
F
G
GB

figure 5.13

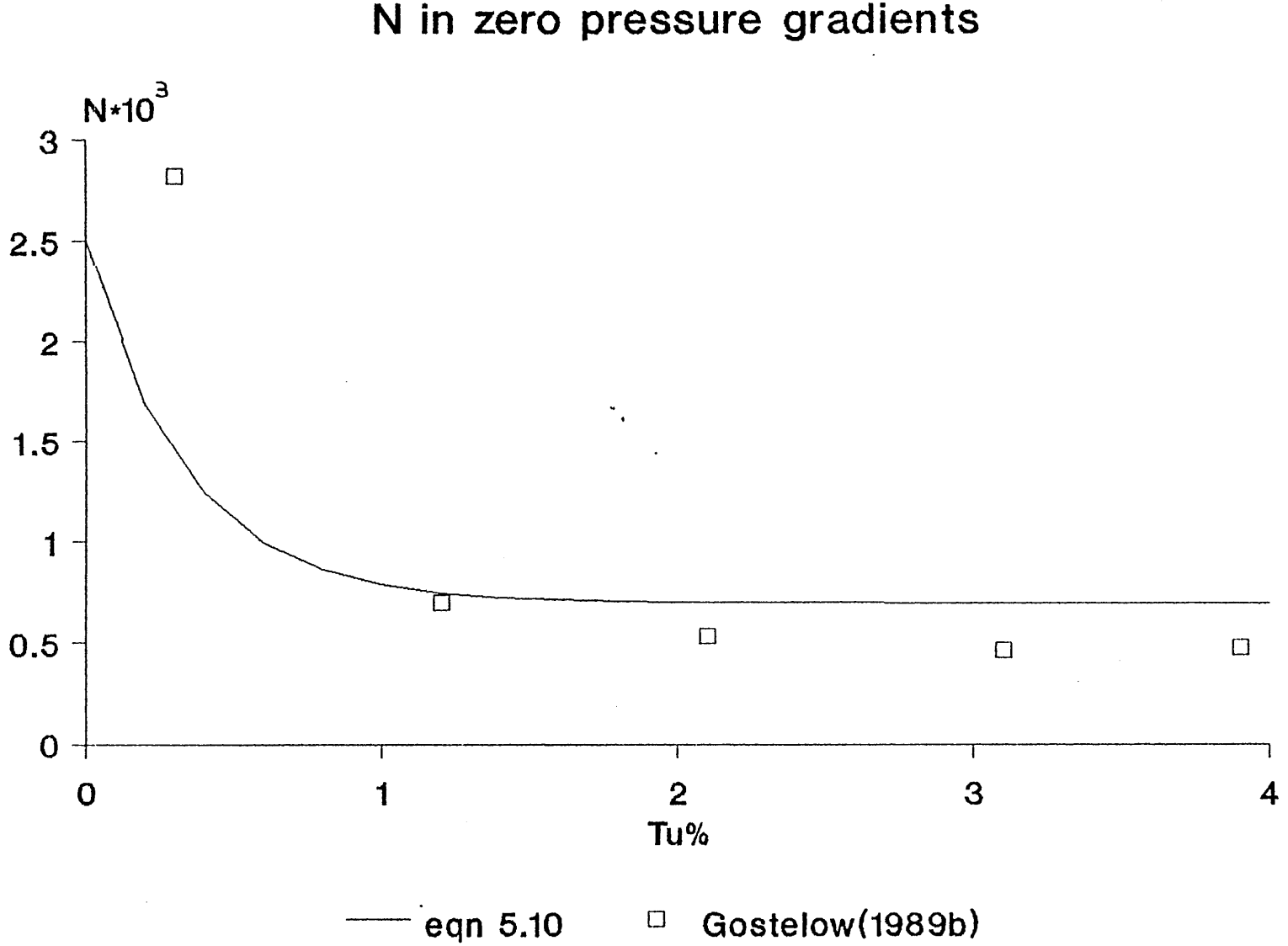
N in zero pressure gradients
N*10^3
3
2.5
2
1.5
1
0.5
0
0
1
2
3
4
Tu%
eqn 5.10
Gostelow(1989b)

figure 5.14

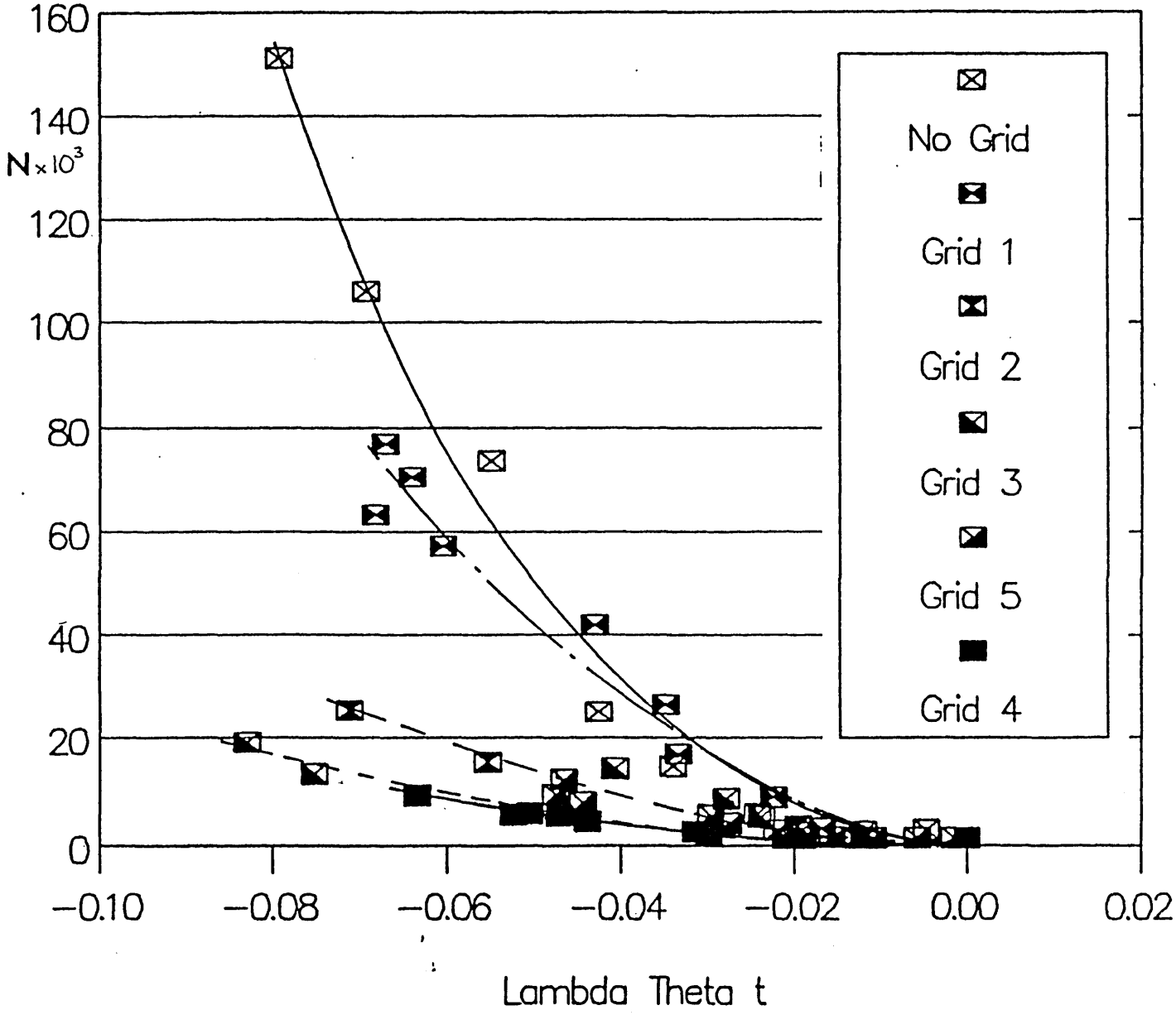

figure 5.15 data of Gostelow (1989b)

N against Tu% at constant pressure gradient parameter, m

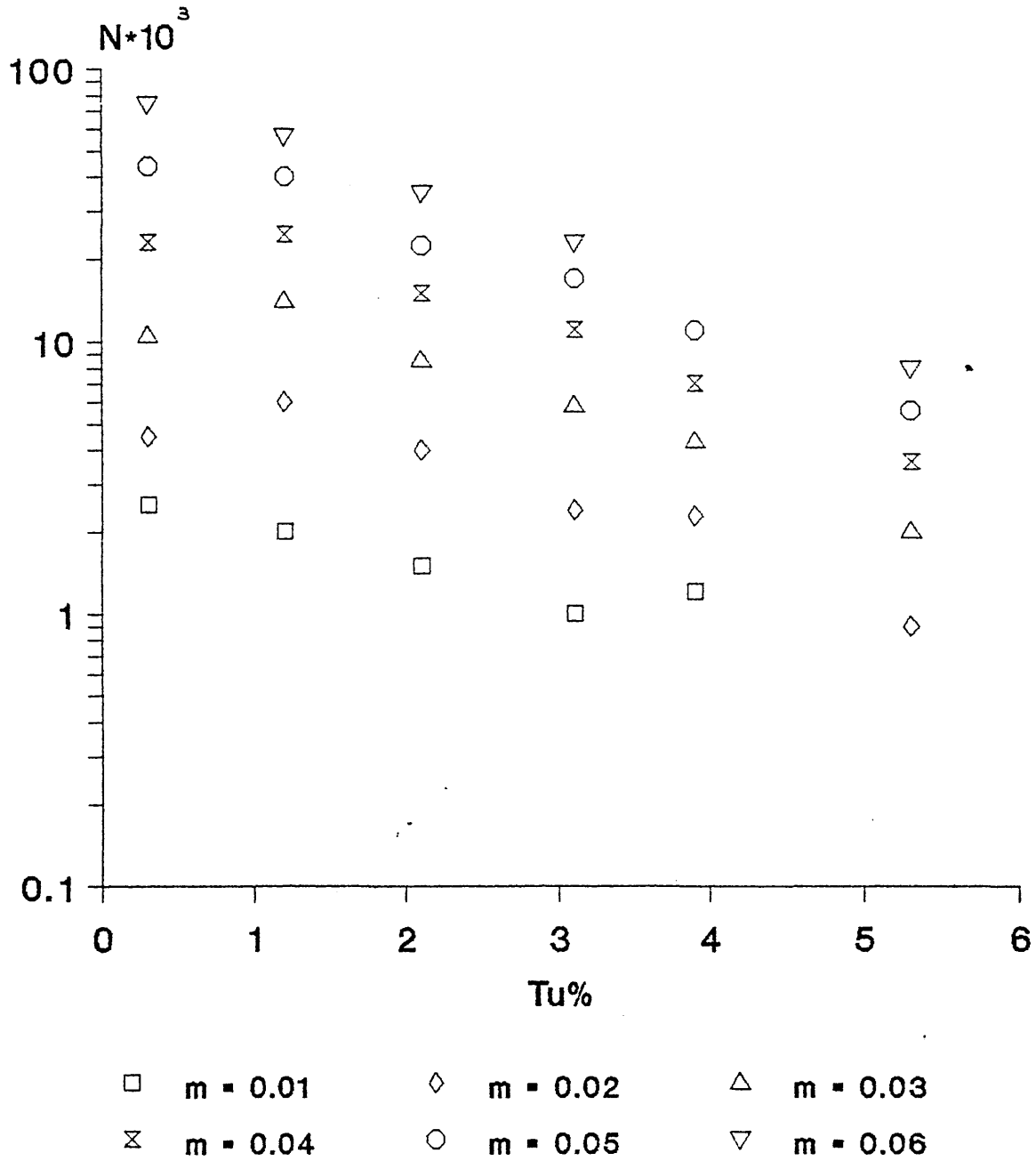

figure 5.16

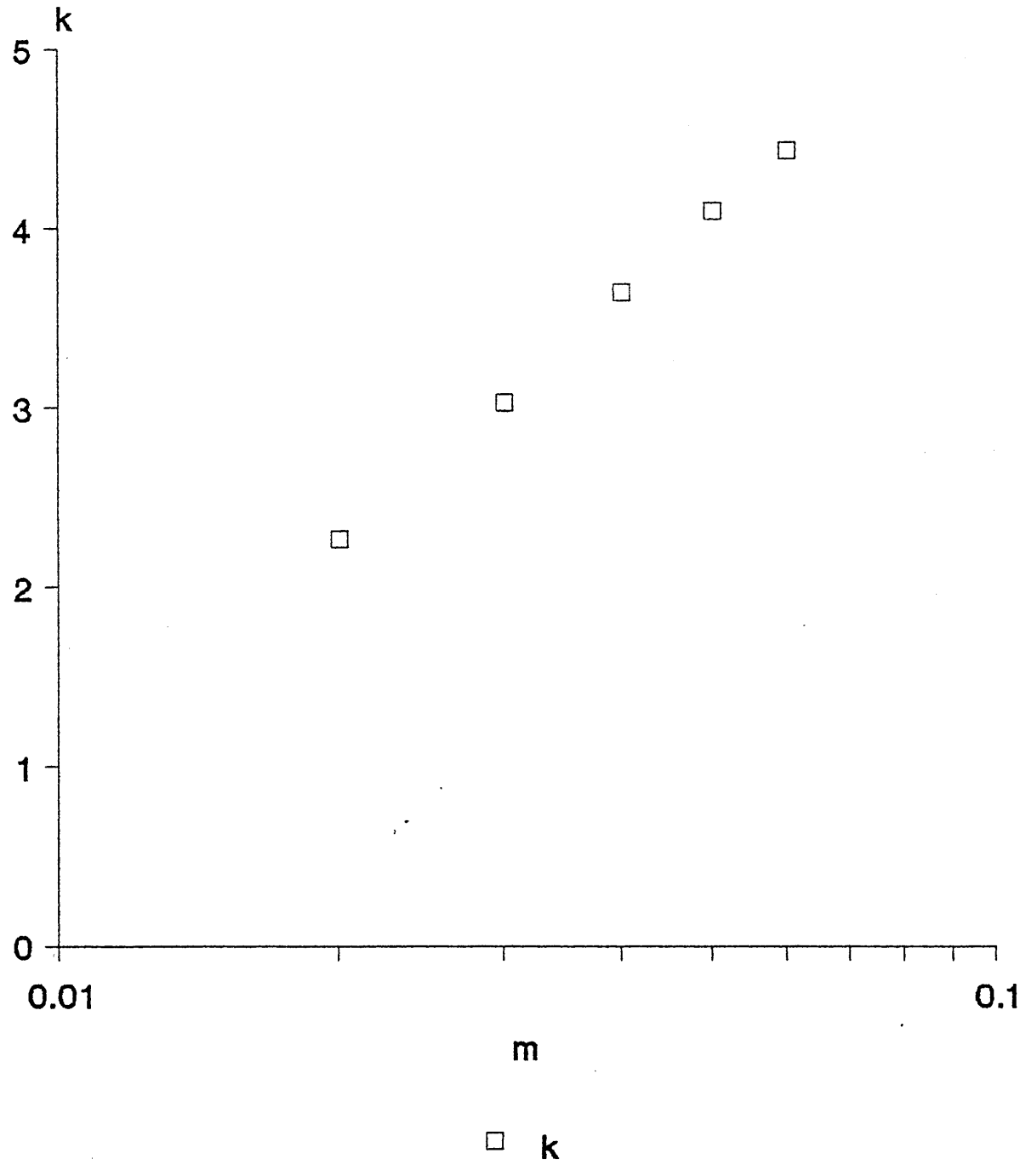

figure 5.17

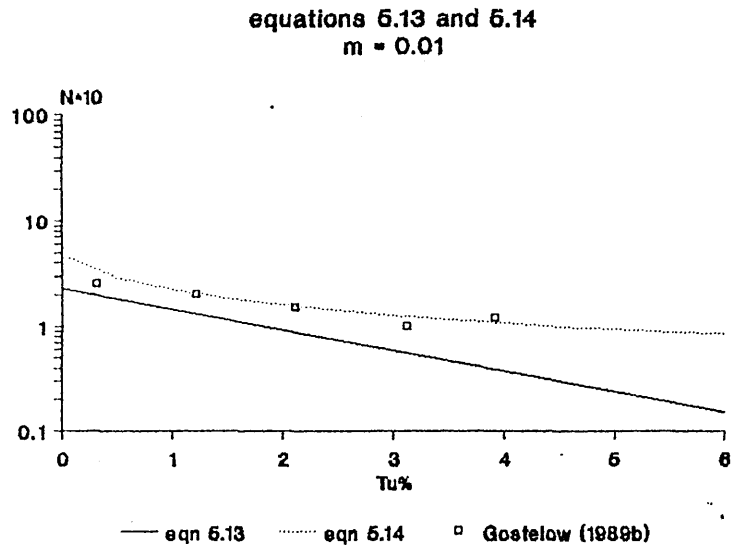

figure 5.18a

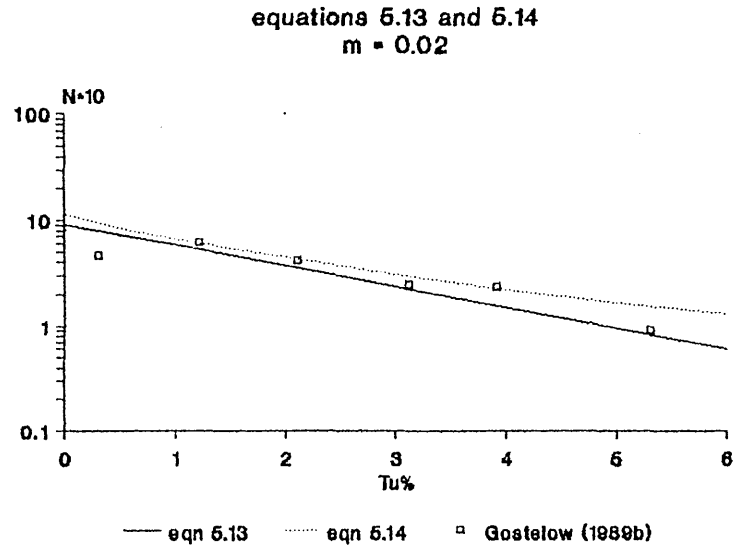

figure 5.18b

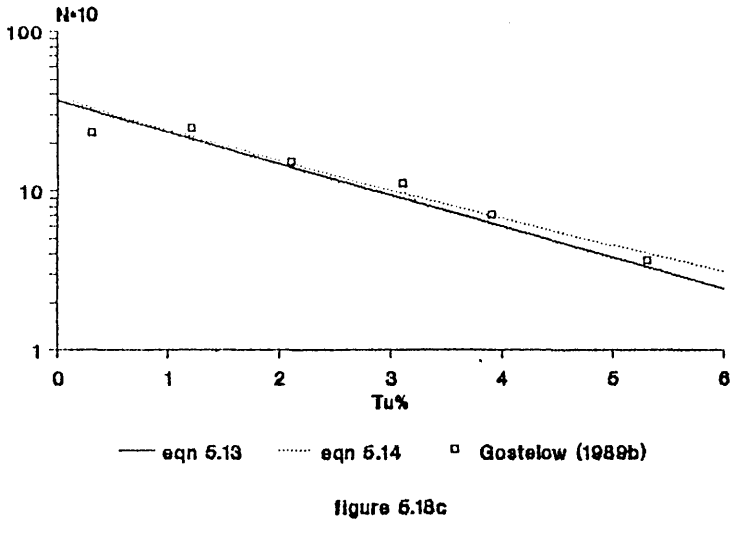

figure 5.18c

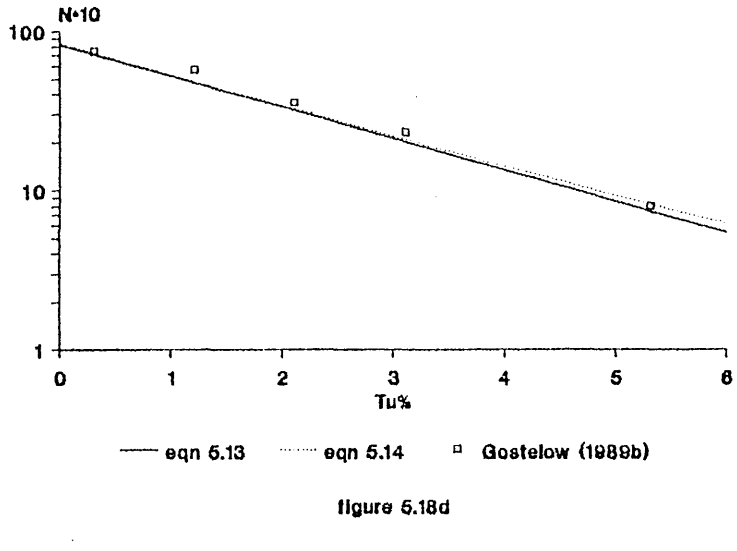

figure 5.18d

figure 5.19 data of Gostelow (1989b) plotted against equation 5.14

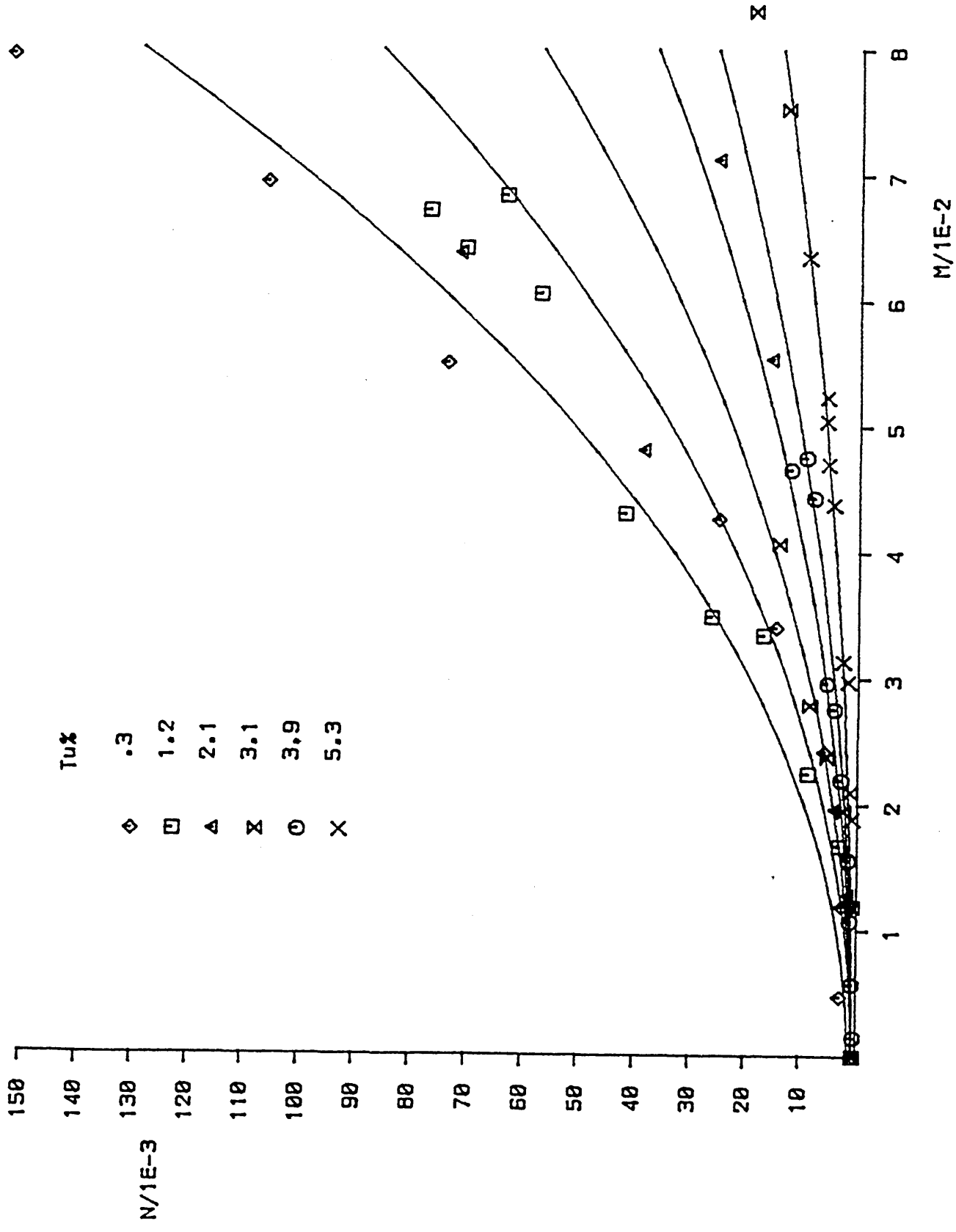

figure 5.20 data of Gostelow (1989b) plotted against equation 5.14

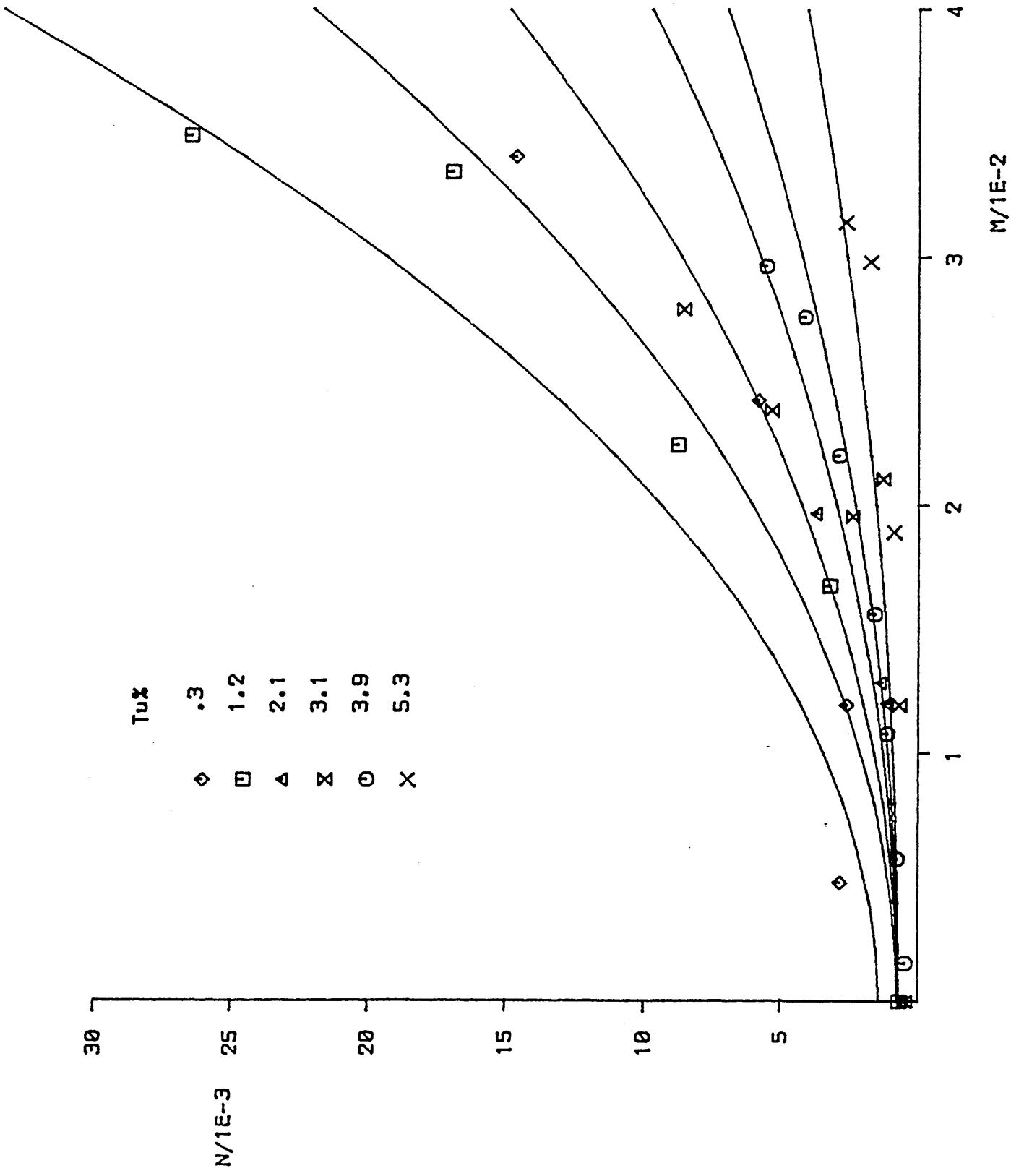

figure 5.21 present data plotted against equation 5.14

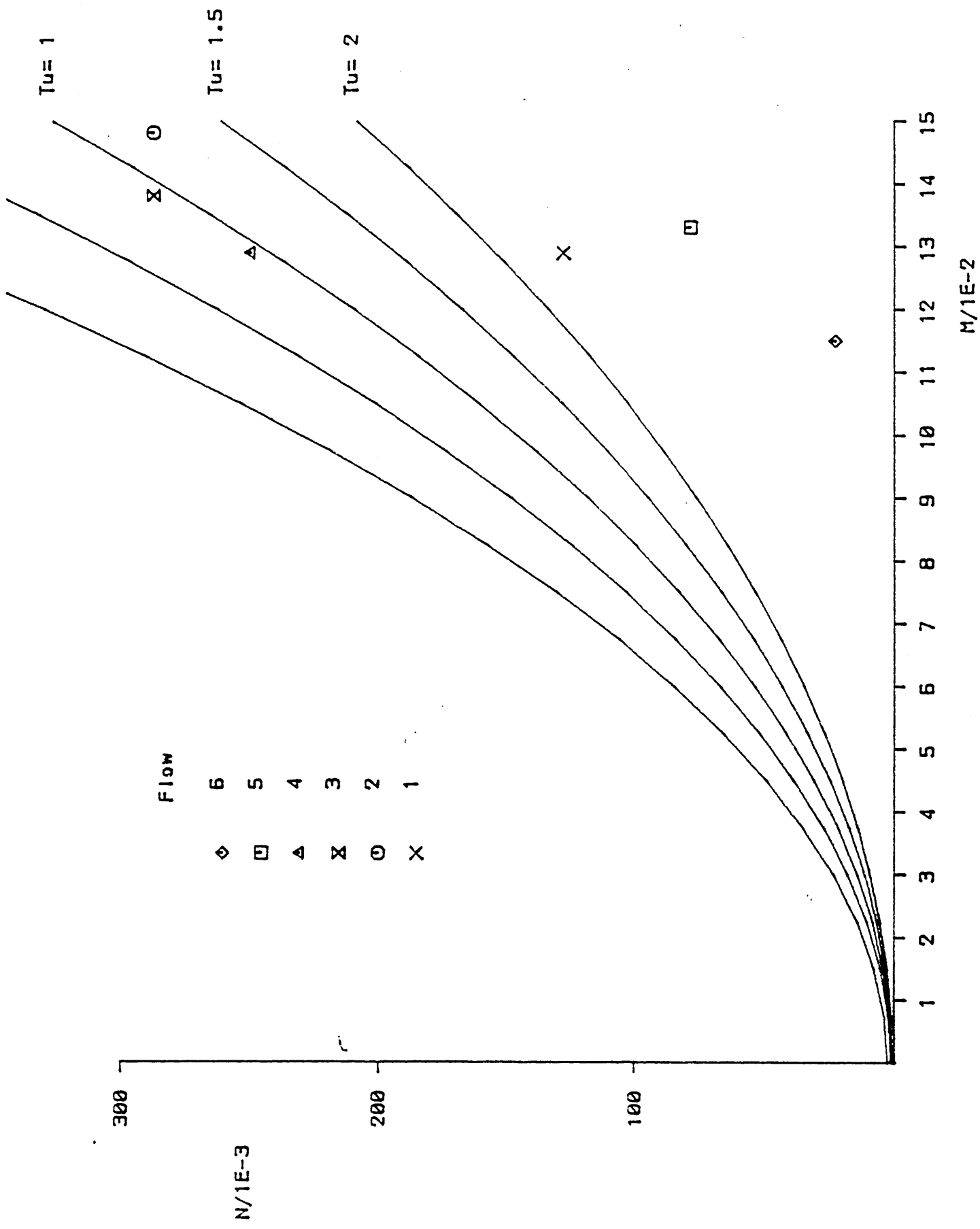

figure 5.22 data of Gardiner (1987) plotted against equation 5.14

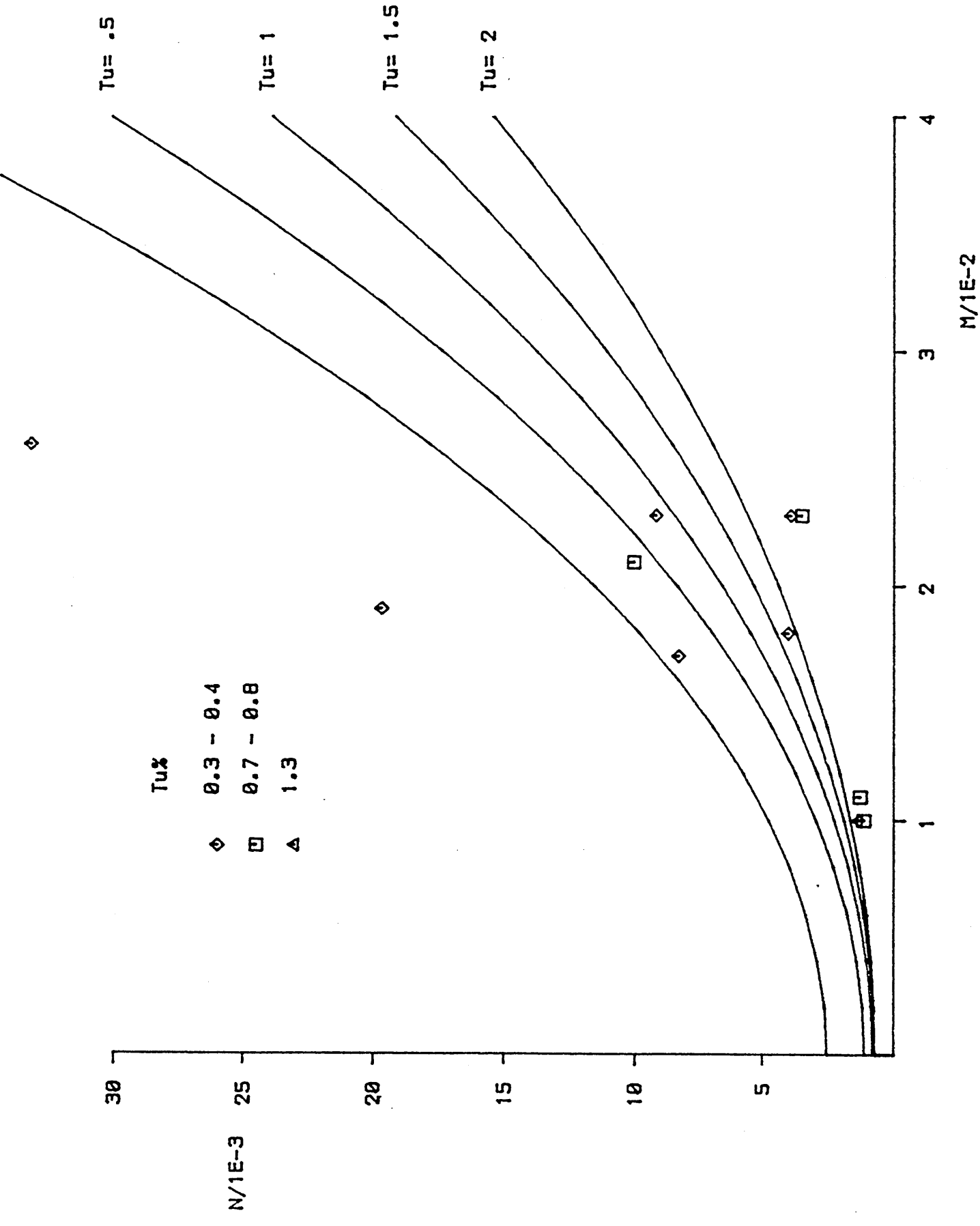

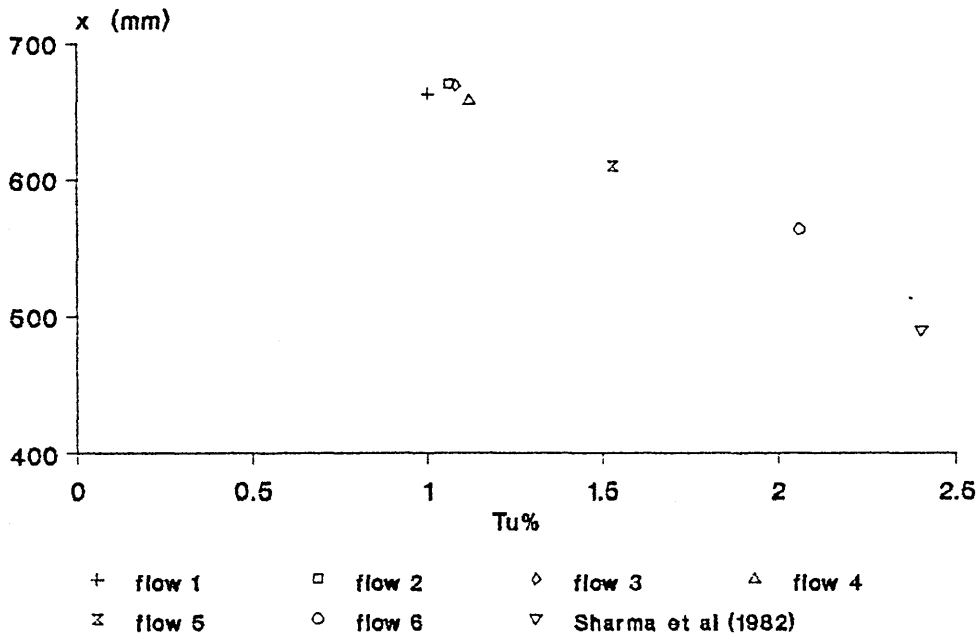

figure 5.23

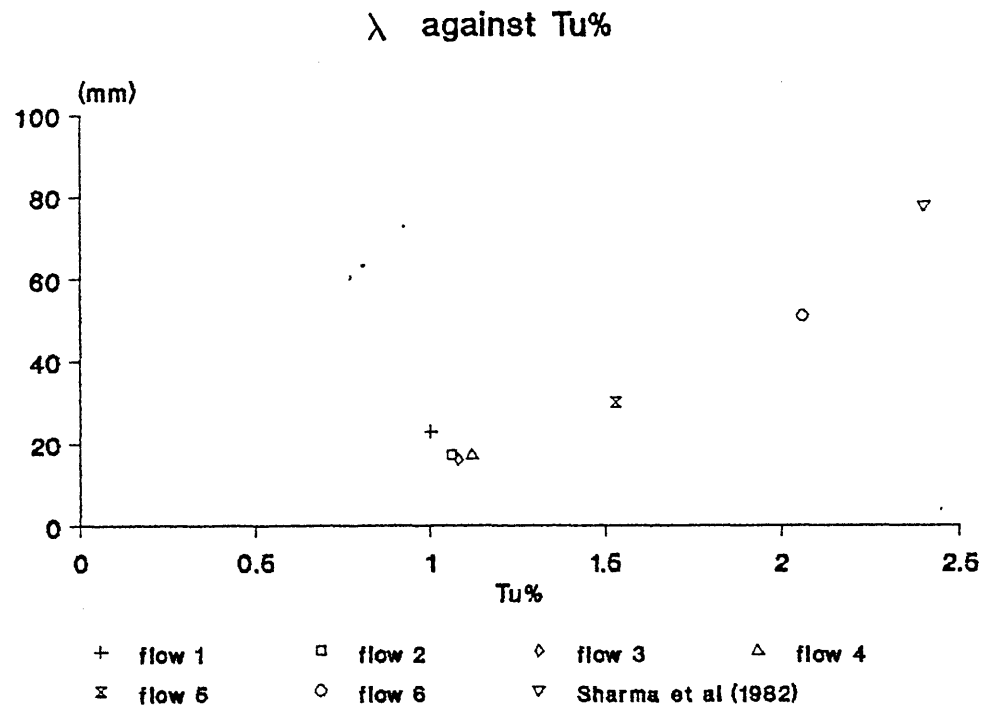

figure 5.24

CHAPTER 6

BOUNDARY LAYER PREDICTION

The so called differential methods of solving the boundary layer equations, which solve the basic partial differential equations numerically, have been developed over the last thirty years. These methods have largely been programmed to run on mainframe or mini computers because of the considerable number of calculations which are required for even fairly simple analyses. However modern microcomputers are having an impact in numbercrunching applications as well as other areas, such as data acquisition. The newer microcomputers have sufficient memory capacity to allow realistic problems to be defined and faster processing speeds allow solutions to be obtained in acceptable times. Thus it is now practical to use differential methods for routine design calculations in many cases. A proven method, which is applicable to laminar and turbulent boundary layers, is that of Cebeci and Smith (1974). This method uses the so called box method due to Keller (1970). A Fortran program for this method is given by Cebeci and Bradshaw (1977) and this was adapted to run, in compiled BASIC, on the Amstrad PC1640 microcomputer. The next section gives a very brief description of the method.

6.1 THE CEBECI-SMITH METHOD

The x-momentum equation can be written for two dimensional, laminar or turbulent boundary layers as

$$u\frac{\partial u}{\partial x} + v\frac{\partial u}{\partial y} = U\frac{dU}{dx} + \frac{1}{\rho}\frac{\partial}{\partial y}\left[\mu\frac{\partial u}{\partial y} + \rho\epsilon\frac{\partial u}{\partial y}\right] \qquad (6.1)$$

where ϵ is the eddy viscosity, which is zero in laminar flow. Equation 6.1 is transformed using the Falkner-Skan transformation. The advantage gained is that the boundary layer thickness in

transformed coordinates remains almost constant in laminar flow and the rate of growth is much reduced in turbulent flow. This means that a relatively simple grid representation can be employed.

The Falkner-Skan transformation is defined by

$$\eta = \left(\frac{U}{\nu x}\right)^{0.5} y \tag{6.2}$$

and a dimensionless stream function, $f(x,\eta)$, is introduced

$$\psi(x,y) = (U \nu x)^{0.5} f(x,\eta) \tag{6.3}$$

After some manipulation equation 6.1 becomes

$$(bf'')' + \left(\frac{m+1}{2}\right) ff'' + m[1 - (f')^2] = x\left[f'\frac{\partial f'}{\partial x} - f''\frac{\partial f}{\partial x}\right] \tag{6.4}$$

where $b = (1 + \epsilon^+)$, with $\epsilon^+ = \epsilon/\nu$ and $m = \frac{x}{U}\frac{\partial U}{\partial x}$ and the prime, $'$, denotes differentiation w.r.t. η

Equation 6.4 is then written as a system of first order P.D.E.s ie.

$$f' = u \tag{6.5a}$$

$$u' = v \tag{6.5b}$$

$$(bv)' + \left(\frac{m+1}{2}\right) fv + m(1-u^2) = x\left[u\frac{\partial u}{\partial x} - v\frac{\partial f}{\partial x}\right] \tag{6.5c}$$

Equations 6.5 are then written in finite difference form using "centred difference" derivatives. An arbitrary grid is assumed in the formulation of the finite difference equations which allows varying step sizes to be used when solving particular problems. The equations are implicit and non linear and are solved using Newton's method. This is carried out using the block elimination method as discussed by Keller (1974) and described in detail by Cebeci and Bradshaw (1977). For laminar boundary layers

the eddy viscosity, ϵ, is zero and the solution of equations 6.5 becomes a purely mathematical problem. Great accuracy can be achieved by using suitable grids and a number of test cases are examined in chapter 8 of Cebeci and Smith (1974).

Predicting turbulent boundary layers is considerably more difficult than predicting laminar boundary layers. Turbulent boundary layers tend to be much thicker than laminar boundary layers yet the velocity gradient, $\partial u/\partial y$, can be greater at the wall. This requires that short steps be taken, in the y direction, close to the wall which would lead to large numbers of points if a constant grid was used. However, because the Cebeci-Smith method allows for an arbitrary grid it is advantageous to use a geometric progression in the y (or η in the transformed equations) direction. This allows fine resolution to be used close to the wall but the spacing becomes larger away from the wall giving an economical number of grid points across the boundary layer. Similarly, varying resolution can be employed in the x direction eg. using finer resolution near separation.

The turbulent boundary layer equations are further complicated by the existance of fluctuation terms, the so called Reynolds stresses. The Reynolds stress terms cannot be obtained analytically and must be modelled. The Cebeci-Smith method uses an eddy viscosity method which relates the Reynolds stresses to the mean flow ie.

$$-\rho\overline{u'v'} = \rho\epsilon\frac{\partial u}{\partial y} \qquad (6.6)$$

The turbulent boundary layer is treated as a composite layer with inner and outer regions and separate expressions are given for the

eddy viscosity in each region. In the inner region the eddy viscosity is defined by a "mixing length" type equation

$$\epsilon_i = L^2 \left|\frac{\partial u}{\partial y}\right| \gamma , \qquad 0 \le y \le y_c \tag{6.7}$$

The mixing length, L, is given by an extended version of Van Driest's model, see Cebeci and Smith (1974). In the transition region the eddy viscosity is weighted by the intermittency and thus affects only the first term in equation 6.4. This is only an approximation since equation 6.4 is non linear but it has been widely used and found to be reliable. A more correct approach would be to solve equation 6.4 separately for the laminar and turbulent components of the flow, and weight the solutions using the intermittency. This is effectively the same technique as that employed by Fraser and Milne (1986) and others for integral methods in that the transitional boundary layer is considered to be a weighted combination of laminar and fully turbulent boundary layers. In the outer region the eddy viscosity is defined by

$$\epsilon_o = \alpha \left| \int_o^\infty (U - u) dy \right| \gamma , \qquad y_c \le y \le \delta \tag{6.8}$$

where α is taken as a universal constant, $\alpha = 0.0168$. y_c is defined as the point where $\epsilon_i = \epsilon_o$.

Because of the difficulty of predicting the location of the start of transition this is normally treated as a direct input. The Cebeci-Smith method uses the method of Chen and Thyson (1971) to calculate the length of the transition region and the intermittency distribution. This method has been found to fare rather poorly when predicting turbine blade flows, usually predicting transition lengths which are far too long. This method is compared, in the

next section, with an alternative based on the correlation described in the previous chapter. Equations 5.10 and 5.14 are used to determine the value of N at the start of transition using the inlet turbulence level and the local pressure gradient parameter. The transition length, in terms of λ, is then obtained from equation 5.7 or 5.8 and the intermittency distribution is given by equation 1.5.

6.2 PERFORMANCE OF THE C-S METHOD

The Cebeci-Smith method has been shown to be reliable for a wide range of laminar and turbulent flows. See, for example, Cebeci and Bradshaw (1977). The method is now compared with some of the present experimental data ie. flow 6. For the present velocity distribution the C-S method predicts laminar separation at about x = 590mm. This ties up with the observation that flows 1 to 5 all exhibit laminar separations prior to the start of transition since the start of transition is later than x = 590mm in all cases (whether defined as x_s or x_t). Although x_t is 592mm in flow 6, x_s is 564mm, therefore the flow will not be completely laminar at x = 590mm. After separation is encountered the C-S method fails since convergence can no longer be attained. Only flow 6 remains attached throughout and this is the only flow that can be calculated completely.

Flow 6 was calculated twice, using both the Chen and Thyson (1971) method and the procedure described in chapter 5 (equation 5.14) for the transition region. The results are shown in figures 6.1, 6.2 and 6.3. Figure 6.1 shows the intermittency distribution. It can be seen that the Chen and Thyson method predicts a much

longer transition region than is actually observed. Of all the present flows the measured value of N for flow 6 gives the poorest agreement with the correlation given by equation 5.14, see figure 5.21. In spite of this, the resulting prediction is an improvement over that obtained using the Chen and Thyson method. This is further illustrated by the predictions of shape factor and momentum thickness Reynolds number through transition, see figures 6.2 and 6.3. The poor performance of the method of Chen and Thyson in turbine blade flows can be attributed to the fact that the spot formation rate parameter, G, which is used, is correlated for zero pressure gradient data only.

Figures 6.4 to 6.14 compare measured mean velocity profiles with those calculated by the C-S method using equation 5.14 for the transition region. The laminar boundary layer is accurately predicted in the region of favourable pressure gradient, as can be seen in figure 6.4, and a fair prediction is obtained in the adverse pressure gradient region as shown in figures 6.5 to 6.7. The early stages of the transition region are not so well predicted, see figures 6.8 and 6.9, and because the predicted transition length is too short the calculated profiles "lead" the measured profiles in the development towards fully turbulent profiles, see figures 6.10 to 6.12. Finally, after transition, reasonable agreement is obtained in the fully turbulent boundary layer as shown in figures 6.13 and 6.14. Better prediction of the transitional velocity profiles may have been achieved by using the procedure described in the previous section ie. by calculating the laminar and turbulent components separately and weighting the solution. This would not, however, have affected the predicted

transition length or intermittency distribution. Future work may show whether the extra computational effort which would be involved is justified by improved accuracy.

The Cebeci-Smith boundary layer calculation method is commonly used to predict flows, such as those over turbine blades, which involve transition in adverse pressure gradients. By using equation 5.14 in conjunction with equations 5.7 and 1.5, which takes account of the effects of adverse pressure gradient, improved prediction of the transition region in such flows is achieved. It is possible to extend the C-S method to calculate separating and reattaching flows by using the so called inverse boundary layer approach, see for example Cebeci et al (1979). This approach requires, however, that the displacement thickness be specified in advance. Cebeci (1989) used the C-S method interactively with an inviscid method to calculate flows over aerofoils which included separation bubbles. Such a procedure should be applicable to flows 1 to 5 of the present work. The improvement of equation 5.14 over the Chen and Thyson model might be expected to be even more marked since the measured values of N for flows 1 to 5 were in better agreement with equation 5.14 than flow 6.

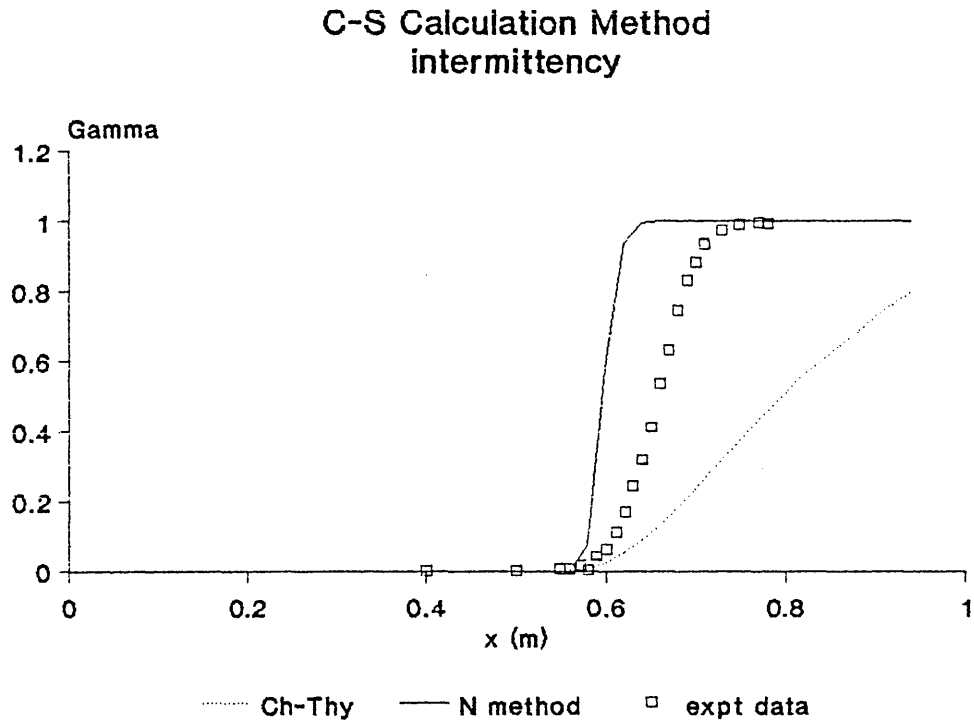

figure 6.1 C-S prediction, flow 6

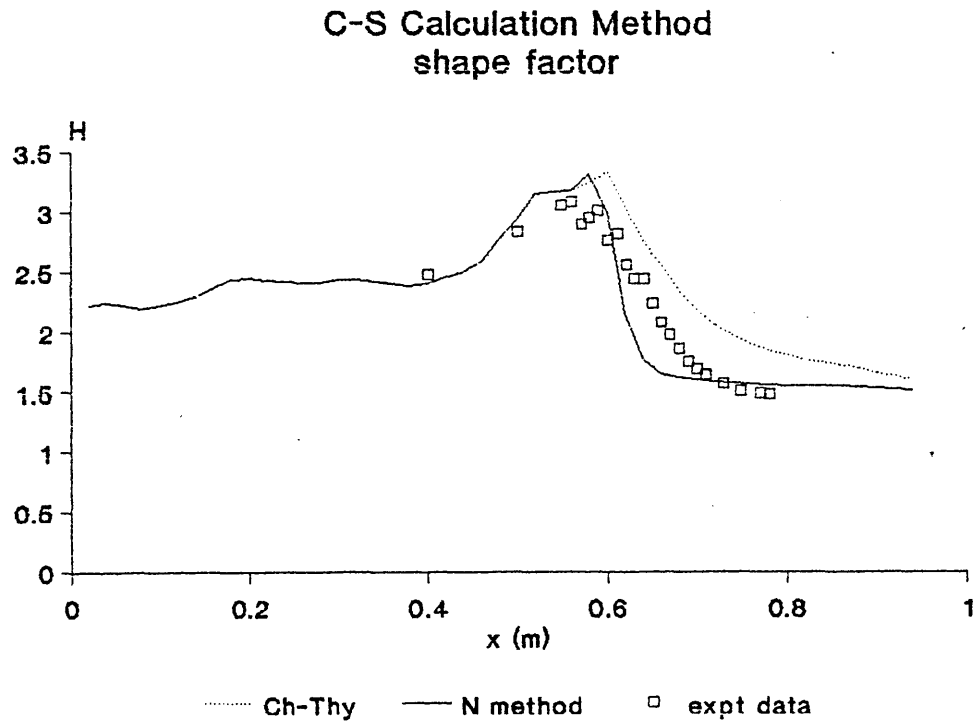

figure 6.2 C-S prediction, flow 6

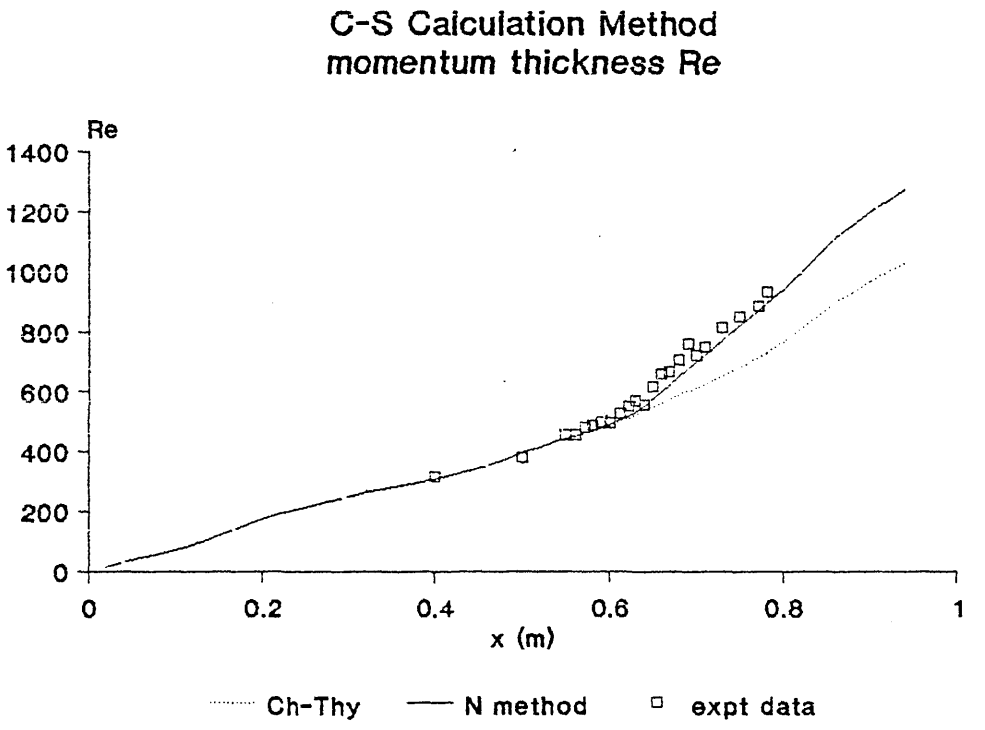

figure 6.3 C-S prediction, flow 6

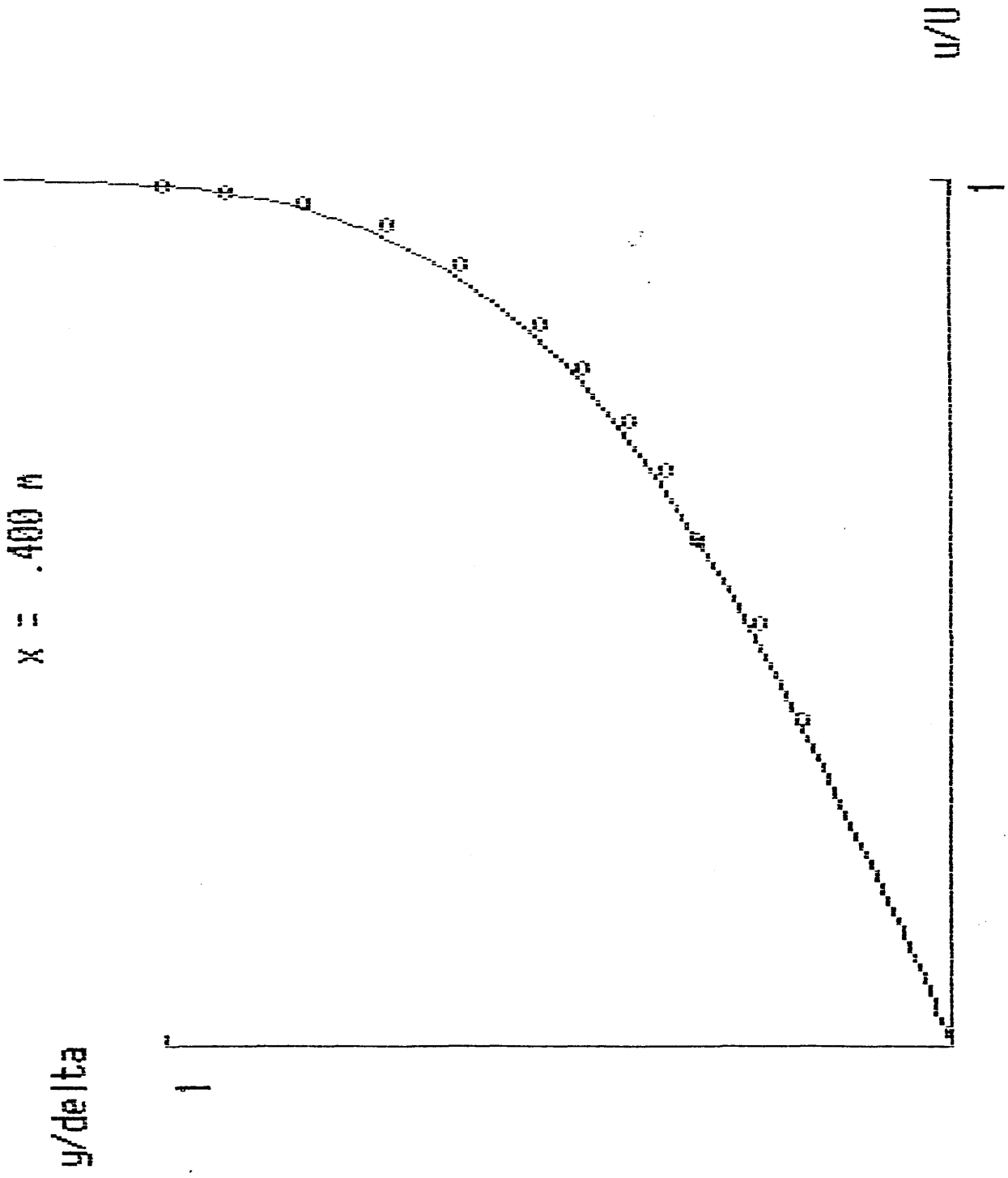

figure 6.4 velocity profile prediction with expt data

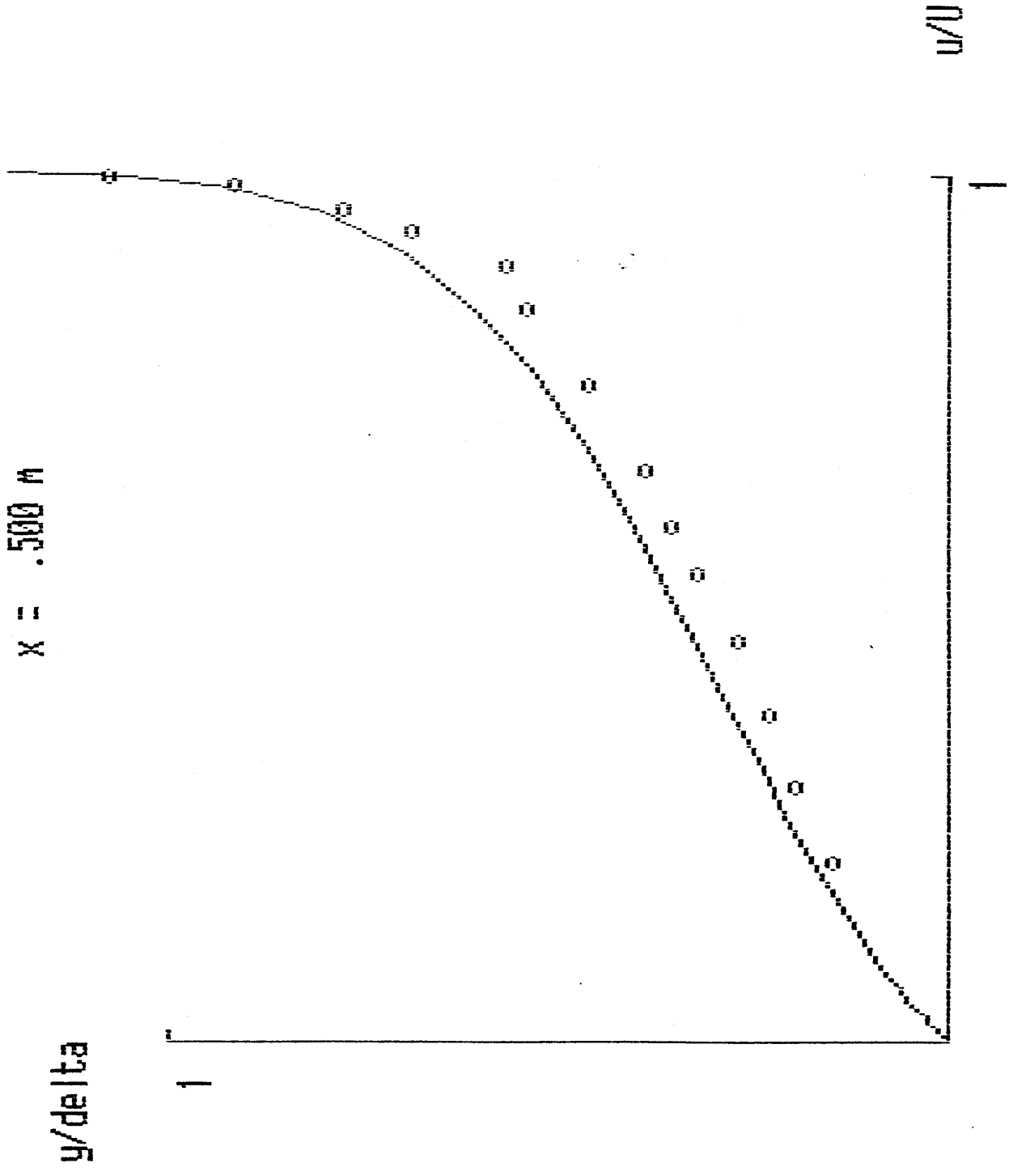

figure 6.5 velocity profile prediction with expt. data

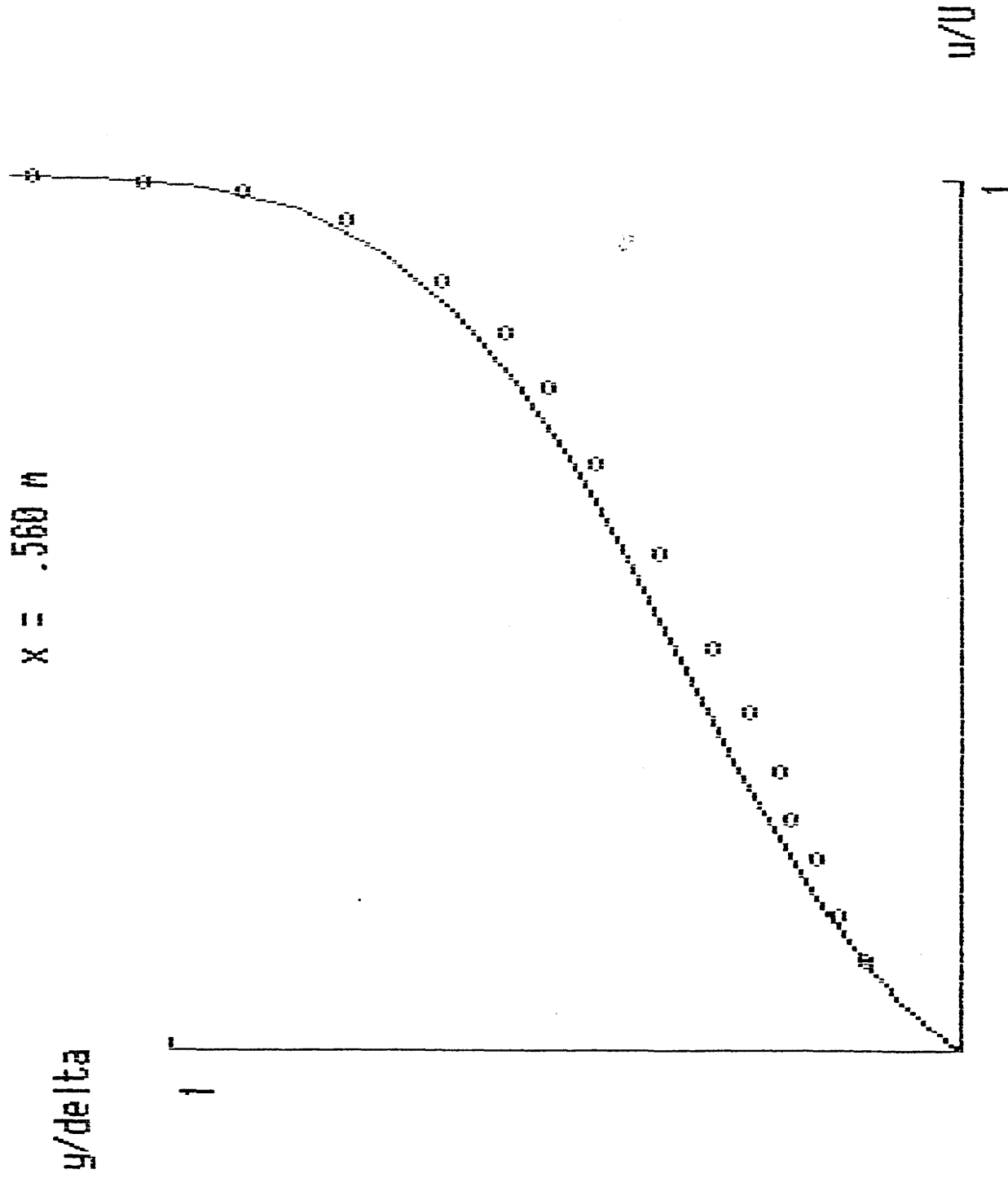

figure 6.6 velocity profile prediction with expt. data

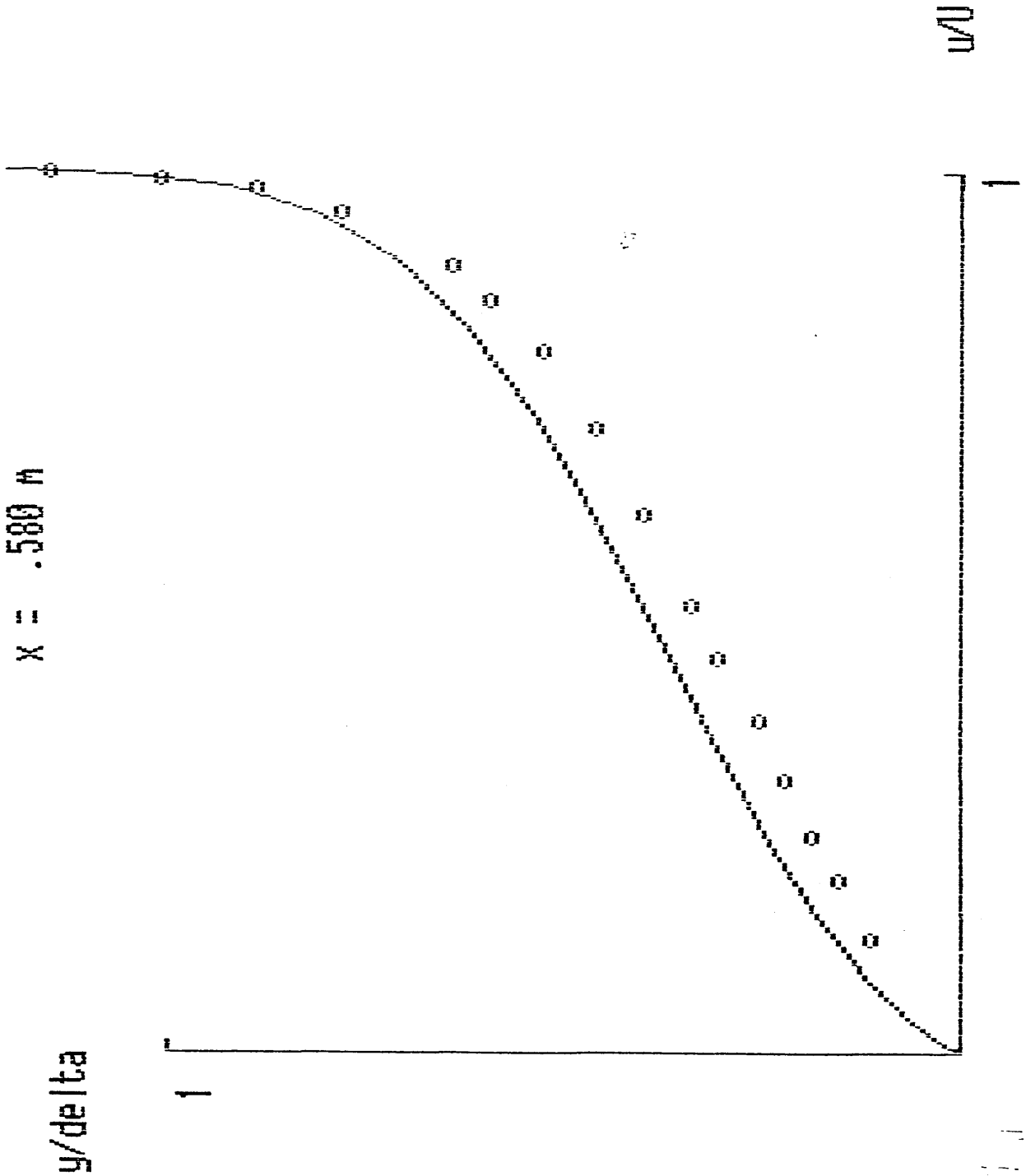

figure 6.7 velocity profile prediction with expt. data

figure 6.8 velocity profile prediction with expt. data

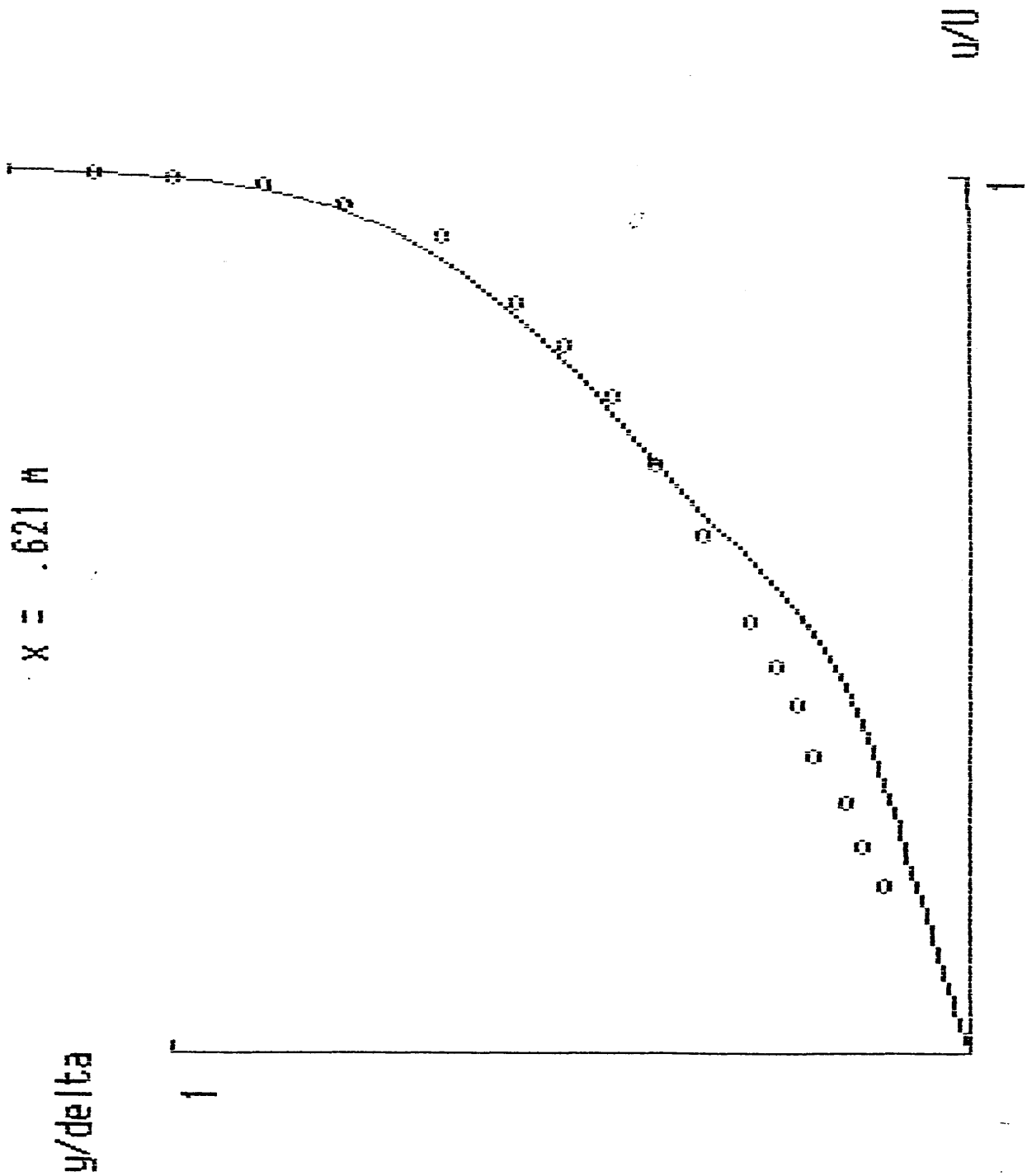

figure 6.9 velocity profile prediction with expt. data

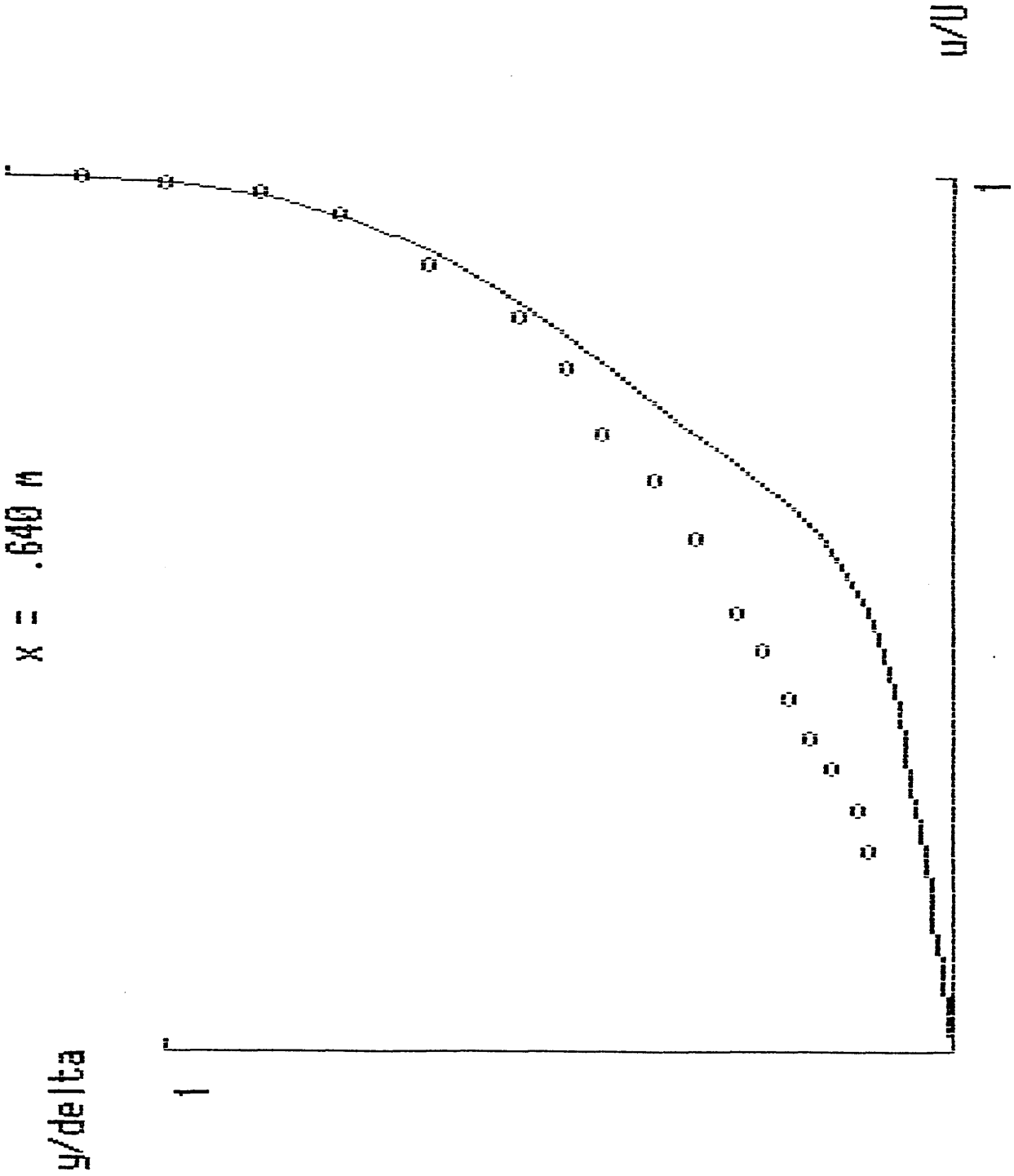

figure 6.10 velocity profile prediction with expt. data

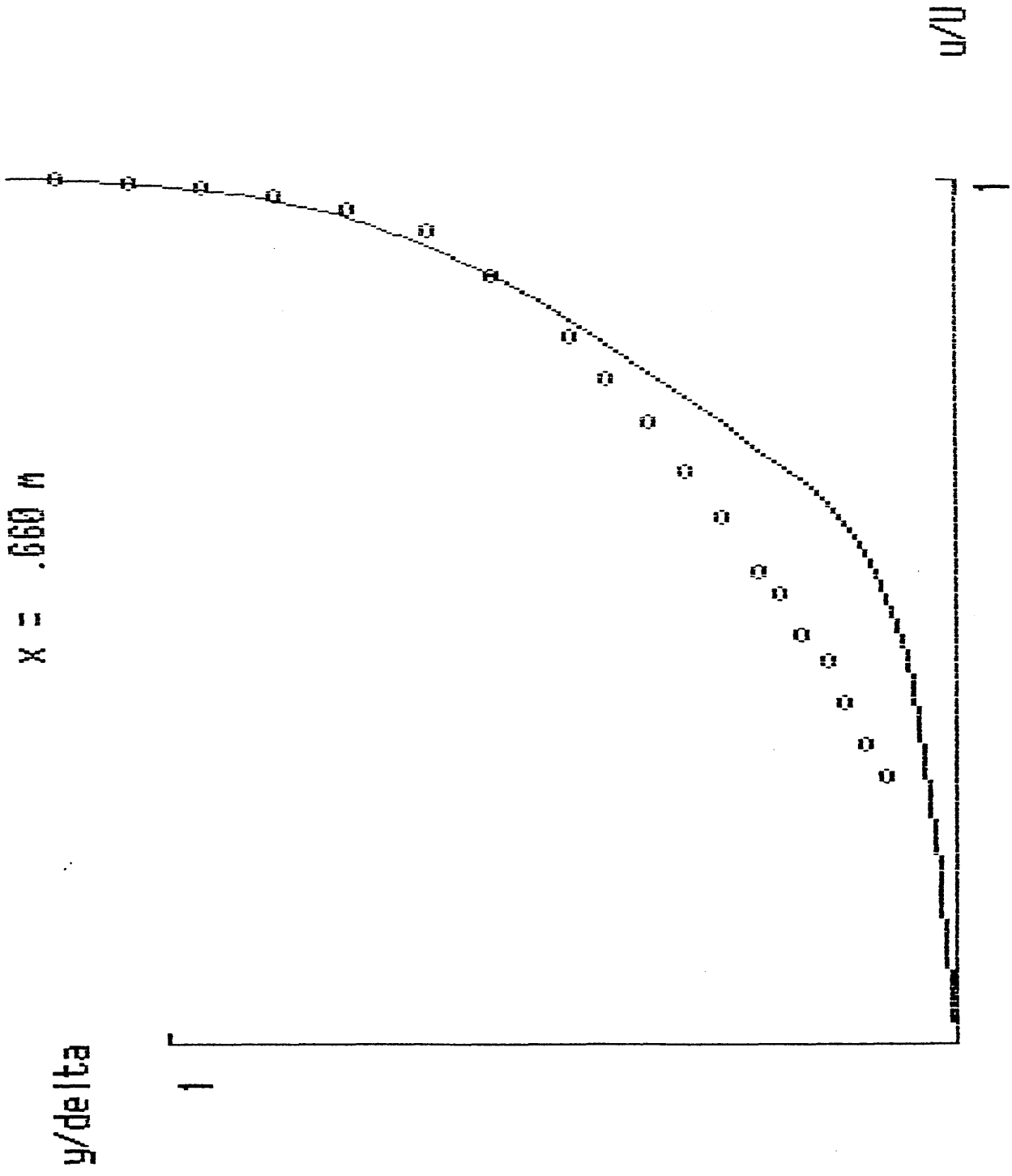

figure 6.11 velocity profile prediction with expt. data

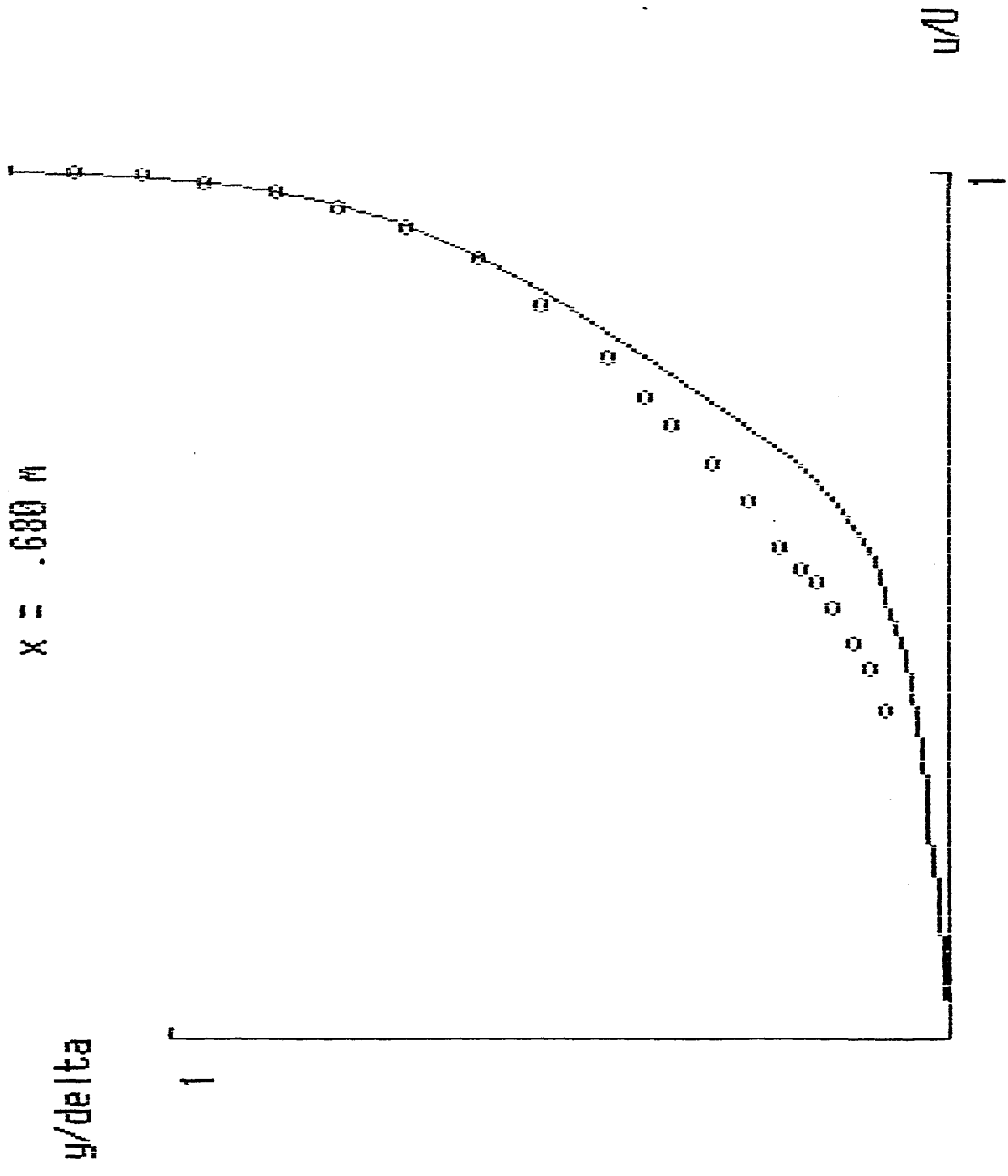

figure 6.12 velocity profile prediction with expt. data

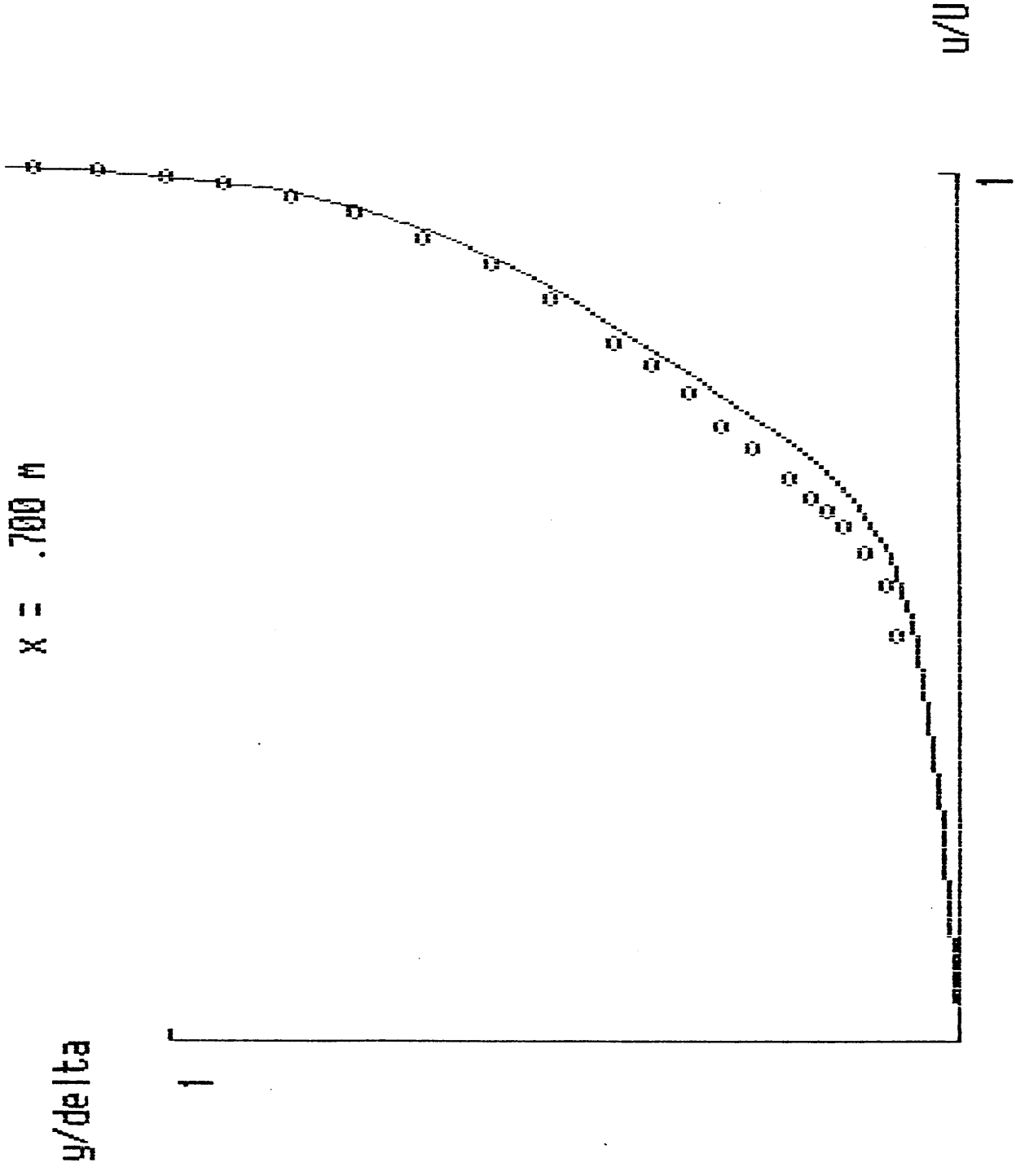

figure 6.13 velocity profile prediction with expt. data

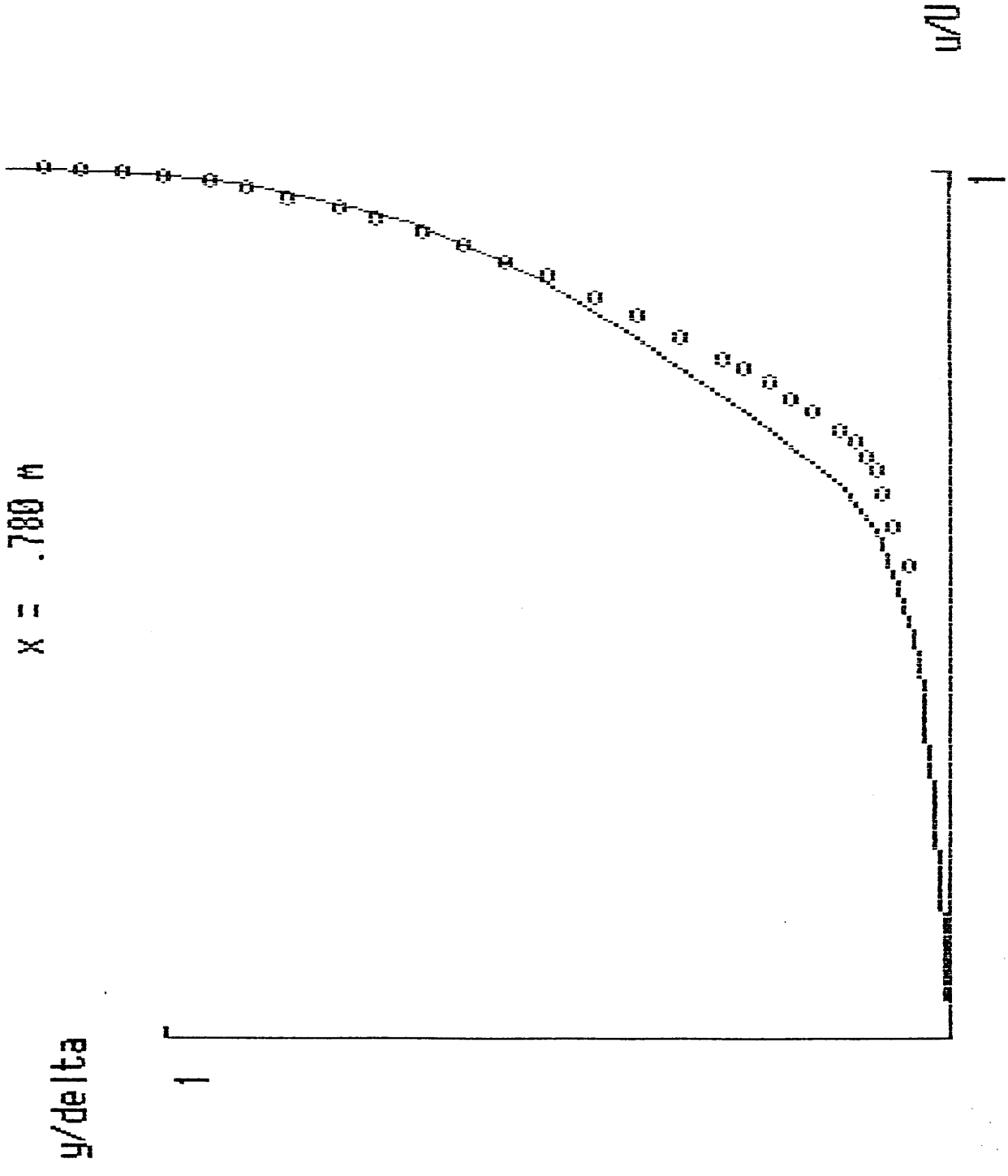

figure 6.14 velocity profile prediction with expt. data

CONCLUSIONS

1. The existing boundary layer wind tunnel has been modified to give a velocity distribution typical of a forward loaded turbine blade ("squared-off" design) over the test plate

2. A data acquisition and control system based on the AMSTRAD PC1640HD20 microcomputer was developed. By utilising assembly language subroutines, very fast sampling rates could be achieved which allowed a detailed digital representation of the raw signal to be captured. The large RAM capacity of the AMSTRAD PC1640 ensured that samples of sufficient length could be stored. The presence of a 20MByte hard disk allowed many such samples to be gathered and stored before subsequent processing at a later, more convenient, time.

3. Software techniques were developed for the calculation of mean flow variables, such as mean velocity and RMS, thus reducing the requirement for external instrumentation. Assembly language subroutines were again necessary to process the large quantities of data involved within acceptable timescales.

4. An algorithm was developed to discriminate between laminar and turbulent flow. This was used to conditionally sample the signal in the transition region and hence provide mean laminar and turbulent velocity profiles in the transition region. It also provided a measurement of the intermittency.

5. Simple intermittency weighting of laminar and turbulent components to give a transitional parameter is not strictly

applicable to the component profiles measured during the present work. A corresponding expression for displacement thickness which takes into account the variation of intermittency in the y direction was developed (equation 4.19). This was shown to be more accurate when applied to the current data.

6. Boundary layer profiles were measured under the imposed velocity distribution at various levels of freestream turbulence.

7. Two methods of defining the start of transition were compared, ie. the 1% intermittency point, x_s, and the method of Narasimha (1985) which gives x_t. In all cases x_s was found to occur earlier than x_t. Conditions at x_t were found to give better results when correlating the spot formation rate parameter, N, (see no. 10).

8. The concept of statistical similarity of transition regions was observed to remain intact for severe adverse pressure gradients, including cases where separation bubbles were present during the early stages of transition.

9. The mean intermittency distributions of Schubauer and Klebanoff (1955) and Dhawan and Narasimha (1958) were compared for the present data. The S-K distribution appears to give the better fit but is likely to be less practical in a calculation scheme since it requires that the 50% intermittency point be known. The D-N distribution depends on x_t which can be difficult to locate accurately.

10. A correlation for the spot formation rate parameter, N, has been developed, equation 5.14, which accounts for the combined effects of freestream turbulence level and pressure gradient (adverse pressure gradients only).

11. Conditionally sampled velocity profiles indicate that intermittently separated laminar flow and attached turbulent flow can occur in the early part of the transition region.

12. The differential boundary layer calculation method of Cebeci and Smith (1974) appears to be better equipped to calculate turbine blade flows as a result of the inclusion of the new correlation.

SUGGESTIONS FOR FUTURE WORK

The transition length obtained from the correlation, equation 5.14, is based on the premise that the most important governing factor is the rate at which spots are formed at the start of transition. Possible variations of the spot propagation characteristics, such as the spread angle, are not explicitly considered. Very little experimental data exist regarding the influence of pressure gradient on the propagation characteristics of turbulent spots and more such data would be helpful in providing improved models of the transition region.

The present work has shown that a high level of sophistication in data acquisition and reduction can be achieved at fairly low cost by using a 16-bit microcomputer. Similar systems could be used to carry out detailed investigations of spot propagation characteristics under the influence of various pressure gradients. Indeed, 16-bit microcomputer based data acquisition and control systems could be used in a wide variety of applications which previously required access to mainframe and mini computers.

REFERENCES

Abu-Ghannam B.J. & Shaw R. - "Natural Transition of Boundary Layers-The Effects of Turbulence, Pressure Gradient and Flow History" Jour Mech. Eng. Science, Vol. 22 1980

Arnal D., Juillen J.C. & Michel R. - "Experimental Analysis and Computation of the Onset and Development of the Boundary Layer Transition". AGARD conf. Proc No. 224, Laminar-Turbulent Transition, paper no 13, 1977 (English translation NASA TM 75325

Birch N.T. - "Navier-Stokes Predictions of Transition, Loss and Heat Transfer in a Turbine Cascade". ASME-GT-22 1987a

Birch N.T. - "Comparison Between Numerical Solutions and Measurements for a High-Speed Turbine Blade". C268/87 I Mech E 1987b

Blair M.F., Bailey D.A. & Schlinker R.H. - "Development of a Large-Scale Wind Tunnel for the Simulation of Turbomachinery Airfoil Boundary Layers". ASME J. of Eng. for Power, Vol 103, 1981

Blair M.F. & Werle M.J. - "The Influence of Freestream Turbulence on the Zero Pressure Gradient Fully Turbulent Boundary Layer". UTRC Report R80-914388-12, 1980

Bluechip Technology - ACM-44 Technical manual, document reference acmu 1011, 1988

Cantwell B., Coles D. & Dimotakis P. - "Structure and Entrainment in the Plane of Symmetry of a Turbulent Spot". J. Fluid Mech., Vol 87, Part 4, 1978

Cebeci T. - "Essential Ingredients of a Method for Low Reynolds-Number Airfoils". AIAA Jour., Vol 27, No 12, 1989

Cebeci T. & Bradshaw P. - "Momentum Transfer in Boundary Layers". McGraw-Hill, 1977

Cebeci T., Keller H.B. & Williams P.G. - "Separating Boundary layer Flow Calculations". Jour. Comp. Phys., Vol. 31, 1979

Cebeci T. & Smith A.M.O. - "Analysis of Turbulent Boundary Layers". Academic Press, New York 1974

Cedar R.D. & Stow P. - "A Compatible Mixed Design and Analysis Finite Element Method for the Design of Turbomachinery Blades". Int. J. for Num. Methods in Fluids. Vol. 5, 331-345 1985

Chen K.K & Thyson N.A. - "Extension of Emmons' Spot Theory to Flows on Blunt Bodies". AIAA Jour. Vol. 9, 1971

Coles D.E. - "The Law of the Wake in the Turbulent Boundary Layer". J. Fluid Mech. Vol 1, 1956

Coles D.E. - "The Young Persons Guide to the Data". Proc. Computation of Turbulent Boundary Layers. Vol II pp 1 - 53, Stanford Conf. 1968

Coles D.E. & Hirst E.A. - "Computation of Turbulent Boundary Layers". AFOSR-IFP-Stanford Conf. Vol II. 1968

Corrsin S. & Kistler A.L. - "Freestream Boundaries of Turbulent Flows". NACA Report 1244, 1955

Dey J. - "An Integral Method for the Calculation of 2-D Transitional Boundary Layers". Ph.D. Thesis, Indian Institute of Science, 1988

Dhawan S. & Narasimha R. - "Some Properties of Boundary Layer Flow During The Transition From Laminar to Turbulent Motion". Jour. Fluid Mech., Vol. 3, 1958

Dzung L.S. & Seippel C. - "Aerodynamic Aspests of Blading Research" Flow Research on Blading. Elsevier Publishing Company, 1970

Emmons H.W. - "The Laminar-Turbulent Transition in a Boundary Layer - Part 1". Jour. Aero. Sci. Vol. 18, 1951

Fraser C.J. - "Boundary Layer Development From Transition Provoking Devices". PhD Thesis, Dundee College of Technology, 1979

Fraser C.J., Gardiner I.D. & Milne J.S. - "A Comparison of Two Integral Techniques for the Prediction of Transitional Boundary Layer Flow". Conf. on Numerical Methods in Laminar and Turbulent Flow, Montreal, 1987

Fraser C.J., Graham D. & Milne J.S. - "Digital Processing of Hot Wire Anemometer Signals in Intermittently Turbulent Flows" Flow Meas. Instrum., Vol 1, 1990

Fraser C.J. & Milne J.S. - "Integral Calculations of Transitional Boundary Layers". Proc. I Mech E, Part C 200, 1986

Fraser C.J., Milne J.S. & Gardiner I.D. - "The Effect of Pressure Gradient and Freestream Turbulence Intensity on the Length of Transitional Boundary Layers". Proc Instn Mech Engrs, Vol 202 No C3, 1988

Fraser C.J., Milne J.S. & Graham D. - "Fast Data Acquisition and Digital Signal Processing in Studies of Turbulent Flow". 4th Joint Int. Conf. on Mech. Eng. & Tech., Zagazig Univ. Cairo, 1989

Gad-el-Hak M., Blackwelder R.F. & Riley J.J. - "On the Growth of Turbulent Regions in Laminar Boundary Layers". J. Fluid Mech. Vol 110, 1981

Gardiner I.D. - "Transition in Boundary Layer Flows". PhD thesis, Dundee College of Technology, 1987

Gardner W.B. - "Energy Efficient Engine Low Pressure Turbine Boundary Layer Program Technology Report". NASA CR-165338 (PWA-5594-141)

Gostelow J.P. - "Adverse Pressure Gradient Effects on Boundary Layer Transition in a Turbulent Free Stream". 9th ISABE, Athens, 1989a

Gostelow J.P. - personal communication, 1989b

Gostelow J.P. & Blunden A.R. - "Investigations of Boundary Layer Transition in an Adverse Pressure Gradient". ASME Paper No 88-GT-298, 1988

Graham D., Fraser C.J. & Milne J.S - "Digital Measurement in Intermittently Turbulent Flows". AMSE conf Signals & Systems, Brighton, 1989

Hall D.J. & Gibbings J.C. - "Influence of Freestream Turbulence and Pressure Gradient Upon Boundary Layer Transition". J. Mech Eng Sci, Vol. 14, No 2, 1972

Horton H.P. - "A Semi-empirical Theory for the Growth and Bursting of Laminar Separation Bubbles". 1967

Kaplan R.E. & Laufer J. - "The Intermittently Turbulent Region of the Boundary Layer". Proc. 12th Int. Cong. of Appl. Mech. Springer-Verlag, 1969

Keller H.B. - "A New Difference Scheme for Parabolic Problems". Numerical Solutions of Partial Differential Equations, Vol. 2, Academic Press, 1970

Keller H.B. - "Accurate Difference Methods for Nonlinear Two-Point Boundary Value Problems". SIAM J. Numer. Anal. Vol 11, 1974

Klebanoff P.S. - "Characteristics of turbulence in a Boundary Layer With Zero Pressure Gradient". NACA Tech note 3178, 1955

Kline S.J., Cockrell D.J., Morkovin M.V. & Sovran G. - "Computation of Turbulent Boundary Layers". AFOSR-IFP-Stanford Conf. Vol I. 1968

Kovasznay L.S.G., Kibens V. & Blackwelder R.F. - "Large-Scale Motion in the Intermittent Region of a Turbulent Boundary Layer". J. Fluid Mech. Vol 41, 1970

Liu Y.C. & Gibson G.A. - "Microprocessor-Based Systems: The 8086/8088 Family". Prentice-Hall, 1984

Ludwieg H. & Tillman W. - "Investigation of the Wall Shearing Stress in Turbulent Boundary Layers". NACA Tech memo 1285, 1950

McCormick M.E. - "An Analysis of the Formation of Turbulent Patches in the Transition Boundary Layer". Trans. ASME, J. App. Mech., Vol 35, 1968

McDonald H. & Fish R.W. - "Practical Calculations of Transitional Boundary Layers". Int Jour Heat & Mass Transfer Vol. 16, No. 9, 1973

Murlis J. - "The Structure of a Turbulent Boundary Layer at Low Reynolds Number". Ph.D. thesis, Imperial College, London, 1975

Murlis J., Tsai H.M. & Bradshaw P. - "The Structure of Turbulent Boundary Layers at Low Reynolds Numbers". J. Fluid Mech. Vol 122, 1982

Narasimha R. - "On the Distribution Of Intermittency in the Transition Region of a Boundary Layer". J. Aero. Sci. Vol 24, 1957

Narasimha R. - "The Laminar-Turbulent Transition zone in the Boundary Layer". Prog. Aerospace Sci. Vol. 22, 1985

Orr W.M.F. - "The Stability or Instability of the Steady Motions of a Perfect Fluid and of a Viscous Liquid". Proc. Royal Irish Acad. Vol. 27 1907

Pohlhausen K. - "Zur Naherungsweisen Integration der Differentialgleichung der Laminaren Reibungsschicht". Zeit fur Ang. Math. & Mech., Vol 1. 1921

Rector R. & Alexy G. - "The 8086 Book". OSBORNE/McGraw-Hill, 1980

Roach P.E. - "A New Boundary Layer Wind Tunnel". Aeronaut. J. June/July 1988

Schubauer G.B. & Klebanoff P.S. - "Contributions on the Mechanics of Boundary Layer Transition". NACA report 1289, 1955

Schubauer G.B. & Skramstad H.K. - "Laminar Boundary Layer Oscillations and Transition on a Flat Plate". NACA Rep. 909. 1948 Laminar Flow"

Sharma O.P., Wells R.A., Schlinker R.H. & Bailey D.A. - "Boundary Layer Development on Turbine Airfoil Suction Surfaces". Trans. ASME Vol 104, 1982

Shaw R., Hardcastle J.A., Riley S. & Roberts C.C. - "Recording and Analysis of Fluctuating Signals Using a Microcomputer". Int. Conf. on The Use of Micros in Fluid Engineering BHRA June, 1983

Sommerfeld A. - "Ein Beitrag zur Hydrodynamischen Erklarung der Turbulenten Flussig-Keitsbeivegungen". Atti 4th Congr. Int. Math., Rome, Vol. 3, 1908

Stow P. "Blading Design For Multi-Stage HP Compressors". AGARD lecture series 167, 1989

Tollmien W. - "Uber Die Entstehung der Turbulenz. 1. Mitteilung". Nach Ger Wiss Gottingen, Math Phy Klasse, 1929

Walker G.J. - "Transitional Flow on Axial Turbomachine Blading". AIAA Paper No. 87-0010, 1987

Walker G.J. & Gostelow J.P. - "Effects of Pressure Gradients on the Nature and Length of Boundary Layer Transition". ASME Gas Turb. Conf, Toronto, 1989

White F.M. - "Viscous Fluid Flow". McGraw-Hill 1974

Wygnanski I., Sokolov M. & Friedman D. - "On a Turbulent 'Spot' in a Laminar Boundary Layer". J. Fluid Mech. Vol 78, part 4, 1976

APPENDIX 1

COMPUTER PROGRAM LISTINGS

ACQ.DG - data acquisition subroutine

```
ACQ:
 MOV CX,02H                    4
 MOV DX,300H                   4
 MOV AX,3000H                  4
START:
 PUSH CX                       10
 MOV ES,AX                     2
 MOV BX,00H                    4
 MOV CX,0FFFFH                 4
CONV_1:
 MOV AL,00H                    4
 OUT DX,AL                     8
 PUSH CX                       10
 MOV CX,24H                    4
DELAY:
 NOP                           3
 LOOP DELAY                    17/5
 POP CX                        8
 IN AL,DX                      8
 MOV ES:[BX],AL                9 + EA + 2(segment override)
 INC BX                        2
 LOOP CONV_1                   17/5
 POP CX                        8
 MOV AX,4000H                  4
 LOOP START                    17/5
 RETF
```

EA (effective address) = 5 for register indirect

TOTAL.DG - totalling subroutine

```
TOTAL:
 MOV CX,02H
 MOV AX,00H
 MOV [0A000H],AX
 MOV [0A002H],AX
 MOV AX,3000H
START1:
 PUSH CX
 MOV ES,AX
 MOV BX,00H
 MOV CX,0FFFFH
TOT1:
 MOV DL,ES:[BX]
 MOV DH,00H
 MOV AX,[0A000H]
 ADD AX,DX
 MOV [0A000H],AX
 MOV AX,[0A002H]
 ADC AX,00H
 MOV [0A002H],AX
 INC BX
 LOOP TOT1
 POP CX
 MOV AX,4000H
 LOOP START1
 RETF
```

RMS2.DG - RMS subroutine

```
RMS:                        ;INITIALISATION
 MOV CX,0FFFFH
 MOV AX,00H
 MOV [0A00CH],AX            ;clear memory locations where
 MOV [0A00EH],AX            ;data is stored by ADD or ADC
 MOV [0A010H],AX            ;instructions
 MOV [0A012H],AX
 MOV [0A014H],AX
 MOV [0A016H],AX
 MOV [0A018H],AX
 MOV [0A01AH],AX
 MOV [0A01EH],CX
 MOV CX,02H
 MOV [0A01CH],CX
 MOV AX,3000H
START2:
 PUSH CX
 MOV ES,AX
 MOV BX,00H
 MOV CX,0FFFFH
RMS1:                       ;START OF LOOP
 MOV AL,ES:[BX]             ;read 8-bit datum into 16-bit
 MOV AH,00H                 ;AX register
 MUL W[0A01CH]              ;calculate A n (datum * no. of points)
 MUL W[0A01EH]
 MOV [0A004H],AX            ;store 32-bit answer
 MOV [0A006H],DX
 MOV AX,[0A006H]            ;SUBTRACT   (An - total)
 CMP AX,[0A002H]            ;compare high bytes of An and total
 JB B_A                     ;if An < total then do (total - An)
 JE LOWER                   ;if equal compare low bytes
A_B:
 MOV AX,[0A004H]            ;32-bit subtraction
 SUB AX,[0A000H]
 MOV [0A008H],AX
 MOV AX,[0A006H]
 SBB AX,[0A002H]
 MOV [0A00AH],AX
 JMP DONE
LOWER:                      ;compare low bytes
 MOV AX,[0A004H]
 CMP AX,[0A000H]
 JNB A_B
B_A:
 MOV AX,[0A000H]            ;32-bit subtraction
 SUB AX,[0A004H]            ;answer stored at &A008 - &A00B
 MOV [0A008H],AX
 MOV AX,[0A002H]
 SBB AX,[0A006H]
 MOV [0A00AH],AX
DONE:
 MOV AX,00H                 ;SQUARING ROUTINE (An - total)
 MOV [0A010H],AX            ;clear memory for answer
 MOV [0A012H],AX
 MOV AX,[0A008H]            ;multiply low bytes
 MUL W[0A008H]
```

```
 MOV [0A00CH],AX
 MOV [0A00EH],DX
 MOV AX,[0A008H]          ;low times high bytes
 MUL W[0A00AH]
 ADD [0A00EH],AX
 ADC [0A010H],DX
 JNC NEXT
 INC B[0A012H]
NEXT
 MOV AX,[0A00AH]          ;low times high bytes
 MUL W[0A008H]
 ADD [0A00EH],AX
 ADC [0A010H],DX
 JNC HIGH
 INC B[0A012H]
HIGH
 MOV AX,[0A00AH]          ;multiply high bytes
 MUL W[0A00AH]
 ADD [0A010H],AX          ;32*32-bit multiplication ref
 ADC [0A012H],DX          ;The 8086 Book ,Rector and Alexy
 MOV AX,[0A00CH]          ;SUMMATION  sigma(An - total)
 ADD [0A014H],AX
 MOV AX,[0A00EH]
 ADC [0A016H],AX
 MOV AX,[0A010H]
 ADC [0A018H],AX          ;64-bit addition
 MOV AX,[0A012H]
 ADC [0A01AH],AX
 INC BX                   ;BX=BX+1 to access next data point
 DEC CX                   ;decrement loop counter
 JCXZ FIN1                ;if CX=0 then finish
 JMP RMS1                 ;repeat loop
FIN1:
 POP CX
 MOV AX,4000H
 DEC CX
 JCXZ FIN2
 JMP START2
FIN2:
 RETF                     ;return to BASIC program
```

GAMMA4.DG - intermittency and conditional sampling routine

```
GAMMA:                          ;INITIALISATION
 MOV AL,2
 MOV [0A018],AL
 MOV AX,00H                     ;clear memory locations which
 MOV BX,0A01AH                  ;receive data via ADD or ADC
 MOV CX,0DH                     ;instructions
CLEAR:
 MOV [BX],AX
 INC BX
 INC BX
 LOOP CLEAR
 MOV AX,3000H
 MOV CX,02H
START3:
 PUSH CX
 MOV ES,AX
 MOV BX,00H                     ;clear BX register
 MOV CX,0FFF6H                  ;load loop counter with 65526
GAMMA1:                         ;START OF MAIN LOOP
 MOV AX,00H                     ;clear memory locations which
 MOV [0A01EH],AX                ;hold "SUM1" and "SUM2"
 MOV [0A030H],AX
 MOV DL,0EH                     ;load DL with 14 to control sub-loop
SUM1:                           ;SUM1  first derivative
 MOV AL,ES:[BX+1]
 MOV AH,00H
 MOV [0A01CH],AX
 MOV AL,ES:[BX]
 MOV AH,00H
 SUB AX,[0A01CH]
 JNS POS1
 NEG AX
POS1:
 ADD [0A01EH],AX
 INC BX
 DEC DL
 JNZ SUM1
 MOV DL,0EH
RESET1:
 DEC BX
 DEC DL
 JNZ RESET1
 MOV DL,0DH
SUM:                            ;SUM2 second derivative
 MOV AL,ES:[BX+1]               ;load the byte at i+1 into
 MOV AH,00H
 MUL B[0A018H]                  ;2*Ui+1
 MOV [0A01CH],AX                ;memory location &A01C
 MOV AL,ES:[BX]                 ;load the byte at i into the
 MOV AH,00H                     ;AX register
 MOV [0A01AH],AX
 MOV AL,ES:[BX+2]
 ADD AX,[0A01AH]
 SUB AX,[0A01CH]                ;subtract
 JNS POS
 NEG AX                         ;ensure the absolute value is returned
```

```
POS:
 ADD [0A030H],AX            ;add into "SUM2"
 INC BX
 DEC DL
 JNZ SUM                    ;loop 14 times ie. 15 points
 MOV DL,0DH
RESET:                      ;loop 9 times to restore BX
 DEC BX
 DEC DL
 JNZ RESET
 MOV AX,[0A01EH]            ;load "SUM1" into AX register
 CMP AX,1AH                 ;compare with 26
 JBE LAMINAR                ;if "SUM" < 26 then LAMINAR
 MOV AX,[0A030H]            ;load "SUM2" into AX
 CMP AX,1AH
 JA TURBULENT               ;ie.  if SUM1 and SUM2 > 26 then TURB
LAMINAR:
 MOV AL,ES:[BX+6]           ;load the value at i+6 into AX
 MOV AH,00H
 ADD [0A020H],AX            ;add the value to laminar total
 ADC [0A022H],00H           ;32-bit addition
 MOV AX,001H
 ADD [0A024H],AX            ;add 1 to laminar counter
 ADC [0A026H],00H
 JMP LAMI                   ;jump to end of loop
TURBULENT:                  ;same procedure if point is
 MOV AL,ES:[BX+6]           ;considered turbulent
 MOV AH,00H
 ADD [0A028H],AX
 ADC [0A02AH],00H
 MOV AX,001H
 ADD [0A02CH],AX
 ADC [0A02EH],00H
LAMI:
 INC BX                     ;inc BX by one
 DEC CX
 JCXZ FINISH
 JMP GAMMA1
FINISH:
 POP CX
 MOV AX,4000H
 DEC CX
 JCXZ FIN3
 JMP START3
FIN3:
 RETF
```

DGDATA5.BAS - data acquisition program

```
REM
REM                              DGDATA5
REM
REM data acquisition (and analysis)        21/4/88 Derek Graham
REM
REM update    21/2/89
REM

REM initialise

PORT = &H300
OUT PORT+2,&H12
OUT PORT+3,1
DIM MEAN(40),B(40),Y(40)
CLS

REM input data

PRINT"SWITCH ON STEPPER MOTOR"
PRINT
INPUT"enter temperature (degrees C)          ",T
INPUT"enter atmospheric pressure (mm Hg)     ",H
INPUT"y datum (mm)                           ",YDAT
INPUT"distance from leading edge (mm)        ",X
INPUT"enter filename                         ",FILE$
PRINT
N = 1
PRINT"MEAN VELOCITY"

REM read probe position

5
B(N) = 0
FOR i=1 TO 500
 OUT PORT,0
 Y(N) = INP(PORT)
 B(N) = B(N) + Y(N)
NEXT i
B(N) = B(N)/500

REM data acquisition

OUT PORT+2,&H10
CALL ACQ

SUB ACQ INLINE
 $INLINE "ACQ.COM"
END SUB

BEEP

REM mean velocity

CALL TOTAL
C1 = PEEK(&HA000)
C2 = PEEK(&HA001)
```

```
C3 = PEEK(&HA002)
C4 = PEEK(&HA003)
TOTAL =  C4*(24) + C3*(26) + C2*256 + C1
MEAN(N) = TOTAL/(65535*2)

REM convert to m/s

MEAN(N) = MEAN(N)/12.5

SUB TOTAL INLINE
 $INLINE "TOTAL.COM"
END SUB

REM dump data to disc

DEF SEG=&H3000
BSAVE FILE$+STR$(2*N-1),0,&HFFFF
DEF SEG=&H4000
BSAVE FILE$+STR$(2*N),0,&HFFFF
DEF SEG

REM print mean velocity

PRINT INT(MEAN(N)*1000+0.5)/1000

REM test for profile completed

IF N < 2 GOTO 420
IF MEAN(N)>=0.995*MEAN(N-1) AND MEAN(N)<=1.005*MEAN(N-1) GOTO 410
GOTO 420
410
IF MEAN(N)>=0.995*MEAN(N-2) AND MEAN(N)<=1.005*MEAN(N-2) GOTO 500
420
OUT PORT+2,&H12
N = N + 1

IF N < 8 THEN
TRAV = 0.5
ELSEIF N < 13 THEN
TRAV = 1.0
ELSE
TRAV = 2
END IF
OUT PORT+3,0
DELAY TRAV
OUT PORT+3,1
GOTO 5

500

REM freestream turbulence

UINF = (MEAN(N) + MEAN(N-1) + MEAN(N-2))/3
TINT = 100*RMS(N)/UINF
PRINT
PRINT"UINF     ",UINF
```

```
PRINT
PRINT"N         ",N
PRINT

REM save data to disk file

OPEN"O",f1,FILE$
WRITEf1,T,H,N,UINF,YDAT,X,TINT
FOR I=1 TO N
 WRITEf1,B(I)
NEXT I
CLOSEf1


END
```

DGDATA6.BAS - data reduction program

```
REM
REM                              DGDATA6
REM
REM data acquisition and analysis        21/4/88 Derek Graham
REM
REM update    20/2/89
REM

DIM MEAN(40),RMS(40),MLAM(40),MTURB(40),GAMMA(40),B(40)
CLS

REM input data

PRINT
INPUT"enter filename                          ",FILE$
PRINT
N = 1
PRINT"MEAN","RMS","MLAM","MTURB","GAMMA"

REM read data file

OPEN"I",f1,FILE$
INPUTf1,T,H,N,UINF,YDAT,X,TINT
FOR I=1 TO N
 INPUTf1,B(I)
NEXT I
CLOSEf1

FOR I=1 TO N

REM load data

DEF SEG=&H3000
BLOAD FILE$+STR$(2*I-1),0
DEF SEG=&H4000
BLOAD FILE$+STR$(2*I),0
DEF SEG

REM mean velocity

CALL TOTAL
C1 = PEEK(&HA000)
C2 = PEEK(&HA001)
C3 = PEEK(&HA002)
C4 = PEEK(&HA003)
TOTAL = C4*(24) + C3*(26) + C2*256 +C1
MEAN(I) = TOTAL/(65535*2)

REM convert to m/s

MEAN(I) = MEAN(I)/12.5

REM RMS velocity

CALL RMS
C1 = PEEK(&HA014)
```

```
C2 = PEEK(&HA015)
C3 = PEEK(&HA016)
C4 = PEEK(&HA017)
C5 = PEEK(&HA018)
C6 = PEEK(&HA019)
C7 = PEEK(&HA01A)
C8 = PEEK(&HA01B)
CA = C8*(26) + C7*(28) + C6*(20) + C5*(22)
CB = C4*(24) + C3*(26) + C2*256 + C1
C = CA + CB
D = C/(65535*2)
E = SQR(D)
RMS(I) = E/(65535*2)

REM convert to m/s

RMS(I) = RMS(I)/12.5

REM intermittency

CALL GAMMA
VL1 = PEEK(&HA020)
VL2 = PEEK(&HA021)
VL3 = PEEK(&HA022)
VL4 = PEEK(&HA023)
VLAM = VL4*(24) + VL3*(26) + VL2*(2) + VL1
CL1 = PEEK(&HA024)
CL2 = PEEK(&HA025)
CL3 = PEEK(&HA026)
CL4 = PEEK(&HA027)
CLAM = CL4*(24) + CL3*(26) + CL2*(2) + CL1
VT1 = PEEK(&HA028)
VT2 = PEEK(&HA029)
VT3 = PEEK(&HA02A)
VT4 = PEEK(&HA02B)
VTURB = VT4*(24) + VT3*(26) + VT2*(2) + VT1
CT1 = PEEK(&HA02C)
CT2 = PEEK(&HA02D)
CT3 = PEEK(&HA02E)
CT4 = PEEK(&HA02F)
CTURB = CT4*(24) + CT3*(26) + CT2*(2) + CT1
IF CTURB = 0 GOTO 10
MTURB(I) = VTURB/CTURB
10 IF CLAM = 0 GOTO 20
MLAM(I) = VLAM/CLAM
20 GAMMA(I) = CTURB/(65526*2)

REM convert to m/s

MLAM(I) = MLAM(I)/12.5
MTURB(I) = MTURB(I)/12.5


REM print out results

BEEP
```

```
PRINT INT(MEAN(I)*1000+0.5)/1000,INT(RMS(I)*1000+0.5)/1000,;
PRINT INT(MLAM(I)*1000+0.5)/1000,INT(MTURB(I)*1000+0.5)/1000,;
PRINT INT(GAMMA(I)*1000+0.5)/1000

NEXT I
500

REM freestream turbulence

UINF = (MEAN(N) + MEAN(N-1) + MEAN(N-2))/3
TINT = 100*RMS(N)/UINF
PRINT
PRINT"UINF      ",UINF
PRINT
PRINT"N         ",N
PRINT

REM save data to disk file

OPEN"O",£1,FILE$
WRITE£1,T,H,N,UINF,YDAT,X,TINT
FOR I=1 TO N
 WRITE£1,MEAN(I),RMS(I),MLAM(I),MTURB(I),GAMMA(I),B(I)
NEXT I
CLOSE£1

SUB TOTAL INLINE
 $INLINE "TOTAL.COM"
END SUB

SUB RMS INLINE
 $INLINE "RMS2.COM"
END SUB

SUB GAMMA INLINE
 $INLINE "GAMMA4.COM"
END SUB

END
```

DATA9.BAS - intermittency display program

```
REM
REM data analysis program                23/3/88        Derek Graham
REM
REM update 13/13/89  S1(t) AND S2(t) criterion
REM

INPUT"no. of points for intermittency calculations";PTS
INPUT"CUT OFF     ";CUT
INPUT"factor for sum";FT

REM read data

PORT = &H300
OUT PORT+2,&H10
print"reading data"

CALL ACQ
N = &H00
BEEP

5 INPUT X
IF X = 99 GOTO 200

REM Mean velocity

CLS
PRINT"Calculating mean velocity"
N = X
VEL = 0
FOR i=1 TO 640
 P% = PEEK(N)
 VEL = VEL + P%
 N=N+1
NEXT i
MEAN = VEL /640

REM rms velocity

BEEP
CLS
PRINT"Calculating RMS velocity"
N = X
TOT = 0
FOR k=1 TO 640
 A% = PEEK(N)
 B = (A% - MEAN)
 N = N + 1
 TOT = TOT + B
NEXT k
C = TOT/640
RMS = SQR(C)
BEEP

REM set up graph

DEF SEG=&H3000
```

```
CLS
N = X
SCREEN 2
LINE(0,180)-(640,180)
LINE(0,180)-(0,0)
LINE(0,80-CUT/FT)-(640,80-CUT/FT)
FOR i=1 TO 640
 P% = PEEK(N)
 PSET(i,(180-P%/2.4))
 N = N + 1
NEXT i

REM intermittency and mean laminar and turbulent velocities

BEEP
DIM VEL(300)
VTURB = 0
VLAM = 0
CTURB = 0
CLAM = 0
N = X
FOR i=1 TO 640
FOR F=0 TO PTS-1
 VEL(F+1) = PEEK(N+F)
NEXT F
SUM1 = 0
SUM2 = 0
FOR Q=1 TO PTS-1
 S = ABS(VEL(Q+1) - VEL(Q))
 SUM1 = SUM1 + S
NEXT Q
FOR Q=2 TO PTS-1
 S = ABS(VEL(Q+1) - 2*VEL(Q) + VEL(Q-1)) REM (VEL(Q+1)-VEL(Q))
 SUM2 = SUM2 + S
NEXT Q
 PSET(i+INT(PTS/2),80-SUM1/FT)
 PSET(i+INT(PTS/2),80-SUM2/FT)
 IF SUM1 > CUT AND SUM2 > CUT GOTO 10
 VLAM = VLAM + VEL(13)
 CLAM = CLAM + 1
 GOTO 20
 10 VTURB = VTURB + VEL(INT(PTS/2))
 CTURB = CTURB + 1
 LINE(i+INT(PTS/2),190)-(i+INT(PTS/2),180)
 20 N = N + 1
NEXT i
IF CTURB = 0 GOTO 30
MTURB = VTURB/CTURB
30 IF CLAM = 0 GOTO 40
MLAM = VLAM/CLAM
40 GAMMA = CTURB/640
INPUT Y

REM convert to volts

MEANV = MEAN/50
```

```
RMSV = RMS/50
MTURBV = MTURB/50
MLAMV = MLAM/50
BEEP
PRINT:PRINT:PRINT
PRINT"Mean velocity                ",INT(MEANV*100+0.5)/100;"Volts"
PRINT
PRINT"RMS velocity                 ",INT(RMSV*100+0.5)/100;"Volts"
PRINT
PRINT"Mean turbulent velocity      ",INT(MTURBV*100+0.5)/100;"Volts"
PRINT
PRINT"Mean laminar velocity        ",INT(MLAMV*100+0.5)/100;"Volts"
PRINT
PRINT"Intermittency                ",GAMMA
GOTO 5
200 STOP
END
```

PROFILE.BAS - profile data display program

```
REM
REM                    PROFILE
REM
REM      b.1. profile display           28/4/88  Derek Graham
REM
REM update 17/1/89
REM

REM read data from disk

DIM MEAN(40),MLAM(40),MTURB(40),GAMMA(40),B(40),UM(40),UL(40)
DIM UT(40),Y(40),Y1(40),RMS(40)

INPUT"enter filename                    ",FILE$
OPEN"I",£1,FILE$
INPUT£1,T,H,N,UINF,YDAT,X,TINT
FOR I=1 TO N
 INPUT£1,MEAN(I),RMS(I),MLAM(I),MTURB(I),GAMMA(I),B(I)
NEXT I
CLOSE£1

REM convert bits in B(n) to mm in Y(n)

FOR I=1 TO N
 Y(I) = YDAT + 0.1979*(B(1) - B(I))
NEXT I

REM convert velocities to dimensionless quantities based on UINF

FOR I=1 TO N
 UM(I) = MEAN(I)/UINF
 UL(I) = MLAM(I)/UINF
 UT(I) = MTURB(I)/UINF
NEXT I

REM estimate Š

FOR I=1 TO N
 IF UM(I) < 0.99 GOTO 100
 DELTA = Y(I) - (Y(I)-Y(I-1))*(UM(I) - 0.99)/(UM(I) - UM(I-1))
 GOTO 110
 100
NEXT I
110

REM non dimensionalise Y

FOR I=1 TO N
 Y1(I) = Y(I)/DELTA
NEXT I

REM estimate gamma (averaged up to y/delta = 0.4)

GAMMA = 0
FOR I=1 TO N
 IF Y1(1) > 0.4 GOTO 150
```

```
 IF Y1(I) > 0.4 GOTO 140
 GAMMA = GAMMA + GAMMA(I)
NEXT I
140
GAMMA = GAMMA/(I-1) : GOTO 160
150
GAMMA = GAMMA(1)
160

REM graphics output

SCREEN 2
200
CLS
PRINT"delta = ",DELTA
PRINT
PRINT"      MENU"
PRINT
PRINT"LAMINAR PROFILE                                    1"
PRINT"TURBULENT PROFILE                                  2"
PRINT"MEAN PROFILE                                       3"
PRINT"LAMINAR AND TURBULENT PROFILES                     4"
PRINT"ALL THREE                                          5"
PRINT"INTERMITTENCY                                      6"
PRINT"GAMMA / KLEBANOFF                                  7"
PRINT"RMS                                                8"
PRINT"PRINT OUT DATA AND END                             9"
INPUT A
CLS
LINE(55,180)-(555,180)
LINE(55,180)-(55,30)
LINE(55,30)-(60,30)
LINE(355,180)-(355,177)
LINE(455,180)-(455,177)
LINE(555,180)-(555,177)
LOCATE 2,1 : PRINT"y/delta";
LOCATE 5,5 : PRINT"1";
IF A = 1 THEN GOSUB 500 : GOTO 300
IF A = 2 THEN GOSUB 600 : GOTO 300
IF A = 3 THEN GOSUB 700 : GOTO 300
IF A = 4 THEN GOSUB 500:GOSUB 600
IF A = 5 THEN GOSUB 500:GOSUB 600:GOSUB 700
IF A = 6 THEN GOSUB 800
IF A = 7 THEN GOSUB 900
IF A = 8 THEN GOSUB 1000
IF A = 9 GOTO 1100
300
INPUT A
IF A = 99 THEN STOP
GOTO 200
500
FOR I=1 TO N
 LINE(300*UL(I-1)+55,(180-150*Y1(I-1)))-
                                    (300*UL(I)+55,(180-150*Y1(I)))
 CIRCLE(300*UL(I)+55,(180-150*Y1(I))),3
NEXT I
```

```
LOCATE 2,40 : PRINT"Lam"
LOCATE 24,45 : PRINT"1";
LOCATE 23,75 : PRINT"u/U"
RETURN
600
FOR I=1 TO N
 LINE(155+300*UT(I-1),(180-150*Y1(I-1)))-
                                    (155+300*UT(I),(180-150*Y1(I)))
 CIRCLE(155+300*UT(I),(180-150*Y1(I))),3
NEXT I
LOCATE 2,52 :PRINT"Turb"
LOCATE 24,57 : PRINT"1";
LOCATE 23,75 : PRINT"u/U"
RETURN
700
FOR I=1 TO N
 LINE(255+300*UM(I-1),(180-150*Y1(I-1)))-
                                    (255+300*UM(I),(180-150*Y1(I)))
 CIRCLE(255+300*UM(I),(180-150*Y1(I))),3
NEXT I
LOCATE 2,65 : PRINT"Mean"
LOCATE 24,70 : PRINT"1";
LOCATE 23,75 : PRINT"u/U"
RETURN
800
CIRCLE(300*GAMMA(1)+55,(180-150*Y1(1))),3
FOR I=2 TO N
 LINE(300*GAMMA(I-1)+55,(180-150*Y1(I-1)))-
                                 (300*GAMMA(I)+55,(180-150*Y1(I)))
CIRCLE(300*GAMMA(I)+55,(180-150*Y1(I))),3
NEXT I
LOCATE 5,60 : PRINT"gamma = ";GAMMA;
LOCATE 24,45 : PRINT"1";
LOCATE 23,75 : PRINT"gamma"
RETURN
900
PSET(355,180)
FOR I=1 TO 25
 YOD = I/20
 C1 = YOD
 C2 = C1*5
 C3 = 1 + C2
 GAM1 = 1/C3
 X = 300*GAM1
 Y = 150*YOD
 LINE -(X+55,180-Y)
NEXT I
IF GAMMA = 0 GOTO 910
X1 = 300*GAMMA(1)/GAMMA + 55 : Y1 = 180 - 150*Y1(1)
CIRCLE(X1,Y1),3
PSET(X1,Y1)
FOR I=2 TO N
 X1 = 300*GAMMA(I-1)/GAMMA + 55 : Y1 = 180-150*Y1(I-1)
 X2 = 300*GAMMA(I)/GAMMA + 55 : Y2 = 180-150*Y1(I)
 PSET(X2,Y2)
 CIRCLE(X2,Y2),3
```

```
NEXT I
910
LOCATE 5,60 : PRINT"gamma = ";GAMMA;
LOCATE 24,45 : PRINT"1";
LOCATE 23,75 : PRINT"gamma"
RETURN
1000
CIRCLE(3000*RMS(1)+55,(180-150*Y1(1))),3
FOR I=2 TO N
 X1 = (3000*RMS(I-1)/UINF+55)
 Y1 = (180-150*Y1(I-1))
 X2 = (3000*RMS(I)/UINF+55)
 Y2 = (180-150*Y1(I))
 LINE(X1,Y1)-(X2,Y2)
 CIRCLE(3000*RMS(I)/UINF+55,(180-150*Y1(I))),3
NEXT I
LOCATE 24,44 : PRINT"10%";
LOCATE 23,75 : PRINT"RMS"
RETURN
1100
CLS
PRINT"Y","Y/DELTA","UM","GAMMA"
PRINT
FOR I=1 TO N
 PRINT INT(Y(I)*1000+0.5)/1000,INT(Y1(I)*1000+0.5)/1000,;
 PRINT INT(UM(I)*1000+0.5)/1000,INT(GAMMA(I)*1000+0.5)/1000
NEXT I

PRINT
PRINT"turbulence intensity        ",TINT,"%"

STOP
```

ANLYS4.BAS - profile reduction program
(outputs integral parameters)

```
REM                        ANALYSIS     (anlys4)
REM
REM
REM profile analysis program          5/5/88        Derek Graham
REM
REM
REM update 16/8/89  modified intermittency analysis
REM

REM read in profile data

DIM MEAN(40),MLAM(40),MTURB(40),GAMMA(40),BI(40),Y(40)
DIM RMS(40),UM(40),UL(40),UT(40),Y1(40),U(40)

INPUT"enter filename           ",FILE$
OPEN"I",f1,FILE$
INPUTf1,T,H,N,UINF,YDAT,X,TINT
FOR I=1 TO N
 INPUTf1,MEAN(I),RMS(I),MLAM(I),MTURB(I),GAMMA(I),BI(I)
NEXT I
CLOSEf1

REM convert bits(B) to mm(Y)

FOR I=1 TO N
 Y1(I) = YDAT + 0.1979*(BI(1) - BI(I))
NEXT I

REM non dimensionalise velocities using UINF

FOR I=1 TO N
 UM(I) = MEAN(I)/UINF
 UL(I) = MLAM(I)/UINF
 UT(I) = MTURB(I)/UINF
NEXT I

REM estimate delta

FOR I=1 TO N
 IF UM(I) < 0.99 GOTO 100
 DELTA = Y1(I)  - (Y1(I)-Y1(I-1))*(UM(I) - 0.99)/(UM(I) - UM(I-1))
 GOTO 110
 100
NEXT I
110

REM non dimensionalise y

FOR I=1 TO N
 Y(I) = Y1(I)/DELTA
NEXT I

REM evaluate fluid properties

MU = (1.725 + 0.004375*T)/1E5
RHO = (0.46535*H)/(T+273)
```

```
NU = MU/RHO

REM calculate Rx

RX = UINF*X/(NU*1000)

REM estimate gamma (up to y/delta = 0.4)

GAMMA = 0
FOR I = 1 TO N
 IF Y(1) > 0.4 GOTO 210
 IF Y(I) > 0.4 GOTO 200
 GAMMA = GAMMA + GAMMA(I)
NEXT I
200
GAMMA = GAMMA/(I-1) : GOTO 220
210
GAMMA = GAMMA(1)
220

REM

LPRINT"FILE NAME                    "FILE$
LPRINT
LPRINT
LPRINT"b.l. thickness               ",INT(DELTA*100+0.5)/100
LPRINT"Intermittency                ",INT(GAMMA*1000+0.5)/1000
LPRINT"freestream velocity          ",INT(UINF*100+0.5)/100
LPRINT"Reynolds number (x)          ",INT(RX*100+0.5)/100
LPRINT
LPRINT
IF GAMMA < 0.01 THEN GOSUB 400:GOSUB 1000:GOSUB 3000 : GOTO 300
                                                      : REM Laminar
IF GAMMA > 0.99 THEN GOSUB 500:GOSUB 2000:GOSUB 4000 : GOTO 300
                                                    : REM Turbulent
GOSUB 1000
GOSUB 2000 : REM transitional
LPRINT
GOSUB 5000
LPRINT
LPRINT"TRANSITIONAL MEAN PROFILE"
LPRINT"_____"
LPRINT

IF GAMMA < 0.5 THEN GOSUB 350:GOSUB 400:GOSUB 1000:GOSUB 3000
                                                    : GOTO 300
GOSUB 350:GOSUB 500:GOSUB 2000:GOSUB 4000


300

STOP

350
OPEN"I",f1,FILE$
INPUTf1,T,H,N,UINF,YDAT,X,TINT
```

```
FOR I=1 TO N
 INPUTf1,MEAN(I),RMS(I),MLAM(I),MTURB(I),GAMMA(I),BI(I)
NEXT I
CLOSEf1

REM convert bits(B) to mm(Y)

FOR I=1 TO N
 Y1(I) = YDAT + 0.1979*(BI(1) - BI(I))
NEXT I

REM non dimensionalise velocities using UINF

FOR I=1 TO N
 UM(I) = MEAN(I)/UINF
 UL(I) = MLAM(I)/UINF
 UT(I) = MTURB(I)/UINF
NEXT I

REM non dimensionalise y

FOR I=1 TO N
 Y(I) = Y1(I)/DELTA
NEXT I

400
FOR I=1 TO N
 MLAM(I) = MEAN(I)
 UL(I) = UM(I)
NEXT I
RETURN

500
FOR I=1 TO N
 MTURB(I) = MEAN(I)
 UT(I) = UM(I)
NEXT I
RETURN

1000

REM
REM laminar b.l. subroutine
REM

REM calculate shear stress

TOL = MU*MLAM(1)/Y1(1)*1000
CFL = 2*TOL/(RHO*UINF)
1110

REM LAMINAR PARINT

SUM1 = 0
SUM2 = 0
SUM3 = 0
```

```
SUM4 = 0
SUM5 = 0

N2 = N - 2

L% = 0

CALL SUMS(UL(),N,L%)

REM laminar b.l. parameters

DEL1L = SUM2
THETAL = SUM1 - SUM3
DEL2L = SUM1 - SUM4
H12L = DEL1L/THETAL
H32L = DEL2L/THETAL
RDISL = (UINF*DEL1L)/(NU*1000)
RMOML = (UINF*THETAL)/(NU*1000)
DEL1LM = DEL1L - GAMMA*SUM5
1800

RETURN

2000

REM
REM turbulent b.l. routine
REM

DIM UTAU(30),ITUT(30),YPLUS(30),UPLUS(30),E(30)

S1 = 0
S2 = 0
S3 = 0
S4 = 0
SUM1 = 0
SUM2 = 0
SUM3 = 0
SUM4 = 0
SUM5 = 0

REM "loglaw" establish utau & velocity profiles

REM in terms of u+ and y+

SUM = 0
L = 0
2150
FOR I=1 TO N
 IF MTURB(I) = 0 GOTO 2450
 UTAU(I) = 1
 GOTO 2200
 2190
 UTAU(I) = ITUT(I)
 2200
 YPLUS(I) = UTAU(I)*Y1(I)/(NU*1000)
```

```
 ITUT(I) = MTURB(I)/(2.439*LOG(YPLUS(I))+5.2)
 E(I) = UTAU(I) - ITUT(I)
 IF ABS(E(I)) < 0.00001 THEN GOTO 2300
 GOTO 2190
 2300
 IF YPLUS(I) <= 30 OR Y(I) >= 0.2 GOTO 2400
 L = L + 1
 SUM = SUM + UTAU(I)
 2400
NEXT I
2450
IF L = 0 THEN GOTO 2510
UTAU1 = SUM/L
FOR I=1 TO N
 UPLUS(I) = MTURB(I)/UTAU1
 YPLUS(I) = UTAU1*Y1(I)/(NU*1000)
NEXT I
YT1 = YPLUS(3)
IF YT1 > 50 GOTO 2500

FOR K=2 TO N
 Y1(K-1) = Y1(K)
 MTURB(K-1) = MTURB(K)
 Y(K-1) = Y(K)
 UT(K-1) = UT(K)
NEXT K
Y1(N) = 0
MTURB(N) = 0
Y(N) = 0
UT(N) = 0
N = N - 1
LPRINT"point nearest the wall has been deleted"
GOTO 2150

2500
REM "wallint" establish the inner profile integral functions up to
REM and including the third data point

C1 = 540.6
C2 = 6546
C3 = 82770
A = 2.439
B = 5.2
PI11 = A*(YT1*(LOG(YT1)-1)-50*(LOG(50)-1))
PI12 = B*(YT1-50)
INT1W = PI11+PI12
PI21 = YT1*(LOG(YT1))-50*(LOG(50))
PI22 = -2*(YT1*(LOG(YT1)-1)-50*(LOG(50)-1))
PI23 = 2*A*B*(YT1*(LOG(YT1)-1)-50*(LOG(50)-1))
PI24 = B*(YT1-50)
INT2W = A*(PI21+PI22)+PI23+PI24
PI31 = YT1*(LOG(YT1))-3*YT1*(LOG(YT1))+6*YT1*(LOG(YT1)-1)
PI32 = -50*(LOG(50))+3*50*(LOG(50))-6*50*(LOG(50)-1)
PI33 = YT1*(LOG(YT1))-50*(LOG(50))
PI34 = -2*(YT1*(LOG(YT1)-1)-50*(LOG(50)-1))
PI35 = 3*A*B*(YT1*(LOG(YT1)-1)-50*(LOG(50)-1))
```

```
PI36 = B*(YT1-50)
INT3W = A*(PI31+PI32)+3*B*A*(PI33+PI34)+PI35+PI36
S1 = (C1 + INT1W)*(NU/UINF)*1000
S2 = (YT1*(NU/UTAU1)*1000) - S1
S3 = (C2 + INT2W)*(NU/UINF)*(UTAU1/UINF)*1000
S4 = (C3 + INT3W)*(NU/UINF)*(UTAU1/UINF)*1000

REM "parint" complete integration from third data point
REM to the edge of th b.l.

L% = 3
GOTO 2520
2510
LPRINT
LPRINT"Simpsons rule is used from the wall"
LPRINT
L% = 0
2520
N2 = N - 2

CALL SUMS(UT(),N,L%)


REM total integrals

SUM1 = SUM1 + S1
SUM2 = SUM2 + S2
SUM3 = SUM3 + S3
SUM4 = SUM4 + S4
SUM5 = SUM5 + S2

REM turbulent b.l. parameters

DEL1T = SUM2
THETAT = SUM1 - SUM3
DEL2T = SUM1 - SUM4
H12T = DEL1T/THETAT
H32T = DEL2T/THETAT
RDIST = (UINF*DEL1T)/(NU*1000)
RMOMT = (UINF*THETAT)/(NU*1000)
CF1 = 0.246/(EXP(1.561*H12T)*RMOMT.268)
CF2 = 2.0*(UTAU1/UINF)
TOT = ((CF1+CF2)/2)*RHO*UINF/2
IF L% = 0 THEN TOT=CF1*RHO*UINF/2: GOTO 2800
WP = 0.205*UINF/UTAU1 - 0.5*LOG(UTAU1*DELTA/(NU*1000))-1.066
2800
DEL1TR = DEL1L*(1-GAMMA) + DEL1T*GAMMA
DEL1TM = GAMMA*SUM5

RETURN

3000

REM laminar printout

LPRINT
```

```
LPRINT"LAMINAR BOUNDARY LAYER PARAMETERS"
LPRINT
LPRINT"displacement thickness              "INT(DEL1L*1000+0.5)/1000
LPRINT"momentum thickness                  "INT(THETAL*1000+0.5)/1000
LPRINT"energy thickness                    "INT(DEL2L*1000+0.5)/1000
LPRINT"shape factor 12                     "INT(H12L*1000+0.5)/1000
LPRINT"shape factor 32                     "INT(H32L*1000+0.5)/1000
LPRINT"displacement thickness Reynolds no"INT(RDISL+0.5)
LPRINT"momentum thickness Reynolds no     "INT(RMOML+0.5)
LPRINT"t0                                  "INT(TOL*1000+0.5)/1000
LPRINT"cf                                  "INT(CFL*1E6+0.5)/1E6
LPRINT

RETURN

4000

REM turbulent printout

LPRINT
LPRINT"TURBULENT B.L. PARAMETERS
LPRINT
LPRINT"displacement thickness              "INT(DEL1T*1000+0.5)/1000
LPRINT"momentum thickness                  "INT(THETAT*1000+0.5)/1000
LPRINT"energy thickness                    "INT(DEL2T*1000+0.5)/1000
LPRINT"shape factor H12                    "INT(H12T*1000+0.5)/1000
LPRINT"shape factor H32                    "INT(H32T*1000+0.5)/1000
LPRINT"displacement thickness Reynolds no"INT(RDIST+0.5)
LPRINT"momentum thickness Reynolds no     "INT(RMOMT+0.5)
LPRINT"cf Lud/Till                         "INT(CF1*1E6+0.5)/1E6
LPRINT"cf log-plot                         "INT(CF2*1E6+0.5)/1E6
LPRINT"wall shear stress                   "INT(TOT*1000+0.5)/1000
LPRINT"wake parameter                      "INT(WP*1000+0.5)/1000
LPRINT


RETURN


5000

REM transitional printout

LPRINT
LPRINT"TRANSITIONAL B.L. PARAMETERS"
LPRINT
LPRINT"PARAMETER","LAMINAR","TURBULENT"
LPRINT"_____"
LPRINT
LPRINT"disp thk",INT(DEL1L*1000+0.5)/1000,INT(DEL1T*1000+0.5)/1000
LPRINT"mom thk",INT(THETAL*1000+0.5)/1000,INT(THETAT*1000+0.5)/1000
LPRINT"energy thk",INT(DEL2L*1000+0.5)/1000,INT(DEL2T*1000+0.5)/1000
LPRINT"H12",INT(H12L*1000+0.5)/1000,INT(H12T*1000+0.5)/1000
LPRINT"H32",INT(H32L*1000+0.5)/1000,INT(H32T*1000+0.5)/1000
LPRINT"Rdisp",INT(RDISL+0.5),INT(RDIST+0.5)
LPRINT"Rmom",INT(RMOML+0.5),INT(RMOMT+0.5)
```

```
LPRINT"Cf",INT(CFL*1E6+0.5)/1E6,"áá"
LPRINT"Cf Lud/till","áá",INT(CF1*1E6+0.5)/1E6
LPRINT"Cf Log-plot","áá",INT(CF2*1E6+0.5)/1E6
LPRINT"TO",INT(TOL*1000+0.5)/1000,INT(TOT*1000+0.5)/1000
LPRINT"Wake par.","áá",INT(WP*1000+0.5)/1000
LPRINT
LPRINT
LPRINT"COMBINED PARAMETERS"
LPRINT
LPRINT"a) Dhawan and Narasimha"
LPRINT"dislacement thickness       ";INT(DEL1TR*1000+0.5)/1000
LPRINT
LPRINT"b) Modified intermittency"
LPRINT"displacement thickness      ";INT((DEL1LM+DEL1TM)*1000+0.5)
                                                              /1000
RETURN


SUB SUMS(U(1),N,L%)

SHARED SUM1,SUM2,SUM3,SUM4,SUM5,DELTA,N2,Y()

DIM A(30),B(30),C(30),DET(30),INT1(30),INT2(30),INT3(30)
DIM INT4(30),INT5(30),INT6(30),INT7(30),INT8(30)
DIM INT1TM(30),INT2TM(30)

FOR K=L% TO N2

 IF U(K+2) = 0 GOTO 2700

 DET1 = 1*(Y(K+1)*Y(K+2)-Y(K+2)*Y(K+1))
 DET2 = Y(K)*(Y(K+2)-Y(K+1))
 DET3 = Y(K)*(Y(K+2)-Y(K+1))
 DET(K) = DET1 - DET2 + DET3

 A1 = U(K)*(Y(K+1)*Y(K+2)-Y(K+2)*Y(K+1))
 A2 = Y(K)*(U(K+1)*Y(K+2)-U(K+2)*Y(K+1))
 A3 = Y(K)*(U(K+1)*Y(K+2)-U(K+2)*Y(K+1))
 A(K) = (A1 - A2 + A3)/DET(K)

 B1 = 1*(U(K+1)*Y(K+2)-U(K+2)*Y(K+1))
 B2 = U(K)*(Y(K+2)-Y(K+1))
 B3 = Y(K)*(U(K+2)-U(K+1))
 B(K) = (B1 - B2 + B3)/DET(K)

 C1 = 1*(Y(K+1)*U(K+2)-Y(K+2)*U(K+1))
 C2 = Y(K)*(U(K+2)-U(K+1))
 C3 = U(K)*(Y(K+2)-Y(K+1))
 C(K) = (C1 - C2 + C3)/DET(K)

 PI11 = A(K)*(Y(K+1)-Y(K))+B(K)*(Y(K+1)-Y(K))/2
 PI12 = C(K)*(Y(K+1)-Y(K))/3
 INT1(K) = PI11 + PI12

 PI21 = A(K)*(Y(K+2)-Y(K+1))+B(K)*(Y(K+2)-Y(K+1))/2
 PI22 = C(K)*(Y(K+2)-Y(K+1))/3
```

```
INT2(K) = PI21 + PI22

PI31 = (1.0-A(K))*(Y(K+1)-Y(K))-B(K)*(Y(K+1)-Y(K))/2
PI32 = -C(K)*(Y(K+1)-Y(K))/3
INT3(K) = PI31+PI32

PI41 = (1.0-A(K))*(Y(K+2)-Y(K+1))-B(K)*(Y(K+2)-Y(K+1))/2
PI42 = -C(K)*(Y(K+2)-Y(K+1))/3
INT4(K) = PI41 + PI42

PI51 = A(K)*A(K)*(Y(K+1)-Y(K))
PI52 = A(K)*B(K)*(Y(K+1)-Y(K))
PI53 = (2*A(K)*C(K)+B(K)*B(K))*(Y(K+1)-Y(K))/3
PI54 = B(K)*C(K)*(Y(K+1)-Y(K))/2
PI55 = C(K)*C(K)*(Y(K+1)-Y(K))/5
INT5(K) = PI51+PI52+PI53+PI54+PI55

PI61 = A(K)*A(K)*(Y(K+2)-Y(K+1))
PI62 = A(K)*B(K)*(Y(K+2)-Y(K+1))
PI63 = (2*A(K)*C(K)+B(K)*B(K))*(Y(K+2)-Y(K+1))/3
PI64 = B(K)*C(K)*(Y(K+2)-Y(K+1))/2
PI65 = C(K)*C(K)*(Y(K+2)-Y(K+1))/5
INT6(K) = PI61+PI62+PI63+PI64+PI65

PI71 = A(K)*A(K)*A(K)*(Y(K+1)-Y(K))
PI72 = 3*A(K)*A(K)*B(K)*(Y(K+1)-Y(K))/2
PI73 = A(K)*(A(K)*C(K)+B(K)*B(K))*(Y(K+1)-Y(K))
PI74 = B(K)*(6*A(K)*C(K)+B(K)*B(K))*(Y(K+1)-Y(K))/4
PI75 = 0.6*C(K)*(A(K)*C(K)+B(K)*B(K))*(Y(K+1)-Y(K))
PI76 = B(K)*C(K)*C(K)*(Y(K+1)-Y(K))/2
PI77 = C(K)*C(K)*C(K)*(Y(K+1)-Y(K))/7
INT7(K) = PI71+PI72+PI73+PI74+PI75+PI76+PI77

PI81 = A(K)*A(K)*A(K)*(Y(K+2)-Y(K+1))
PI82 = 3*A(K)*A(K)*B(K)*(Y(K+2)-Y(K+1))/2
PI83 = A(K)*(A(K)*C(K)+B(K)*B(K))*(Y(K+2)-Y(K+1))
PI84 = B(K)*(6*A(K)*C(K)+B(K)*B(K))*(Y(K+2)-Y(K+1))/4
PI85 = 0.6*C(K)*(A(K)*C(K)+B(K)*B(K))*(Y(K+2)-Y(K+1))
PI86 = B(K)*C(K)*C(K)*(Y(K+2)-Y(K+1))/2
PI87 = C(K)*C(K)*C(K)*(Y(K+2)-Y(K+1))/7
INT8(K) = PI81+PI82+PI83+PI84+PI85+PI86+PI87

REM simpsons rule integration for modified disp thk

SUM = 0
C=0
FOR I=Y(K) TO Y(K+1) STEP (Y(K+1) - Y(K))/10
 IF C=0 OR C=10 THEN MUL = 1 : GOTO 2550
 IF C/2 = INT(C/2) THEN MUL = 2 ELSE MUL = 4
 2550
 SA = 1 - (A(K) + B(K)*I + C(K)*I)
 SB = 1 + 5*I
 S = SA/SB
 S = MUL*S
 SUM = SUM + S
 C=C+1
```

```
 NEXT I
 INT1TM(K) = SUM*(Y(K+1) - Y(K))/30

 SUM = 0
 C=0
 FOR I=Y(K+1) TO Y(K+2) STEP (Y(K+2) - Y(K+1))/10
  IF C=0 OR C=10 THEN MUL = 1 : GOTO 2560
  IF C/2 = INT(C/2) THEN MUL = 2 ELSE MUL = 4
  2560
  C=C+1
  SA = 1 - (A(K) + B(K)*I + C(K)*I)
  SB = 1 + 5*I
  S = SA/SB
  S = MUL*S
  SUM = SUM + S
 NEXT I
 INT2TM(K) = SUM*(Y(K+2) - Y(K+1))/30

 IF K = L% GOTO 2600
 GOTO 2610
 2600
 SUM1 = SUM1 + INT1(K)
 SUM2 = SUM2 + INT3(K)
 SUM3 = SUM3 + INT5(K)
 SUM4 = SUM4 + INT7(K)
 SUM5 = SUM5 + INT1TM(K)
 2610
 IF K < N2 AND K > L% GOTO 2620
 GOTO 2630
 2620
 SUM1 = SUM1 + 0.5*(INT1(K) + INT2(K-1))
 SUM2 = SUM2 + 0.5*(INT3(K) + INT4(K-1))
 SUM3 = SUM3 + 0.5*(INT5(K) + INT6(K-1))
 SUM4 = SUM4 + 0.5*(INT7(K) + INT8(K-1))
 SUM5 = SUM5 + 0.5*(INT1TM(K) + INT2TM(K-1))
 2630
 IF K = N2 GOTO 2640
 GOTO 2650
 2640
 SUM1 = SUM1 + 0.5*(INT1(K) + INT2(K-1)) + INT2(K)
 SUM2 = SUM2 + 0.5*(INT3(K) + INT4(K-1)) + INT4(K)
 SUM3 = SUM3 + 0.5*(INT5(K) + INT6(K-1)) + INT6(K)
 SUM4 = SUM4 + 0.5*(INT7(K) + INT8(K-1)) + INT8(K)
 SUM5 = SUM5 + 0.5*(INT1TM(K) + INT2TM(K-1)) + INT2TM(K)
 2650
NEXT K

2700

SUM1 = DELTA*SUM1
SUM2 = DELTA*SUM2
SUM3 = DELTA*SUM3
SUM4 = DELTA*SUM4
SUM5 = DELTA*SUM5

END SUB
```

CS.BAS - C-S boundary layer calculation method

```
REM
REM CS-METHOD                    12/9/88
REM
REM Numerical method of Cebeci and Smith (1977)
REM
REM Revised 18/10/89

REM
REM Main controlling program
REM

REM Dimension arrays

DIM X(1001),UE(1001),M(1001),ALPH(1001)
DIM H(61),ETA(61),DELV(61),F(61,2),U(61,2),V(61,2),B(61,2)
DIM S1(61),S2(61),S3(61),S4(61),S5(61),S6(61),R1(61),R2(61),R3(61)
DIM W1(61),W2(61),W3(61),A11(61),A12(61),A13(61),A21(61),A22(61)
DIM A23(61),G11(61),G12(61),G13(61),G21(61),G22(61),G23(61)
DIM DELU(61),DELF(61),A(61)

REM

ITMAX = 10
ALPH(1) = 0
NX = 1

GOSUB 1000 : REM Input
GOSUB 2000 : REM grid
GOSUB 3000 : REM Initial profile

OPEN"O",£1,FILE$+".DAT"
OPEN"O",£2,FILE$+".ERR"
OPEN"O",£3,FILE$+".PRO"

WRITE£1,FILE$,NXT
WRITE£3,NXT

PRINT

25

LOCATE 10,16 : PRINT" X",X(NX);"m    "
LOCATE 12,16 : PRINT"NX",NX

IT = 0
RX = UE(NX)*X(NX)/NU
IF NX >= NTR-1 AND NX < NTR THEN RXTR = RX
IF NX >= NTR AND NX < NTR+1 THEN GOSUB 3500
IF NX > 1 THEN ALPH(NX) = 0.5*(X(NX)+X(NX-1))/(X(NX)-X(NX-1))
M1 = 0.5*(M(NX)+1)
ALPH1 = M1 + ALPH(NX)
ALPH2 = M(NX) + ALPH(NX)
IF NX < NTR THEN STATU$ = "Laminar b.l." : GOTO 40
IF NX>=NTR AND NX<NTR+1 THEN STATU$ = "TRANSITION POINT" : GOTO 40
IF NX > NTR AND GAMTR < 0.99 THEN STATU$ = "Transitional b.l."
                                    ELSE STATUs = "Turbulent b.l."
```

```
40
LOCATE 16,16 : PRINT"**** ";STATU$;" ****"
IF NX < NTR GOTO 60
GOSUB 4000 : REM Eddy subroutine
60
IT = IT+1
IF IT>ITMAX THEN PRINT"Max iterations exceeded at x = ";NX;:GOTO 90

GOSUB 5000 : REM CMOM
GOSUB 6000 : REM SOLV3

REM Check for convergence

61
IF NX > NTR GOTO 62
REM Laminar flow
IF ABS(DELV(1)) > 1.0E-5 GOTO 60
GOTO 75
REM Turbulent flow
62
IF ABS(DELV(1))/(V(1,2)+0.5*DELV(1)) > 0.02 GOTO 60

REM check for growth
75
IF NX = 1 GOTO 90
IF NP = 61 GOTO 90
IF ABS(V(NP,2)) < 1.0E-3 GOTO 90
GOSUB 7000 : REM growth
GOTO 60
90
GOSUB 8000 : REM output
GOTO 25

1000
REM
REM input subroutine
REM

ETAE = 8
NU = 1.5E-5
XSTART = 0
XEND = 950
ST = 20
INPUT"transition location (mm)        ";XTRANS
INPUT"file name                       ";FILE$
INPUT"freestream turbulence (%)       ";TU
NXT = (XEND - XSTART)/ST + 1
NTR = 1 + (NXT-1)*(XTRANS - XSTART)/(XEND - XSTART)

H(1) = 0.01
K = 1.14

FOR I=0 TO NXT-1
 X(I+1) = (XSTART + I*ST)/1000
 READ UE(I+1)
NEXT I
```

```
DATA 0,2,4,5.4,7.3,9.4,11,12.4,13,13.2,13.4,13.6,13.8,14,14.2,14.3
DATA 14.4,14.5,14.7,14.8,15,15,15,15,14.8,14.7,14.5,14.4,14.3,14.2
DATA 14.1,13.9,13.8,13.6,13.5,13.4,13.3,13.2,13.1,13,12.9,12.8,12.6
DATA 12.5,12.4,12.4,12.3,12.3,12.3

REM calculation of pressure gradient parameter m

M(1) = 1
1050
FOR I=2 TO NXT
 IF I = NXT GOTO 1060
 A1 = (X(I)-X(I-1))*(X(I+1)-X(I-1))
 A2 = (X(I)-X(I-1))*(X(I+1)-X(I))
 A3 = (X(I+1)-X(I))*(X(I+1)-X(I-1))
 DUDX = -(X(I+1)-X(I))/A1*UE(I-1) + (X(I+1)-2*X(I)+X(I-1))/A2*UE(I)
                                        + (X(I)-X(I-1))/A3*UE(I+1)
 GOTO 1070
 1060
 A1 = (X(I-1)-X(I-2))*(X(I)-X(I-2))
 A2 = (X(I-1)-X(I-2))*(X(I)-x(I-1))
 A3 = (X(I)-X(I-1))*(X(I)-X(I-2))
 DUDX = (X(I)-X(I-1))/A1*UE(I-2) - (X(I)-X(I-2))/A2*UE(I-1)
                                  + (2*X(I)-X(I-2)-X(I-1))/A3*UE(I)
 1070
 M(I) = X(I)/UE(I)*DUDX
NEXT I

RETURN

2000
REM
REM grid subroutine
REM

IF (K - 1) < 0.001 GOTO 2005
NP = LOG((ETAE/H(1))*(K-1)+1)/LOG(K) + 1.0001
GOTO 2010
2005
NP = ETAE/H(1) + 1.0001
2010
IF NP < 61 GOTO 2015
PRINT"NUMBER OF VERTICAL GRID POINTS EXCEEDED 61"
STOP
2015
ETA(1) = 0
FOR J=2 TO 61
 H(J) = K*H(J-1)
 A(J) = 0.5*H(J-1)
 ETA(J) = ETA(J-1) + H(J-1)
NEXT J

RETURN

3000
REM
```

```
REM initial profile subruotine
REM

ETANPQ = 0.25*ETA(NP)
ETAU15 = 1.5/ETA(NP)
FOR J=1 TO NP
 ETAB = ETA(J)/ETA(NP)
 ETAB2 = ETAB
 F(J,2) = ETANPQ*ETAB2*(3 - 0.5*ETAB2)
 U(J,2) = 0.5*ETAB*(3 - ETAB2)
 V(J,2) = ETAU15*(1 - ETAB2)
 B(J,2) = 1.0
NEXT J

RETURN

3500
REM
REM  transition point
REM

RTHTR = RTHETA
MTR = -RTHTR*NU*M(NX)/(X(NX)*UE(NX))
N0 = 0.7 + EXP(0.588 - 3*TU)
N = (N0 + 22705*MTR*EXP(-0.45*TU))*1E-3
N = 0.0222
RLAMBDA = SQR((0.411*RTHTR)/N)
LAMBDA = RLAMBDA*NU/UE(NX)
PRINT
PRINT"lambda =  "LAMBDA
RETURN

4000
REM
REM eddy subroutine
REM

GAMTR = 1
BETA = (X(NX) - XTRANS/1000)/LAMBDA
EXPTM = 0.411*BETA
IF EXPTM < 10 GOTO 4015
GOTO 4020
4015
GAMTR = 1.0 - EXP(-EXPTM)
4020
IFLGD = 0
RX2 = SQR(RX)
RX4 = SQR(RX2)
PPLUS = M(NX)/(RX4*V(1,2).5)
RX216 = RX2*0.16
CN = SQR(1 - 11.8*PPLUS)
CRSQV = CN*RX4*SQR(V(1,2))/26
J = 1
EDV0 = 0.0168*RX2*(ETA(NP)-F(NP,2) + F(1,2))*GAMTR
4050
IF IFLGD = 1 GOTO 4100
```

```
YOA = CRSQV*ETA(J)
EDVI = RX216*ETA(J)*V(J,2)*(1 - EXP(-YOA))*GAMTR
IF EDVI < EDVO GOTO 4200
IFLGD = 1
4100
EDV = EDVO
GOTO 4300
4200
EDV = EDVI
4300
B(J,2) = 1 + EDV
J = J + 1
IF J < NP GOTO 4050

RETURN

5000
REM
REM coefficients subroutine
REM

FOR J=2 TO NP

 REM present station

 USB = 0.5*(U(J,2)+U(J-1,2))
 FVB = 0.5*(F(J,2)*V(J,2)+F(J-1,2)*V(J-1,2))
 FB  = 0.5*(F(J,2)+F(J-1,2))
 UB  = 0.5*(U(J,2)+U(J-1,2))
 VB  = 0.5*(V(J,2)+V(J-1,2))
 DERBV = (B(J,2)*V(J,2)-B(J-1,2)*V(J-1,2))/H(J-1)
 IF NX > 1 GOTO 5010

 REM previous station

 CFB = 0.0
 CVB = 0.0
 CFVB = 0.0
 CUSB = 0.0
 GOTO 5020
 5010
 CFB  = 0.5*(F(J,1)+F(J-1,1))
 CVB  = 0.5*(V(J,1)+V(J-1,1))
 CFVB = 0.5*(F(J,1)*V(J,1)+F(J-1,1)*V(J-1,1))
 CUSB = 0.5*(U(J,1)+U(J-1,1))
 CDERBV = (B(J,1)*V(J,1)-B(J-1,1)*V(J-1,1))/H(J-1)

 REM coefficients of the differenced momentum eqn

 5020
 S1(J) = B(J,2)/H(J-1)+(ALPH1*F(J,2)-ALPH(NX)*CFB)*0.5
 S2(J) = -B(J-1,2)/H(J-1)+(ALPH1*F(J-1,2)-ALPH(NX)*CFB)*0.5
 S3(J) = 0.5*(ALPH1*V(J,2)+ALPH(NX)*CVB)
 S4(J) = 0.5*(ALPH1*V(J-1,2)+ALPH(NX)*CVB)
 S5(J) = -ALPH2*U(J,2)
 S6(J) = -ALPH2*U(J-1,2)
```

```
 REM definitions of RJ

 IF NX = 1 GOTO 5030
 M1A = 0.5*(M(NX-1)+1)
 CLB = CDERBV+M1A*CFVB+M(NX-1)*(1 - CUSB)
 CRB = -M(NX)+ALPH(NX)*(CFVB-CUSB)-CLB
 GOTO 5035
 5030
 CRB = -M(NX)
 5035
 R2(J) = CRB-(DERBV+ALPH1*FVB-ALPH2*USB-ALPH(NX)*(CFB*VB-CVB*FB))
 R1(J) = F(J-1,2)-F(J,2)+H(J-1)*UB
 R3(J-1) = U(J-1,2)-U(J,2)+H(J-1)*VB

NEXT J

R1(1) = 0
R2(1) = 0
R3(NP) = 0

RETURN

6000
REM
REM SOLV3 block elimination method
REM

REM W-Elements for J=1

W1(1) = R1(1)
W2(1) = R2(1)
W3(1) = R3(1)

REM ALPHA - elements for J=1

A11(1) = 1.0
A12(1) = 0
A13(1) = 0
A21(1) = 0
A22(1) = 1.0
A23(1) = 0

REM GAMMA elements for J=2

G11(2) = -1.0
G12(2) = -0.5*H(1)
G13(2) = 0
G21(2) = S4(2)
G23(2) = -2*S2(2)/H(1)
G22(2) = G23(2)+S6(2)

REM Forward sweep

FOR J=2 TO NP
 IF J=2 GOTO 6100
```

```
 DEN = (A13(J-1)*A21(J-1)-A23(J-1)*A11(J-1)-A(J)*(A12(J-1)*A21(J-1)
                                                  -A22(J-1)*A11(J-1)))
 DEN1 = A22(J-1)*A(J)-A23(J-1)
 G11(J) = (A23(J-1)+A(J)*(A(J)*A21(J-1)-A22(J-1)))/DEN
 G12(J) = -(A(J)+G11(J)*(A12(J-1)*A(J)-A13(J-1)))/DEN1
 G13(J) = (G11(J)*A13(J-1)+G12(J)*A23(J-1))/A(J)
 G21(J) = (S2(J)*A21(J-1)-S4(J)*A23(J-1)+A(J)*(S4(J)*A22(J-1)-S6(J)
                                                 *A21(J-1)))/DEN
 G22(J) = (-S2(J)+S6(J)*A(J)-G21(J)*(A(J)*A12(J-1)-A13(J-1)))/DEN1
 G23(J) = G21(J)*A12(J-1)+G22(J)*A22(J-1)-S6(J)

 6100
 A11(J) = 1.0
 A12(J) = -A(J)-G13(J)
 A13(J) = A(J)*G13(J)
 A21(J) = S3(J)
 A22(J) = S5(J)-G23(J)
 A23(J) = S1(J)+A(J)*G23(J)

 W1(J) = R1(J)-G11(J)*W1(J-1)-G12(J)*W2(J-1)-G13(J)*W3(J-1)
 W2(J) = R2(J)-G21(J)*W1(J-1)-G22(J)*W2(J-1)-G23(J)*W3(J-1)
 W3(J) = R3(J)
NEXT J
6500

REM backward sweep

DELU(NP) = W3(NP)
E1 = W1(NP)-A12(NP)*DELU(NP)
E2 = W2(NP)-A22(NP)*DELU(NP)
DELV(NP) = (E2*A11(NP)-E1*A21(NP))/(A23(NP)*A11(NP)-A13(NP)*A21(NP))
DELF(NP) = (E1-A13(NP)*DELV(NP))/A11(NP)
J = INT(NP)
6600
J = J-1
E3 = W3(J)-DELU(J+1)+A(J+1)*DELV(J+1)
DEN2 = A21(J)*A12(J)*A(J+1)-A21(J)*A13(J)-A(J+1)*A22(J)*A11(J)
                                                  +A23(J)*A11(J)
DELV(J) = (A11(J)*(W2(J)+E3*A22(J))-A21(J)*W1(J)-E3*A21(J)*A12(J))
                                                        /DEN2
DELU(J) = -A(J+1)*DELV(J)-E3
DELF(J) = (W1(J)-A12(J)*DELU(J)-A13(J)*DELV(J))/A11(J)
IF J > 1 GOTO 6600

FOR J=1 TO NP
 F(J,2) = F(J,2) + DELF(J)
 U(J,2) = U(J,2) + DELU(J)
 V(J,2) = V(J,2) + DELV(J)
NEXT J
U(1,2) = 0

RETURN

7000
REM
```

```
REM Growth subroutine
REM

NPO = NP
NP1 = NP+1
NP  = NP+1
IF NX = NTR THEN NP = NP + 3
IF NP > 61 THEN NP = 61

REM definition of profiles for new np

FOR J = NP1 TO NP
 F(J,1) = U(NPO,1)*(ETA(J)-ETA(NPO))+F(NPO,1)
 U(J,1) = U(NPO,1)
 V(J,1) = 0
 B(J,1) = B(NPO,1)
 F(J,2) = U(NPO,2)*(ETA(J)-ETA(NPO))+F(NPO,2)
 U(J,2) = U(NPO,2)
 V(J,2) = V(J,1)
 B(J,2) = B(NPO,2)
NEXT J
NNP = NP-(NP1-1)
WRITE£2,NX,NNP

RETURN

8000
REM
REM output subroutine
REM

  WRITE£3,X(NX),NP,UE(NX)
  FOR J=1 TO NP
   WRITE£3,ETA(J),U(J,2)
  NEXT J

IF NX = 1 GOTO 8210
F1 = 0
THETA1 = 0
FOR J=2 TO NP
 F2 = U(J,2)*(1-U(J,2))
 THETA1 = THETA1+(F1+F2)*0.5*H(J-1)
 F1 = F2
NEXT J
THETA = THETA1*X(NX)/SQR(RX)
DELS = (ETA(NP)-F(NP,2))*X(NX)/SQR(RX)
H = DELS/THETA
CF = 2.0*V(1,2)/SQR(RX)
RTHETA = UE(NX)*THETA/NU
RDELS = UE(NX)*DELS/NU
WRITE£1, X(NX),THETA,DELS,H,CF,RX,RTHETA,RDELS,UE(NX),M(NX),GAMTR


8210
NX = NX+1
IF NX > NXT THEN CLOSE£1:CLOSE£2:CLOSE£3:END
```

```
REM shift profiles

FOR J=1 TO NP
 F(J,1) = F(J,2)
 U(J,1) = U(J,2)
 V(J,1) = V(J,2)
 B(J,1) = B(J,2)
NEXT J

RETURN
```

APPENDIX 2

EXPERIMENTAL DATA - INTEGRAL PARAMETERS

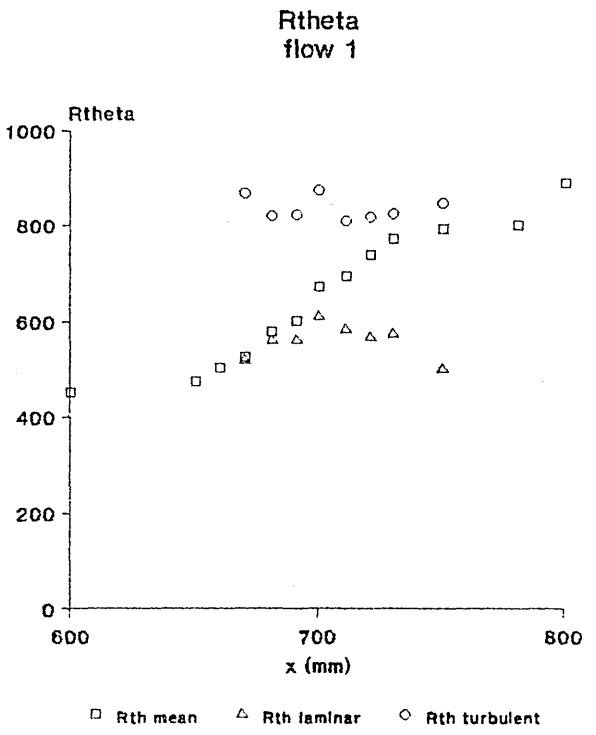

figure A2.1 momentum thickness Re number

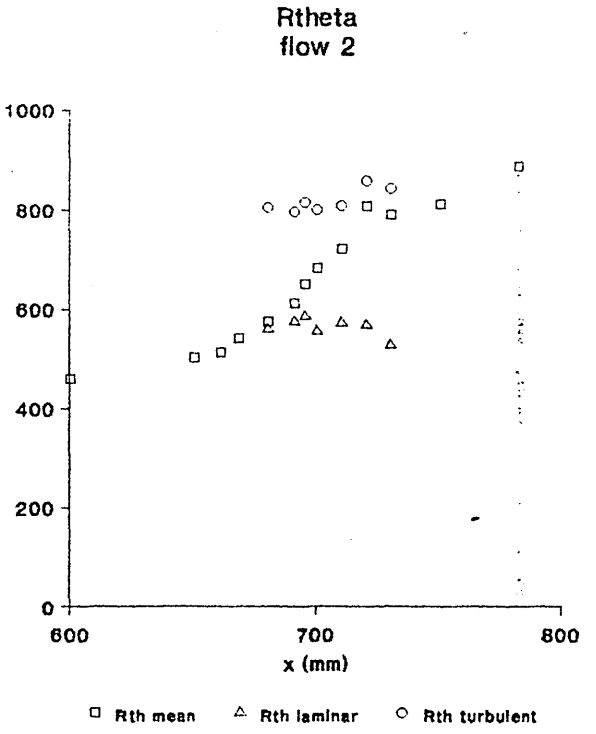

figure A2.2 momentum thickness Re number

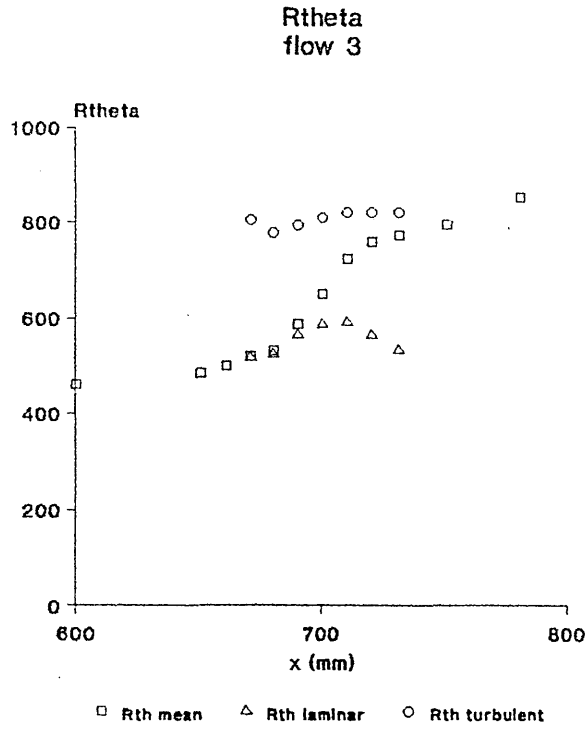

figure A2.3 momentum thickness Re number

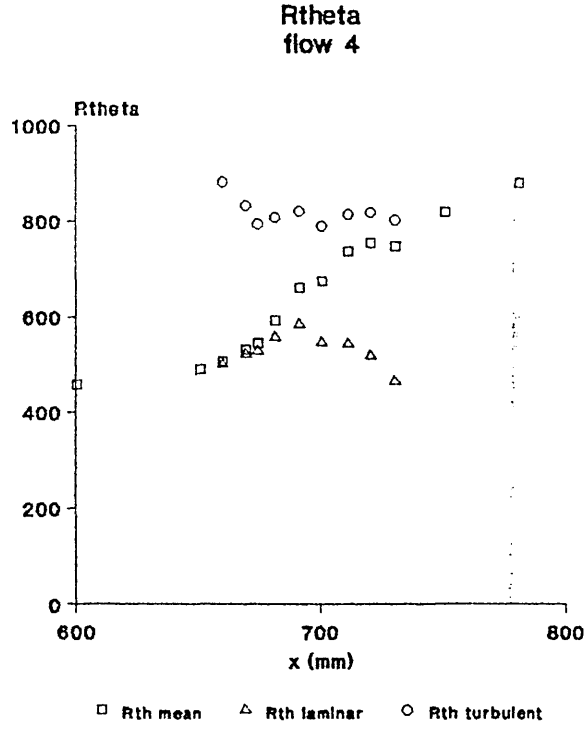

figure A2,4 momentum thickness Re number

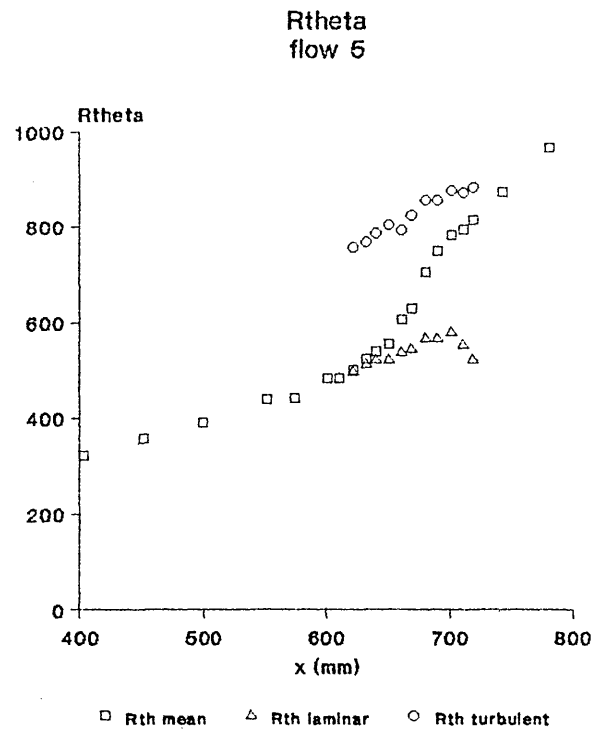

figure A2.5 momentum thickness Re number

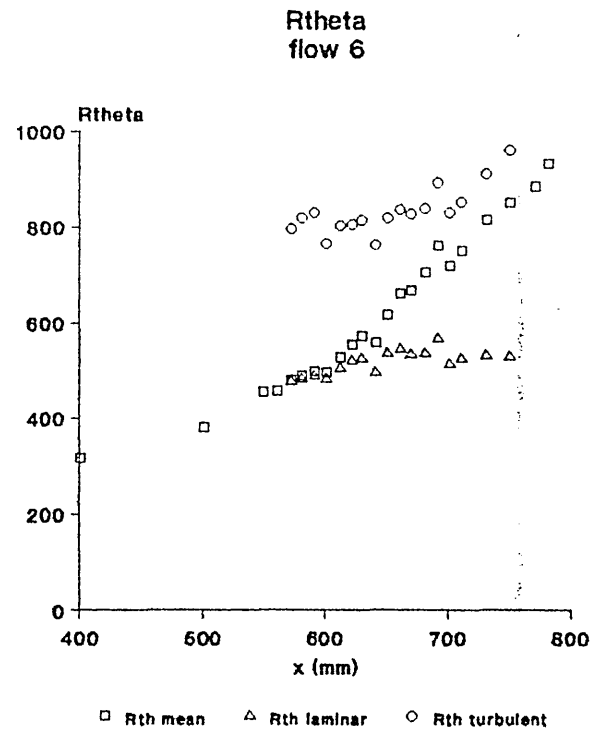

figure A2.6 momentum thickness Re number

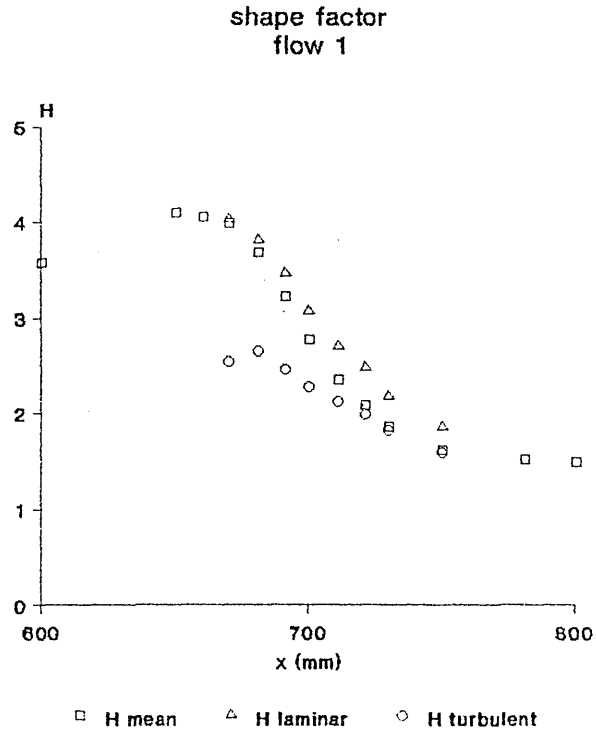

figure A2.7 shape factor

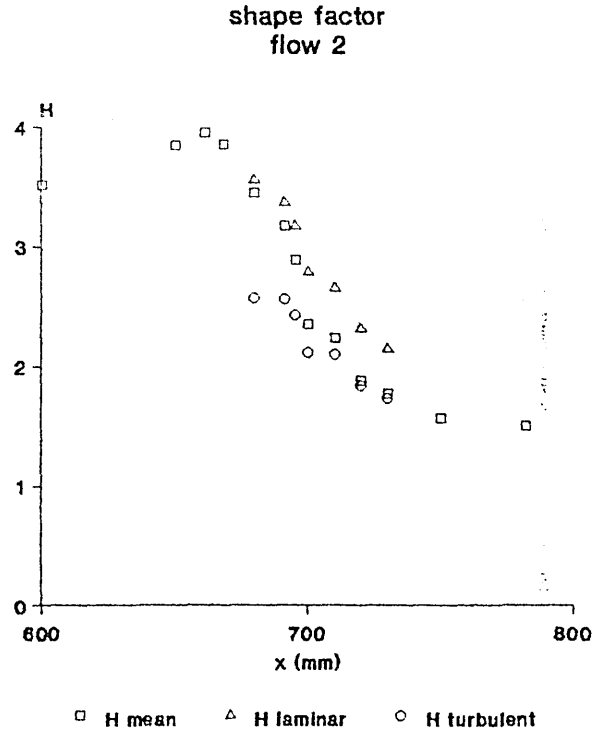

figure A2.8 shape factor

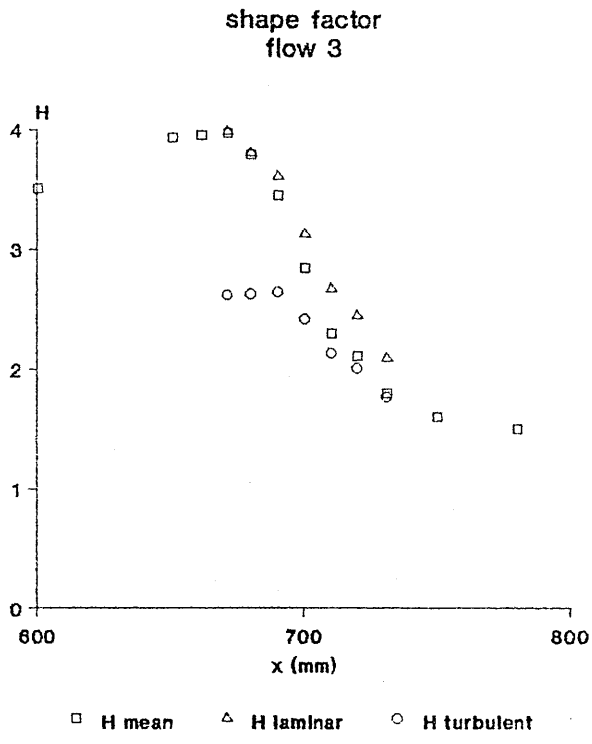

figure A2.9 shape factor

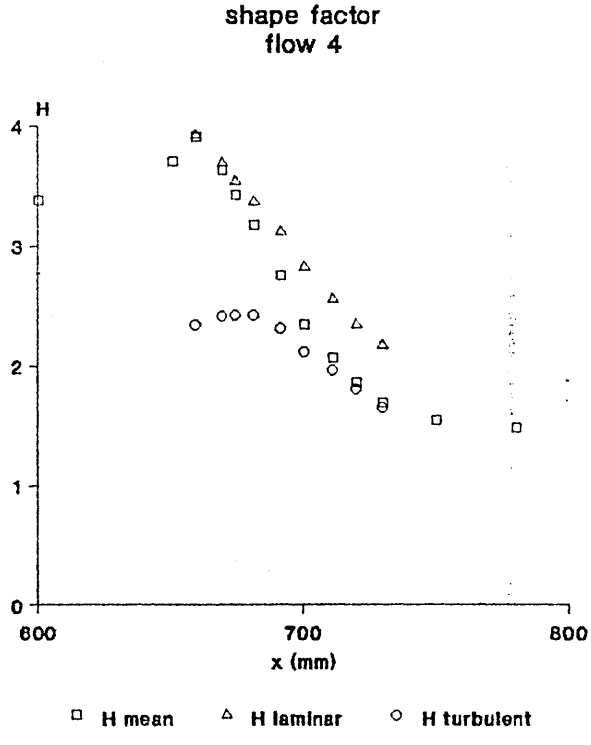

figure A2.10 shape factor

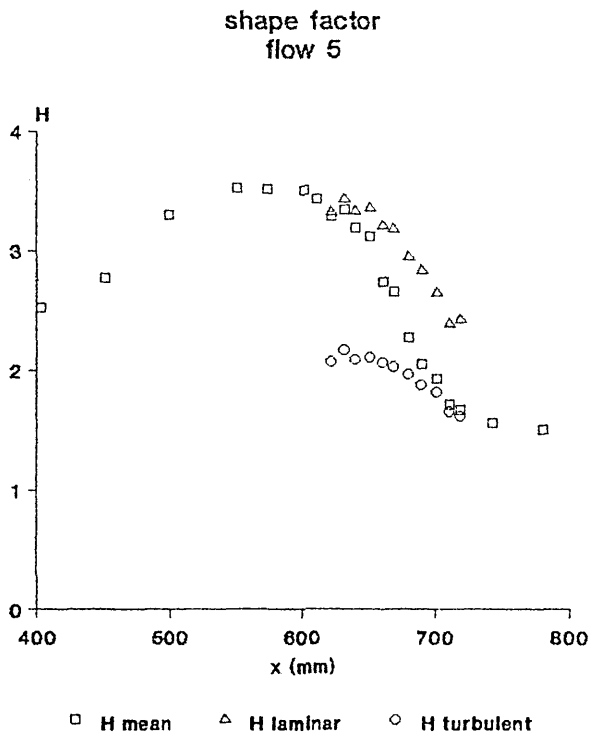

figure A2.11 shape factor

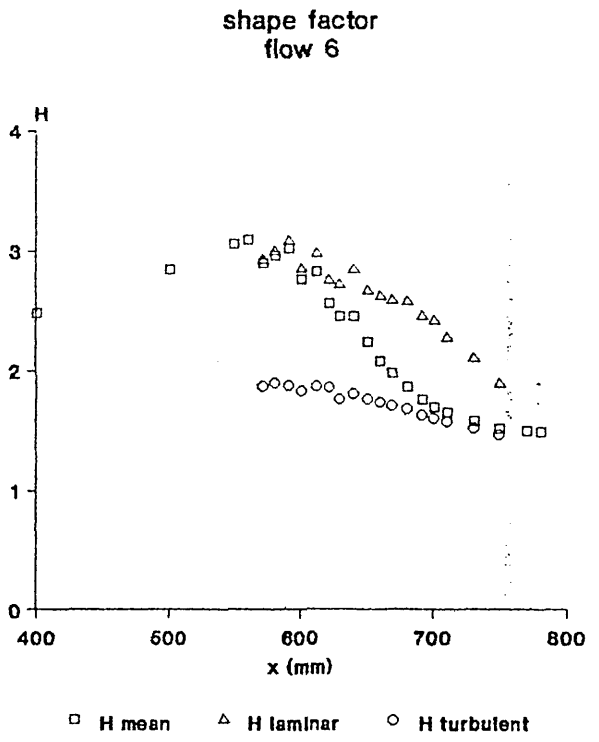

figure A2.12 shape factor

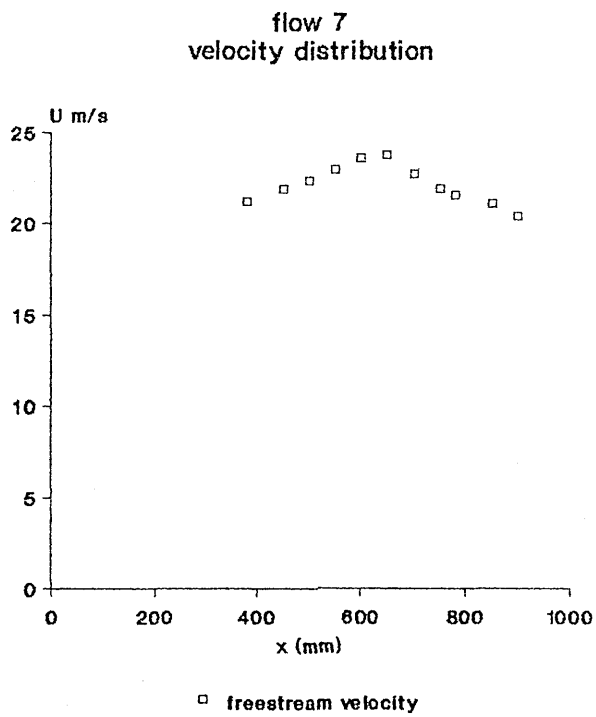

figure A2.13 velocity distribution for flow 7

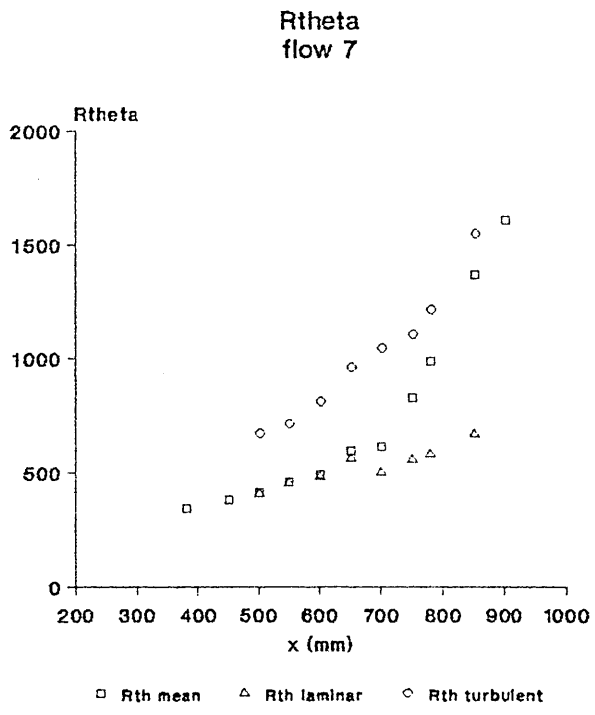

figure A2.14 momentum thickness Reynolds number

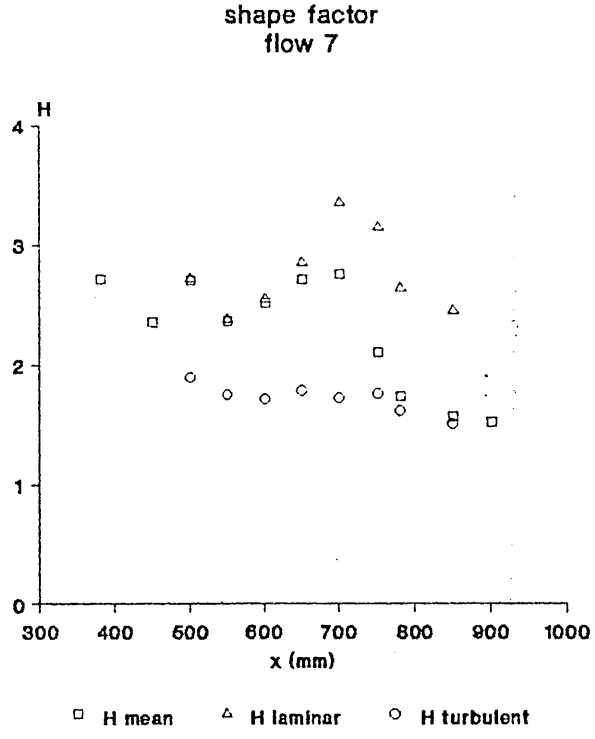

figure A2.15 shape factor

APPENDIX 3

EXPERIMENTAL DATA - VELOCITY PROFILES

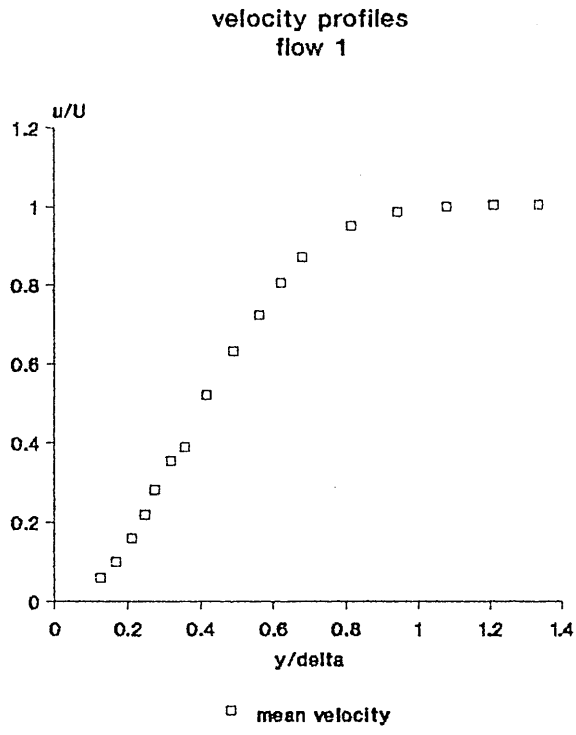

figure A3.1 x = 600

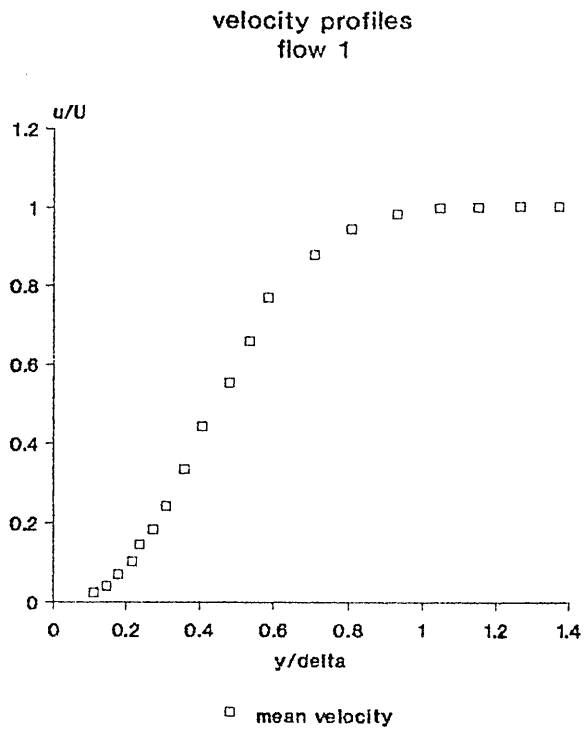

figure A3.2 x = 650

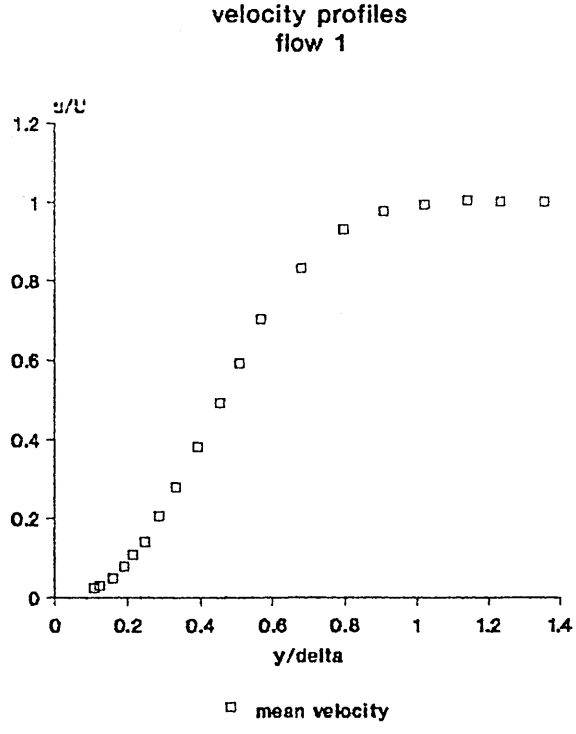

figure A3.3 x = 660

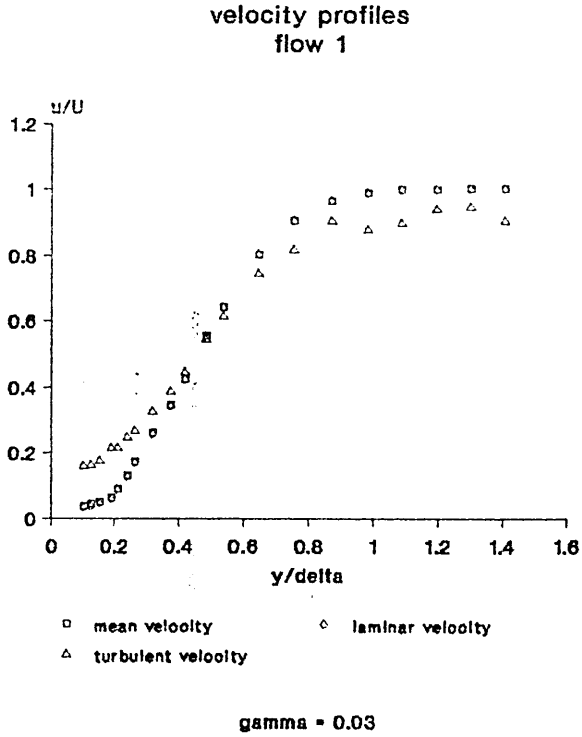

gamma = 0.03

figure A3.4 x = 670

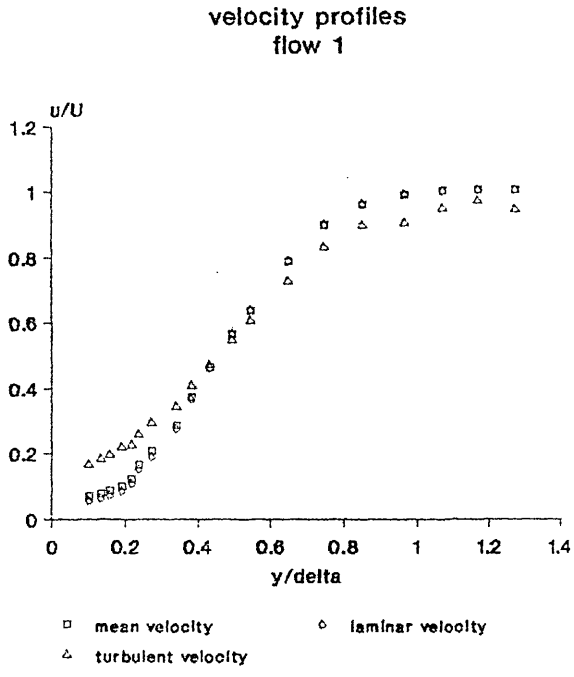

gamma = 0.12

figure A3.5 x = 681

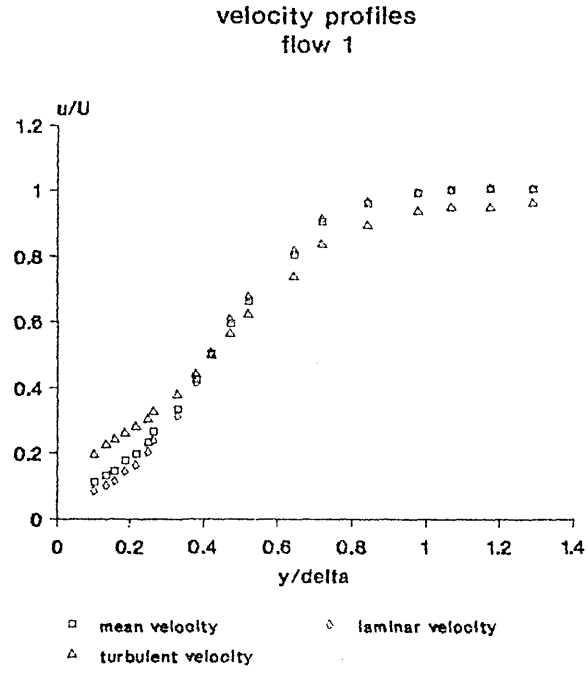

gamma = 0.27

figure A3.6 x = 691

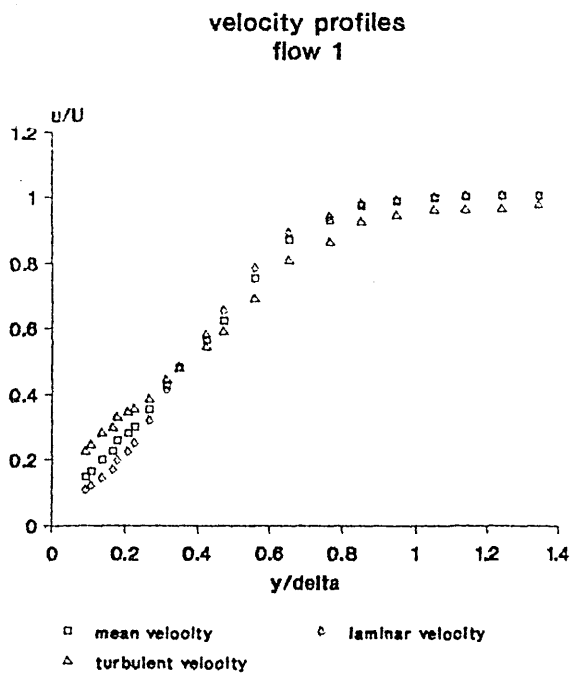

gamma = 0.44

figure A3.7 x = 700

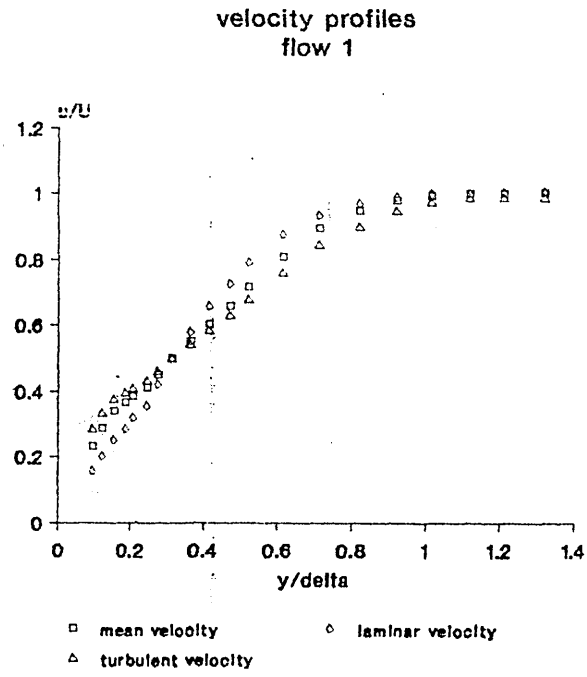

gamma = 0.72

figure A3.8 x = 711

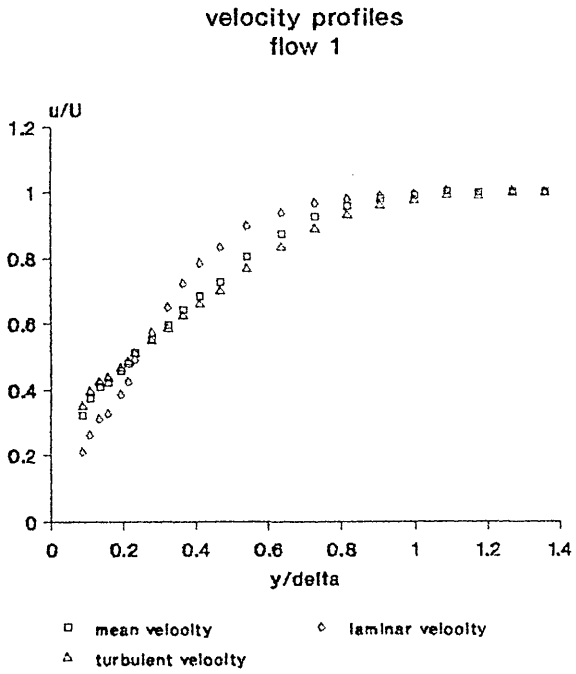

gamma = 0.86

figure A3.9 x = 721

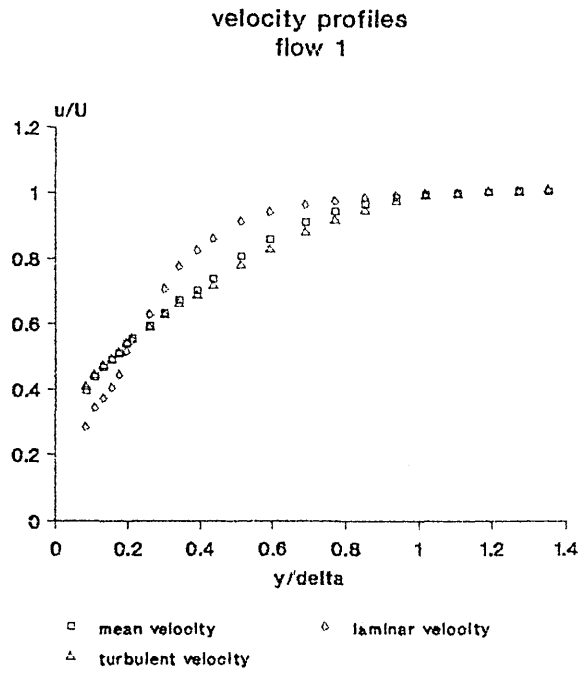

gamma = 0.93

figure A3.10 x = 730

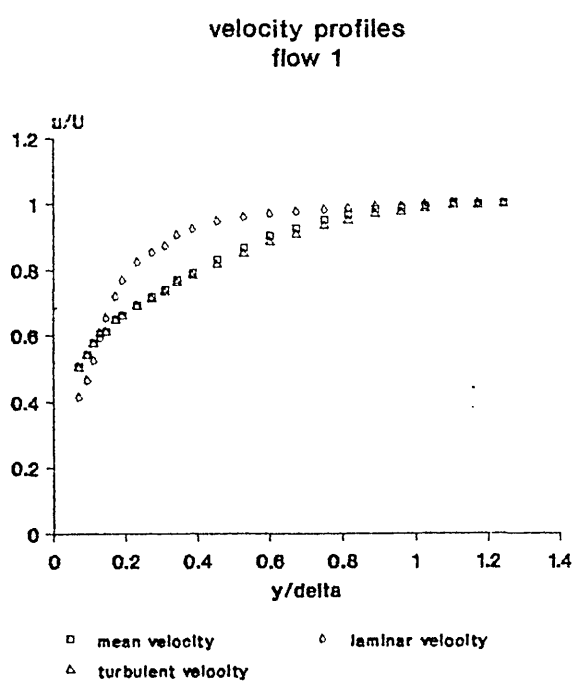

gamma = 0.98

figure A3.11 x = 760

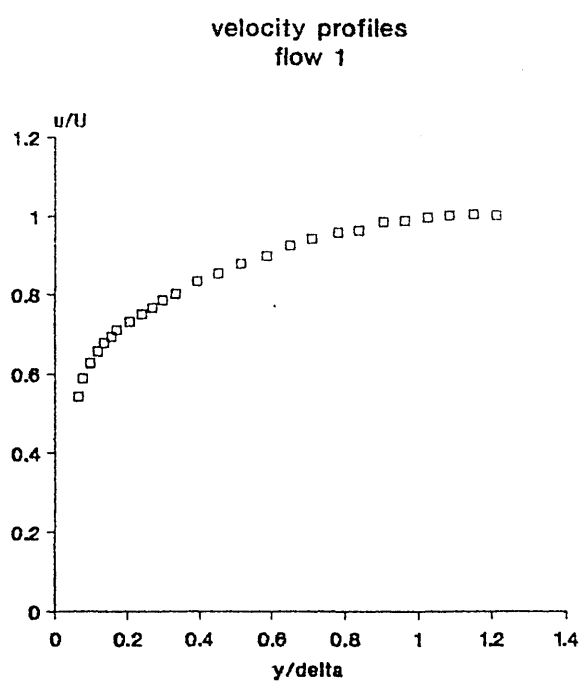

figure A3.12 x = 781

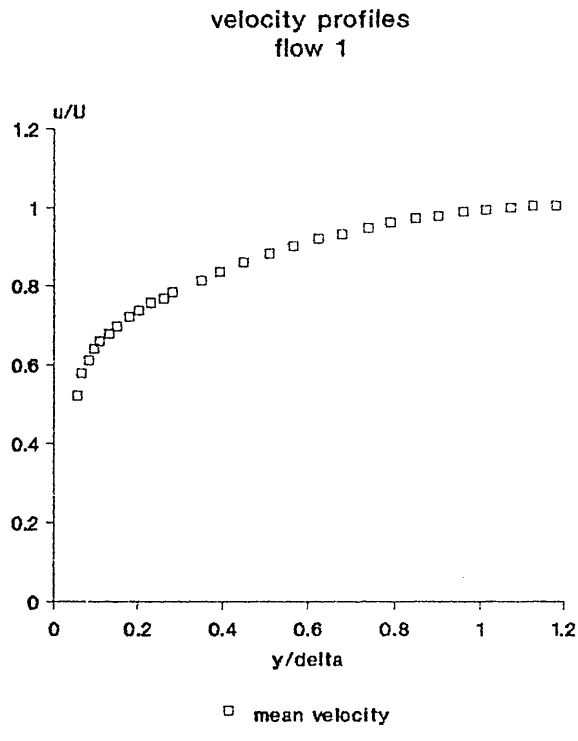

figure A3.13 x = 800

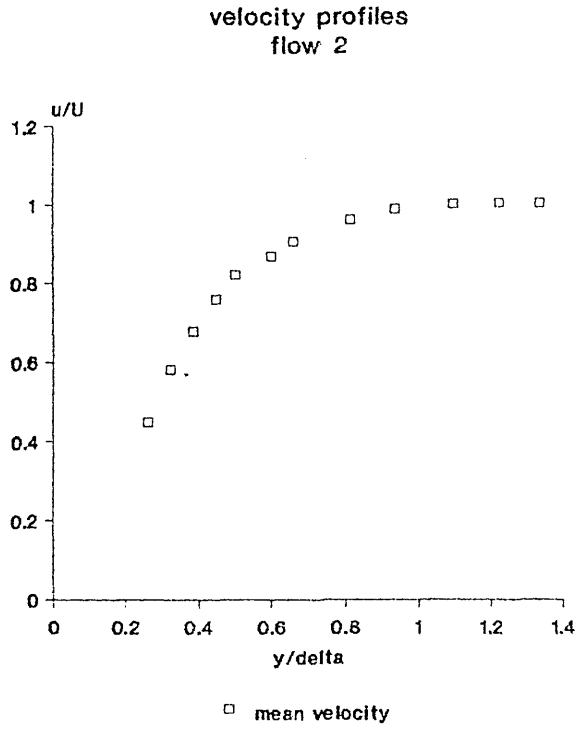

figure A3.14 x = 301

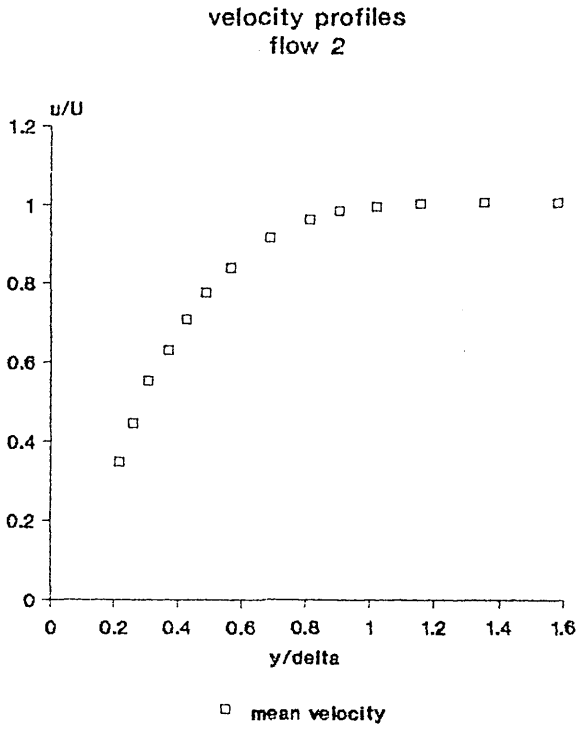

figure A3.15 x = 401

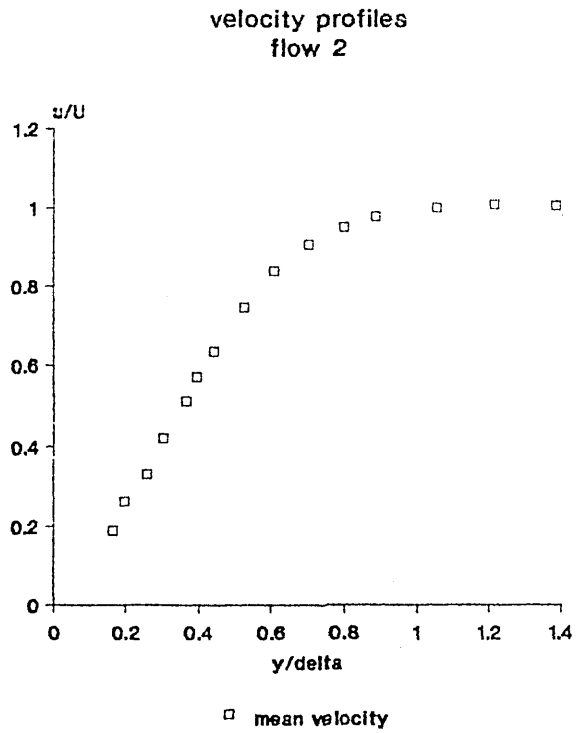

figure A3.16 x = 500

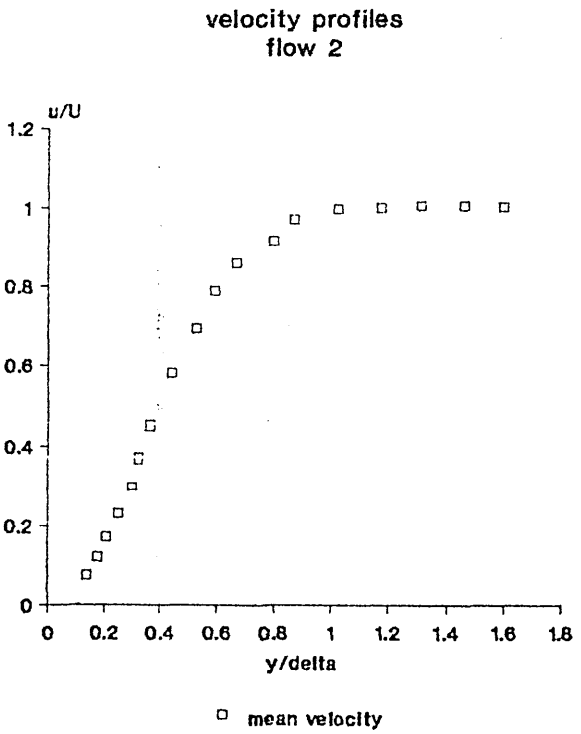

figure A3.17 x = 649

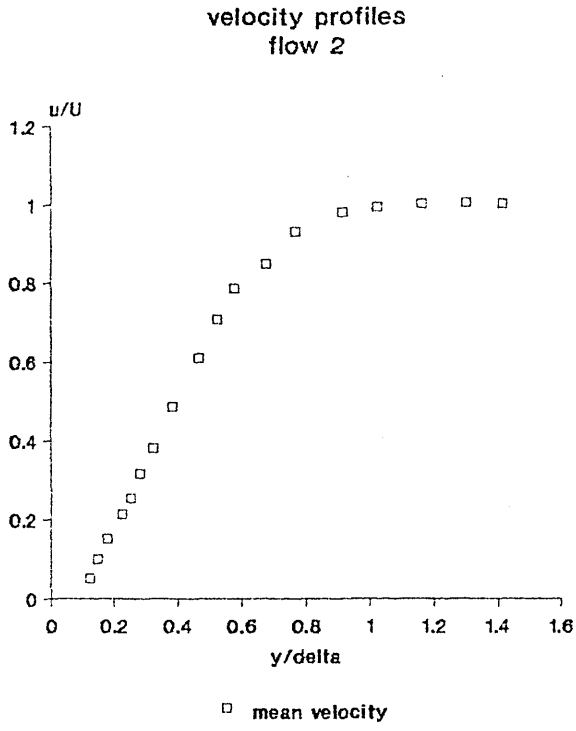

figure A3.18 x = 600

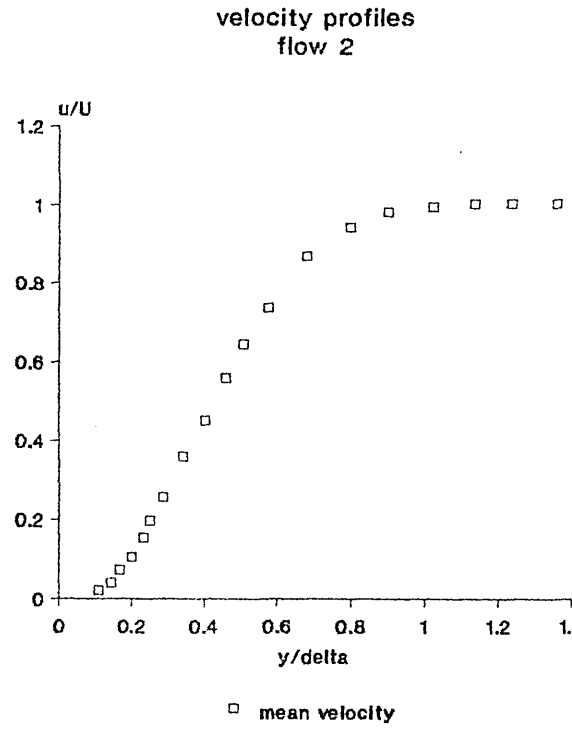

figure A3.19 x = 650

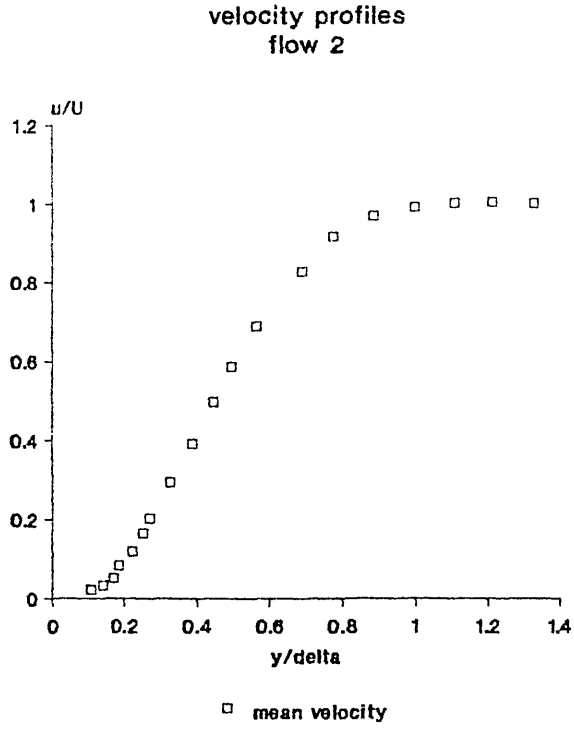

figure A3.20 x = 661

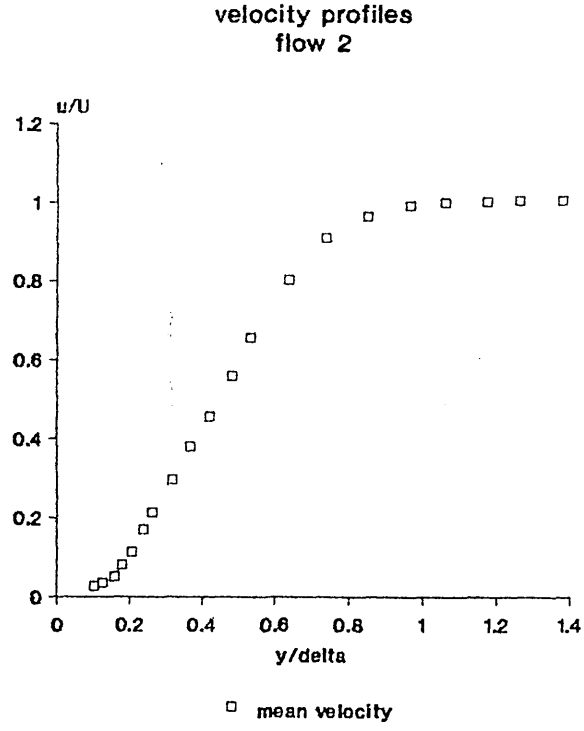

figure A3.21 x = 668

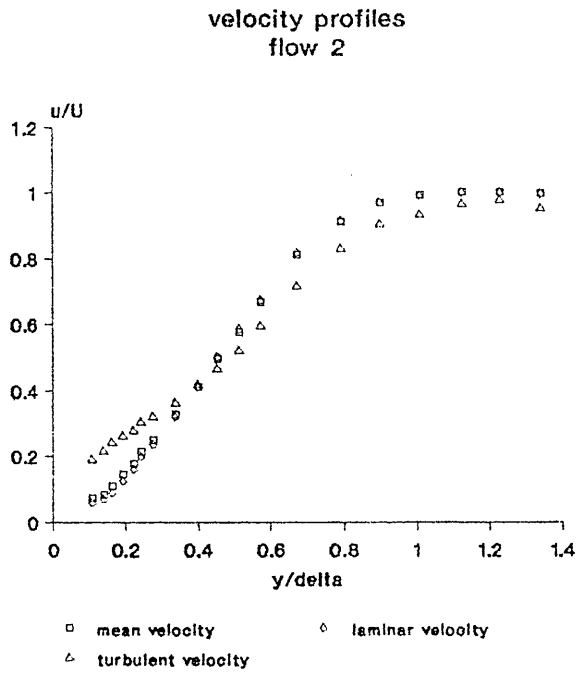

gamma = 0.12

figure A3.22 x = 680

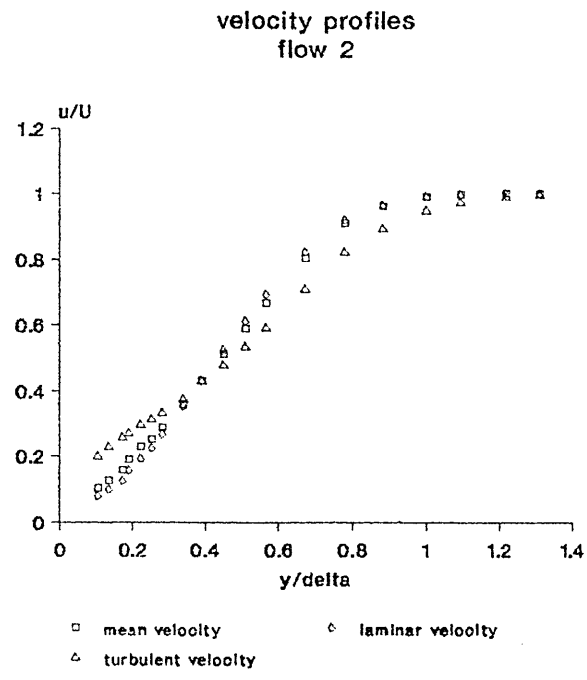

gamma = 0.28

figure A3.23 x = 691

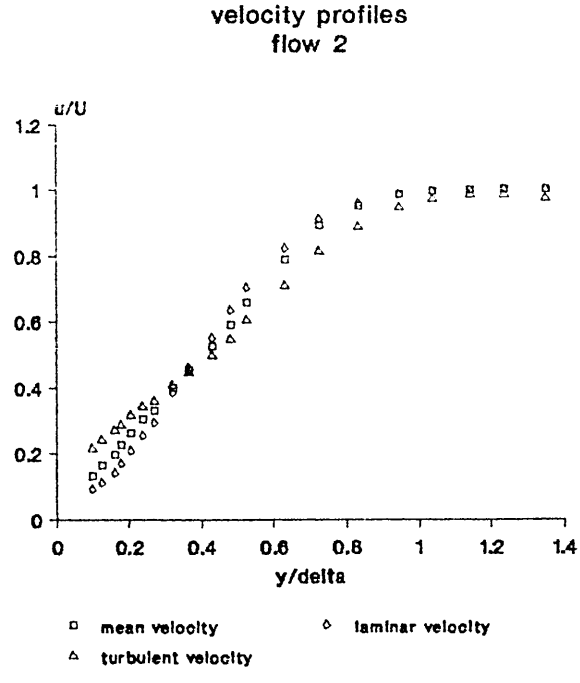

gamma = 0.47

figure A3.24 x = 695

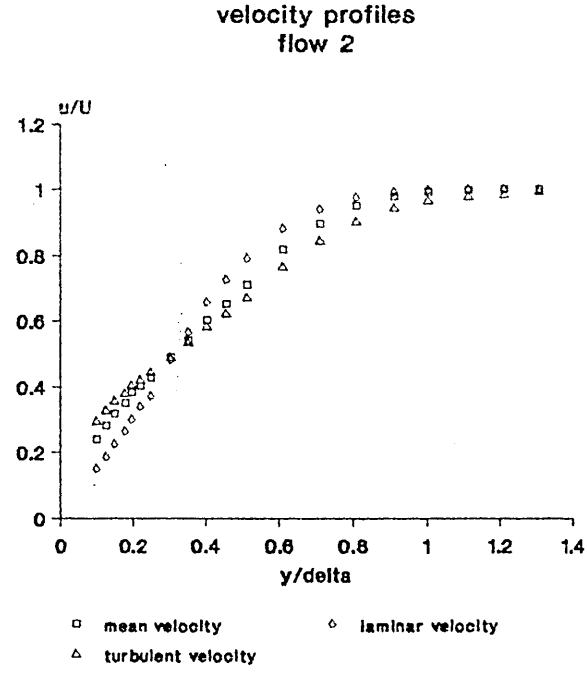

gamma = 0.73

figure A3.25 x = 700

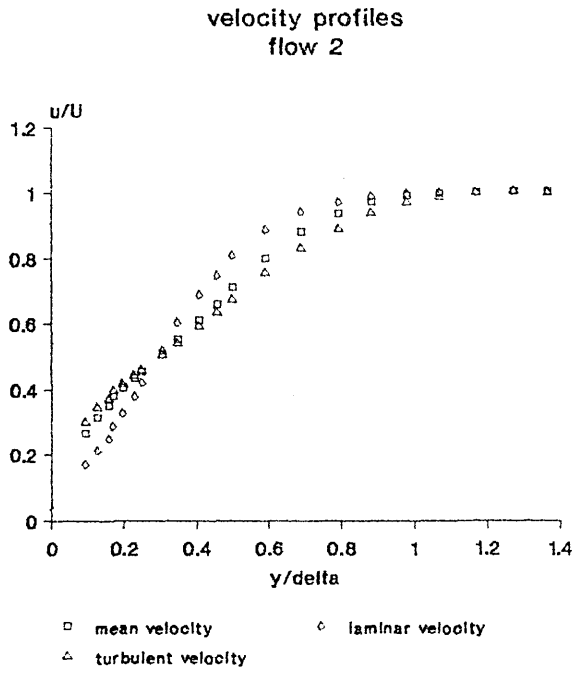

gamma = 0.82

figure A3.26 x = 710

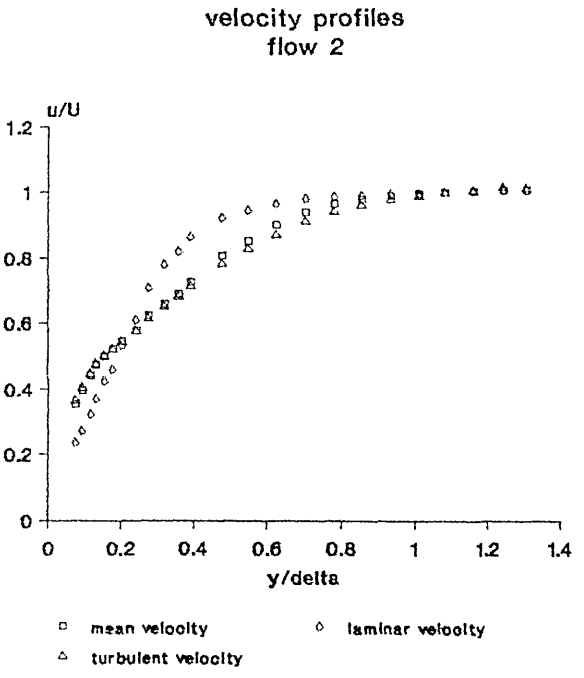

gamma = 0.95

figure A3.27 x = 720

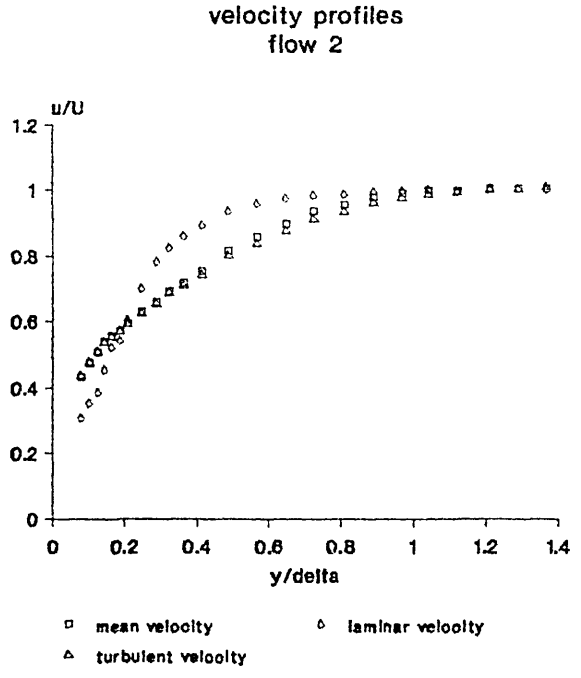

gamma = 0.98

figure A3.28 x = 730

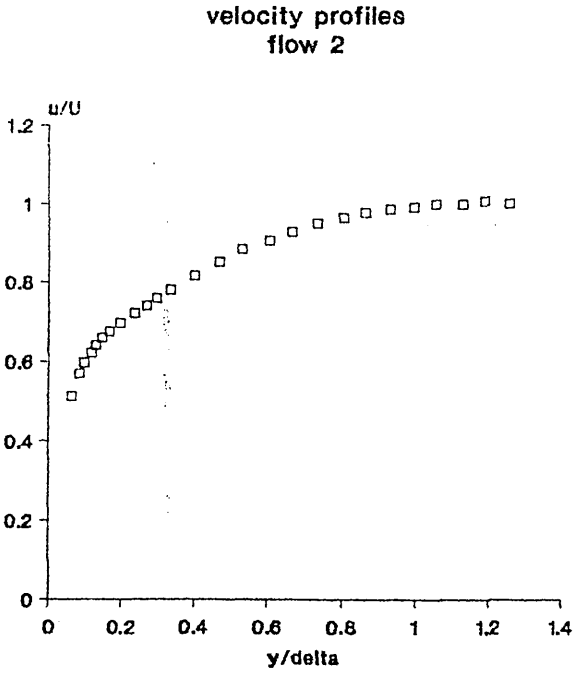

figure A3.29 x = 760

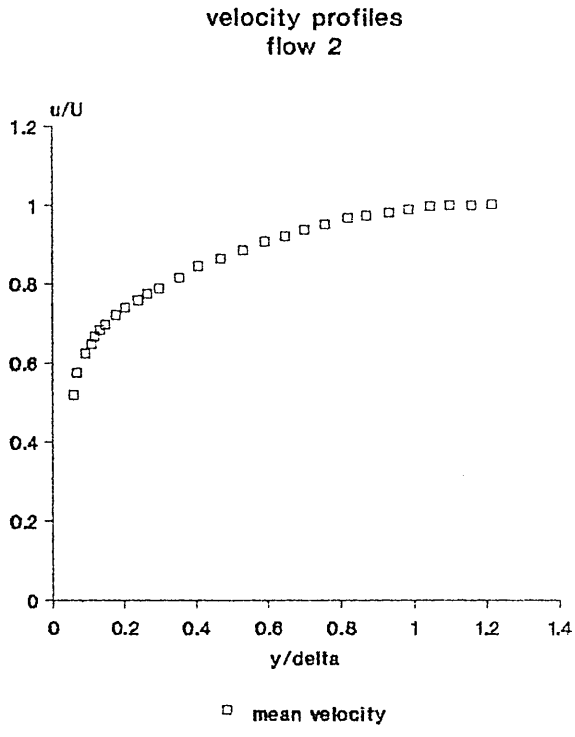

figure A3.30 x = 782

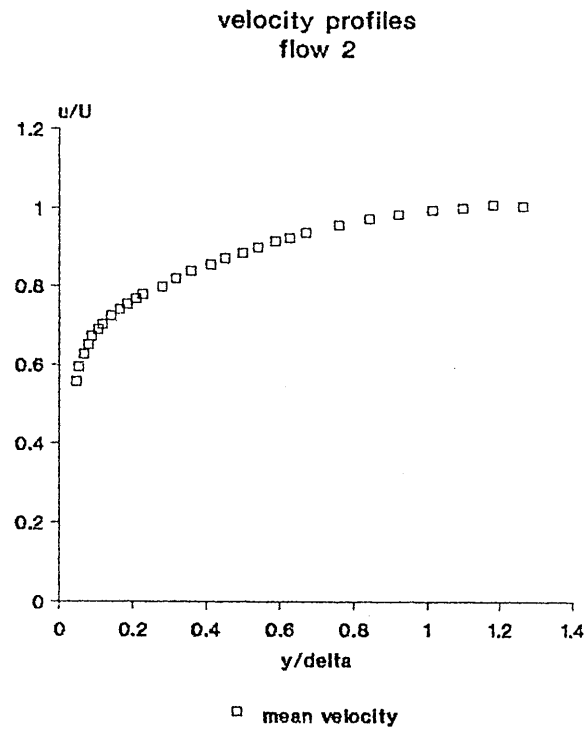

figure A3.31 x = 849

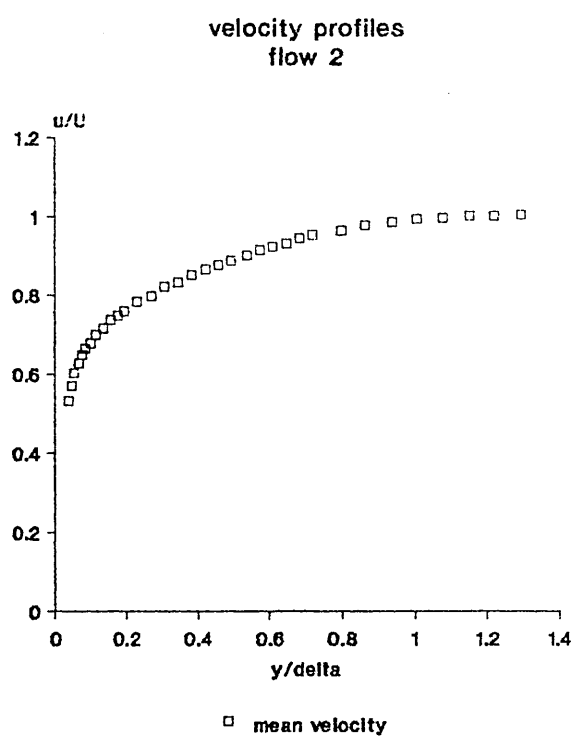

figure A3.32 x = 902

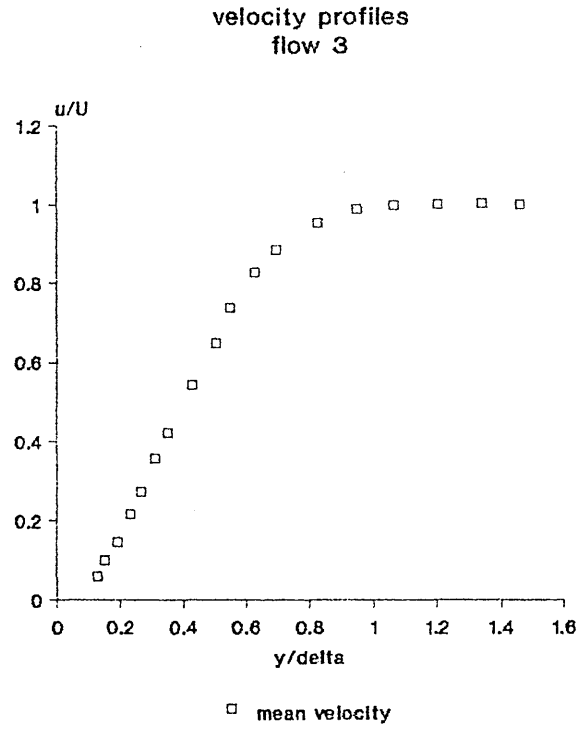

figure A3.33 x = 600

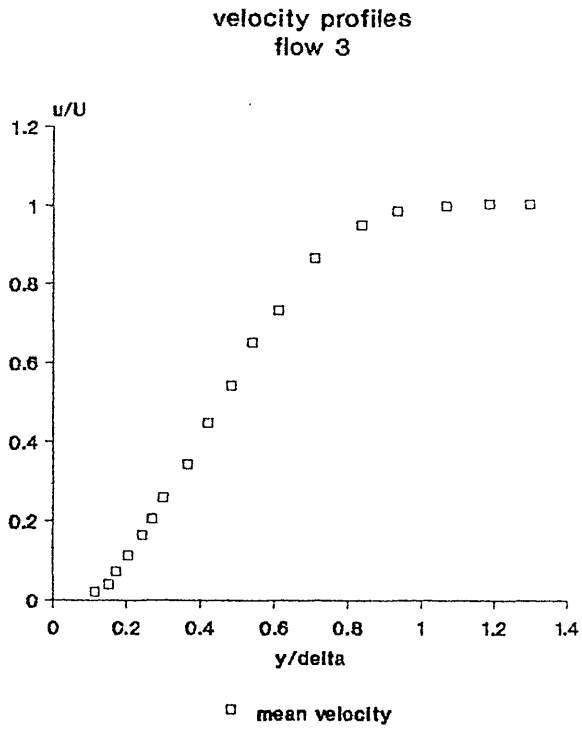

figure A3.34 x = 650

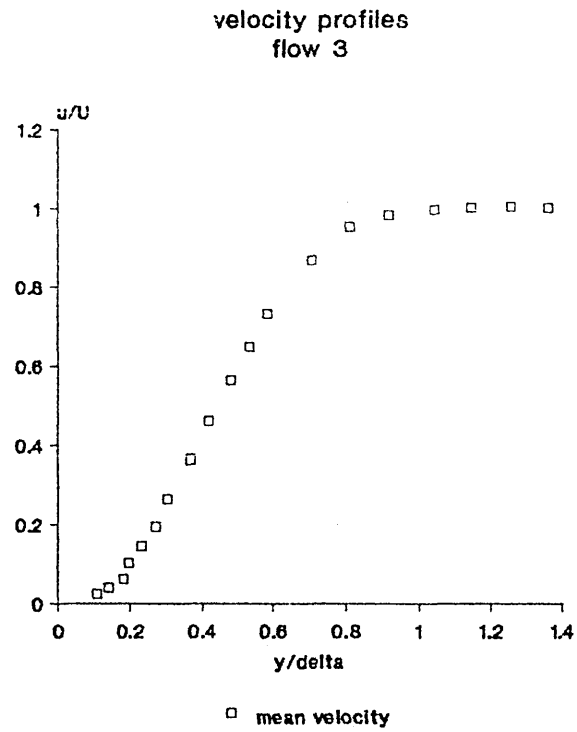

figure A3.35 x = 661

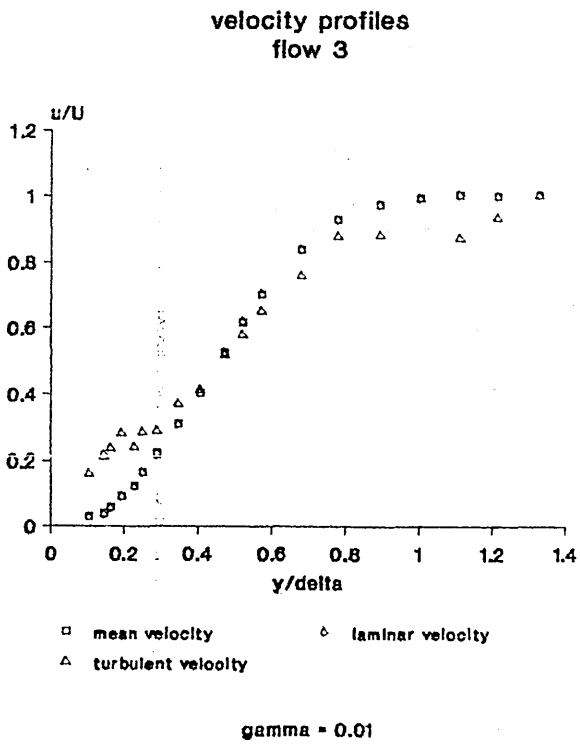

gamma = 0.01

figure A3.36 x = 671

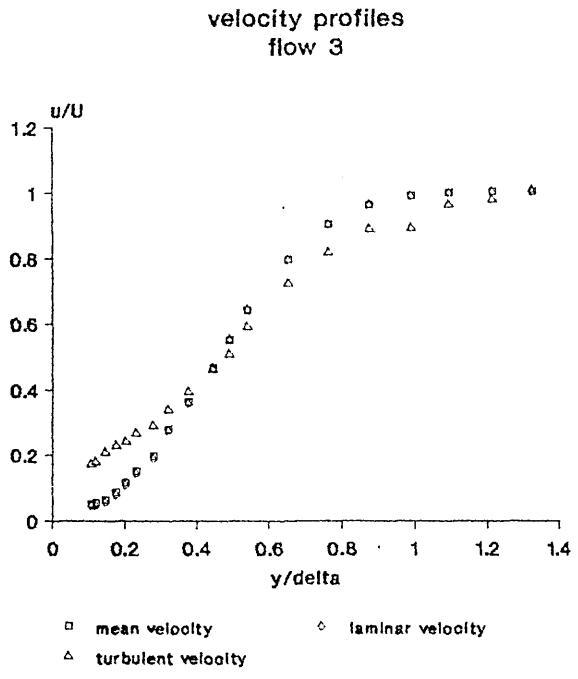

gamma = 0.05

figure A3.37 x = 680

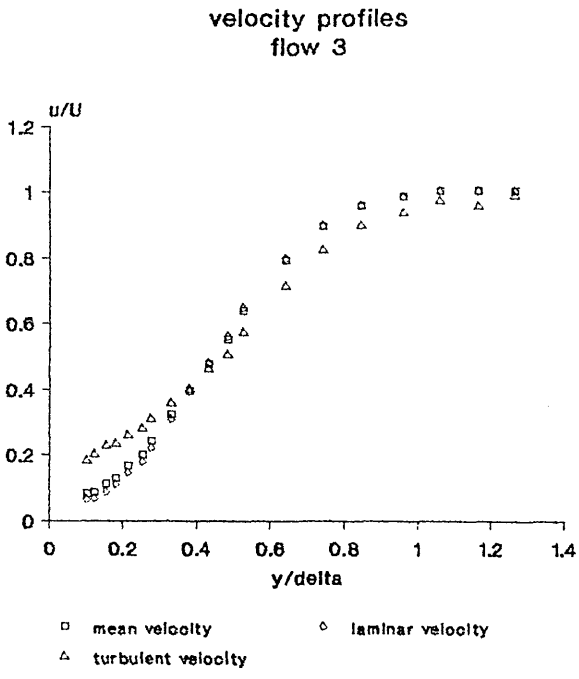

gamma = 0.17

figure A3.38 x = 690

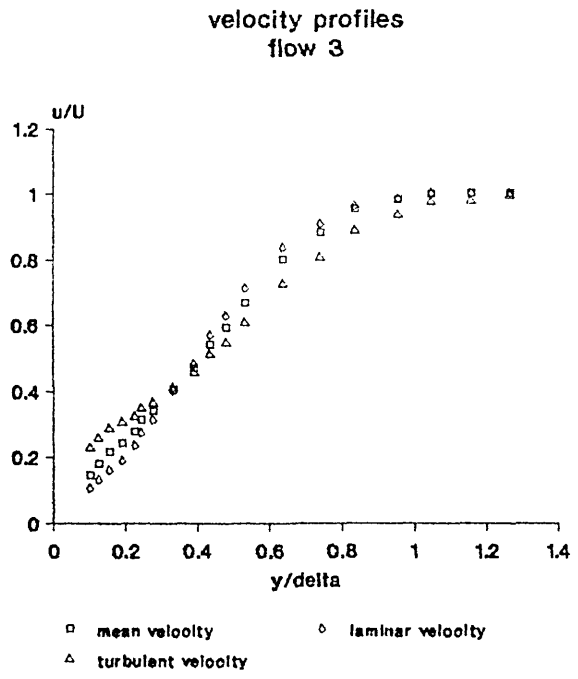

gamma = 0.46

figure A3.39 x = 700

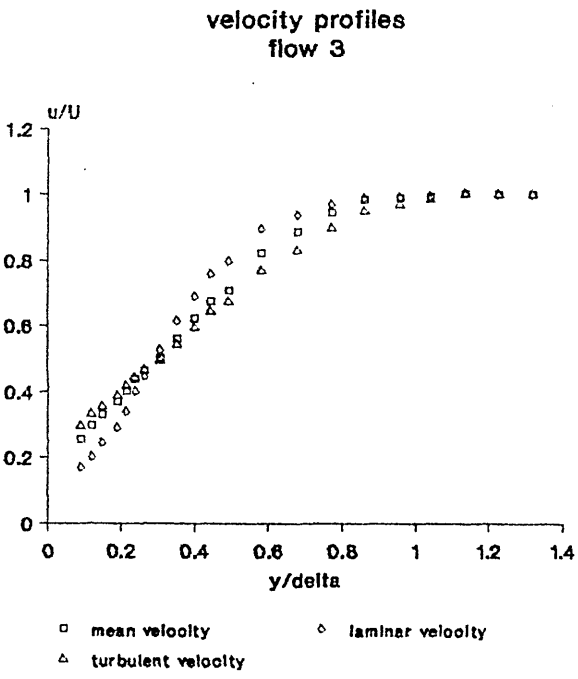

gamma = 0.77

figure A3.40 x = 710

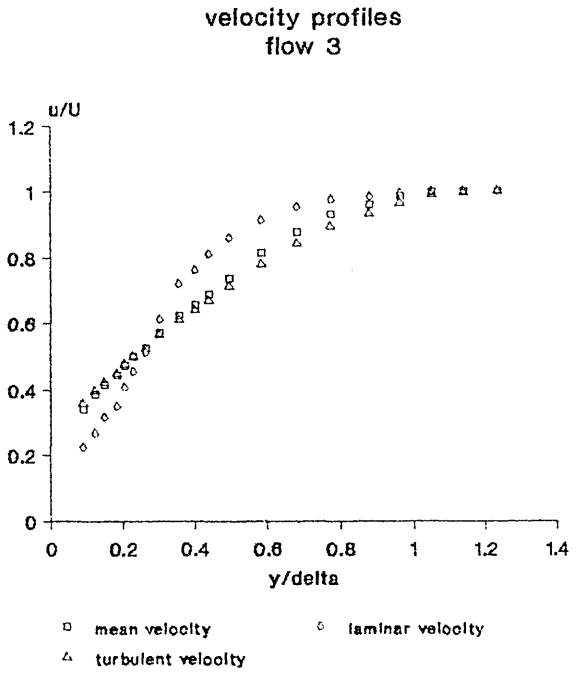

gamma = 0.91

figure A3.41 x = 720

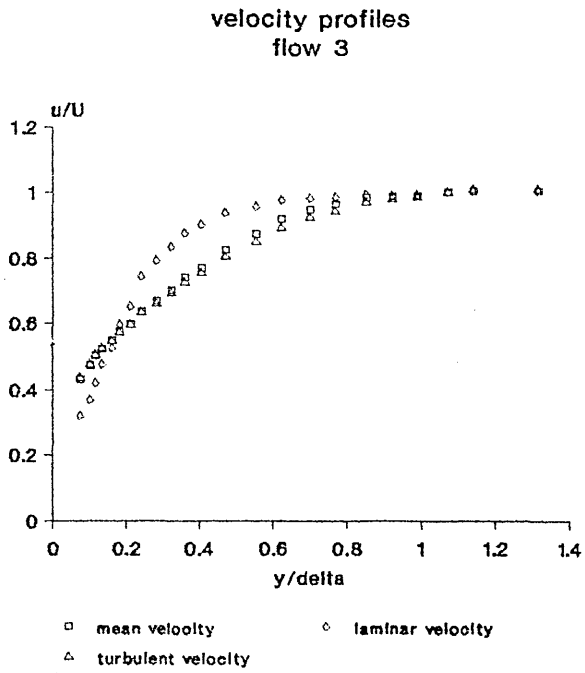

gamma = 0.96

figure A3.42 x = 731

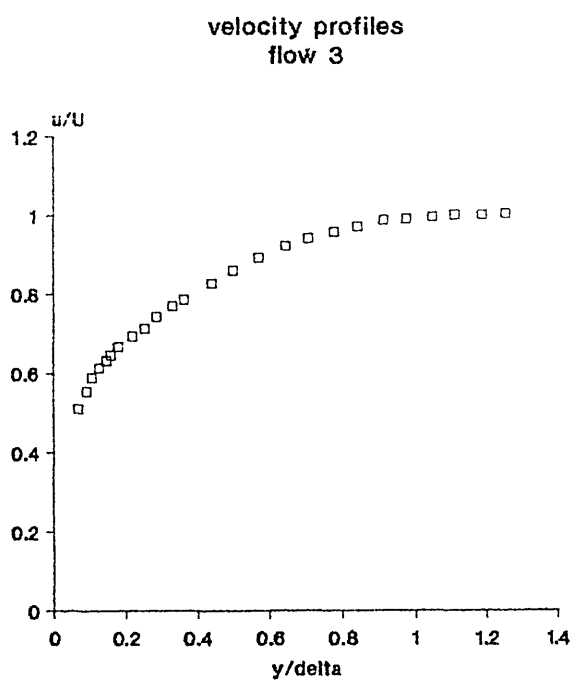

figure A3.44 x = 750

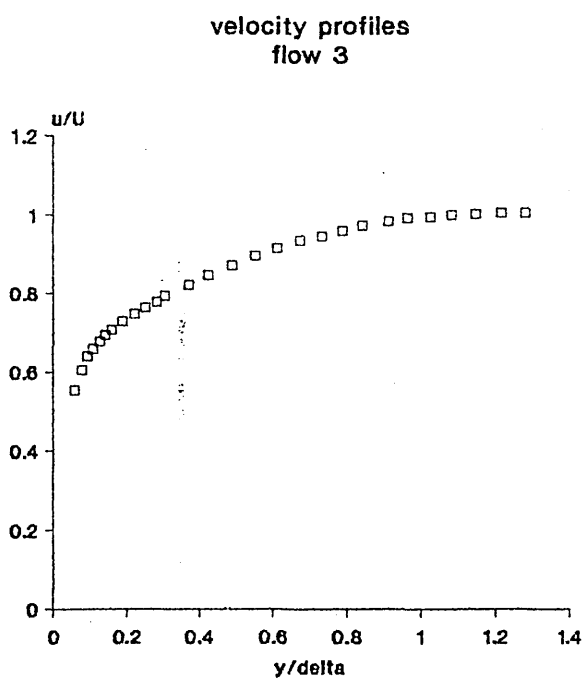

figure A3.44 x = 780

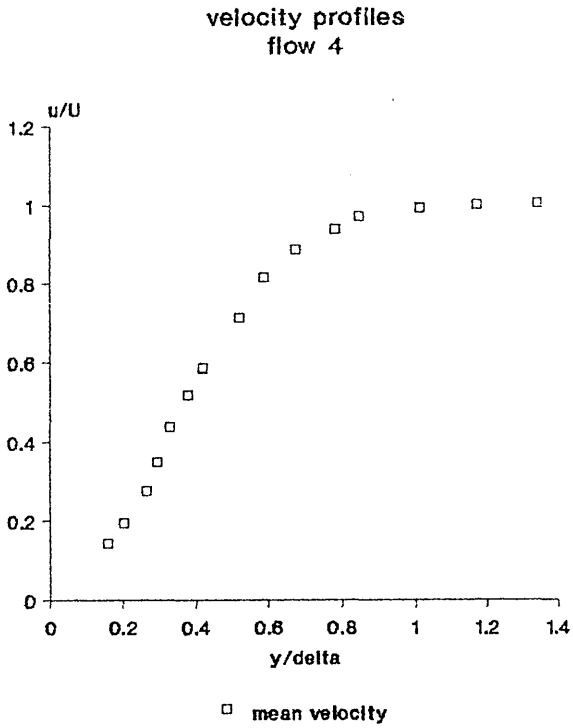

figure A3.45 x = 501

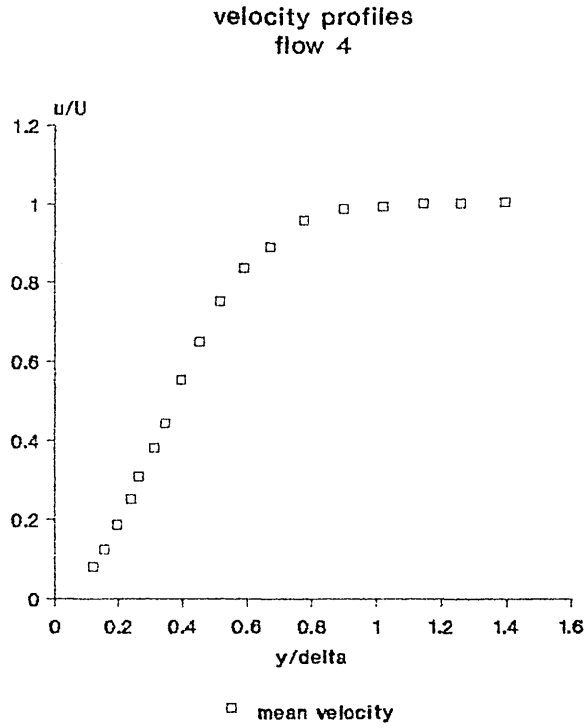

figure A3.46 x = 600

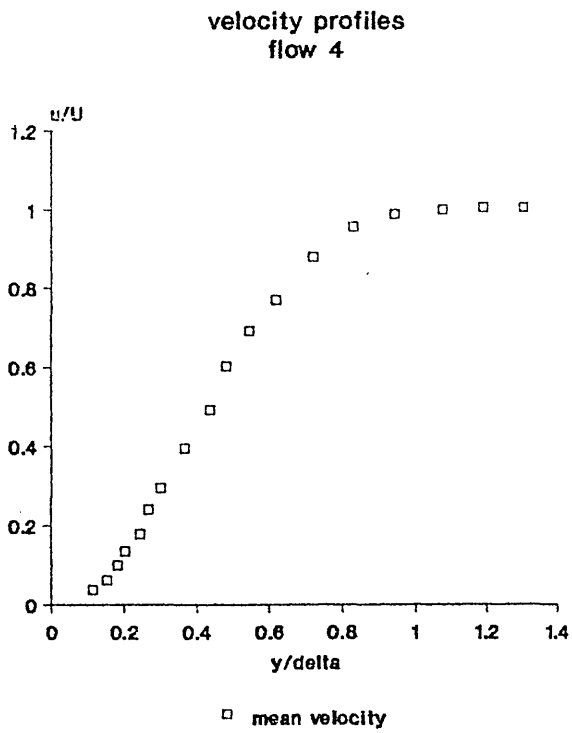

figure A3.47 x = 650

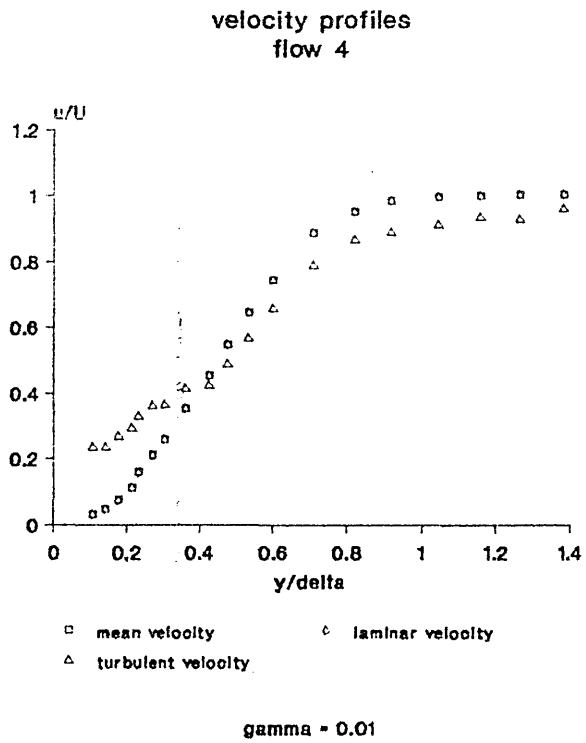

gamma = 0.01

figure A3.48 x = 659

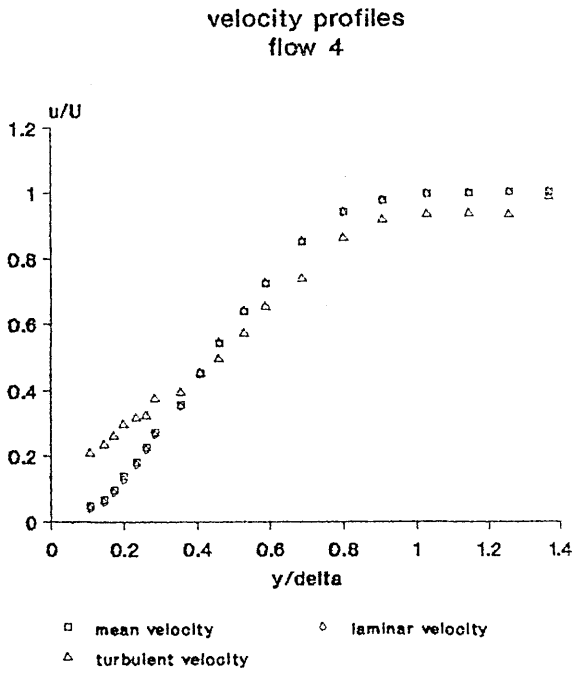

gamma = 0.05

figure A3.49 x = 669

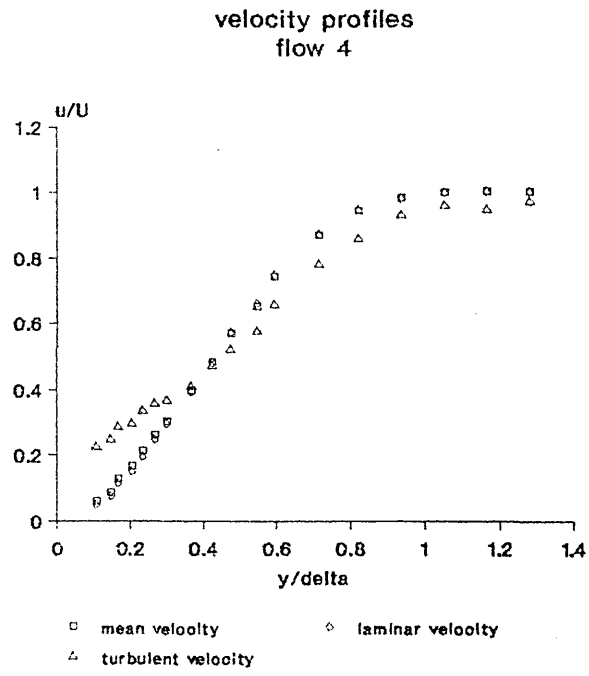

gamma = 0.10

figure A3.50 x = 674

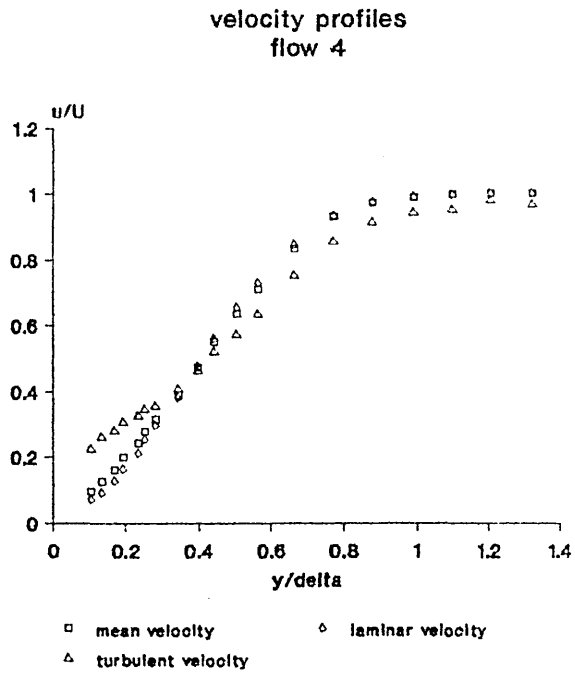

gamma = 0.24

figure A3.51 x = 681

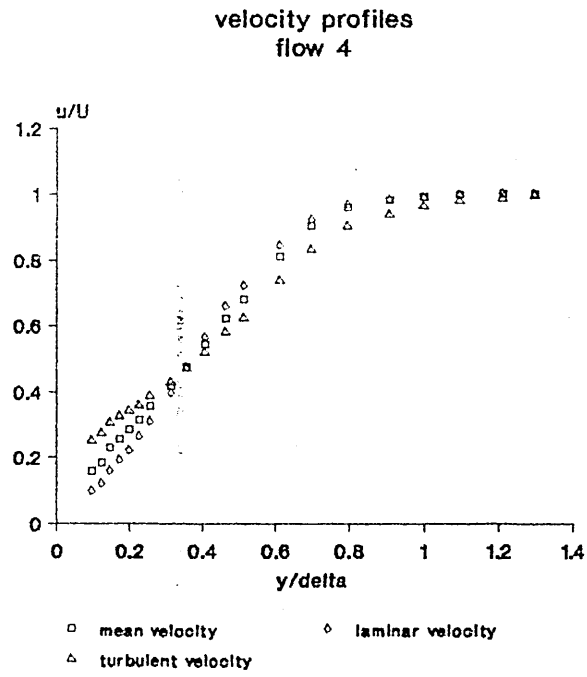

gamma = 0.49

figure A3.52 x = 691

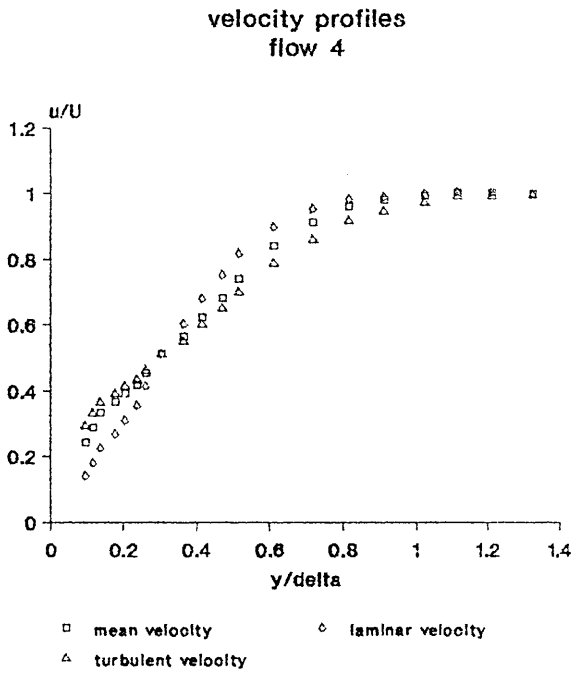

gamma = 0.77

figure A3.53 x = 700

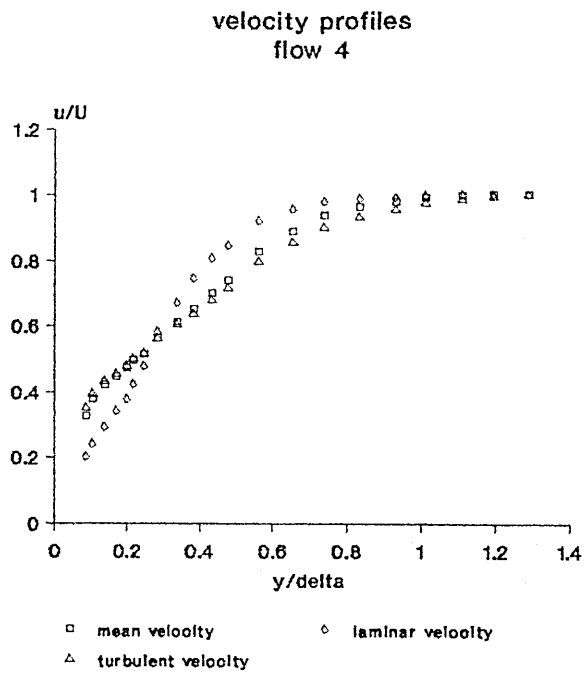

gamma = 0.80

figure A3.54 x = 711

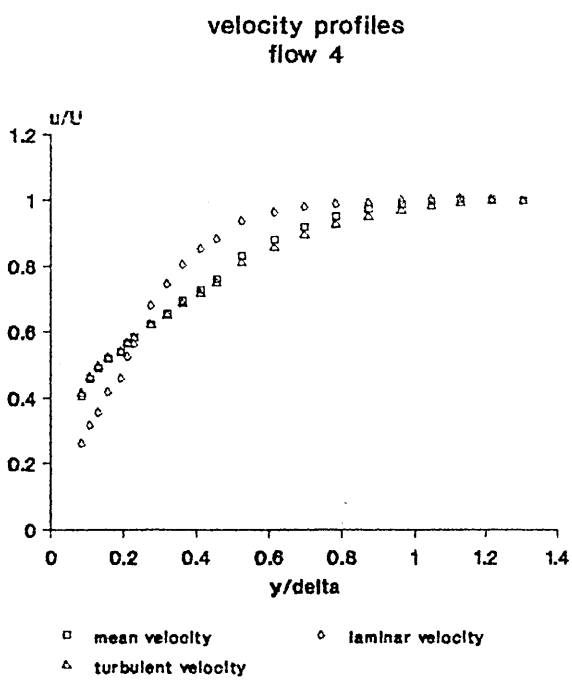

gamma = 0.96

figure A3.55 x = 720

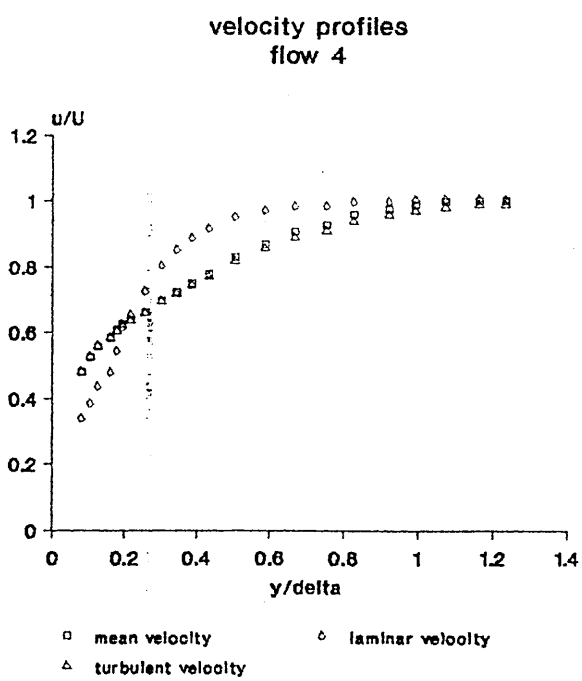

gamma = 0.99

figure A3.56 x = 730

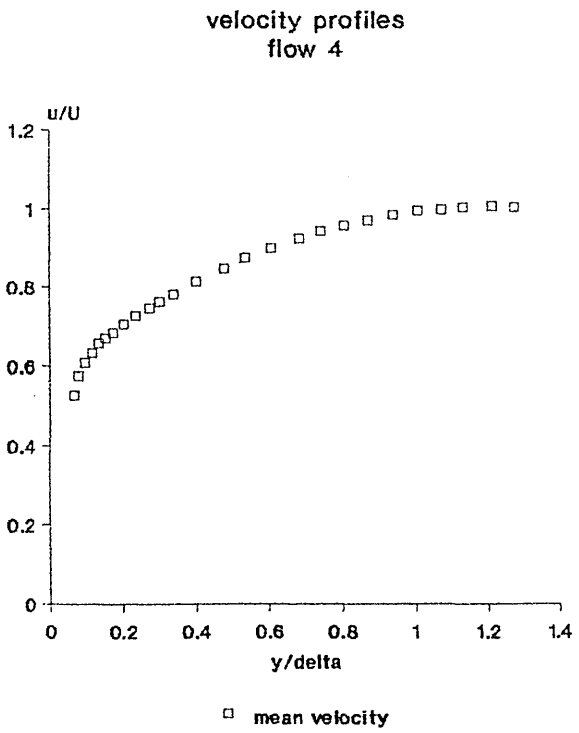

figure A3.57 x = 760

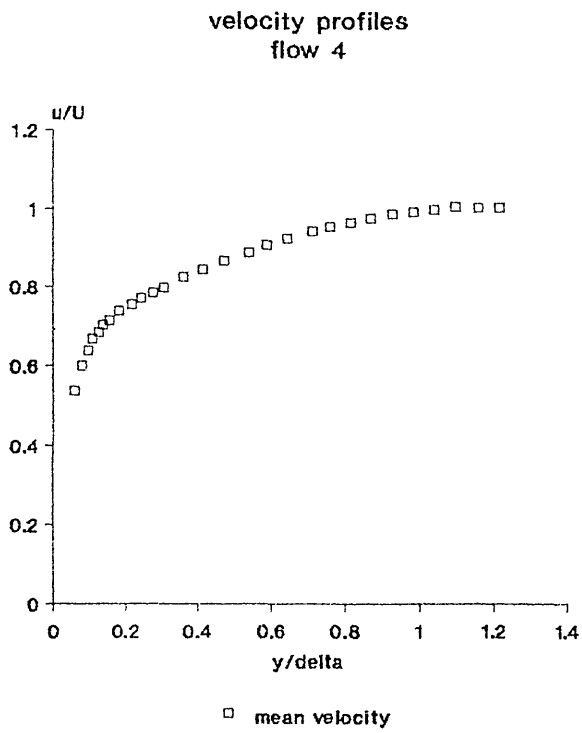

figure A3.58 x = 780

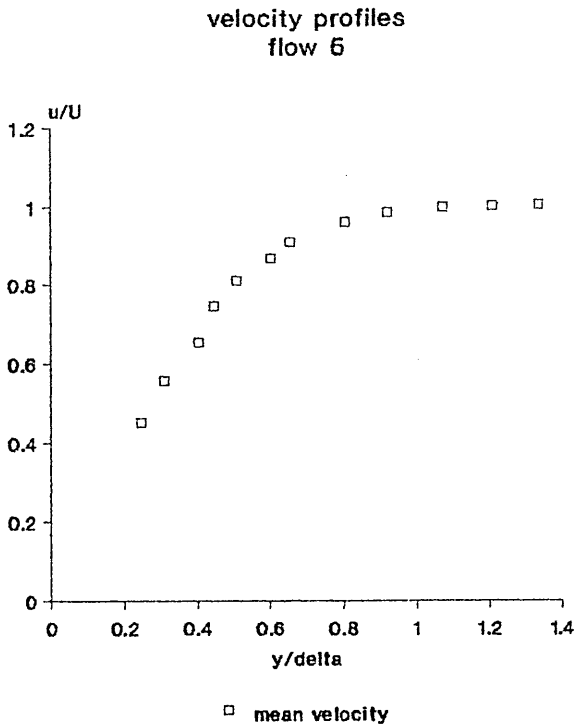

figure A3.59 x = 300

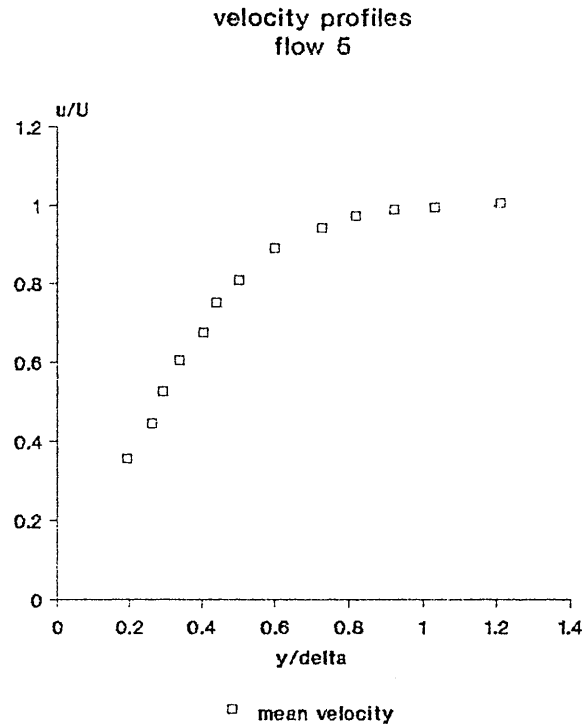

figure A3.60 x = 402

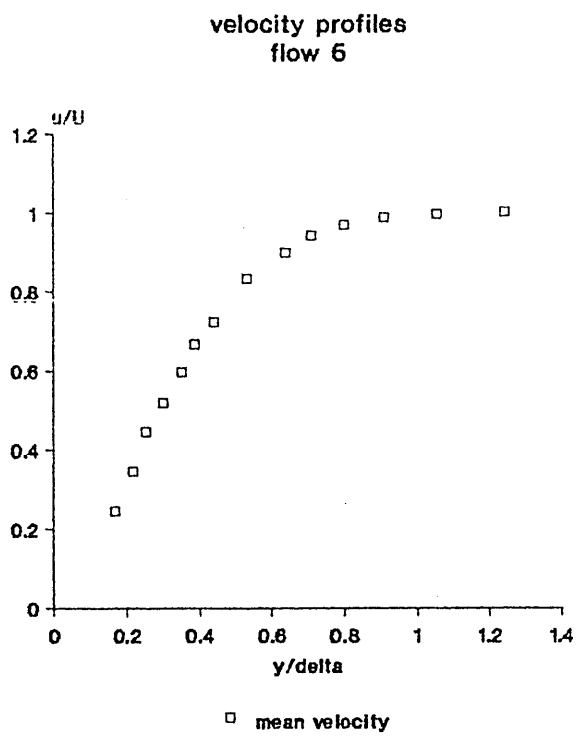

figure A3.61 x = 450

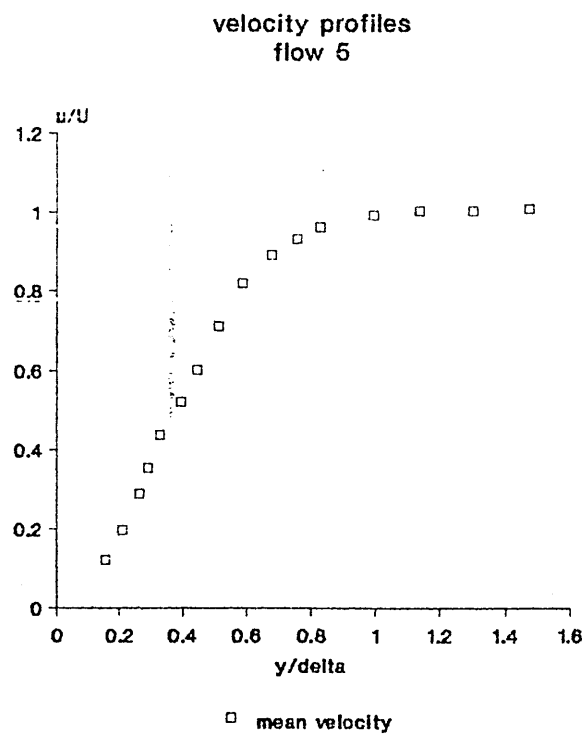

figure A3.62 x = 498

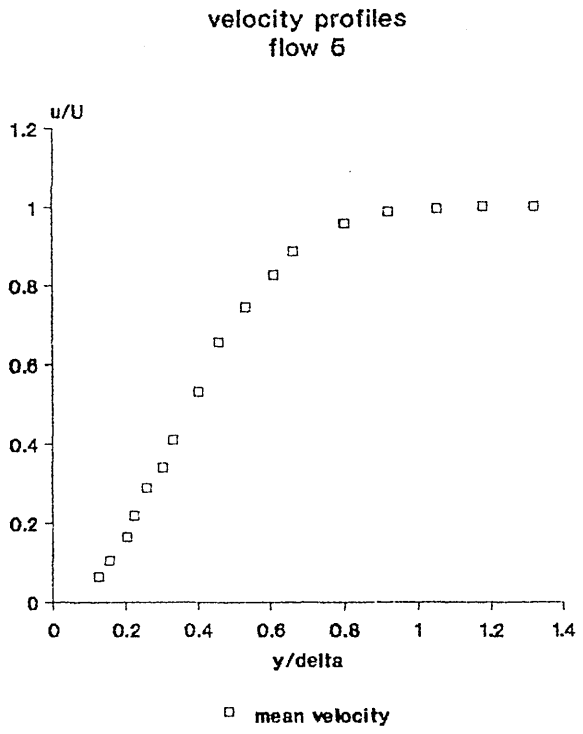

figure A3.63 x = 560

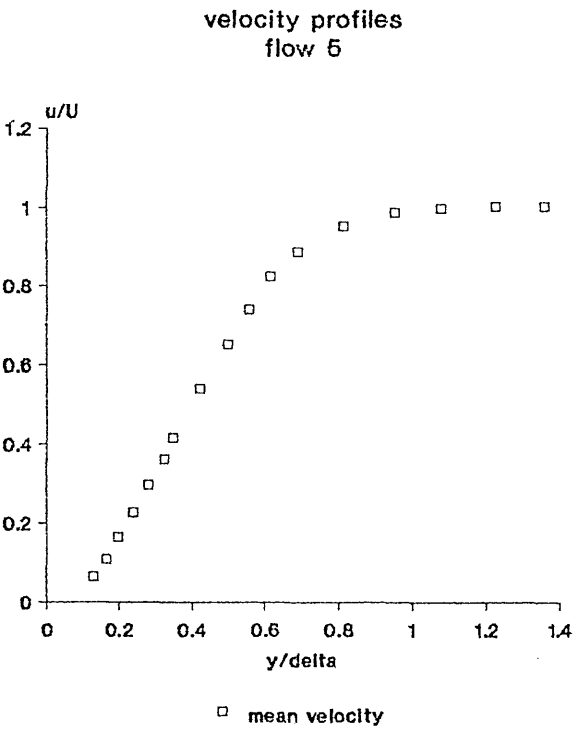

figure A3.64 x = 573

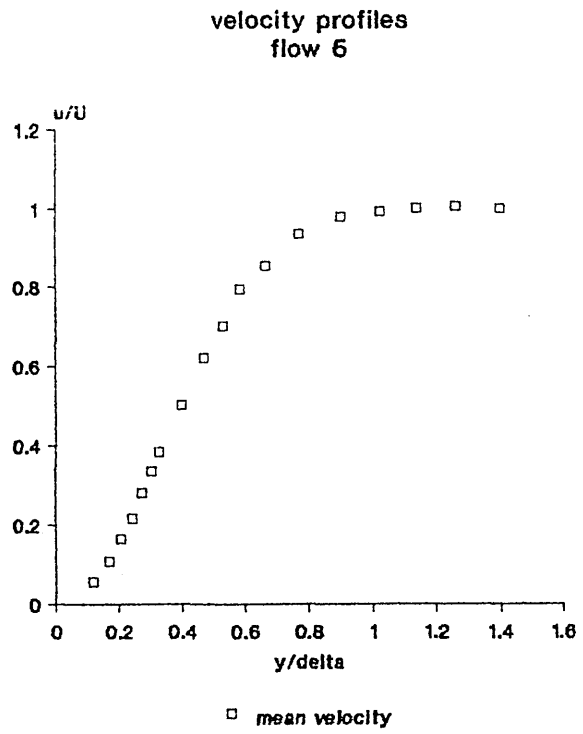

figure A3.65 x = 600

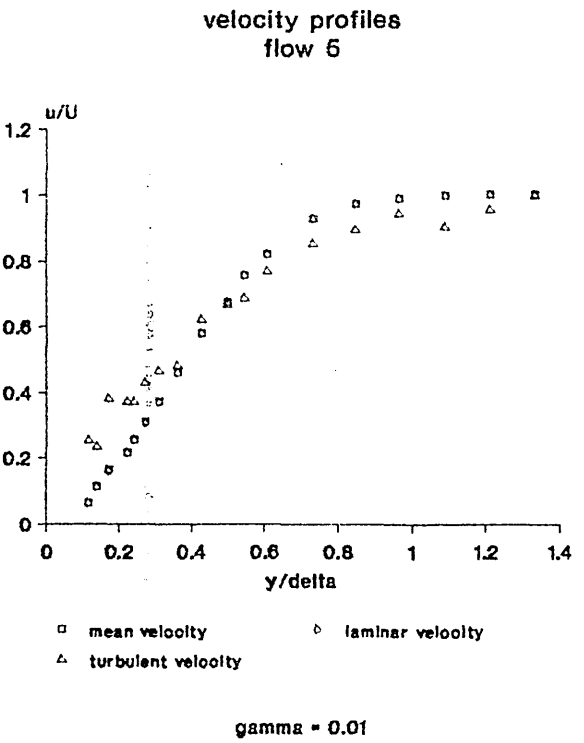

gamma = 0.01

figure A3.66 x = 610

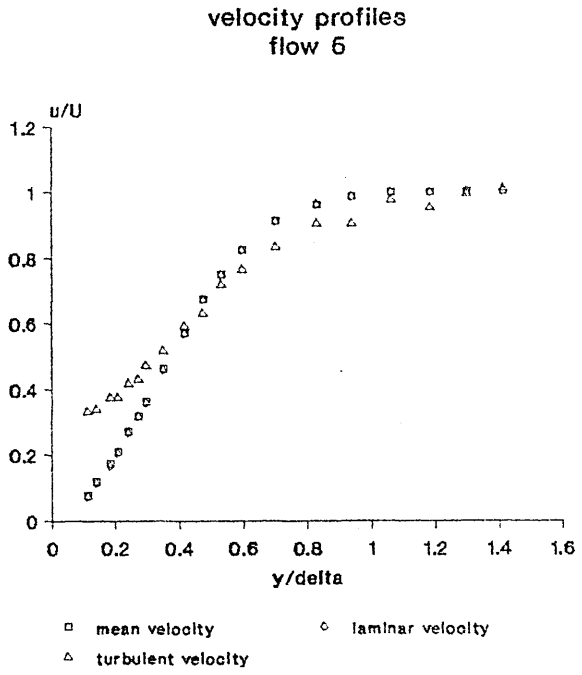

gamma = 0.02

figure A3.67 x = 621

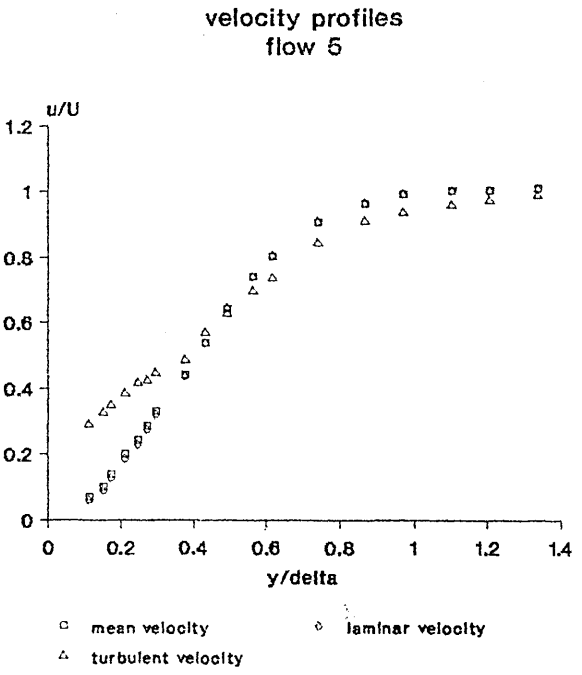

gamma = 0.06

figure A3.68 x = 631

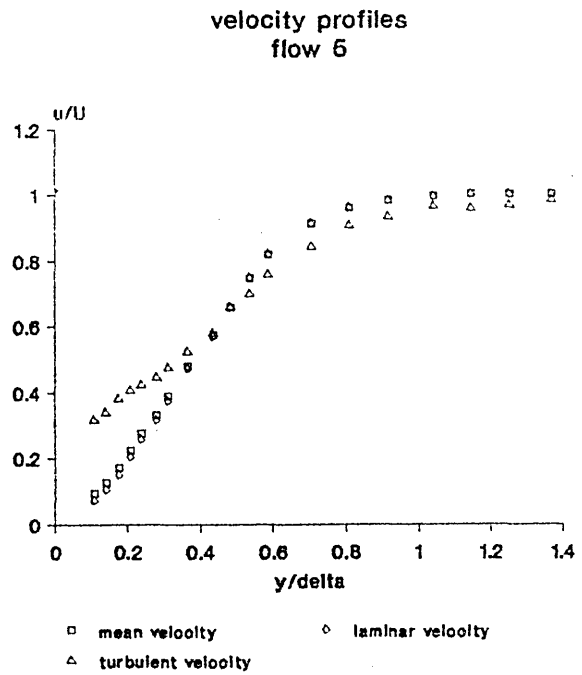

gamma = 0.10

figure A3.69 x = 639

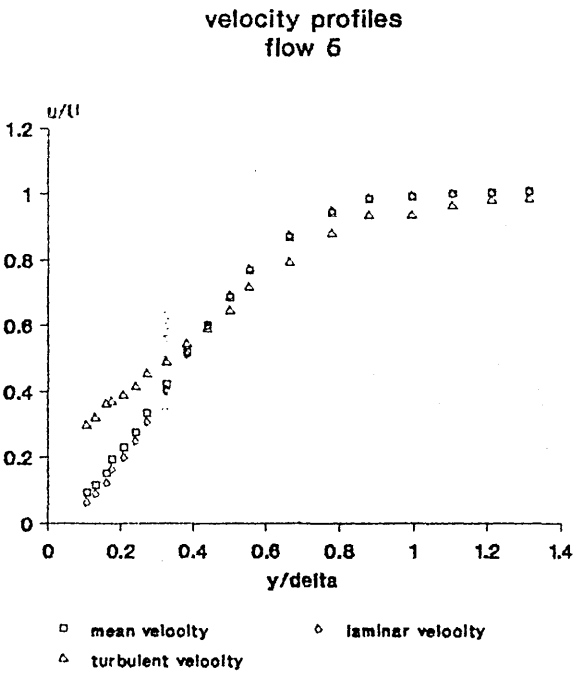

gamma = 0.16

figure A3.70 x = 650

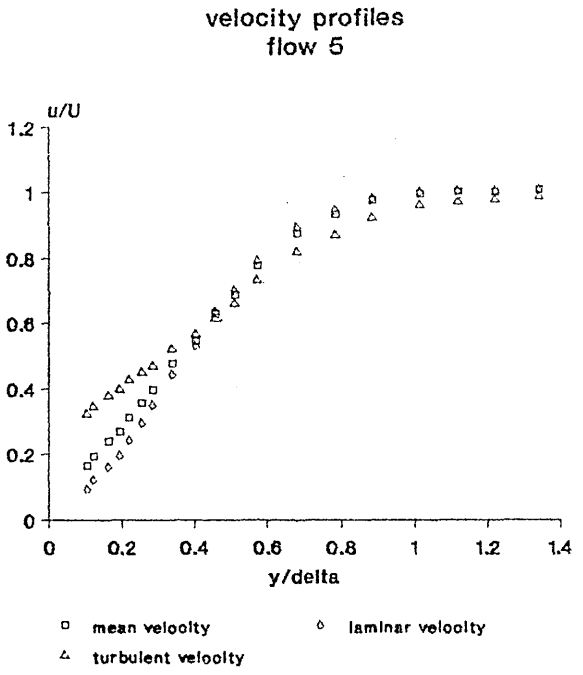

gamma = 0.36

figure A3.71 x = 660

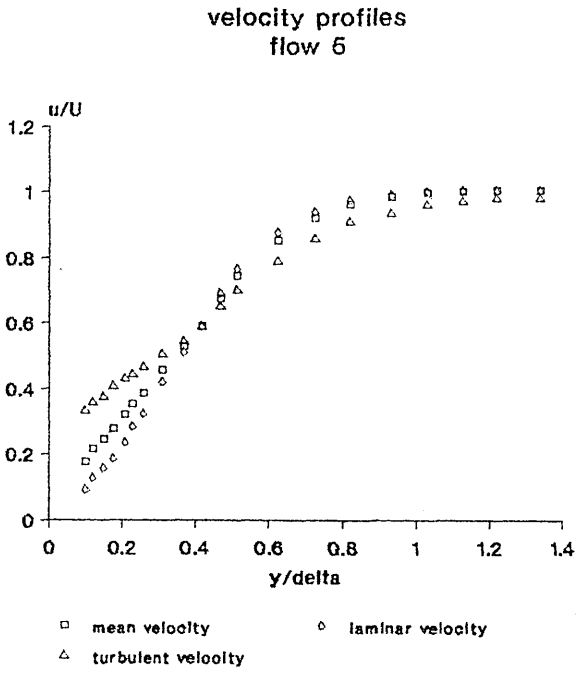

gamma = 0.41

figure A3.72 x = 668

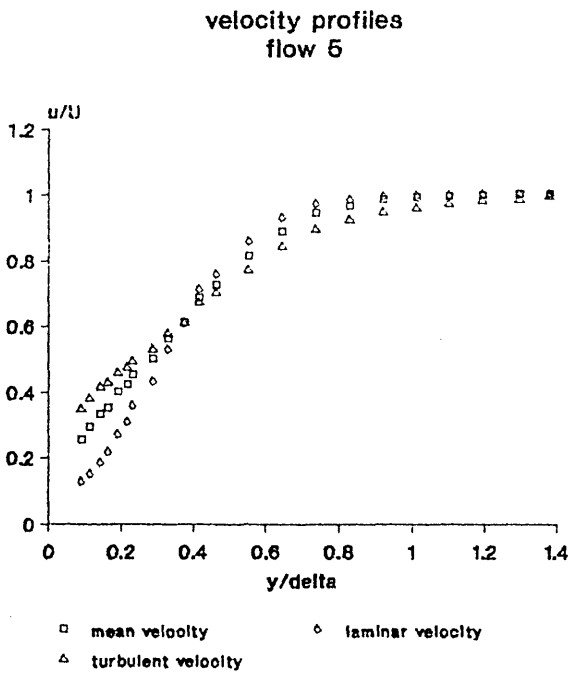

gamma = 0.65

figure A3.73 x = 679

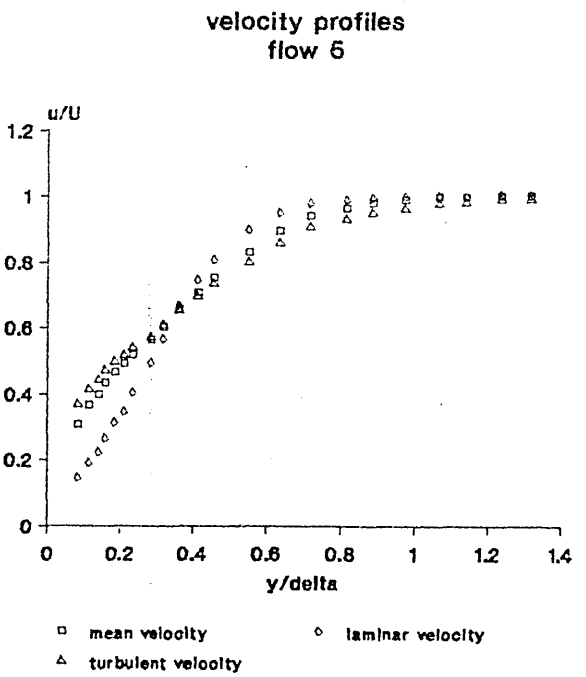

gamma = 0.82

figure A3.74 x = 689

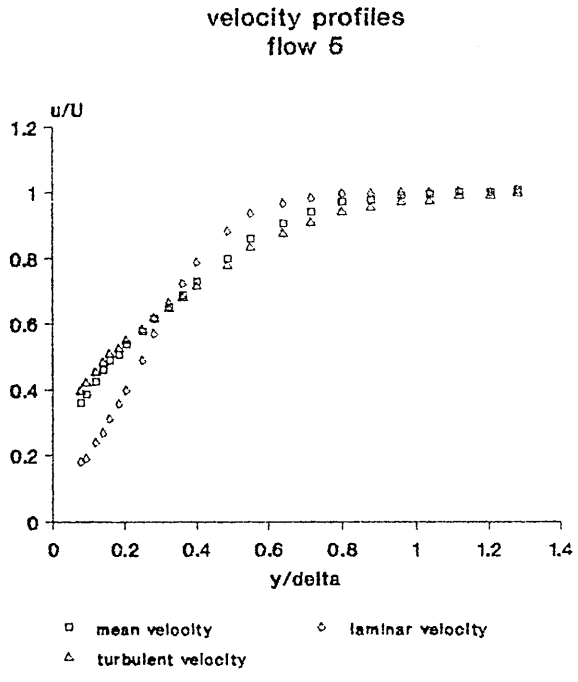

gamma = 0.88

figure A3.75 x = 700

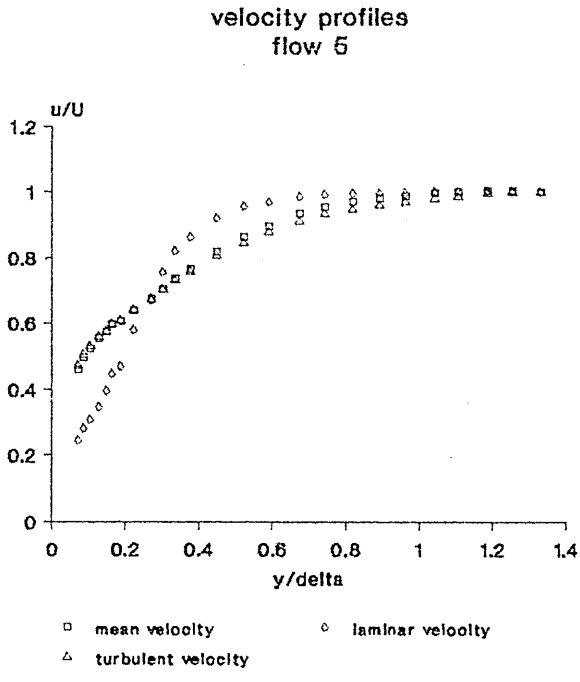

gamma = 0.96

figure A3.76 x = 710

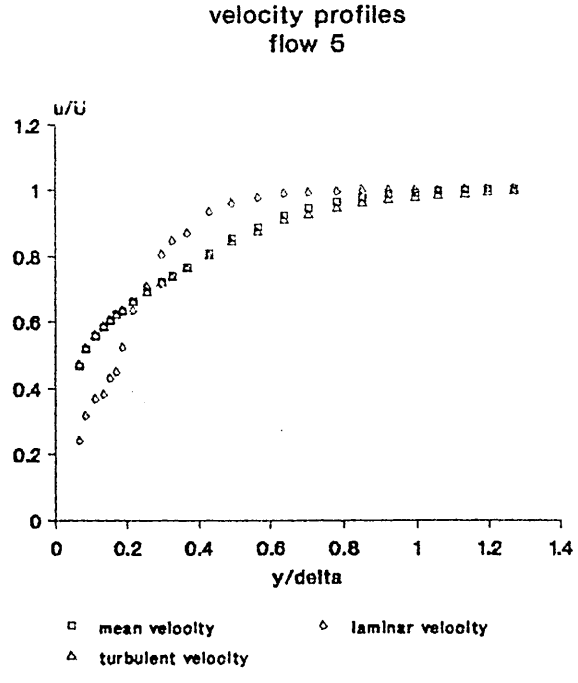

gamma = 0.98

figure A3.77 x = 718

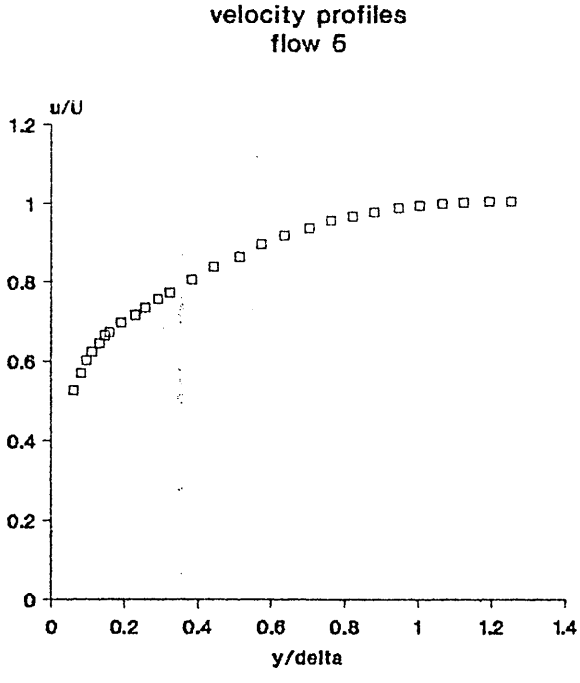

figure A3.78 x = 741

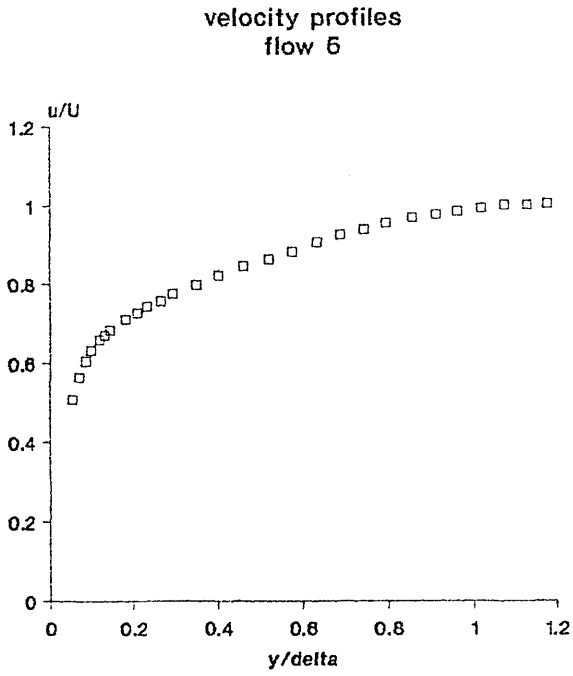

figure A3.79 x = 779

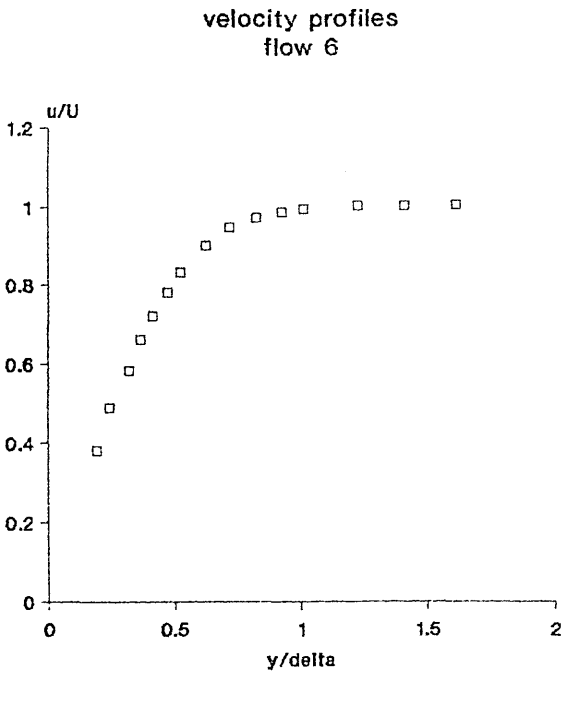

figure A3.80 x = 400

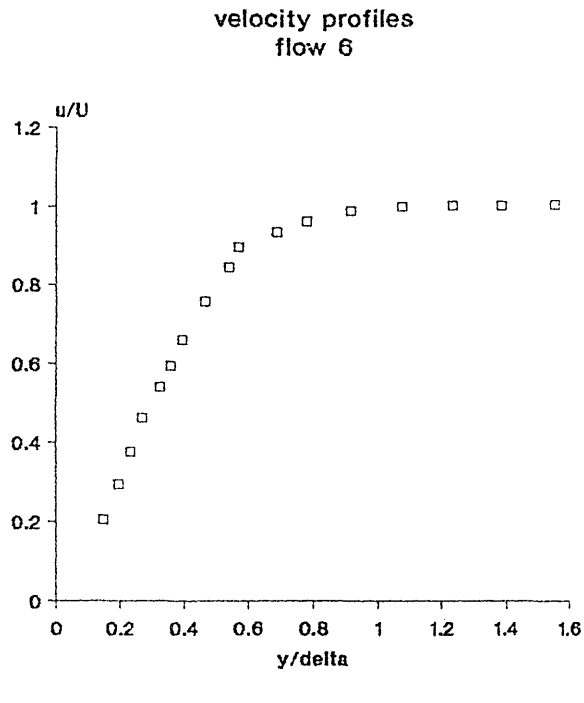

figure A3.81 x = 500

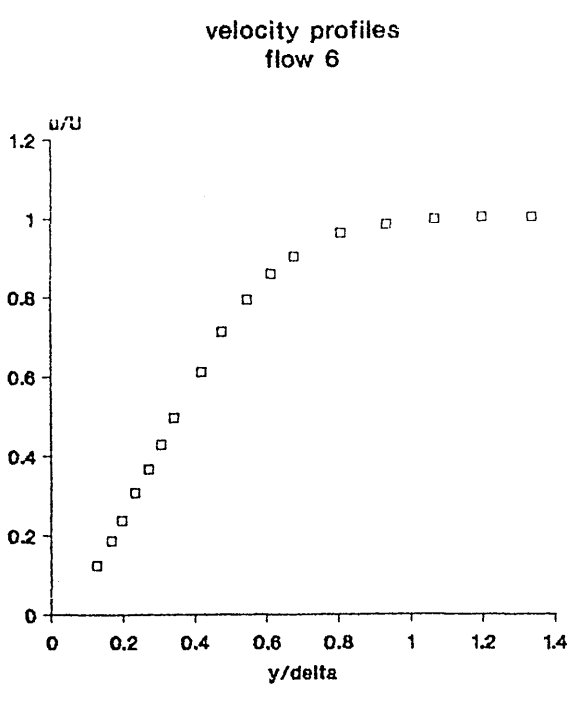

figure A3.82 x = 549

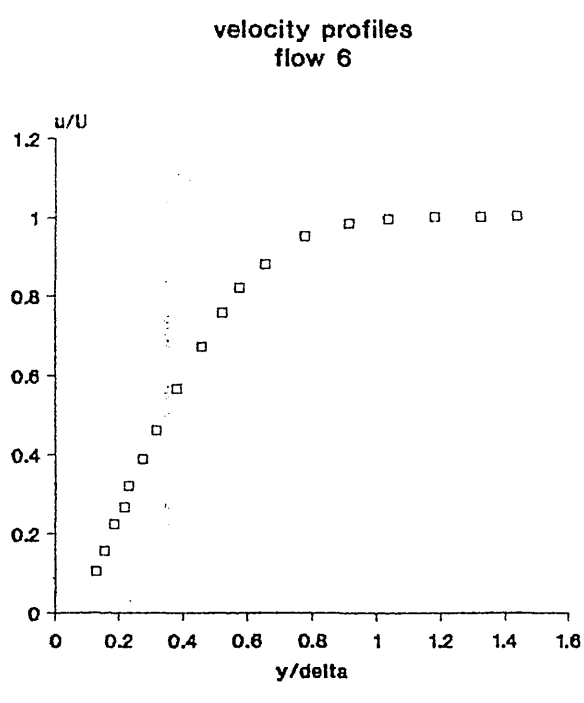

figure A3.83 x = 560

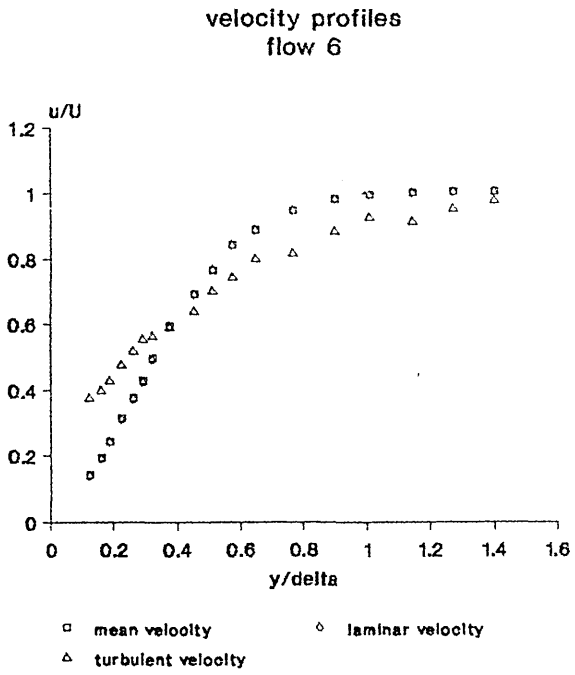

gamma = 0.02

figure A3.84 x = 571

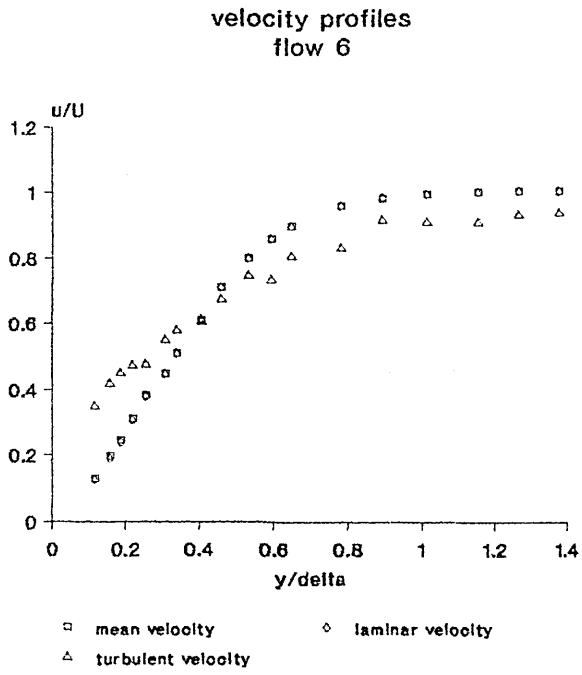

gamma = 0.03

figure A3.86 x = 580

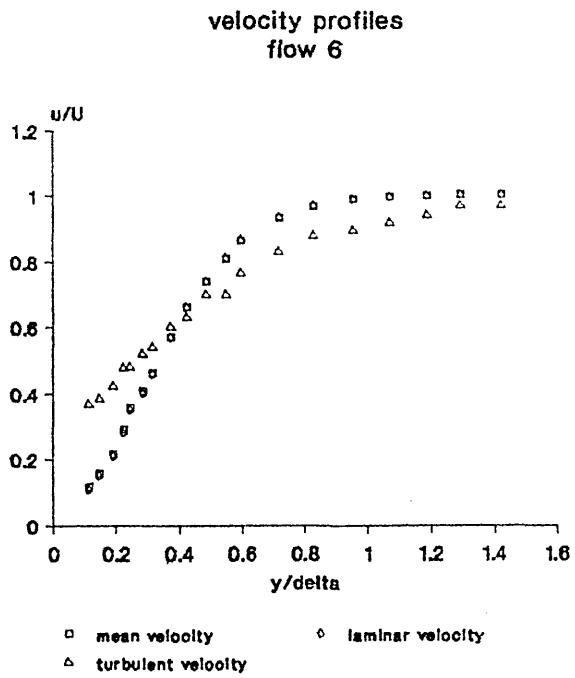

gamma = 0.04

figure A3.86 x = 590

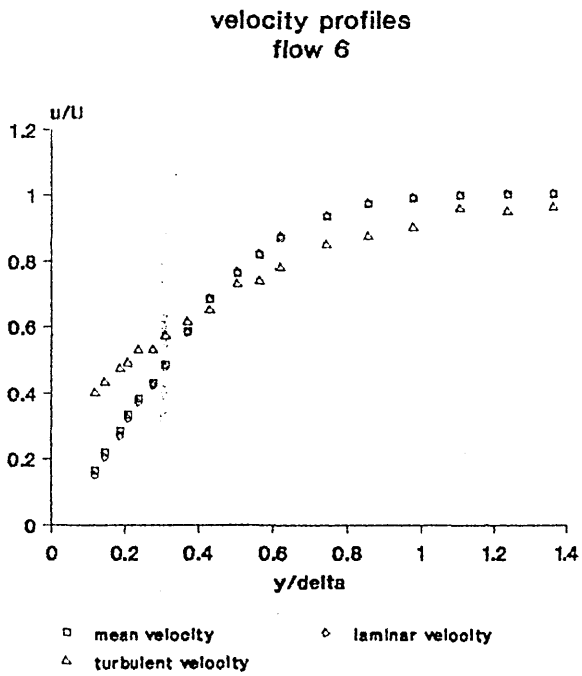

gamma = 0.06

figure A3.87 x = 600

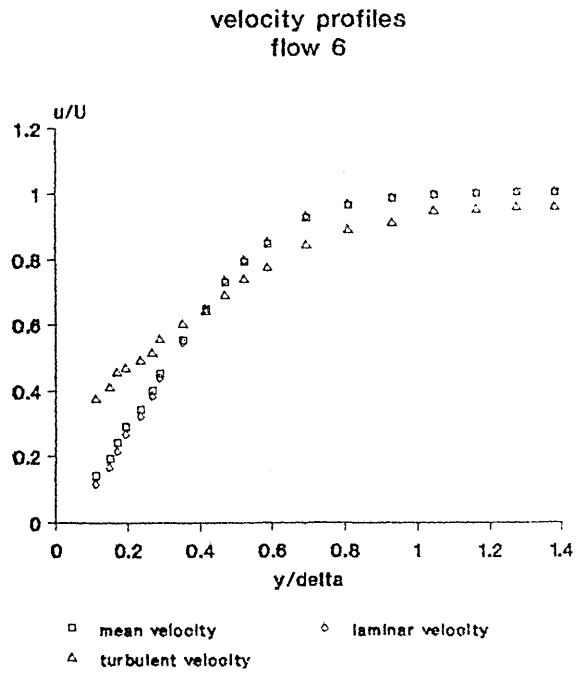

gamma = 0.11

figure A3.88 x = 611

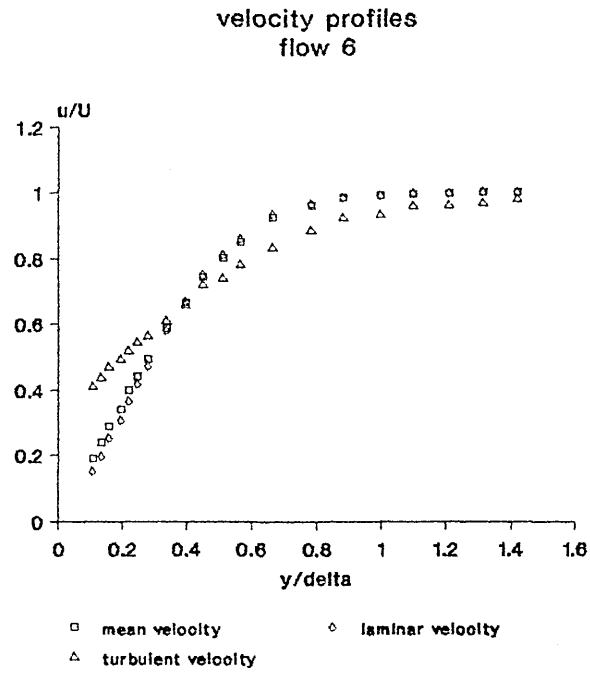

gamma = 0.17

figure A3.89 x = 621

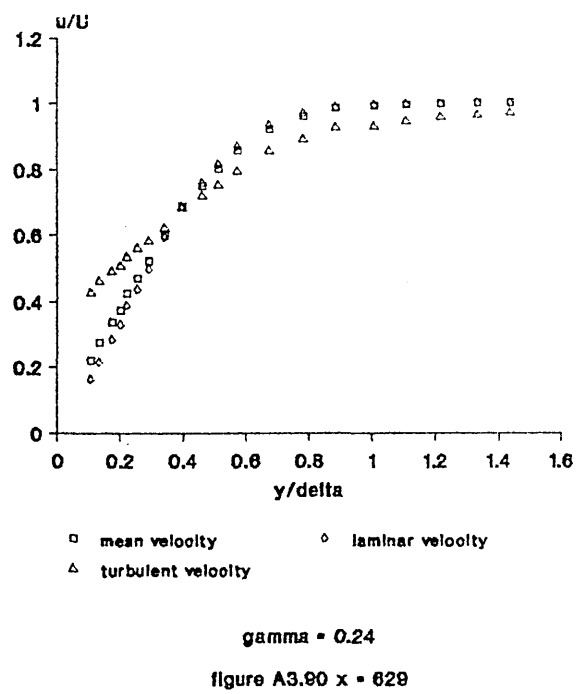

gamma = 0.24

figure A3.90 x = 629

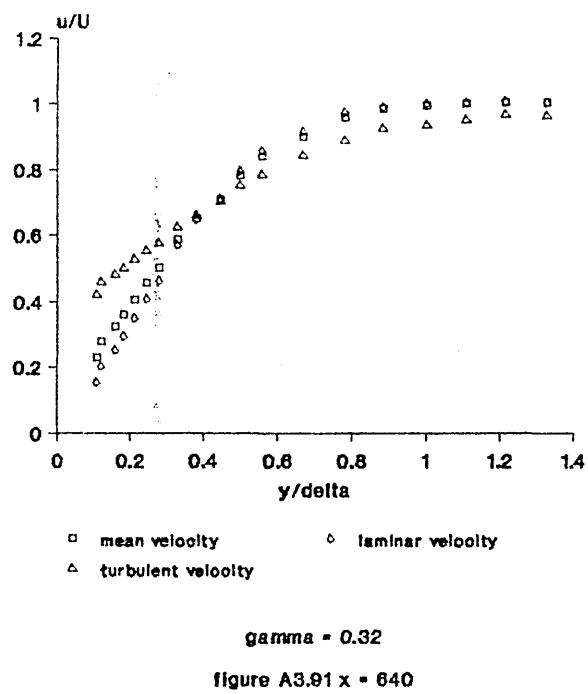

gamma = 0.32

figure A3.91 x = 640

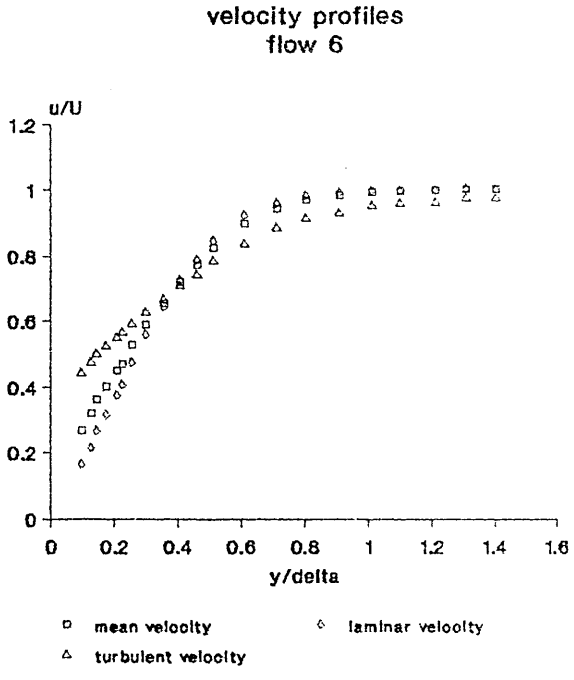

gamma = 0.41

figure A3.92 x = 650

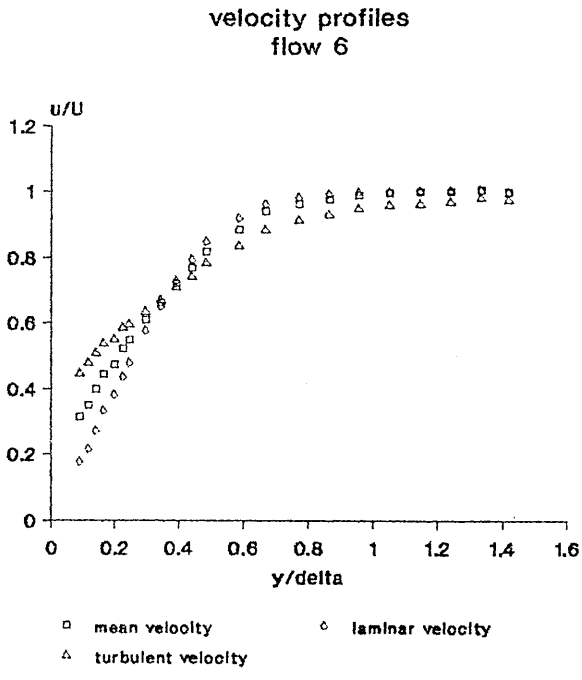

gamma = 0.53

figure A3.93 x = 660

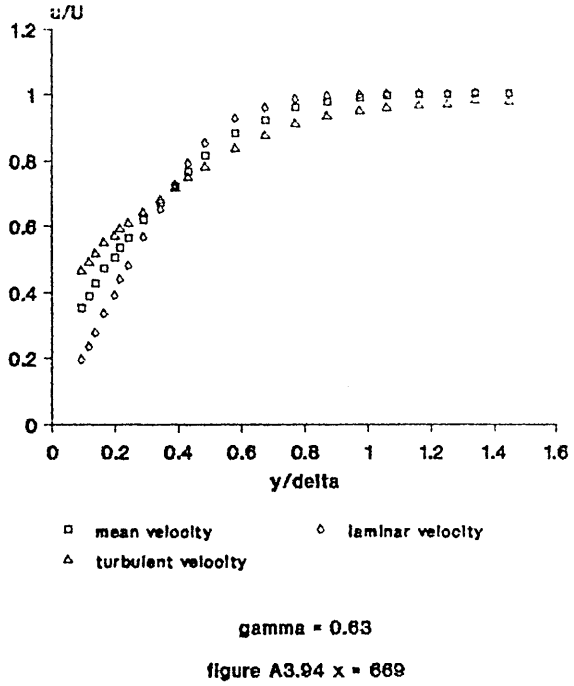

gamma = 0.63

figure A3.94 x = 669

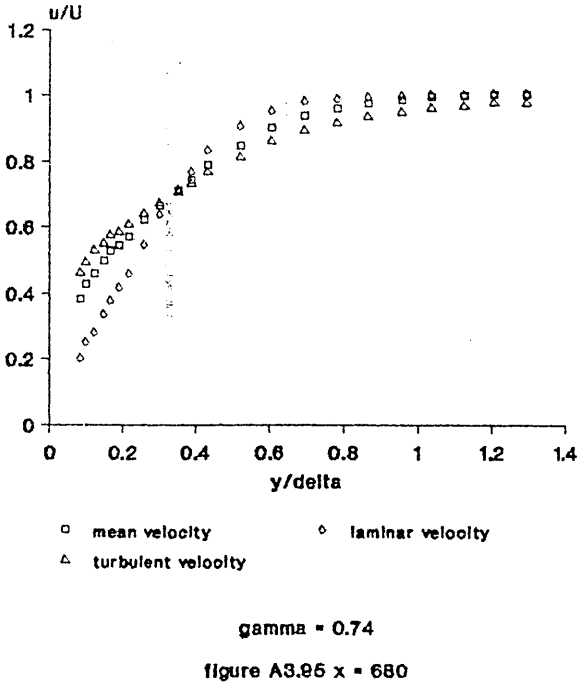

gamma = 0.74

figure A3.95 x = 680

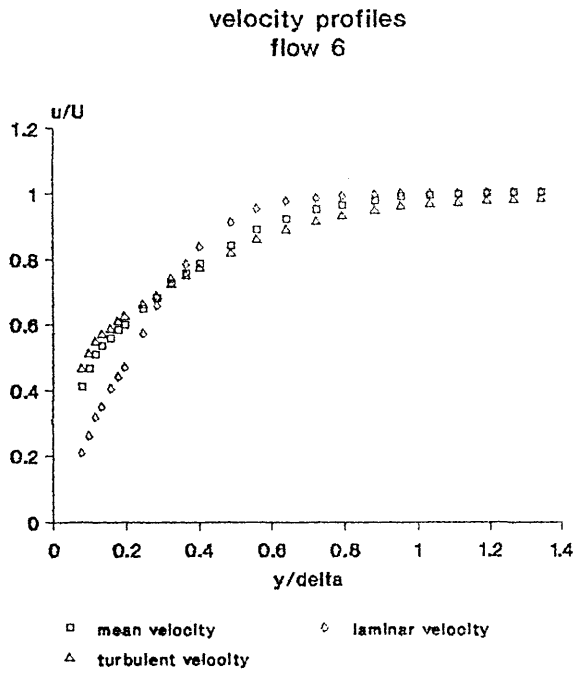

gamma = 0.83

figure A3.96 x = 691

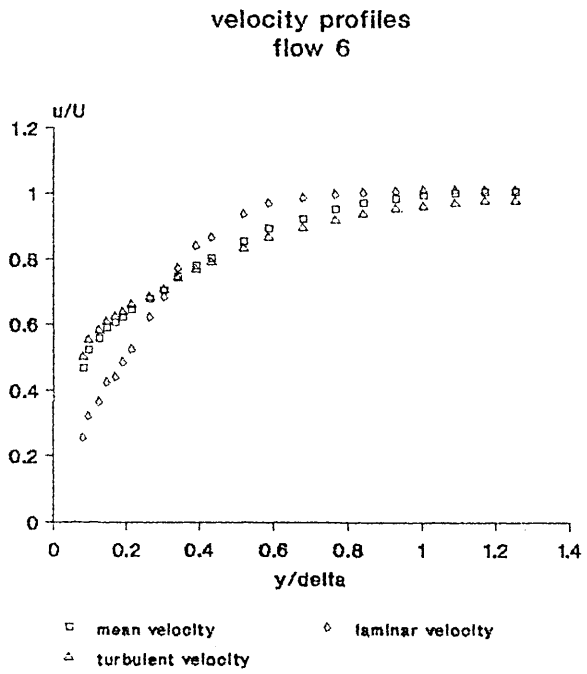

gamma = 0.88

figure A3.97 x = 700

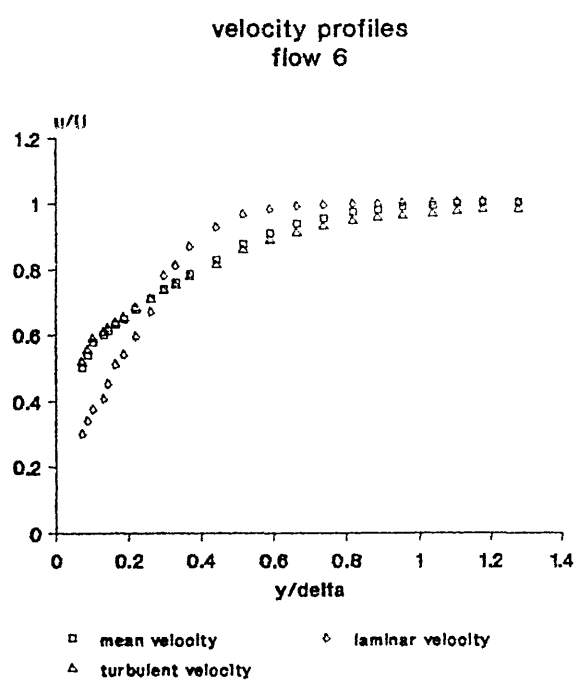

gamma = 0.94

figure A3.98 x = 710

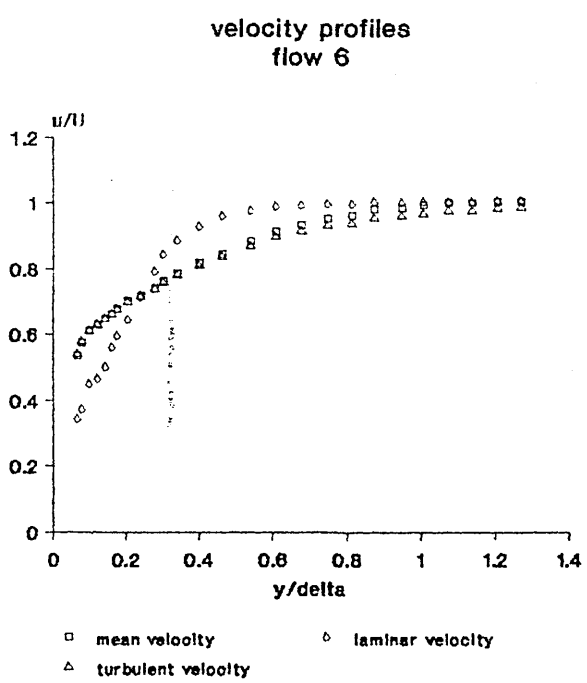

gamma = 0.98

figure A3.99 x = 730

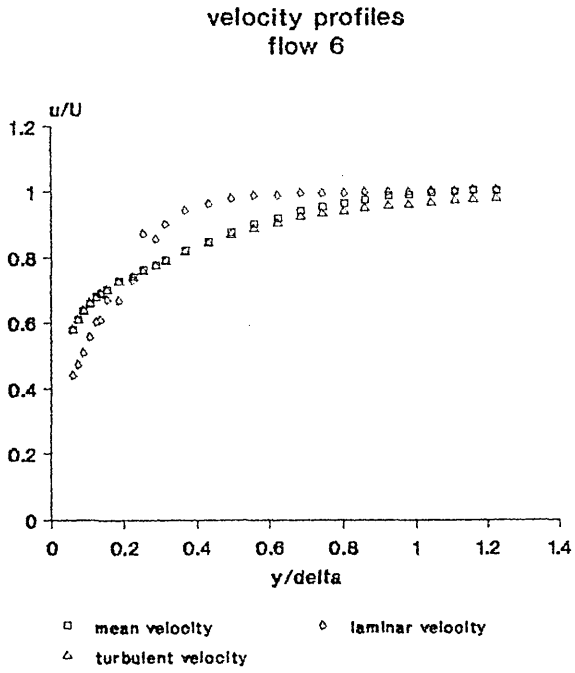

gamma = 0.99

figure A3.100 x = 749

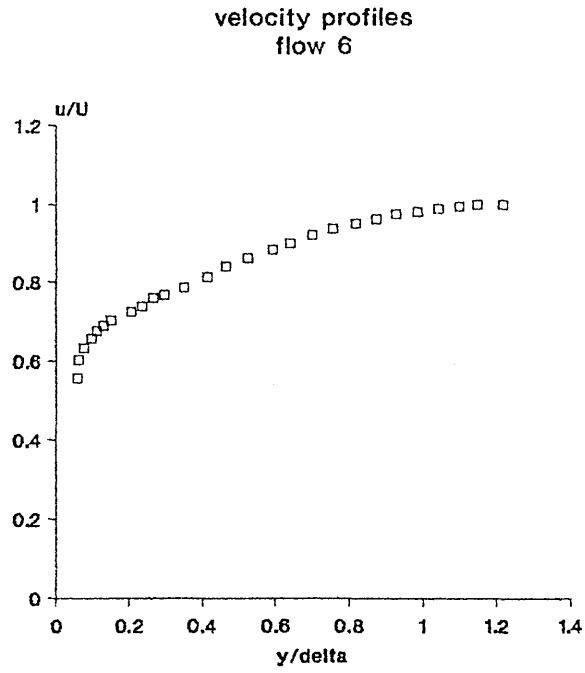

figure A3.101 x = 770

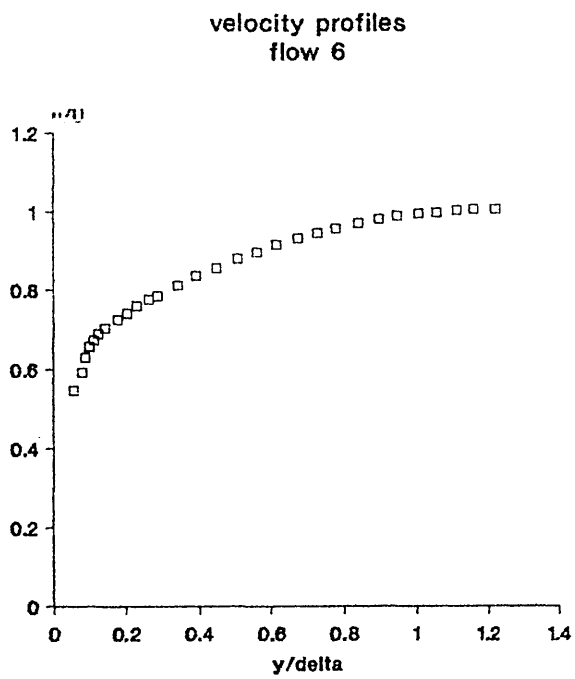

figure A3.102 x = 780

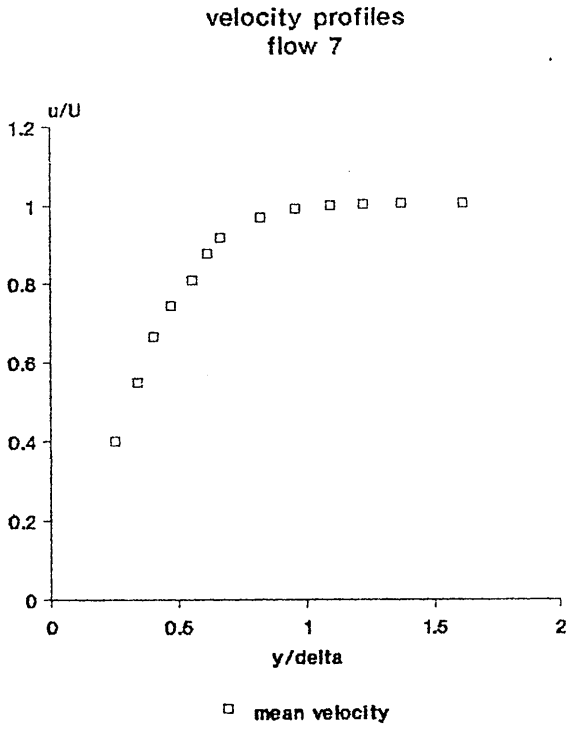

figure A3.103 x = 380

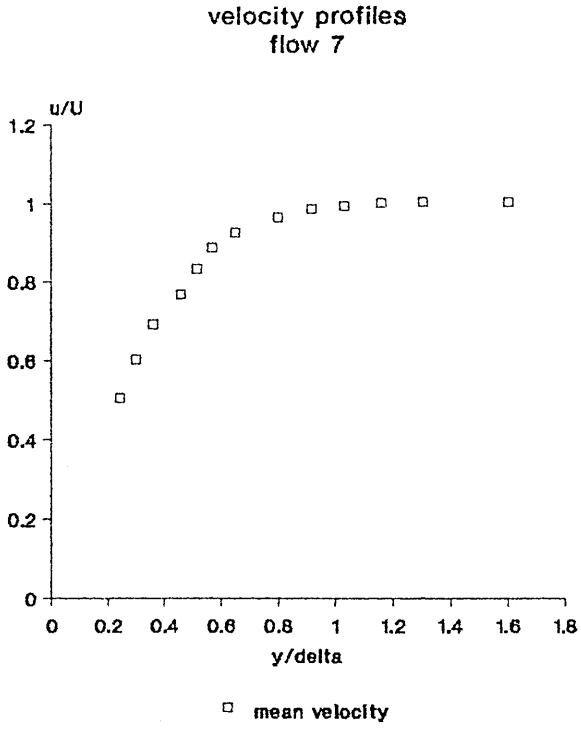

figure A3.104 x = 460

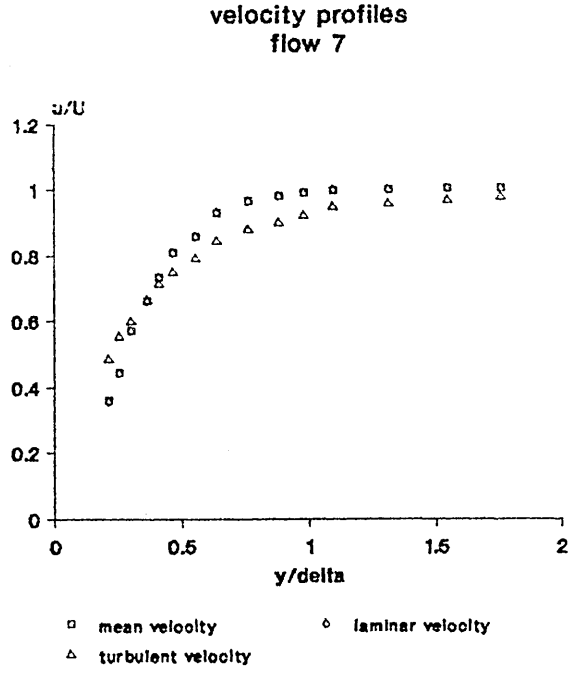

gamma = 0.01

figure A3.105 x = 500

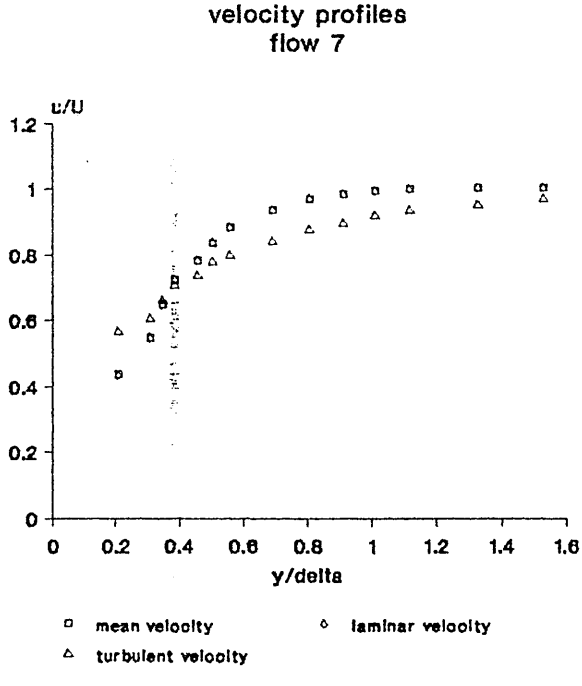

gamma = 0.02

figure A3.106 x = 550

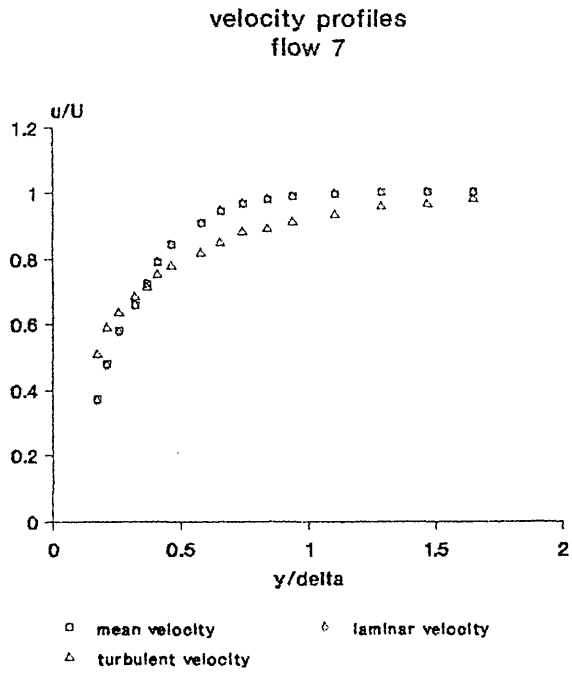

gamma = 0.03

figure A3.107 x = 600

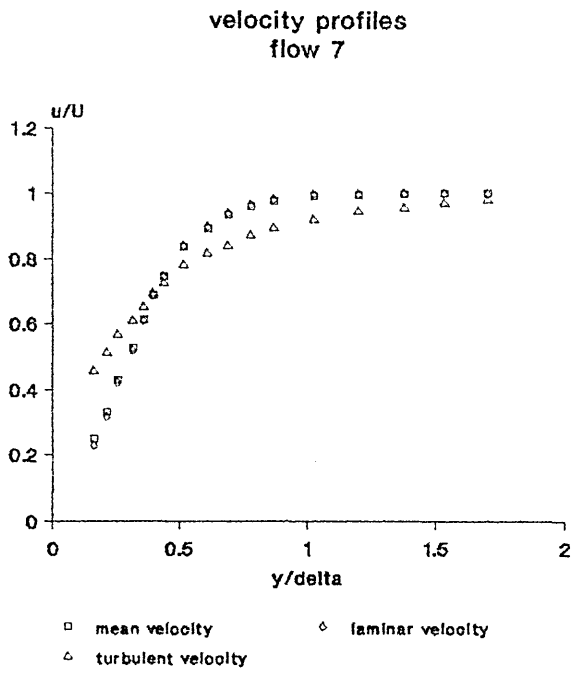

gamma = 0.07

figure A3.108 x = 650

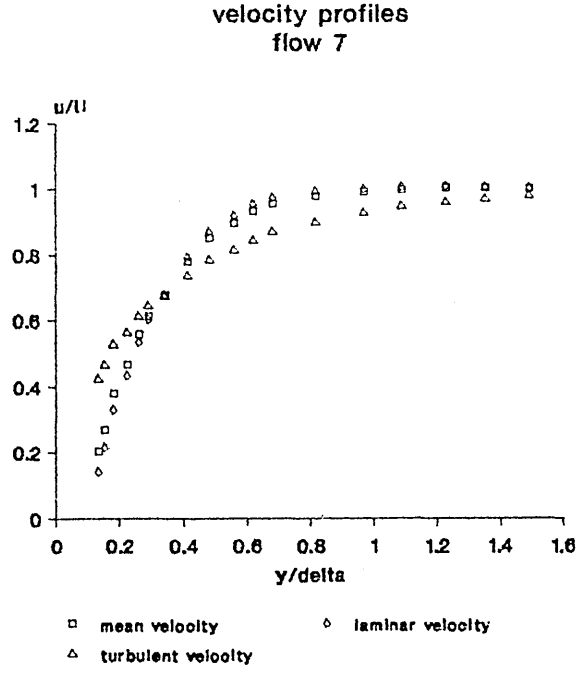

gamma = 0.24

figure A3.109 x = 700

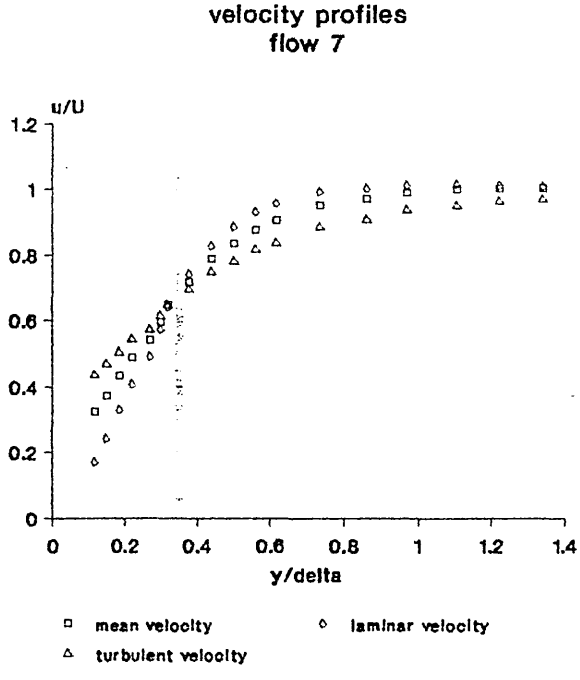

gamma = 0.68

figure A3.110 x = 750

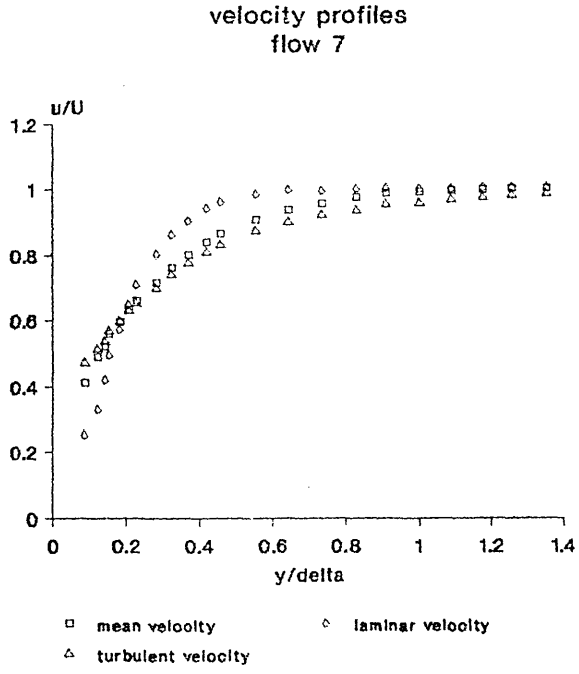

gamma = 0.86

figure A3.111 x = 780

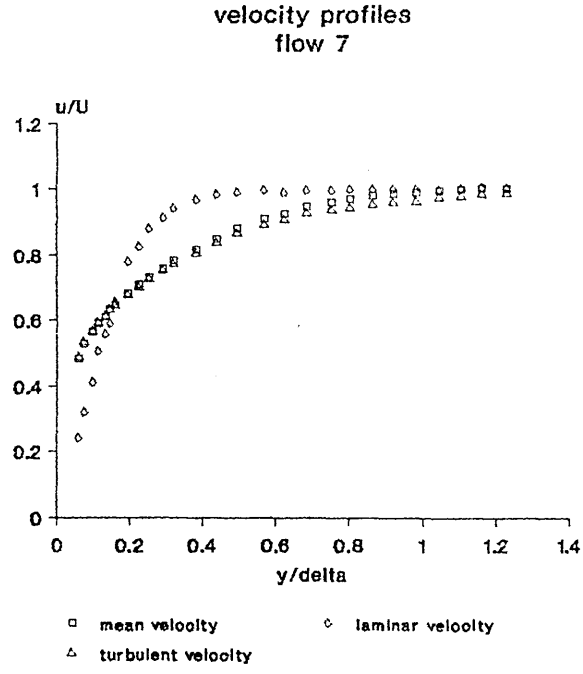

gamma = 0.97

figure A3.112 x = 850

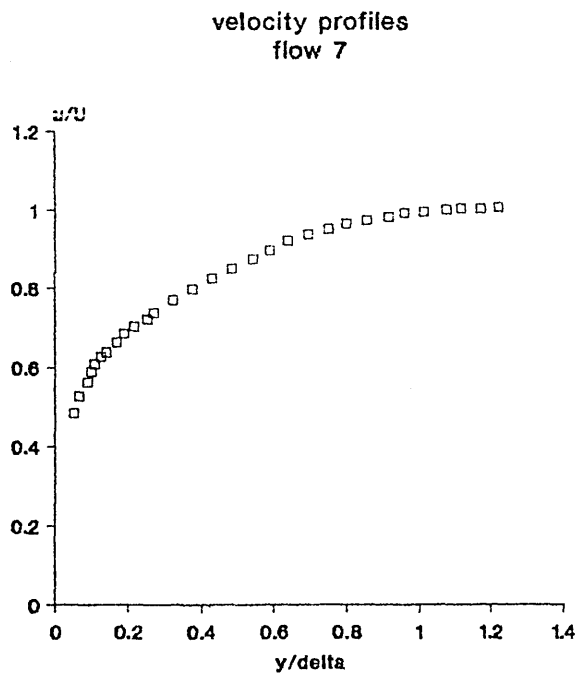

figure A3.113 x = 900

APPENDIX 4

DIGITAL PROCESSING OF HOT WIRE ANEMOMETER SIGNALS IN INTERMITTENTLY TURBULENT FLOWS